Experimental and theoretical investigation of systems with potential for terabit capacity

Clausen, Anders

Publication date:
2006

Document Version
Publisher's PDF, also known as Version of record

Experimental and theoretical investigation of systems with potential for terabit capacity

Anders Thomas Dræborg Clausen

August 1, 2006

Department of Communications, Optics and Materials
Technical University of Denmark
Building 345V
2800 Kgs. Lyngby
Denmark

Contents

Abstract

Internet traffic has been growing with tremendous speed in the last decade and analysis indicate that the growth will continue in the future. The apparent unlimited capacity will within a few years be utilised completely, thus preventing the expected boom in new broadband demanding services. New techniques for utilising the existing Internet infrastructure more efficiently, either by replacing or complementing existing techniques, are therefore indispensable.

Optical Time Division Multiplexing (OTDM) is one option out of a number of schemes, which offer more efficient utilisation of the bandwidth either alone or in conjunction with e.g. Wavelength Division Multiplexing (WDM) or with advanced modulation formats.

The objective of this thesis is to extract and provide design parameters allowing an optimised performance of an OTDM system. A basic point-to-point bit interleaved OTDM system can be divided into a few sub-systems and each chapter in the thesis is dedicated to a specific part. The first sub-system attended is the pulse source, where the temporal Full Width Half Maximum (FWHM) width and the Pulse Tail Extinction Ratio (PTER) are examined. Subsequently, Clock Recovery is covered, by deriving a modified Phase Locked Loop theory, which is useful when extracting a base rate clock from an aggregated high-speed OTDM signal. Stability of the modified Clock Recovery sub-systems is analysed using Bode plots with special emphasise on impact of the often-substantial optical time delays within the loop. Extraction of the tributary channels using switches for demultiplexing is presented, and design parameters in terms of temporal FWHM width, Extinction Ratio and timing jitter are provided. Error-free experimental demultiplexing of 320 to 10 Gbit/s using a Non-linear Optical Loop Mirror (NOLM) is shown. Finally, some of the additional required functionalities when expanding from OTDM point-to-point systems to networks are discussed, with special focus on channel identification schemes.

Resumé (in Danish)

Internet trafikken er steget med fantastisk fart den sidste dekade og analyser antyder at stigningen vil fortsætte i fremtiden. Den kapacitet som hidtil har syntes ubegrænset vil indenfor de kommende år være fuldstændig udnyttet, hvorved det forventede boom i nye bredbåndskrævende services vil blive forhindret. Nye teknikker der vil kunne udnytte den allerede eksisterende Internet kapacitet mere effektivt, enten ved at udskifte eller komplementere nuværende teknikker, vil derfor blive uundværlige.

Optical Time Division Multiplexing (OTDM) er én mulighed ud af mange teknikker som tilbyder en mere effektiv udnyttelse af båndbredden, enten alene eller sammen med f.eks. Wavelength Division Multiplexing (WDM) eller med avancerede modulationsformater.

Formålet med denne afhandling er at udlede og formidle design parametre som tillader en optimeret ydelse af et OTDM system. Et basalt punkt-til-punkt bit sammenflettet OTDM system kan blive inddelt i nogle få undersystemer og hvert kapitel i denne afhandling er dedikeret til en specifik del. Det første undersystem er pulskilden, som er blevet undersøgt mht. den tidslige Full Width Half Maximum (FWHM) bredde samt Pulse Tail Extinction Ratio. Derefter er klokke gendannelsessystemer blevet behandlet ved at udlede en modificeret Phase Locked Loop (PLL) teori som er brugbar når en klokke svarende til den grundlæggende frekvens af de enkelte kanaler skal ekstraheres fra højhastigheds OTDM signalet. Stabilitet af det modificerede klokke gendannelsessystem er analyseret vha. Bode plot med særlig fokus på indflydelsen af de ofte betydelige optiske tidslige forsinkelser internt i loopet. Separation af de enkelte kanaler vha. demultiplexing i switches er præsenteret og design parametre såsom den tidslige FWHM bredde, udslukningsforhold samt tidslig jitter bliver formidlet. Fejlfri eksperimental demultiplexing fra 320 til 10 Gbit/s vha. af en Non-linear Optical Loop Mirror (NOLM) bliver dokumenteret. Til sidst bliver de ekstra funktionaliteter der er nødvendige for at udvide et punkt-til-punkt system til netværk diskuteret med særlig fokus på kanal genkendelsessystemer.

Acknowledgements

The progress of this PhD has been a long and adventurous journey, which I have enjoyed tremendously partly due to the interesting topic and partly due to the good colleagues I have been fortunate to work with.

First of all I would like to express my sincere gratitude to my supervisor Palle Jeppsen, for giving me the opportunity for concentrating on high-speed communication systems and to pursue a PhD degree.

The work presented in this thesis is carried out within the OTDM group, a sub-group of the System Competence Area. I would like to thank all the members, both current, Leif K. Oxenløwe, Jorge Seoane, Michael Galili, Hans Christian Hansen Mulvad and Darko Zibar, and previous, Andrei Siahlo, Kim Berger, Jon Bennike, Andrea Tersigni and Steinar Boge, for their dedicated work on high-speed OTDM systems, the good collaboration and friendly spirit within the group.

I would also like to thank all the members of System Competence Area both "new" and "old" members for contributing to the good and pleasant environment, lunchtime is NEVER boring together with you.

Thank you to Henrik "Kloopf" Poulsen for many cheerful moments at the office and over-sea friendship. Leif K. Oxenløwe is acknowledged for his helpfulness and for his weird sense of humour, which is disturbingly similar to my own. Christophe Peucheret for always finding the time in his tight schedule to discuss topics of both professional relevance and topics of more private character such as mutual passion for ducks. Alvaro Buxéns for technical assistance and for friendly encouragement by means of ice cream. Lars Grüner-Nielsen and Stig Nissen Knudsen current and former employee at OFS are acknowledged for their helpfulness when fibres with very specific characteristics were needed in the experiments, even when requested with very short notice.

Most of the work has been funded by the European IST project TOPRATE and it has been a pleasure working with colleagues from partners all over Europe. Especially the joint experiments with Roberto Llorente from Universidad Politecnica de Valencia and Olaf Brox from Heinrich-Hertz-Institut in Berlin were memorable. Alcatel SEL is acknowledged for their generosity lending COM•DTU essential equipment.

I am indebted to Henrik N. Poulsen, Alvaro Buxéns, Leif K. Oxenløwe and Jorge Seoane for proofreading the thesis and giving me thorough feedback, which certainly improved the readability of this thesis.

Thank you to my parents, my sister and my in-laws for their support and for not being bored when I explained the wonders of OTDM. Finally, and most importantly, I would like to thank Nina for her love and never ever decreasing support.

Kgs. Lyngby 2006 07 31 Anders Thomas Dræborg Clausen

List of Acronyms

ACTS	Advanced Communications and Technology and Services
AM	Amplitude Modulation
ASE	Amplified Spontaneous Emission
ASK	Amplitude Shift Keying
BER	Bit Error Rate
BOD	Bandwidth On Demand
BPSK	Binary Phase Shift Keying
CDPF	Comb-like Dispersion Profiled Fibre
CW	Continuous Wave
CLW	Clockwise
CCLW	Counter-clockwise
COM•DTU	Department of Communications, Optics and Materials
CR	Clock Recovery
CW	Continuous Wave
DCF	Dispersion Compensating Fibre
DDF	Dispersion Decreasing Fibre
DFB	Distributed Feedback
DFF	Dispersion Flattened Fibre
DSF	Dispersion Shifted Fibre
EAM	Electroabsorption Modulator
EDF	Erbium Doped Fibre
EDFA	Erbium Doped Fibre Amplifier
ERGO	Erbium Glass Laser Oscillator
ETDM	Electrical Time Division Multiplexing
ETH	Eidgenössische Technische Hochschule
EOP	Eye Opening Penalty
ER	Extinction Ratio
FIS	Fibre based interferometric switch
FM	Frequency Modulated
FNIS	Fibre based non-interferometric switch
FOD	Fourth Order Dispersion
FROG	Frequency Resolved Optical Gating
FWHM	Full Width Half Maximum
FWM	Four Wave Mixing
GBW	Guaranteed Bandwidth
GS-DFB	Gain-switched Distributed Feedback
GVD	Group Velocity Dispersion

HIGHWAY	Photonic technologies for ultra-high-speed information highways
HNLF	Highly Non-linear Fibre
IP	Internet Protocol
ISI	Intersymbol Interference
IST	Information Society Technologies
ITU	International Telecommunication Union
LAN	Local Area Network
MAC	Media Access Control
MAN	Metropolitan Area Network
ML-FRL	Mode-locked Fibre Ring Laser
MLL	Mode-locked Laser
MMLL	Monolithic Mode-Locked Laser
MZI	Mach-Zehnder Interferometer
NF	Noise Figure
NLE	Non-linear Element
NLSE	Non-linear Schrödinger equation
NOLM	Non-linear Optical Loop Mirror
NRZ	Non-Return to Zero
OA	Operational Amplifier
OADM	Optical Add Drop Multiplexer
OBF	Optical Bandpass Filter
OEO	Opto-Electronic Oscillator
OE-PLL	Opto-electronic Phase Locked Loop
OPD	Optical Phase Detection
OSNR	Optical Signal to Noise Ratio
OTDM	Optical Time Division Multiplexing
PBS	Polarisation Beam Splitter
PC	Polarisations Control
PCF	Photonic Crystal Fibre
Pdf	Probability density function
PD	Phase Detector
PD-EAM	Photo-diode integrated with an EAM
PDL	Polarisation Dependent Loss
PD-SMZI	Polarization-Discriminating Symmetric Mach-Zehnder Interferometer
PLC	Planar Lightwave Circuit
PLL	Phase Locked Loop
PM	Phase Margin
PMD	Polarisation Mode Dispersion
PM-DSF	Polarisation Maintaining Dispersion Shifted Fibre
PRBS	Pseudo Random Bit Sequence
PTER	Pulse Tail Extinction Ratio
PZT	Pietzo

RF	Radio Frequency
RIN	Relative Intensity Noise
RZ	Return to Zero
RX	Receiver
SCOOP	Semiconductor components for optical signal processing
SESAM	Semiconductor saturable absorber mirror
SIS	SOA based interferometric switch
SLALOM	Semiconductor Laser Amplifier Loop Mirror
SNR	Signal to Noise Ratio
SNIS	SOA based non-interferometric switch
SOA	Semiconductor Optical Amplifier
SOA-MZI	Semiconductor Optical Amplifier based Mach-Zehnder interferometer
SOP	State of polarisation
SPM	Self Phase Modulation
SSB	Single Side Band
SSMF	Standard Single Mode Fibre
SW	Switching Window
TL	Transform Limited
TOAD	Terahertz Asymmetric Optical Demultiplexing
TOD	Third Order Dispersion
TOPRATE	Terabit/s Optical Transmission Systems based on Ultra-high Channel Bitrate
TX	Transmitter
UNI	Ultrafast Nonlinear Interferometer
VCO	Voltage Controlled Oscillator
VOA	Variable Optical Attenuator
WDM	Wavelength Division Multiplexing
WTPS	Wavelength Tuneable Pulse Source
XGM	Cross Gain Modulation
XPM	Cross Phase Modulation

List of figures

List of tables

Chapter 1
Introduction

1.1 Motivation for work

Year 2006 is the year of the 40th anniversary for the conceptual invention of data transmission over optical fibres [1.1], [1.2], an invention which have had a profound impact on the telecommunication scene. With the wide spreading of the Internet, the evolution of telecommunication was further accelerated and in the end 90es an often cited remark was "the Internet is doubling every 100 days" corresponding to an increase in traffic between 8 and 16 times a year. Studies in retrospect have revealed that the Internet indeed was exploding with 1000 % per year, but only in a very limited period on a specific installed network [1.3]. It has been speculated whether the company WorldCom deliberately mislead the marked by claiming that this doubling every 100 days indeed was an universal law, thus keeping their stocks on an unrealistic high level [1.4] [1.5]. The entire marked accepted the mantra of "the Internet is doubling every 100 days" basing their business strategies on these growth rates, despite other analysis indicating growth of 100 % per year [1.3], impressive but not comparable to the 1000 % growth. In 2002 the optimism combined with risky investments lead to the burst of the telecommunication bubble [1.6] and every player in the telecommunication sector had to adjust to the realities leading to bankruptcy, substantial cut-downs and reorganisation of companies.

Despite the regression in telecommunication business the Internet traffic and capacity continued to increase and in the years 2003 to 2005 the annual increase in Internet traffic was ~50 % or more as seen in Table 1.1 [1.7][1.8][1.9].

Year	Internet traffic Annual increase in %	Internet capacity Annual increase in %
2003	67	78
2004	115	46
2005	49	42

Table 1.1: Annual increase in global Internet traffic and capacity in year 2003, 2004 and 2005. Notice, the increment in Internet traffic in 2003 is based only on figures for the first quarter of 2003 [1.7][1.8][1.9]

Now, 4 years after the crash, the optimism is back in the telecommunication industry. The Internet traffic is continuously increasing and trends in the telecommunication strategies suggest that the data traffic will increase further - the telephone companies start offering triple play services, by integrating voice, data and video services, over broadband connections to the costumers [1.10], and in response the service providers prepare bandwidth demanding data applications like voice-over-IP, IP video and soon high-definition TV [1.11]. Fibres-to-the-premises (Fibres-to-the-home) is back on the agenda as means for increasing the capacity in the access net [1.12] and decreasing the price per bit [1.10]. Despite the troubles in predicting the future, it nevertheless appears that the regression is over and confident prospects exist.

Predictions, which indicate that the apparently unlimited fibre capacity will be insufficient long before 2025, even if the capacity is increased with 20 % each year [1.13] represents a potential cup of bitterness. The analysis indicates that incrementing the number of Wavelength Division Multiplexing (WDM) channels employing existing commercial bit rates of 2.5, 10 and 40 Gbit/s will not necessarily fulfil the capacity requirements, partly due to the limited low-loss transmission window of the optical fibres. Albeit, forecasts are in its nature based on assumptions and thus should be interpreted with caution, the analysis emphasise the importance of searching for alternative schemes and technologies which can either replace or supplement the existing systems.

Increasing the bit rates has historically been accepted as one way to increase the total capacity of commercial communication systems, while reducing the price per bit. Thus increasing the bit rate by four only increases the price with a factor of two [1.14]. Since the first systems at 45 Mbit/s in 1980 [1.2], the bit rates have been incremented regularly and systems at 40 Gbit/s are now maturing, see e.g. [1.15]. However, research is continuing to increase the bit rate further by carefully optimising the materials and the design of the opto-electronic components, and at the moment there is a lot of focus on 100 Gbit/s Ethernet development, see e.g. [1.11][1.16][1.17].

1.2 OTDM systems

The high-speed systems currently deployed commercially and researched upon are based on time multiplexing a number of relative low bit rate signals up to a high-speed signal in the electrical domain, hence the name Electrical Time Division Multiplexing (ETDM). The aggregated bit rate is consequently determined by the bandwidth of the electronics, a bottleneck, which is reasonably easy to overcome by time multiplexing in the optical domain instead. This technique, which is called Optical Time Division Multiplexing (OTDM), was recognised almost at the same time as the conceptual idea of optical fibres was presented, as some of the first OTDM schemes were reported in the end of the 1960es/beginning of the 1970es according to [1.18]. In Figure 1.1 the basic point-to-point bit interleaved OTDM system is shown.

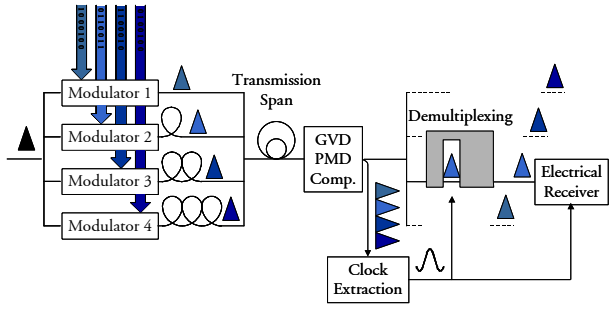

Figure 1.1: Point-to-point bit interleaved Optical Time Division Multiplexed (OTDM) system

Figure 1.1 is a returning figure in the next chapters, as each chapter emphasises specific sub-systems of the OTDM system. The pulse source is the main component of the transmitter. It generates a pulse train of Return-to-Zero (RZ) pulses characterised by e.g. shape, temporal Full Width Half Maximum (FWHM) width, timing jitter and repetition rate B, labelled the base rate frequency. The pulse train is split into N branches, each including an external modulator which intensity modulates the pulse trains with unique data streams. If the pulses are sufficiently narrow, a specifically designed time delay in each branch, allows the N data signals to be bit interleaved, i.e. multiplexed, thus generating an aggregated OTDM data signal with a bit rate of NB bit/s. The OTDM signal is injected into a transmission fibre span before it is received. In the receiver the physical distortion of the signal due to the properties of the fibres, e.g. due to Group Velocity Dispersion (GVD) and Polarisation Mode Dispersion (PMD), is compensated if possible. After transmission and compensation of impairments, the ultra fast OTDM data signal should be downscaled in bit rate, allowing electronics to process the signal. In the

transmitter, it was relatively easy to overcome the potential bit rate limitations induced by the low bandwidth of the electronics. However, in the receiver, the OTDM scheme takes its toll, as detection of the signal is very challenging; both clock recovery and demultiplexing of each tributary channel are required. A part of the OTDM signal is tapped for the Clock Recovery (CR) circuit, which extracts a clock corresponding to the base rate frequency B of the OTDM signal. Because the OTDM signal does not include a distinct frequency component at B, the clock extraction is challenging and modifications of existing Clock Recovery schemes are required. The base rate clock is applied as a control signal to the switches, used to optically demultiplex each individual time channel from the aggregated data signal. As no existing switches offer demultiplexing of all channels using only one single switch, an array of switches is used as sketched in Figure 1.1. Each of the demultiplexed base rate signals can subsequently be detected, by injecting the signals into base rate receivers triggered by the base rate clock. Hence, by using relatively slow electronics, very high-speed optical signals can be generated and impressive results of e.g. 320 [1.19], 640 [1.20] and 1280 Gbit/s [1.21] have been demonstrated.

Comparing with 40 or 100 Gbit/s ETDM systems, currently OTDM has the potential to increase the bit rate with factors from 10 to 30, thus offering attractive technology, which empowers system designers to enlarge the capacity of each wavelength channel significantly. Furthermore according to [1.14], an increase in speed per wavelength gives better bandwidth efficiency, is easier to manage, introduce lower footprint and in principle lower power consumption. OTDM systems also face challenges, which need to be solved before OTDM represents a realistic option. However, some of these challenges appear to be depending on each other. As an example, the benefits presented in [1.14] have not been confirmed yet, because no component vendor has invested the required resources in refining laboratory implementations or proto-types of e.g. the necessary high-speed switches used for signal processing, because presently there is no market for commercial OTDM systems. Consequently, no system vendor will offer OTDM systems because no cheap and reliable components are available. So the two main issues, i.e. costs and stability, still remain unanswered questions and thus prevent a final evaluation of whether OTDM can penetrate the barrier to commercial applications.

OTDM represents an attractive option for increasing the total capacity of optical communication systems, but should not necessarily be regarded as the stand-alone answer to ensure sufficient capacity for the expected continued increase in data traffic. OTDM can, as vaguely indicated in the previous paragraph, be combined with WDM, by using OTDM on several parallel WDM channels, see e.g. [1.22]. OTDM has also been reported combined with advanced modulation formats thus increasing the spectral efficiency as reported in e.g. [1.23] [1.24]. Finally, OTDM offers the possibility for paving the way for

high-speed ETDM systems by offering an easy way for generating the required high-speed data signals required to characterise e.g. designed transmission spans or detectors, without having access to full ETDM systems. In conclusion, OTDM is still an important player when considering the challenges of offering sufficient of capacity that can cover the needs of the future.

1.3 Structure of the thesis

The thesis is organised by addressing specific sub-systems of the bit interleaved OTDM system in separate chapters. In chapter 2 the pulse source is addressed. The most important characterisation parameters of the pulse sources allowing high-speed system implementation are extracted before a summary of the most promising pulse sources for OTDM systems is presented. A detailed simulation tool is presented in order to determine the strict requirements the pulses need to fulfil in terms of temporal FWHM width and Pulse Tail Extinction Ratio (PTER). H. N. Poulsen has contributed with parts of the used simulation code. In chapter 3, the Clock Recovery sub-system is described. A survey of reported OTDM Clock Recovery schemes is presented before the standard theory for Phase Locked Loops (PLL) are modified in order to allow for extraction of a base rate clock signal from a high-speed OTDM signal without any distinct frequency component at the base rate frequency. By including a fast switch in the set-up, which is used as a harmonic mixer, thus generating an output signal, which reflects the offset between the phases of the two signals, a modified PLL for clock extraction can be implemented, controlled by the phase difference. However, because the control signal inherently includes an offset signal, Clock Recovery is not possible unless further modifications of the sub-system are introduced. Four different techniques for compensating the offset are compared and one is chosen as the preferred scheme. A discussion between L. K. Oxenløwe and the author about how the often substantial time delays within the PLL affects the clock extraction, resulted in a simple model of evaluating the stability of the Clock Recovery sub-system, which is presented and a numerical example emphasise how strict the requirements to the acceptable delay are. Chapter 4 is devoted to demultiplexing the tributary channels from the aggregated OTDM signal. Because no switches presently can separate all the OTDM channels simultaneously an array of switches is needed, and different array structures are briefly examined. A survey of the most successful switches is presented. A simple simulation model is used to evaluate the impact of different parameters of an ideal switch, in terms of temporal FWHM width, shape and timing jitter. Finally, a simple model of the preferred Non-linear Optical Loop Mirror (NOLM) switch is derived and examined numerically, before an experimental 320 to 10 Gbit/s demonstration is presented. The experiment was performed primarily in collaboration with A. I. Siahlo and J. Seoane. Applying the OTDM technique to network structures, the point-to-point system

sketched in Figure 1.1 needs to be modified to include more nodes and include additional functionalities, e.g. enabling the possibility of dropping an OTDM channel in one node and add a new channel in the vacant timeslot of the signal. In chapter 5 these additional functionalities are discussed, before one is addressed in more detail. An indispensable functionality is channel identification, thus allowing the system to identify which channel is targeted for being dropped in the node. A short summary of reported channel identification techniques is presented before a novel scheme based on pilot tone modulation is suggested. The pilot tone modulation scheme is numerically investigated before an experimental characterisation is presented. The experiments were performed in collaboration with J. Bennike. Finally a short introduction to reported packet switched OTDM networks is given. In chapter 6 the results are summarised.

The thesis is covering important parts of bit interleaved OTDM systems but certainly not every aspect of OTDM systems. Inspecting Figure 1.1 it is noticed that especially the transmission span is not addressed in this thesis, albeit it is equally interesting and a very important part of any optical system. Thus, design of the transmission span in terms of maximum GVD and dispersion slope, PMD and suppression of the detrimental non-linear processes otherwise likely to make error-free operation impossible is not addressed.

1.4 References to chapter 1

[1.1] K. C. Kao, G. A. Hockham, "Dielectric-fibre surface waveguides for optical frequencies", Proceedings of the institution of Electrical Engineers (IEE), Vol. 113, No. 7, pp. 1151-1158 (1966).

[1.2] G. P. Agrawal, "Fiber-Optic Communication Systems", John Wiley & Sons, Inc., Second edition, United States of America (1997).

[1.3] A. M. Odlyzko, "Internet traffic growth: Sources and implications", proceedings of the international society for optical engineering (SPIE) – Optical transmission systems and equipment for WDM networking II, Vol. 5247, pp. 1-15 (2003).

[1.4] D. Moberg, E. J. Romar, "WorldCom", http://www.scu.edu/ethics/dialogue/candc/cases/worldcom-update.html

[1.5] E. J. Romar, M. Calkins, "WorldCom Case Study update 2006", http://www.scu.edu/ethics/dialogue/candc/cases/worldcom.html

[1.6] Fibers.org – the optical communication source, "www.fibers.org" (2002)

[1.7] TeleGeography, "Global Internet Geography 2004 - Executive summary", "www.telegeography.com" (2004)

[1.8] TeleGeography, "Global Internet Geography 2005 - Executive summary", "www.telegeography.com" (2005)

[1.9] TeleGeography, "Global Internet Geography 2006 - Executive summary", "www.telegeography.com" (2006)

[1.10] Fibers.org – the optical communication source, "www.fibers.org" (2006)

[1.11] M. Duelk, "Next-generation 100G Ethernet", Proceedings of the 31st European Conference on Optical Communication (ECOC'05), Glasgow, United Kingdom, paper Tu3.1.2 (2005).

[1.12] E. Zouganeli, "Optical Networks: From point-to-point transmission to full networking capabilities", Telektronikk, Vol. 101, No. 2, pp. 3-19 (2005).

[1.13] E. Dseurvire, "Optical communication in 2025", Proceedings of the 31st European Conference on Optical Communication (ECOC'05), Glasgow, United Kingdom, paper Mo2.1.3 (2005).

[1.14] R. Ludwig, S. Ferber, C. Boerner, C. Schubert, C. Schmidt-Langhorst, M. Kroh, V. Marembert, H. G. Weber, " Ultrafast transmission technology", Proceedings of the 31st European Conference on Optical Communication (ECOC'05), Glasgow, United Kingdom, tutorial We1.6 (2005).

[1.15] Mintera Optical Networks, http://www.mintera.com/prod_trans.html

[1.16] R. Lewén, S. Irmscher, U. Westergren, L. Thylén, "Travelling-wave electrode Electroabsorption Modulators toward 100 Gb/s", Technical Digest of conference on Optical Fiber Communication (OFC'04), Los Angeles, California, USA, paper FL1 (2004).

[1.17] A. Beling, H-G. Bach, G. G. Mekonnen, R. Kunkel, D. Schmidt, "Miniaturized Waveguide-Integrated p-i-n Photodetector with 120-GHz Bandwidth and high responsivity", Photonics Technology Letters, Vol. 17, No. 10, pp. 2152-2154 (2005).

[1.18] R. S. Tucker, G. Eisenstein, S. K. Korotky, “Optical Time-Division Multiplexing for very high bit-rate transmission”, Journal of Lightwave Technology, Vol. 6, No. 11, pp. 1737-1749 (1988).

[1.19] A. T. Clausen, A. Siahlo, J. Seoane, L. K. Oxenløwe, P. Jeppesen, "320 to 10 Gbit/s demultiplexing using a NOLM based on commercially available components”, Electronics Letters, Vol. 41, No. 5, pp. 265-266 (2005).

[1.20] A. I. Siahlo, A. T. Clausen, L. K. Oxenløwe, J. Seoane, P. Jeppesen, "640 Gb/s OTDM Transmission and Demultiplexing using a NOLM with Commercially Available Highly Non-linear Fiber", Technical Digest of Conference on Lasers & Electro-Optics (CLEO 2005), Baltimore, Maryland, USA, paper CTuO1 (2005) (Invited).

[1.21] M. Nakazawa, T. Yamamoto, K.R. Tamura, "1.28Tb/s - 70 km OTDM transmission using third- and fourth-order simultaneous dispersion compensation with a phase modulator", Electronics Letters, Vol. 36, No. 24, pp. 2027-2029 (2000).

[1.22] M. Schneiders, S. Vorbeck, R. Leppla, E. Lach, M. Schmidt, S B. Papernyi, K. Sanapi, “Field transmission of 8 x 170 Gb/s over high-loss SSMF link using third-order distributed Raman amplification”, Journal of Lightwave Technology, Vol. 24, No. 1, pp. 175-182 (2006).

[1.23] T. Tokle, L. K. Oxenløwe, J. Seoane, A. T. Clausen, P.Jeppesen, “160 Gbit/s Single Channel Data Generation using Multilevel Optical RZ-DPSK-ASK Modulation and Optical Time Division Multiplexing”, Proceedings of the 31st European Conference on Optical Communication (ECOC'05), Glasgow, United Kingdom, paper We3.2.5 (2005).

[1.24] H. G. Weber, S. Ferber, M. Kroh, C. Schmidt-Langhorst, R. Ludwig, V. Marembert, C. Boerner, F. Futami, S. Watanabe, C. Schubert,"Single Channel 1.28 Tbit/s and 2.56 Tbit/s DQPSK Transmission", Proceedings of the 31st European Conference on Optical Communication (ECOC'05), Glasgow, United Kingdom, post-deadline paper Th4.1.2 (2005).

Chapter 2
Pulse Source Requirements

2.1 Introduction

A number of research groups at universities and companies worldwide are investigating high-speed data transmission, both on aggregated bit rates approaching Tbit/s on a single wavelength, based entirely on Optical Time Division Multiplexing (OTDM) techniques, OTDM combined with advanced modulation formats and finally on a combination of OTDM and Wavelength Division Multiplexing (WDM) techniques, by generating 160 or 320 Gbit/s OTDM signals at several wavelengths. For all approaches the systems are based on Return-to-Zero (RZ) pulses, and the objective of this chapter is to identify and extract the requirements for pulse sources to be used in such systems.

Different schemes, techniques and components have been developed for generating RZ pulses. In the next section of this chapter a short overview of some of the existing components is presented. In general, with few exceptions, the reported pulse trains are characterised in two ways. Either the pulses are characterised by the temporal Full Width Half Maximum (FWHM) pulse width and the deviation from the ideal pulse in terms of residual pedestal energy, see e.g. [2.1], or the pulses are characterised in terms of performance when implemented in an OTDM system, see e.g. [2.2]. However, the link between development of the pulse source and the expected behaviour in the system has only very briefly been addressed in the literature, see e.g. [2.3], [2.4] and [2.5]. Consequently it is the objective of this chapter to provide the link between characterisation of the pulse source and the expected behaviour in an OTDM system.

The principal OTDM communication system can be illustrated as in Figure 2.1. A thorough description of the system is found in chapter 1 and only a short resume is presented below. A pulse source generating a pulse train of RZ pulses with a repetition rate of B is the main component of the transmitter. The pulse

train is split into N branches, each including an external modulator. After modulation, each data train is delayed with a specific delay in order to interleave, i.e. multiplex, the N number of data signals to a single aggregated signal. The data signal, with the aggregated bitrate of NB bit/s, is injected into the transmission span. The impact of e.g. Group Velocity Dispersion (GVD), dispersion slope and Polarisation Mode Dispersion (PMD) of the transmission span is compensated before each of the OTDM channels are demultiplexed optically to the base rate. The demultiplexed signal can then be converted to the electrical domain and processed electronically.

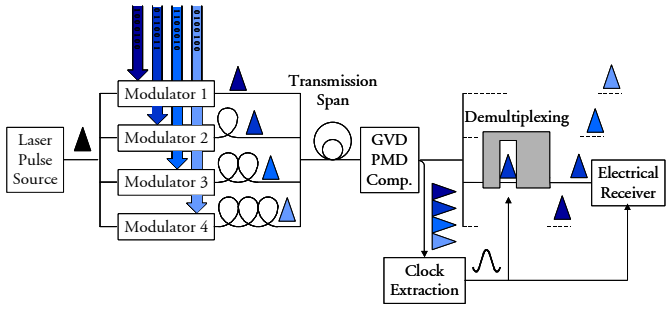

Figure 2.1: Basic OTDM communication system.

Figure 2.1 illustrates how the entire bit-interleaved point-to-point OTDM system is based on several subsystems, e.g. multiplexing, dispersion compensation and clock-recovery. The total performance of the OTDM system is an interaction between all the subsystems, and consequently the requirements for each subsystem can in principle not be extracted before all the subsystems are developed and combined in a complete communication system. However, it is possible to design and evaluate the subsystems individually, by neglecting the impact of interaction between some of the subsystems and idealise the impact of other subsystems. By making these assumptions, the specific subsystem, which is investigated, can be designed.

The structure of this chapter is as follows. First a short discussion of the requirements, which need to be clarified when choosing a laser pulse source for the OTDM system is described, followed by a short review of some of the most promising available RZ pulses reported in literature and from commercial vendors. As will be argued in subsequent sections, the temporal FWHM pulse width should be on the order of 0.40 times the time slot width of the OTDM signal. As only very few pulse sources fulfil these requirements for 320 Gbit/s and above, additional pulse compression is required. A short introduction to the pulse compression technique utilised at Department of Communications, Optics and Materials (COM•DTU) within the European Information Society Technologies (IST) project Terabit/s Optical Transmission Systems based on

Ultra-high Channel Bitrate (TOPRATE) is presented. Finally, the requirements to the pulse source are extracted by means of simulations. To this end, a simplification of the OTDM system is proposed, the detrimental physical effects, which have an impact on the requirements, are described before the actual implementation of the program for simulating the system is sketched. The results from the simulation are presented and compared to existing literature and finally the requirements are extracted.

2.2 Parameters to evaluate OTDM RZ pulse sources

In order to design a functioning OTDM system, a high-quality pulse source fulfilling a number of requirements is indispensable.

In Figure 2.1 it is tacitly assumed that the repetition rate of the pulse source is equal to the base rate of the OTDM data signal and that the pulse source and the data modulation is synchronised.

First, it is essential that the pulse source and the data modulation are synchronised, to ensure correct data modulation of the pulses. Even the slightest mismatch between the two frequencies will impair the system performance. Two approaches for synchronisation exist – external synchronisation of the pulse source as shown in Figure 2.2A or clock extraction from the pulse train to synchronise the data modulation module as depicted in Figure 2.2B.

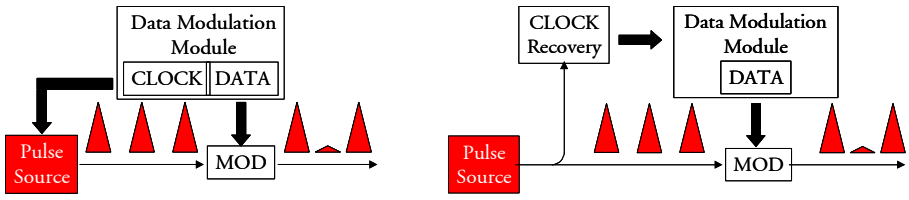

Figure 2.2: Two approaches for synchronising pulse source and data modulation module.

External synchronisation of the pulse source is implemented by applying the electrical base rate clock from the data modulation module to the pulse source. The shape and amplitude of the clock signal should be matched to the requirements of the pulse source[1]. If external synchronisation of the pulse

[1] The clock signal required for the commercial pulse sources available at COM•DTU operate fine with a sinusoidal shape.

source is not an option, and the pulse source inherently generates a pulse train with a repetition frequency in the vicinity of the OTDM base rate frequency, synchronisation of the data modulation module is needed. A small branch of the emitted pulse train is injected into a Clock Recovery (CR) circuit, which extracts the clock and applies the synchronisation signal to the data modulation module. Clock extraction from a RZ pulse shaped base rate signal is not difficult and can be implemented by small modifications of existing Phase Locked Loop (PLL) CR configurations, see chapter 3. However, the introduction of a CR circuit in the transmitter will increase the complexity and the cost of the system, and consequently constitute an inefficient system approach. Furthermore, the required synchronisation of the data modulation module can be quite complex, depending on how the actual data is generated. If the data originates from a number of electrical low speed channels and multiplexed up in bit rate, i.e. Electrical Time Division Multiplexing (ETDM), the extracted clock need to be applied at several levels in the data modulation module and at different clock speeds. This is a challenging task, but can without doubt be implemented, though introducing a complex architecture. In conclusion, a pulse source, which can be synchronised to an external signal constitute the most simple and efficient solution.

The relation between the OTDM base rate frequency B and the repetition frequency rate of the pulse source B_P need to be $B = q\,B_P$, where q is an integer. The situation with $i = 1$ is assumed in Figure 2.1, but is not a strict requirement. Pulse sources fulfilling the repetition frequency requirement with $q > 1$ can also be utilised in an OTDM system by passively multiplexing the pulse train up to B using e.g. a Planar Lightwave Circuit (PLC) [2.6]. The requirements to the multiplexer are as strict as for the OTDM multiplexer shown in Figure 2.1 in terms of amplitude fluctuations and temporal precision, see e.g. [2.7]. Synchronisation of the pulse source to the data modulation module needs a low speed clock, which can be extracted from the base rate clock by a clock divider generating the required sub-harmonic signal or by applying a low frequency clock from the data modulation module if available. A pulse source offering a bit rate corresponding to B leads to the simplest architecture, and will be preferred whenever possible.

The wavelength of the emitted pulse train should match the designed system wavelength, hence wavelength tuneability is not a prerequisite. However, in a laboratory environment as the facilities of COM•DTU, it is a highly appreciated option as tuneability offers the possibility for optimising system performance, e.g. for transmission or signal processing in terms of demultiplexing, as seen in chapter 4. Furthermore, wavelength tuneability of the pulse sources suggests the possibility for using a number of similar pulse sources in a WDM OTDM system where several high-speed OTDM data signal

at different wavelengths are transmitted simultaneously. If the pulse sources are not tuneable, each wavelength needs to be fixed at the factory.

The pulse shape, the width of the pulses and the energy in the pedestals are vital for the system. In subsequent sections, the requirements to the FWHM temporal width and the Pulse Tail Extinction Ratio (PTER) are determined for Gaussian pulses by means of simulations[2]. The spectral width of the pulses should be as small as possible, in order to minimise the impact of GVD and higher order dispersion terms. For any pulse shape with a specific temporal width, there exists a minimum spectral width due to the correlation between time and frequency. A pulse train with a minimum spectral width for a specific temporal width is Transform Limited (TL). If standard OTDM systems, as shown in Figure 2.1, are used, transform limited pulses are preferred. Some transmission schemes are based on pre-processing of the pulses before launching the signal into the transmission span, e.g. pre-chirping as reported in [2.8] or [2.9]. However, these schemes are founded on an exact external control of the spectral properties of the pulse train. Consequently, transform-limited input pulses before spectral manipulation even in these configurations will be the preference. Timing jitter of the pulses is equally important as it can impose large penalties on the system performance if the magnitude is too high. The impact of timing jitter can however not be regarded without including the timing jitter originating from the transmission span and the receiver. In this thesis, no work has been dedicated to determining requirements to timing jitter, except illustrating the impact of timing jitter on the switching performance in chapter 4. Finally, the output power, the Optical Signal to Noise Ratio (OSNR) and the Relative Intensity Noise (RIN) can impose restrictions on the system performance, and should be addressed. However, it appears from a practical point of view, that the quality with respect to these two parameters is sufficiently high for the available actual pulse sources. Consequently, the work has been focussed on determining the requirements to FWHM and PTER in this thesis.

In summary, a pulse source operating in an OTDM system should primarily be examined for the following parameters

- Narrow temporal FWHM width fulfilling requirements.
- High PTER fulfilling requirements.
- Transform Limited.
- Low timing jitter fulfilling requirements.
- Wavelength tuneable.
- Synchronisation to an external signal possible.

[2] A general note on the pulse shapes utilised in all the chapters of the thesis. Because the mathematical manipulation of temporal Gaussian pulses often offers the possibility for obtaining analytical expressions, Gaussian pulses are preferred.

- Repetition frequency of emitted pulse train equal to base rate of OTDM signal.
- Stability.
- High OSNR fulfilling requirements.
- Low RIN fulfilling requirements.

And finally more subjective criteria such as

- Complexity of pulse source scheme.
- Complexity of operation.

2.3 Reported OTDM pulse sources

A number of strong candidates aspire to become the pulse source of choice in OTDM systems and in the following section a short presentation of the present status on available sources is given.

2.3.1 Gain-switched DFB lasers (GS-DFB)

A pulse source, which has been used in numerous OTDM experiments in the past years, is the Gain-switched Distributed Feedback semiconductor laser (GS-DFB), which constituted the main pulse source in e.g. the European Advanced Communications and Technology and Services (ACTS) project Photonic technologies for ultra-high-speed information highways (HIGHWAY). The laser operation can be explained by using the relation between the applied bias current I and the optical output power P. By biasing the laser below the threshold current I_{th}, at which the laser will start lasing, and applying a sinusoidal modulation of the current, the Distributed Feedback (DFB) laser will, if proper designed, emit a pulse train synchronised to the electrical sinusoidal signal, see e.g. [2.10] [2.11]. The principle is sketched in Figure 2.3.

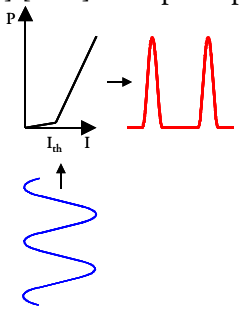

Figure 2.3: Simple illustration of the principle behind gain-switching of a laser.

The GS-DFB laser represents a good pulse source candidate at modest OTDM bit rates, i.e. 40 and 80 Gbit/s, as the modulation of the laser is simple and

offers narrow pulses with timing jitter less than 1 ps [2.12] at repetition frequencies at 10 GHz and above. The temporal FWHM width of the pulses are typically in the range between 20 ps [2.10] to 35 ps [2.12], but can be compressed down to 5.7 ps [2.10] or even down to 3.4 ps [2.13] by transmitting the pulses through normal dispersive fibre, e.g. Dispersion Compensating Fibre (DCF). This is a direct artifact of a deliberate laser design, as the laser is optimised to have a high Frequency Modulation efficiency in order to generate a large frequency chirp [2.11].
Summarising the advantages of the GS-DFB

- Small.
- Simple to operate.
- Transform limited pulses after pulse compression in DCF.
- External synchronisation feasible within a limited frequency span[3].

The disadvantages of the GS-DFB can be summarised

- No wavelength tuning.
- Relatively broad pulses after linear compression on the order of 3-5 ps.

For bit rates above 80 Gbit/s the linearly compressed pulses from the GS-DFB lasers are too broad and unsuited for ultra-high OTDM signals. However, GS-DFB may e.g. be used in conjunction with adiabatic pulse compression schemes to reach 160 Gbit/s [2.14].

2.3.2 Mode-locked Fibre Ring Laser (ML-FRL)

The mode-locked Fibre Ring Laser (ML-FRL) has been used in some of the most successful OTDM transmission experiments. As an example, the pulse source used in the first 640 Gbit/s OTDM experiment ever was a regenerative ML-FRL [2.2] with additional pedestal suppression [2.15]. In Figure 2.4 the principle of an active ML-FRL is shown.

[3] The applied sinusoidal control signal only exists the first period of the relaxation oscillation [2.11], which is closely related to the specific design of the GS-DFB. Consequently, an arbitrary tuning of the applied signal frequency is not possible.

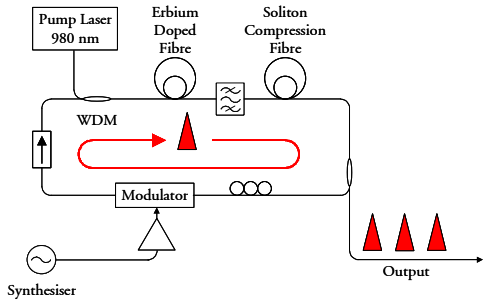

Figure 2.4: Actively Mode-Locked Fibre Ring Laser

The principle of a ML-FRL can be found in e.g. [2.16]. A laser diode is pumping the Erbium Doped Fibre (EDF) in order to introduce the required population inversion, i.e. gain, within the cavity. When the gain is sufficiently high, the threshold condition is fulfilled for a large number of longitudinal modes around the gain peak, i.e. gain equal loss in the cavity. The frequency spacing between the modes is related to the length of the cavity and the refractive index. A modulator controlled by an external sinusoidal signal from e.g. a synthesiser is used to lock the phase differences between the longitudinal modes within the laser, thus mode-locking the laser. The modulator can be either amplitude modulators, which are often utilised, or phase modulators. As modulators can be polarisation dependent, e.g. the $LiNbO_3$ modulator, a polarisation controller can be included before the modulator. An Optical Bandpass Filter (OBF) is used to select the centre wavelength of the pulses emitted from the laser and an isolator ensures uni-directional operation.

In Figure 2.4 an additional coil of fibre is included within the cavity, i.e. the Soliton Compression Fibre, which is not required for the actual mode-locking of the laser. However, its presence can cause an increase in the total aggregated OTDM bit rate as it can compress the temporal width of the output pulses. If the gain of the EDF is sufficiently high and if the Soliton Compression Fibre is dimensioned correctly in terms of length and dispersion, adiabatic pulse compression in non-linear fibre can reduce the temporal pulse width significantly. In [2.17] a reduction of the pulse width from 7.0 to 2.7 ps was reported by the inclusion of 190 m of Dispersion Shifted Fibre. Pulse compression is briefly explained in a subsequent section.

The cavity loop length is substantial, typically more than 200 meters [2.17] [2.18] and the impact of even small perturbations in terms of e.g. mechanical vibrations or thermal changes applied to the cavity can severely influence the stability or even jeopardise the locking of the laser as perturbations affecting the effective optical length of the cavity immediately influences the temporal position of the pulses [2.17]. This can be overcome by introducing the

regenerative ML-FRL, as shown in Figure 2.5A. A branch of the output signal is injected into a CR circuit, extracting a sinusoidal clock signal from the pulse train. By applying this clock to the internal modulator, pulses within the cavity, which are temporally displaced compared to the ideal temporal position, will experience higher loss, as they will be completely or partly suppressed by the modulator. Hence the regenerative ML-FRL suppresses the impact of environmental perturbations.

In 1994, M. Nakazawa et al reported the generation of a 10 GHz train of 2.7 ps FWHM pulses using a regenerative ML-FRL [2.17]. The technique was refined by other groups and in 1999 a 40 GHz pulse train composed of 1.6 ps temporal FWHM width pulses was reported [2.18]. The length of the cavity is, due to the pulse compression stages included in the cavity, often substantial and are in the two mentioned examples 200 m and 1000 m, respectively. By substituting the compression stage fibres with Photonic Crystal Fibre (PCF), the length of non-linear fibre can be reduced to 10 m, which results in a total cavity length of ~ 30 m. With this configuration a 10 GHz pulse train of 1 ps pulses and only 78 fs timing jitter has been reported [2.19].

However, the proposed stabilisation of the cavity is on the expense of external synchronisation. In [2.20] a novel design is suggested, offering both the advantage of regenerative stabilisation and the possibility of synchronising the pulse train to an external electrical signal. The set-up after [2.20] is shown in Figure 2.5B.

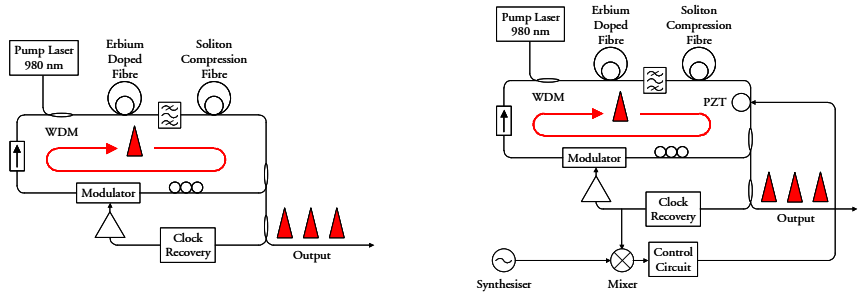

A B

Figure 2.5: A) shows the principle of a regenerative ML-FRL. B) A regenerative ML-FRL offering the possibility for external synchronisation [2.20].

By mixing the external signal from the synthesiser with the clock extracted from the pulse train within the cavity, a beat-signal including the phase difference between the two signals can be generated. By lowpass filtering the phase difference signal and applying it to a pietzo (PZT) element, the part of the Soliton Compression Fibre coiled up on this will be stretched/compressed, effectively changing the cavity length. When a perfect match between the pulse

train within the cavity and the external signal is obtained, the control signal to the PZT will be kept constant. Using this configuration, a 40 GHz pulse train tuneable from 1530 to 1560 nm composed by 0.9 ps pulses was generated with only 120 fs timing jitter [2.21]. Using the same configuration, only exchanging the amplitude modulator with a phase modulator, 850 fs pulses were generated.

Summarising the advantages of the ML-FRL
- Transform limited pulses.
- Temporal FWHM width less than 1 ps achievable.
- Tuneable in the C-band.
- External synchronisation feasible.

The disadvantages of the ML-FRL can be summarised
- Complex architecture.
- Bulky.
- Immediate locking of the ML-FRL when applying external signal can not be expected – a number of operation parameters need to be optimised[4].

During the European IST project TOPRATE a commercial actively ML-FRL was available and was used in some of the experiments reported in the PhD publication list, see e.g. [2.22], [2.23].

2.3.3 Semiconductor Mode-locked Lasers (MLL)

The Semiconductor Mode-Locked Laser is based on a Semiconductor Optical Amplifier (SOA) sandwiched between two mirrors. By applying a current to the SOA, the population inversion threshold in which the gain equals the loss is reached, and the structure starts lasing. Similar to the ML-FRL, the structure supports a number of longitudinal modes. By designing the laser to include a section where the loss (or gain) can be varied in time, the phase of the longitudinal modes supported in the laser are fixed and mode locking is induced [2.24]. One approach for designing a mode locked semi-conductor laser is to incorporate a saturable absorber within the cavity, whose opacity decreases for increased intensity. Mode-locking semiconductor lasers is now a well-established technique to generate high-quality pulse trains. As an example of the excellent properties of the Semiconductor MLL, a laser was reported in [2.25] which was tuneable from 1440 to 1560 nm, tuneable in repetition

[4] This is an observation done in the laboratory facilities of department COM•DTU, when operating a commercial available ML-FRL. It is observed how the operation parameters for the exact same lasing conditions, i.e. wavelength and repetition frequency, are not identical from time to time and the required time adjusting the control parameters before a high quality pulse train is generated can vary from 3 to 30 minutes.

frequency from 1 to 14 GHz and tuneable in temporal pulse width from 180 fs to 17 ps. For a more thorough discussion and presentation of Semiconductor MLLs refer to [2.26].

Summarising the advantages of the Semiconductor MLL
- Small.
- Tuneable in wavelength beyond C-band.
- Tuneable in temporal FWHM width.
- Tuneable in repetition frequency.
- External synchronisation both optically and electrically.
- Transform limited pulses.

The disadvantages of the Semiconductor MLL can be summarised
- Medium complex to operate – a number of parameters can be adjusted e.g. currents for the different sections.
- Trailing pulses can appear[5].

In the last period of the European IST project TOPRATE both a commercial and a research MLL developed within the Danish National Technical Research Council programme project Semiconductor components for optical signal processing (SCOOP) [2.26] were available.

2.3.4 Erbium Glass Laser Oscillator (ERGO)

Yet another pulse source candidate is the Erbium Glass Laser Oscillator (ERGO), which has been demonstrated operating at 10 [2.27] and 40 GHz [2.28], see Figure 2.4. Erbium Ytterbium doped (Er:Yb) glass is situated in the cavity of the laser and by injecting a 976 nm beam through a beam splitter into the cavity, the doped glass is pumped, offering the required gain within the cavity. Due to the small emission cross-section in the glass, the mode-locked pulse train will experience large variations in amplitude, referred to as Q-switched mode-locking [2.24]. By including a Semiconductor saturable absorber mirror (SESAM) in the cavity, this effect is minimised and a high-quality pulse train is emitted [2.27]. A tuneable etalon within the cavity is used to select the wavelength of the emitted pulse train.

[5] This has been observed in commercially available semiconductor based MLLs, probably due to the quality of the Antireflection Coating used.

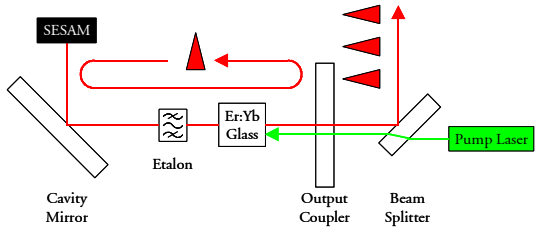

Figure 2.6: Illustration of the principle behind the ERGO laser [2.28].

An important feature of the laser is the possibility for synchronising the repetition frequency of the emitted pulse train to an external electrical RF signal. This is accomplished by using a PLL to control the cavity length of the ERGO laser. According to [2.28], the laser operates in the fundamental mode and only a single pulse circulates within the cavity, yielding negligible pulse-to-pulse jitter. Values in the order of 70-80 fs are reported.

Summarising the advantages of the ERGO
- Simple to operate.
- Small.
- Tuneable in wavelength.
- External electrical synchronisation.
- Transform limited pulses.

The disadvantages of the ERGO can be summarised
- Tuning range of repetition frequency is very small.
- Trailing pulses can appear[6].

A number of the high-speed experiments reported in this thesis are based on commercial available ERGO lasers, including the 320 Gbit/s demultiplexing experiment reported in chapter 4.

2.3.5 Electroabsorption Modulator (EAM) based pulse sources

The Electroabsorption Modulator (EAM) is a versatile component, as it can be used both in the transmitter and in the sub-systems constituting the receiver, i.e. the Clock Recovery circuit and the Demultiplexing circuit, see chapter 3 and 4. The component is relatively easy to manufacture, simple to operate and has consequently attracted considerable interest the last few years, see e.g. [2.3][2.29] for EAM based system experiments.

[6] This has been observed in commercially available ERGO lasers, probably due to the quality of the Antireflection Coating used.

The EAM based pulse source has attracted considerable interest in the last few years. It offers the possibility for upgrading existing Non-Return to Zero (NRZ) systems in a simple way, as shown in Figure 2.7, by simply placing the EAM between the CW laser and the external modulator. Using this configuration the system designer can preserve already developed wavelength stabilising control circuitry for the CW laser source, i.e. the DFB laser, hereby potentially reducing the cost from upgrading the system from NRZ to RZ format. Further advantages of the EAM are the compact size of the component, the possibility for integrating the device with the modulator, which can be an additional EAM [2.3] and finally the simple set-up for generating the pulses. The operation of the semiconductor EAM is based on the ability to control the absorption of injected light by the applied reverse bias. In [2.30] a typical example of an increase in insertion loss, i.e. increased absorption, for increased reverse bias is shown. By modulating the bias with a sinusoidal electrical signal, the insertion loss will consequently be synchronised to the applied signal and an injected Continuous Wave (CW) signal will be pulse shaped at the output of the component.

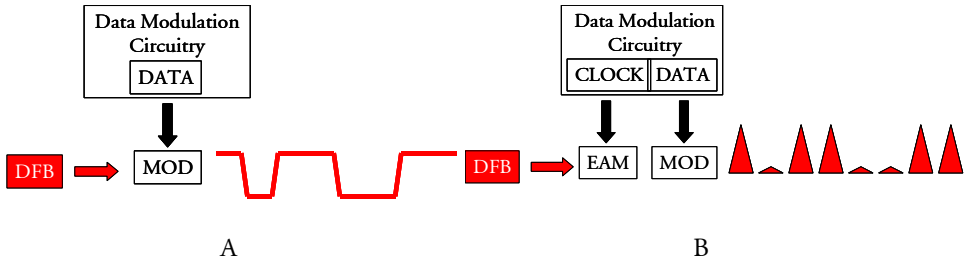

Figure 2.7: The upgrade from NRZ (A) to RZ (B) format using an EAM

A disadvantage of the components is the temporal relative broad pulses generated. Due to the sinusoidal-like shape of the absorption when varying the applied voltage [2.30], the temporal FWHM pulse widths will typically correspond to 10 to 20 % of the timeslot of the external signal, i.e. 10-15 ps at 10 GHz [2.31], 6 ps at 30 GHz and 5 ps at 40 GHz [2.32]. Unless more advanced schemes are use, e.g. by concatenating EAM devices operating at different bit rates, generating complex voltage signals or using pulse compression schemes, it appears that EAM can only be utilised in OTDM systems, where the aggregated OTDM signal is composed of ~4-8 time channels in total. No timing jitter values have been found in literature, but it is expected that the jitter will primarily origin from the Radio Frequency (RF) synchronisation source.

Summarising the advantages of the EAM
- Simple to operate.
- Small.

- Tuneable in wavelength.
- External electrical synchronisation.
- Transform limited.

The disadvantages of the EAM can be summarised
- High insertion loss.
- Relatively broad pulses – pulse width related to frequency of external signal.
- Pulse source in OTDM systems with limited number of time channels.
- Need external CW source.

The EAM based pulse source has been the focus of the partners within the European IST project TOPRATE working on systems combining 160 Gbit/s OTDM signals with WDM. However, no experiments reported in this thesis have been based on this pulse source.

Finally, a more complex configuration based on injection locking of an EAM is reported. As the concept of injection locking has proven to be very successful at clock extraction, a short introduction can be found in chapter 3. Using the EAM in the simplified configuration shown in Figure 2.8 a 10 GHz pulse train of 20 ps pulses is generated [2.33].

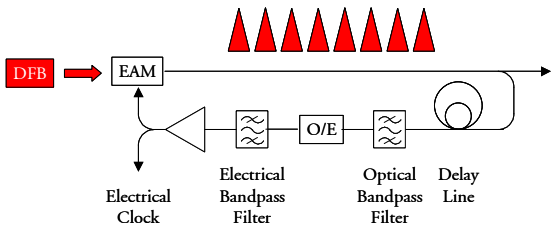

Figure 2.8: Pulse source based on injection locking of EAM [2.33].

2.3.5 Summary on pulse sources

The advantages and disadvantages of the pulse sources explained in the previous sections and extracted from the listed references of each pulse source type are summarised in Table 2.1.

	GS-DFB	ML-FRL	MLL	ERGO	EAM
Pulse width	4-5 ps	1-2 ps	Variable 180 fs – 17 ps	1-2 ps	10-15 ps (10 GHz) 5 ps (40 GHz)
PTER	NA	NA	NA	NA	NA
TL	Yes (after DCF)	Yes	Yes	Yes	Yes
Timing jitter	< 1 ps	< 100 fs	~ 100 fs	< 80 fs	NA
Wavelength variable	No	Yes	Yes	Yes	Yes
External sync	Yes	Yes	Yes	Yes	Yes
Repetition rate variable	Small	Large	Large	Small	Large
Stability	High	Low	High	High	High
Scheme Complexity	Simple	Complex	Simple	Complex	Simple
Operation	Simple	Complex	Medium	Simple	Simple
Misc			Trailing pulses	Trailing pulses	High insertion loss

Table 2.1: Summary of existing OTDM pulse sources. NA: Not available

No values are listed for the PTER as this is not stated in specifications of the commercial pulse sources. The timing jitter values are extracted from numerous references. However, the timing jitter of most of the pulse sources is dependent on the RF source used to synchronise the repetition rate.

2.4 Wavelength tuneable pulse source

In the experimental work comprising the work in the European IST project TOPRATE and the work presented in this thesis, all the above mentioned pulse sources were, as mentioned, not available at all time. In some experiments only a single pulse source was available at a fixed wavelength not suitable for the experiment, e.g. the wavelength did not correspond to the wavelength at which the total accumulated dispersion of the transmission span was zero. In other experiments a single wavelength tuneable pulse source was available, but pulse trains at two different wavelengths were required, e.g. for demultiplexing as reported in chapter 4. One approach to overcome these obstacles is to wavelength convert the pulse train from the available pulse source to the target wavelength. It should be emphasised that wavelength converting the pulse train

is only an acceptable option if pulse sources are not available due to the complexity of the set-up.

In this section wavelength conversion based on Four Wave Mixing (FWM) in a Highly Non-linear Fibre (HNLF) is presented, partly based on [2.34]. In the actual implementation of the wavelength tuneable pulse source (WTPS), see Figure 2.9A, the pulse source with fixed wavelength is a GS-DFB laser modulated at 10 GHz. The temporal FWHM width of the pulses, after compression in a DCF is 6.3 ps. The RZ pulses are amplified and filtered using an OBF, before being launched through an asymmetric coupler (1:10 dB) into the HNLF. The CW source is a commercially available laser source, with a wavelength (λ_{CW}) tuning range from 1525 nm to 1610 nm. The CW probe is amplified but not filtered, hereby simplifying the operation of the scheme, when λ_{CW} is tuned. A polarisation-controller (PC) in front of the coupler allows for aligning the polarisation state of the CW probe to be co-polarised with the RZ signal. The power levels at the input to the HNLF for the RZ signal and CW probe are +10 and +5 dBm, respectively, as seen from the input spectrum to the HNLF (Figure 2.9B). Because the wavelength of the GS-DFB (λ_{RZ} = 1553.6 nm) corresponds to the zero-dispersion wavelength (λ_0) of the HNLF, it is well suited as the pump in an efficient FWM process [2.35]. Furthermore, the fibre used in this experiment was a newly developed HNLF with a high non-linear coefficient, i.e. γ = 10.6 $W^{-1}km^{-1}$. The dispersion-slope, S, and attenuation, α, are 0.022 ps/nm/km^2 and 0.87 dB/km, respectively. Due to the large γ, the needed length of fibre is reduced significantly compared to standard Dispersion Shifted Fibre (DSF) often utilised as the non-linear medium in previous experiments, see e.g. [2.36], and the length in this specific implementation is only ~ 500 m[7]. The advantages of a reduced length of fibre are, a) a reduced impact of environmental conditions, and b) a large FWM bandwidth, when combined with a low slope S [2.35] [2.37] [2.38]. In the HNLF, a partly degenerated FWM process generates new frequencies, as seen at the output spectrum from the HNLF, Figure 2.9C. The wavelength of the FWM signal is $\lambda_{FWM} = (2/\lambda_{RZ}-1/\lambda_{CW})^{-1}$ [2.36]. Consequently, by tuning λ_{CW} the wavelength λ_{FWM} can be tuned. The converted pulses are optically bandpass filtered and used in the experiments. Because the RZ signal is used as the pump, the scheme can be expanded to provide a multi-wavelength WTPS, by launching several CW probes at different wavelengths into the HNLF. This is indicated with dots in Figure 2.9A.

[7] The experiments were conducted in 1999 when only a few groups worldwide had access to HNLF.

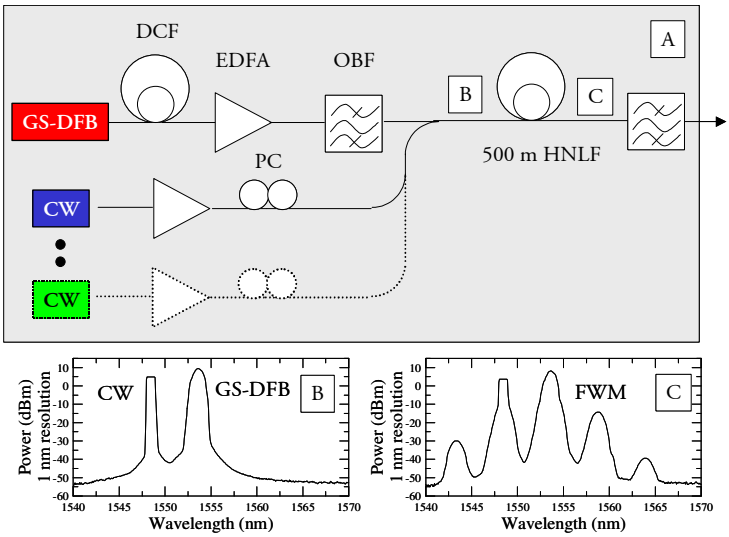

Figure 2.9: A) Principle set-up for wavelength converting a pulse train. B) Optical spectrum at the input to the HNLF. C) Optical spectrum at the output of the HNLF containing the generated FWM product.

When tuning λ_{CW} from 1546 to 1558 nm a small increase in pulse width, when compared to the pulses from the GS-DFB, is observed. A temporal FWHM width of ~ 7 ps pulses with small variations up to ±0.4 ps over the entire tuning range was observed. In order to evaluate the quality of the converted pulses, the pulses are externally modulated and detected using a 10 Gbit/s Bit Error Rate (BER) pattern-generator and detector and a pre-amplified receiver. In Figure 2.10 the variation in sensitivity, relative to the best-measured sensitivity, is shown as function of the detuning (λ_{FWM} - λ_{RZ}), revealing a maximum variation of ~ 1 dB. In order to estimate the tuning range of the FWM process in the HNLF, a CW pump and probe were launched into the fibre, and the conversion efficiency, defined as the power of the generated FWM product at the output of the fibre divided by the power of the input CW pump [2.37], versus the detuning was measured and added to Figure 2.10. The measured spectral FWHM bandwidth of the conversion efficiency is > 68 nm limited by the tuning range of the CW source, and estimated to 76 nm assuming symmetry around λ_0. Consequently, it is expected that the tuning range of the converted pulses in a practical implementation will be limited by the gain bandwidth of the Erbium Doped Fibre Amplifier (EDFA) (also represented in the figure) and not the HNLF.

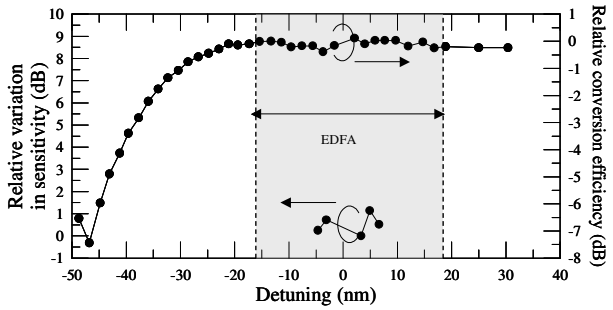

Figure 2.10: Relative variation in sensitivity, relative conversion efficiency for HNLF and EDFA gain bandwidth (~1535-1570 nm) (marked as grey box) all as function of detuning.

An important aspect when evaluating the quality of the pulses is not only the back-to-back performance, but also if the converted pulses introduce an additional power penalty when transmitted e.g. due to chirp. The converted pulses were externally modulated with a Pseudo Random Bit Sequence (PRBS) of 2^{31}-1 in a $LiNbO_3$ Mach-Zehnder modulator, amplified and launched into two transmission spans with a total length of 160 km of Standard Single Mode Fibre (SSMF) and 24 km of DCF [2.39]. In the receiver, the signal was pre-amplified, filtered using an OBF and detected in a BER detector, which was triggered by an electrical Clock Recovery. For comparison the same experiment was carried out using the original pulses from the GS-DFB. The penalty for converting the pulses from 1553.6 nm to 1557 nm using the above scheme is ~ 0.7 dB. For transmitting the original pulses the introduced penalty is ~ 1 dB, whereas the penalty for transmitting the converted pulses is ~ 0.7 dB. This is explained by an additional OBF in front of the two transmission spans, which reduces the Amplified Spontaneous Emission (ASE) noise from the amplifiers. In conclusion the converted pulses have approximately the same performance as the original pulses in terms of transmission properties.

To evaluate the feasibility of using the converted pulses in OTDM systems, the 10 Gbit/s modulated signal was multiplexed to 40 Gbit/s using fibre-delays. The signal was subsequently demultiplexed to 10 Gbit/s using a 10 GHz modulated EAM and detected. The penalty for multiplexing and demultiplexing the converted signal is ~ 0.9 dB, which represents a negligible increase compared with the penalty for the original signal, i.e. ~ 0.7 dB. Finally, as indicated in Figure 2.9A, the principle of the set-up can be expanded to generate multiple converted pulse trains simultaneously. This is demonstrated for two wavelengths by injecting two CW probes into the HNLF. The wavelengths of the CW probes are 1547 and 1550 nm, respectively, which generate pulses at 1557 and 1560 nm. The output spectrum for one and two CW input probes, showed no measurable difference in conversion efficiency.

Furthermore, no impact on the pulse width was observed, i.e. 7.0 ps FWHM, for one and two CW probes. The converted pulses at 1560 nm were filtered out, modulated and received for one and two input CW probes. The corresponding BER measurements showed a small penalty of 0.3 dB ascribed to insufficient filtering. In conclusion the principle of multiple converted pulses can be expanded to a multi-wavelength WTPS. Pump-depletion, bandwidth management, filtering and cross-talk between the different signals will determine the actual number of available wavelengths generated with this scheme.

The principle has been used successfully in a number of experiments, see e.g. [2.40], [2.22], [2.23], [2.41].

As the scheme is based on wavelength converting a pulse train, any scheme which is sufficiently fast to wavelength convert the narrow pulses without any significant pulse distortions e.g. in terms of broadening can be used. This is exemplified e.g. in [2.42] where a 10 GHz pulse train at 1531 nm is injected into a Non-linear Optical Loop Mirror (NOLM) as the control signal, imposing the required phase change on the CW probe beam at 1557 nm, resulting in a wavelength conversion.

2.5 Soliton Pulse Compression

The pulse widths reported so far of commercial available pulse sources are typically on the order of 1-5 ps, see Table 2.1, corresponding to between ~ 15 to 80 % of a 160 Gbit/s timeslot. In section 2.6 simulations show that the required FWHM width of the pulses should not exceed 0.40 times the timeslot. Hence, when the bit rate is increased further, even narrower pulses are required and consequently schemes for generating narrower pulses based on existing high quality pulses are needed. In [2.16], a thorough survey of compression techniques is presented and consequently only soliton compression utilised in system experiments in this thesis will be presented.

Soliton compression has its origin in the non-linear Schrödinger equation (NLSE), describing the evolution of pulses transmitted through fibres [2.16].

$$\frac{\partial A}{\partial Z}+\frac{\alpha}{2}A+\frac{i\beta_2}{2}\frac{\partial^2 A}{\partial T^2}-\frac{\beta_3}{6}\frac{\partial^3 A}{\partial T^3}-\frac{i\beta_4}{24}\frac{\partial^4 A}{\partial T^4}= i\gamma\left(|A|^2 A+\frac{i}{\omega_0}\frac{\partial}{\partial T}(|A|^2 A)-T_R A\frac{\partial |A|^2}{\partial T}\right) \tag{2.1}$$

A is the slowly varying field envelope, α is the loss parameter, β_2, β_3, β_4 are the GVD, the Third Order Dispersion (TOD) and the Fourth Order Dispersion (FOD) respectively, T is the retarded time frame, ω_0 is the carrier frequency, γ is the non-linear coefficient and T_R is the Raman resonant time.

The pulse injected into the fibre, is characterised by the soliton order N, which is defined as

$$N^2 = \frac{\gamma P_0 T_0^2}{|\beta_2|} \tag{2.2}$$

where P_0 and T_0 is the peak power and the pulse width at e^{-1} intensity point, respectively. The non-linear pulse compression is divided into two subcategories – adiabatic soliton pulse compression and soliton compression.

2.5.1 Adiabatic soliton pulse compression

When a hyperbolic secant shaped pulse (sech) which fulfils N = 1 is injected into a fibre span with anomalous dispersion, i.e. $\beta_2 < 0$, the pulse will remain the same shape during propagation as the effect of Self Phase Modulation (SPM) and GVD exactly cancel out. The fundamental soliton, i.e. N = 1, is resilient to small perturbations in the parameters governing the pulse propagation, see eq. (2.1) and remains in principle a soliton. This implies conservation of the energy, hence the term adiabatic, which leads to the following useful relation between the width of the pulse at the input and the width of the pulse at position z in the fibre [2.43]

$$T_{FWHM}(z) = \frac{\beta_2(z)\,\gamma(0)\,T_{FWHM}(0)}{\beta_2(0)\,\gamma(z)\,G} \tag{2.3}$$

G is the gain in the transmission medium. Note that for passive fibres, the gain resembles the fibre loss, i.e. $e^{-\alpha z}$. From eq. (2.3) the principle behind pulse compression of the fundamental soliton can be recognised. In order to reduce the pulse width of the output pulse compared to the input pulse width, 3 parameters can be changed, individually or together

- Reduce the dispersion along the fibre.
- Increase the non-linear coefficient along the fibre.
- Increase the gain along the fibre.

A few references addressing pulse compression by e.g. decreasing the dispersion and/or increasing the gain has been reported, see e.g. [2.44]. How the dispersion should decrease as function of the length has been evaluated in [2.45], where four different dispersion profiles were investigated – linear, hyperbolic, exponential and Gaussian Dispersion Decreasing Fibre (DDF). When a single fibre segment with decreasing dispersion is not available, the equivalent to a DDF can be constructed, by designing a fibre span based on segments of different dispersion values spliced together. By carefully combining 4 different segments of fibre, each with different dispersion, a span with an effective decrement in dispersion along the propagation length was constructed [2.46]. Another approach to obtain an equivalent to a DDF is to use only two different fibre types, hence reducing the complexity of the fibre management. By designing a number of segments, each segment including a specific length of each fibre type with a total specific average dispersion, and splicing the segments together so the average dispersion of each concatenated segment will gently decrease, a Comb-Like Dispersion Profiled Fibre (CDPF) designed to resemble the DDF can be constructed. In [2.47] and reported in [2.48] a CDPF compression stage was designed based on 10 segments of alternating SMF and DSF.

2.5.2 Higher order soliton compression

If the soliton order of the input pulse to the compression stage is higher than 1, the pulse compression is categorised as a higher order soliton compression. As opposed to adiabatic pulse compression, the pulse does not maintain the pulse shape when propagating through the fibre but instead changes periodically along the fibre. The period, after which the pulse has recovered its original shape, is characterised as the soliton period [2.49]. Due to the properties of the solitons, the initial pulse will experience narrowing just before recovering the original shape, and can, consequently be utilised for pulse compression [2.49]. By increasing the soliton order the obtained pulse compression factor, defined as the ratio between the original pulse width and the resulting pulse width, can be increased significantly, compared to adiabatic pulse compression [2.43]. However, the obtained increased compression factor is at the expense of an increased required input power, see eq. (2.2), which for high soliton orders can be difficult to realise, even with the aid of an EDFA. Furthermore, the quality of the pulse is reduced for increased soliton orders, as an increasing part of the total pulse energy will be transferred from the narrow peak to the accompanying temporal pulse pedestals. As the compressed pulses are intended to be used in OTDM systems, the broad pedestals can enter the neighbouring time channels, hence jeopardise the performance of the system. In section 2.6 the impact of pedestals is evaluated numerically. In [2.49] a numerical example shows how the energy in the pedestals exceed the energy in the peak for $N \sim 5$.

Obviously, this is unacceptable for an OTDM system and clearly a trade-off exists between the quality of the pulses and the achievable compression factor versus the length of the fibre and the soliton order. In [2.43] a trade-off is suggested, by using pulses of the order of $1 < N < 2$ in DDF. Using this approach it is argued by simulated examples, that pulses with e.g. a soliton order of $N = 1.7$ can be compressed up to 41 times with approximately 20 % of the energy in the pedestals in a linear profiled DDF fibre of only 1.5 times the soliton period. This should be compared to adiabatic pulse compression where the highest achievable compression factor is 18 in a linear profiled DDF almost 6 times longer than the soliton compression. However, as opposed to the soliton compression, the adiabatic pulse compression only had approximately 2 % of the energy in the pedestals, hence demonstrating a significantly better quality [2.43].

2.5.3 Available pulse compression stages

The adiabatic CDPF pulse compression stage reported in [2.48] was available at COM•DTU for the first initial experiments focusing on OTDM systems with an aggregated bit rate of 160 Gbit/s. The compressed pulses of 1.06 ps de-convoluted should in principle be sufficient for bit rates < 400 Gbit/s assuming an acceptable FWHM pulse width of 0.4 times the time slot. However, within the European IST project TOPRATE, an ambitious objective was to strive for Tbit/s and consequently higher compression factors were required. As opposed to [2.48] where the compression factor was 5, a compression factor of 18 was required and consequently a new pulse compression stage was designed and implemented.

A compression factor of 18 represents the absolute maximum value for adiabatic compression assuming an ideal implementation [2.43]. Instead of a new adiabatic pulse compression stage, it was decided to design the new compression stage using the principle based on higher order soliton compression technique outlined in [2.43], i.e. $1 < N < 2$ by means of a decreasing dispersion profile implemented as a CDPF. In [2.50] an 8 segment CDPF is presented with a total length of 2.448 km of fibre, divided into a total length of 0.289 km SSMF and 2.158 km of DSF[8]. Notice how the total fibre length is reduced with a factor of ~ 4 compared to the adiabatic pulse compression stage in [2.48]. According to simulations, the 5 ps pulses should be compressed down to 800 fs. The experimental characterisation of the compression scheme, needed to confirm the simulated results, was impeded, as the compression stage was designed to match a specific GS-DFB laser, which unfortunately degraded. Hence the compression stage was evaluated with a GS-

[8] Designed, implemented and characterised by Kim Berg.

DFB laser, with altered parameters in terms of wavelength, chirp and particularly pulse width, which was broadened to 14 ps. Injecting a 10 GHz pulse train based on these pulses, compressed pulses of 2.5 ps were obtained. Modifying the simulations to adapt the changed input pulse parameters, the compressed pulses according to simulations should be 2.6 ps, revealing an excellent prediction of the performance of the compression stage. Thus it was believed that 800 fs pulses could be generated, using the specific compression stage. However, 800 fs pulses would only be sufficient for ~500 Gbit/s signals, according to simulations presented in subsequent sections of this chapter. Furthermore, the pulses were accompanied by relative large pedestals, with a suppression of only 20 dB, which exceeds the acceptable value for Pulse Tail Extension Ratio (PTER), defined in the following. While not perfect, the compression stage still represented an important upgrade of the existing high-speed systems, and was used in some of the high-speed experiments in the PhD publication list, see e.g. [2.51].

Finally, within the European IST project TOPRATE, two DDF's were kindly provided by Alcatel SEL for system experiments. The fibres were only available in the last year of the project, but were used in the 320 Gbit/s demultiplexing experiment presented in chapter 4. The available fibre parameters are summarised in table 2.2. Information regarding the DDF profile between in- and output was not stated, and the profile could not be measured with the dispersion measuring technique used at COM•DTU.

Label	**Length (m)**	**Input dispersion D_{In} at 1550 nm (ps/nm/km)**	**Output dispersion D_{Out} at 1550 nm (ps/nm/km)**
DDF 1	1000	10.45	0.47
DDF 2	1060	11.31	-0.219

Table 2.2: Parameters for available DDFs used in system experiments in chapter 4.

2.6 Pulse source requirements

2.6.1 Subsystem for evaluating pulse source requirements

In order to identify the parameters relevant for designing a transmitter, the system in Figure 2.1 is simplified to include only the modulation, optical multiplexing and demultiplexing. As the demultiplexing is used to address a specific channel, an idealised square shaped demultiplexing window with infinite extinction ratio is used. Using the square shaped demultiplexing window, the obtained results are as generalised as possible, as the impact of shaping the demultiplexed channel, due to a specific demultiplexing window

shape, is avoided[9]. With these simplifications, requirements to the FWHM pulse width and the extinction ratio can be derived. In Figure 2.11 an example is shown of a number of pulses optically multiplexed together and the square shaped demultiplexing window, used to extract the target channel.

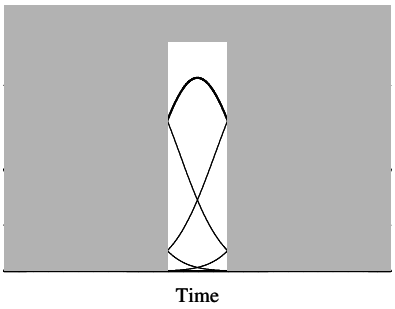

Figure 2.11: Impact of neighbouring channels on a specific channel, introducing crosstalk.

The pulses in Figure 2.11, which are multiplexed together, are very broad with pulse tails entering into several neighbouring channels. When a specific channel is optically demultiplexed, indicated with the grey shade on top of the multiplexed signal, the signal at the base rate is to some extent deteriorated by the presence of the pulse tails. The illustration in Figure 2.11 shows that irrespective of the sampling time when detecting the demultiplexed signal, pulse tail contributions from several of the neighbouring channels will be detected as well. The effect of interfering electric fields is well known, see e.g. [2.52], and consequently only a brief summary focusing on the impact of interfering electric fields on a demultiplexed channel will be given.

2.6.2 Classification of noise

For illustration, the situation in Figure 2.11 is simplified, so the demultiplexed channel with electric field $\overline{E}_0$ is only superimposed by two pulse tails $\overline{E}_1$ and $\overline{E}_2$. The three electric fields are injected into a photo-detector with a responsivity R equal to 1 for convenience. The bandwidth of the photo-detector is assumed infinite, so the total bandwidth of the electrical detection is defined by the bandwidth B_e of the electric lowpass filter. The example can be illustrated as in Figure 2.12.

[9] Bell-shaped Gaussian and Super Gaussian switching windows are addressed in chapter 4.

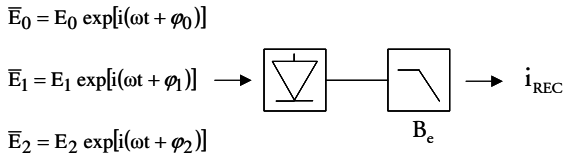

Figure 2.12: Example for illustrating crosstalk in OTDM systems. Three electric fields are injected into a photo-detector, before filtering in a lowpas filter.

It is assumed that the State Of Polarisation (SOP) is aligned to be parallel for the three electric fields. This is justified according to [2.53] where simulations and experiments showed, that the SOP of the signals, statistically will be aligned to the worst case, or close to worst case, i.e. parallel polarisation.

The total received electric field at the input to the photo-detector, $\bar{E}_{Rec}$, can be described as

$$\bar{E}_{Rec} = E_0 \exp\left[i\left(\omega t + \varphi_0\right)\right] + E_1 \exp\left[i\left(\omega t + \varphi_1\right)\right] + E_2 \exp\left[i\left(\omega t + \varphi_2\right)\right] \tag{2.4}$$

E_0, E_1 and E_2 are the amplitudes of the demultiplexed channel and the two pulse tails from the neighbouring channels. The optical carrier is denoted ω and the phases of the signals are φ_0, φ_1 and φ_2. As the electrical bandwidth $B_e << 2\omega$, the double frequency terms is filtered away, and the received photo-current i_{REC} can be described as

$$\begin{aligned} i_{REC} &\propto \frac{1}{2}\bar{E}_{REC}\,\bar{E}^*_{REC} \\ &= \frac{E_0^2}{2} + \frac{E_1^2}{2} + \frac{E_2^2}{2} \\ &\quad + E_0E_1\cos(\varphi_0 - \varphi_1) + E_0E_2\cos(\varphi_0 - \varphi_2) + E_1E_2\cos(\varphi_1 - \varphi_2) \end{aligned} \tag{2.5}$$

Introducing the optical power of the demultiplexed channel and the two pulse tails, P_0, P_1 and P_2 respectively as[10]

[10] Ignoring the factor η^{-1} [2.24]

$$P_0 = \frac{1}{2}\bar{E}_0\,\bar{E}_0^* = \frac{E_0^2}{2} \Leftrightarrow E_0 = \sqrt{2P_0}$$
$$P_1 = \frac{1}{2}\bar{E}_1\,\bar{E}_1^* = \frac{E_1^2}{2} \Leftrightarrow E_1 = \sqrt{2P_1} \qquad (2.6)$$
$$P_2 = \frac{1}{2}\bar{E}_2\,\bar{E}_2^* = \frac{E_2^2}{2} \Leftrightarrow E_2 = \sqrt{2P_2}$$

The total received photo-current i_{REC} consist of the following terms

$$i_{REC} \propto P_0 + P_1 + P_2 + 2\sqrt{P_0P_1}\cos(\varphi_0 - \varphi_1) + 2\sqrt{P_0P_2}\cos(\varphi_0 - \varphi_2) + 2\sqrt{P_1P_2}\cos(\varphi_1 - \varphi_2) \qquad (2.7)$$

The first term represents the actual channel with no deterioration and term two and three represent the crosstalk due to Intersymbol Interference (ISI) from the neighbouring channels. Term four, five and six represent interferometric crosstalk. If the OTDM signal is generated as shown in Figure 2.1, the three fields are emitted from the same laser. If the delay between the pulses is less than the coherence time of the pulses, then the phases in term four to six are approximately constant, and the terms are denoted coherent crosstalk [2.52]. As opposed to this situation, the delay in the modulation and multiplexing in the transmitter part can exceed the coherence time, and the phases of the three fields will change randomly with a corresponding random change in intensity. As these fluctuations vary very quickly, the threshold within the receiver cannot be adjusted sufficiently fast, and thus the impact of the fluctuations is similar to noise. This phenomenon is classified as incoherent crosstalk [2.52]. The impact of incoherent crosstalk compared to coherent crosstalk and to ISI is significantly more severe, and therefore requirements to the pulse sources should be based on the assumption that the system introduces incoherent crosstalk. It should furthermore be noted, that term six often will be negligible compared to term four and five, as the amplitudes of the pulse tails are small compared to the demultiplexed channel.

With the proposed simplified OTDM system consisting of pulse source, modulation, delay, multiplexing, demultiplexing and detection, and with identification of the limiting phenomena, the model for extracting the requirements can be described.

2.6.3 Model for evaluating pulse source requirements

In the previous section, the simplified OTDM system to evaluate the pulse source requirements was proposed. The physical phenomena, which are expected to influence the requirements, were identified. In this section the proposed system is described in more detail.

The pulses in Figure 2.11 were ideal Gaussian pulses as the envelope of the pulses was entirely described by a Gaussian function. However, pulse trains actually emitted from lasers will consist of pulses, which can be described by e.g. Gaussian or Hyperbolic Secant pulse shapes, with an additional pedestal. The quality of the pulses can be evaluated by the parameter PTER - sometimes referred to as extinction ratio. The exact definition of the parameter is not completely consistent in the literature. It can be defined as the amplitude of optical power in the centre of the neighbour pulse, or the amplitude of the pulse measured at a time infinitely far from the centre of the pulse. In this thesis, the PTER is defined as the ratio between the peak power of the pulse and the level of an additional constant pedestal added to the ideal pulse. The definition of PTER is shown in Figure 2.13 where the difference between pulses with and without pedestals is illustrated.

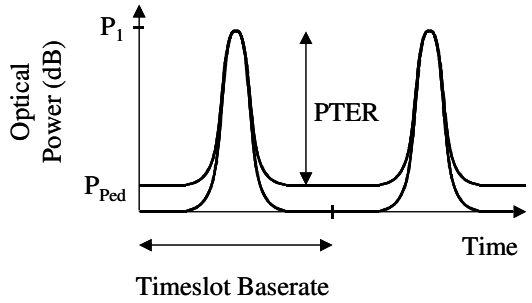

Figure 2.13: Definition of Pulse Tail Extinction Ratio for pulses with an additional pedestal.

From Figure 2.13, the PTER can be defined as the relation between the peak power in the pulse, P_1, and the power in the pedestal, P_{ped}.

$$\mathrm{PTER} = \frac{P_1}{P_{\mathrm{Ped}}} \quad ; \quad \mathrm{PTER}_{\mathrm{dB}} = 10\log\left(\frac{P_1}{P_{\mathrm{Ped}}}\right) \tag{2.8}$$

The pulses are intensity modulated with a PRBS using an external modulator with an extinction ratio, r_{ext}. The extinction ratio is defined as the relation between the signal power in a mark, P_1, and the signal power in a space, P_0.

$$r_{ext} = \frac{P_1}{P_0} \quad ; \quad r_{ext.dB} = 10 \log\left(\frac{P_1}{P_0}\right) \tag{2.9}$$

Using these definitions a model for the modulated signal can be developed. The electric field for the Gaussian pulse with an added pedestal is expressed as

$$E_G(t) = \left[c + (A - c) \exp\left(\frac{-t^2}{2T_0^2}\right)\right] \exp\left[i(\omega t + \varphi)\right] \tag{2.10}$$

Here c is the amplitude of the pedestal, (A-c) is the amplitude of the Gaussian pulse thus resulting in a total amplitude of A, as indicated in Figure 2.13, t is time, T_0 is the half-width at the e^{-1}- intensity point, ω is the carrier frequency and φ is the phase.

For an intensity-modulated signal, the electric field is expressed as

$$E(t) = \sum_k d_k \, E_G(t - t_k) \quad ; \quad t_k = kT_S \quad ; \quad d_k = \begin{cases} \dfrac{1}{\sqrt{r_{ext}}} \\ 1 \end{cases} \tag{2.11}$$

T_S is the period of the pulse train, t_k is the centre of bit number 'k' and d_k represents the logical values 0 and 1 for a signal with finite extinction ratio.

N numbers of channels, each defined as above, are multiplexed together forming an OTDM bit stream, with an aggregated bit rate of N/T_S. Finally the OTDM signal is demultiplexed with an ideal square shaped window, with a width corresponding to the timeslot width of the aggregated bit rate and with infinite extinction ratio.

Because the neighbouring channels have a finite PTER, the electric field within the demultiplexing window, will include contributions from these (N-1) channels as well.

In order to illustrate the impact of crosstalk on the demultiplexed signal, the previous example used to classify the different terms of crosstalk, can be expanded to show the impact of the PTER from two neighbouring channels on the demultiplexed channel. The example will derive an expression for the crosstalk in channel 0 originating from channel 1 and 2. The obtained result can easily be generalised to an OTDM signal of N channels.
If it is assumed that the pulses are sufficiently narrow so the impact of the ideal Gaussian pulse tails can be neglected, only the pedestal will affect the electric

field from channel 0. Labelling timeslot k as 0 and the neighbour channel (k-1) and (k+1) as 1 and 2, as sketched in Figure 2.12, the received electric field, $E_{rec}(t)$ when extracting the content of timeslot k is

$$\begin{aligned}\bar{E}_{rec}(t) = d_0 \left[c + (A-c) \exp\left(\frac{-(t-t_0)^2}{2T_0^2} \right) \right] \exp\left[i(\omega t + \varphi_0) \right] \\ + d_1\, c \exp\left[i(\omega t + \varphi_1) \right] + d_2\, c \exp\left[i(\omega t + \varphi_2) \right]\end{aligned} \tag{2.12}$$

If the receiver consists of a photo-detector and an electrical bandpass filter with a bandwidth $B_e << 2\omega$, see Figure 2.12, the received photo-current $i_{rec}(t)$, at the decision time $t = t_0$ is then

$$\begin{aligned} i_{rec}(t_0) &\propto \frac{1}{2} \bar{E}_{rec}(t_0)\, \bar{E}^*_{rec}(t_0) \\ &= \frac{1}{2} d_0^2\, A^2 + \frac{1}{2} d_1^2\, c^2 + \frac{1}{2} d_2^2\, c^2 + \\ &\quad d_0\, d_1\, c\, A \cos(\varphi_0 - \varphi_1) + \\ &\quad d_0\, d_2\, c\, A \cos(\varphi_0 - \varphi_2) + \\ &\quad d_1\, d_2\, c^2 \cos(\varphi_1 - \varphi_2) \end{aligned} \tag{2.13}$$

By introducing the following relations for the power in channel 0, P_1, and the power in the pedestal, P_{Ped},

$$P_1 = \frac{1}{2} A^2 \quad ; \quad P_{Ped} = \frac{1}{2} c^2 \quad ; \quad PTER = \frac{P_1}{P_{Ped}} \tag{2.14}$$

combined with the definition of PTER, the received power can be expressed as

$$i_{rec}(t_0) \propto d_0^2\, P_1 + \frac{P_1}{PTER}\left[d_1^2 + d_2^2\right] +$$

$$2\frac{P_1}{\sqrt{PTER}}\left[d_0\, d_1 \cos(\varphi_0 - \varphi_1) + d_0\, d_2 \cos(\varphi_0 - \varphi_2)\right] +$$

$$2\frac{P_1}{PTER} d_1\, d_2 \cos(\varphi_1 - \varphi_2) \qquad (2.15)$$

The first term represents the original power within channel 0, bit k. Term two is the power of the neighbouring channels within channel 0, i.e. power addition crosstalk or ISI. Term three and term four are the interferometric crosstalk.

The expression for crosstalk can easily be generalised to an OTDM signal of N channels

$$i_{rec}(t_0) \propto d_0^2\, P_1 +$$

$$\sum_{l\neq 0}^{N-1} d_l^2 \frac{P_1}{PTER} +$$

$$2\sum_{m\neq 0}^{N-1} d_0 d_m \frac{P_1}{\sqrt{PTER}} \cos(\varphi_0 - \varphi_m) + \qquad (2.16)$$

$$2\sum_{\substack{l\neq 0 \\ l\neq m}}^{N-1}\sum_{m\neq 0}^{N-1} d_l d_m \frac{P_1}{PTER} \cos(\varphi_l - \varphi_m)$$

From this expression a worst-case scenario can be derived. For a received space originating from channel 0, i.e. $d_0 = (r_{ext})^{-½}$ the most deteriorating effect is when all the neighbouring channels are marks, i.e. $d_l = 1$, and the phase-difference ($\varphi_0 - \varphi_m$) equals $2\pi p$, where p is an integer, and as a consequence the relation $\varphi_m = \varphi_l + 2\pi q$, where q is an integer. The received photo-current is then

$$i_{rec}(t_0) \propto \frac{P_1}{r_{ext}} + (N-1)\frac{P_1}{PTER} + 2(N-1)\frac{1}{\sqrt{r_{ext}}}\frac{P_1}{\sqrt{PTER}} + 2(N-1)\frac{P_1}{PTER} \tag{2.17}$$

For a received mark originating from channel 0, i.e. $d_0 = 1$, the most deteriorating effect is when all the neighbouring channels are marks, i.e. $d_m = 1$, and the phase-difference $(\varphi_0 - \varphi_m)$ equals $\pi + 2\pi p$, where p is an integer, which establish the same relation for the phases of the neighbouring channels $\varphi_m = \varphi_l + 2\pi q$, where q is an integer. The received photo-current is then

$$i_{rec}(t_0) \propto P_1 + (N-1)\frac{P_1}{PTER} - 2(N-1)\frac{P_1}{\sqrt{PTER}} + 2(N-1)\frac{P_1}{PTER} \tag{2.18}$$

As an example of the optical power reduction of the marks and the increased optical power of the spaces, described by the right side of eq. (2.17) and (2.18) is shown in Figure 2.14. An input signal with +10 dBm in the mark, corresponding to P_1 and an extinction ratio r_{ext} = 13 dB, is deteriorated by the neighbouring channels within the OTDM signal. The worst-case crosstalk scenario described with eq. (2.17) and (2.18) is calculated for 4, 8, 16 and 32 channels as function of the PTER. From Figure 2.14, it is apparent how devastating the crosstalk can be, even for relatively small pedestal values, i.e. high PTER levels. For e.g. an 8 channel OTDM signal based on pulses with PTER = 30 dB, the mark-level has decreased from +10 dBm to +7.6 dBm and the space-level has increased from –3 dBm to +2.1 dBm, corresponding to a decrease in the eye-opening from 13 dB to 5.5 dB. It should also be emphasised that the impact of power addition crosstalk, i.e. term 2, is significantly less devastating than the impact of incoherent crosstalk in term 3. For a received space, the contribution from power addition crosstalk is ~ -11.5 dBm compared to the ~ 0 dBm from the incoherent crosstalk in term 3, emphasising the importance of evaluating the impact of incoherent crosstalk on the transmitter.

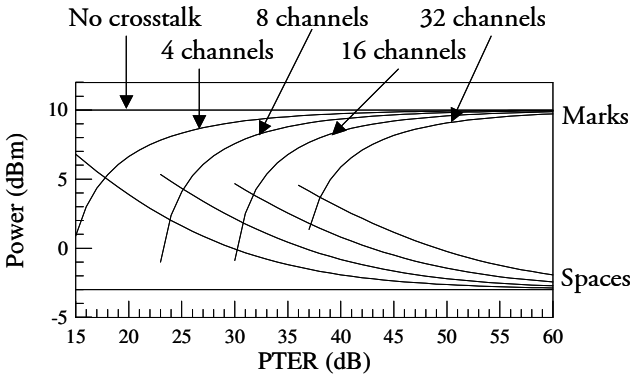

Figure 2.14: Example of worst-case crosstalk scenario for an input signal with +10 dBm in mark and modulation extinction ratio of 13 dB. The crosstalk is calculated for 4, 8, 16 and 32 channel OTDM signal.

2.6.4 Scalability

From the expression for introduced crosstalk from neighbouring channels within the OTDM signal, it is obvious that the impact of crosstalk is not related to the bit rate, but the number of channels multiplexed together. An OTDM signal with four channels, each at a base rate of 10 Gbit/s or 40 Gbit/s, i.e. the aggregated bit rate is 40 and 160 Gbit/s, respectively, will experience the same crosstalk penalty if the pulses in every respect in terms of e.g. shape, polarisation and PTER are identical besides the scaling in time. The scaling in time should be based on a constant relation between the temporal Full Width Half Maximum width and the width of the OTDM timeslot, i.e. 25 and 6.25 ps respectively. It should be stressed that even though the requirements in principle are the same, the actual development of a pulse source fulfilling these requirements are much more challenging at 40 than at 10 GHz.

In Figure 2.15 power penalties versus PTER is shown for 4 x 10 Gbit/s and 4 x 40 Gbit/s. The actual simulations are based on the program described below and will not be described further in this section. The example is included in order to illustrate and support the arguments for scalability. In the figure the full line represents the 4 x 40 Gbit/s system, and the circles represents the 4 x 10 Gbit/s system. The small deviations between the two sets of results are ascribed to the receiver specific parameters, e.g. filtering effects and impact of noise.

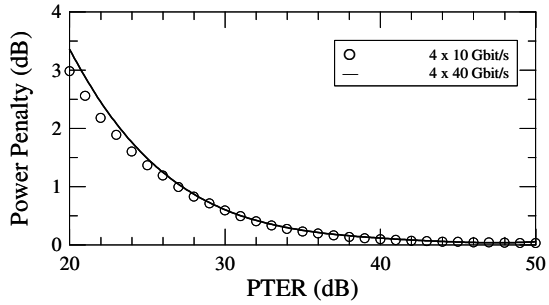

Figure 2.15: Comparison of induced power penalty versus PTER for a 4 x 10 Gbit/s system (o) and a 4 x 40 Gbit/s (-).

2.6.5 Simulation tool

Two techniques to investigate the impact of pulse tail induced crosstalk have been demonstrated in literature. One principle is based on a statistic description of the probability density function (pdf) in terms of Moment Generating Functions [2.54]. The other technique is based on a Monte Carlo approach, where the appropriate parameters are changed randomly, and the calculations are carried out a number of times. The two techniques have been shown to generate approximately the same results, and consequently the choice of technique is free. In this chapter the Monte Carlo approach has been chosen.

The simulation model consists in principle of only two sub modules, the transmitter and the receiver, and they are described in the following.

The transmitter consists of a pulse source, which generates a pulse train at the base rate of the OTDM signal, i.e. 10 or 40 Gbit/s. The pulses are characterised by the pulse shape and the temporal Full Width Half Maximum (FWHM) width. In principle the simulations can be expanded to include SuperGaussian, Hyperbolic Secant pulses and specific pulse shapes either simulated or measured. Each pulse is assigned a random phase, evenly distributed between 0 and 2π, which corresponds to the optical phases in Figure 2.12. The pulse train at the base rate is externally modulated, based on an NRZ modulator with a specified extinction ratio. The data sequence is generated with a PRBS of 127 bits, generated by a random start sequence in the 7-bit array [2.55]. A number of signals at the base rate with random phase are multiplexed together. The number of signals corresponds to the number of channels in the OTDM signal. Hereby the impact of the pulse tails and the additional pedestal, due to the random phase that each pulse is assigned, can be evaluated.

The receiver consists of optical demultiplexing generated by a square window equal to the width of the timeslot of the OTDM signal. The extinction ratio of the switching window is assumed infinite. The demultiplexed channel and the pedestals from the neighbouring channels are injected into an optical preamplifier with a Noise Figure (NF), an optical filter with bandwidth B_O, an O/E converter and an electrical filter with bandwidth B_e, before the Bit Error Rate analyser processes it. The BER-analyser first determines the optimum sampling time, before it determines the optimum threshold of the signal, by minimizing the probability of errors. A feedback loop, determines the required input power to the preamplifier, in order to establish the power sensitivity.

For a specific pulse description in terms of shape, FWHM and PTER, the sensitivity is calculated for all the OTDM channels a number of times, and an average sensitivity is calculated for each channel and compared to a back-to-back scenario with no multiplexing.

The simulations can be summarised as in the diagram in Figure 2.16.

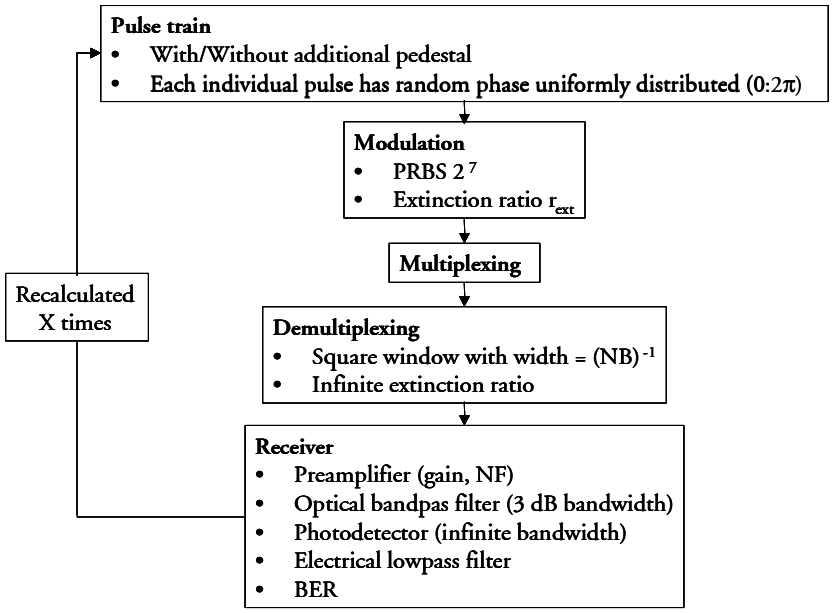

Figure 2.16: Diagram of power penalty simulations for different pulses.

2.6.6 Pulse source requirements for ideal pulse with no pedestal

Before realistic data streams based on pulses with pedestals are simulated, the impact of multiplexing ideal transform-limited Gaussian pulses is evaluated.

The objective of this simulation is to obtain the power penalty for a specific width of the pulses. This limit represents the best possible pulse quality at a given pulse width, and the results will be used in the next section when pulses with a finite PTER are simulated.

In order to predict the results for ideal pulses, the following illustrative example is used. A pulse train with an aggregated bitrate of 160 Gbit/s is shown in Figure 2.17. The OTDM signal is shown for three different pulse widths, 0.625, 3.125 and 5.625 ps, corresponding to 0.1, 0.5 and 0.9 times the OTDM timeslot of 6.250 ps.

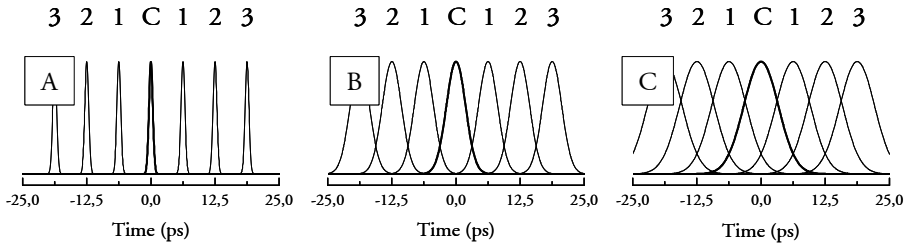

Figure 2.17: Electric field of a 160 GHz pulse train based on Gaussian pulses. The numbers refer to the number from the central channel C. A) T_{FWHM} equal to 0.1 of the timeslot T_S, i.e. 0.625 ps. B) T_{FWHM} equal to 0.5 of the timeslot T_S, i.e. 3.125 ps. C) T_{FWHM} equal to 0.9 of the timeslot T_S, i.e. 5.625 ps.

The example illustrates how the amplitude of the pulse tails in the neighbouring channels are increased for increased pulse width. However, it also demonstrates that a specific channel is only significantly affected by the two immediate neighbour channels. When calculating the actual amplitude contribution of the ideal neighbouring Gaussian pulses relative to the amplitude of the affected channel, this is confirmed. In table 2.3 the relative amplitude in dB at the time corresponding to the centre of the central channel C is calculated as function of the ratio between the FWHM pulse width, T_{FWHM}, and the OTDM timeslot, T_S. For narrow pulses the amplitude can be neglected, even for the immediate neighbours, i.e. channel 1 left and right. For increased pulse width up to 0.9, the amplitude for all the neighbour channels except channel 1, are negligible.

T_{FWHM}/T_S	Channe l 3 Left	Channe l 2 Left	Channe l 1 Left	Center	Channe l 1 Right	Channe l 2 Right	Channe l 3 Right
0.1				0			
0.2				0			
0.3			-67	0	-67		
0.4			-38	0	-38		
0.5		-96	-24	0	-24	-96	
0.6		-67	-17	0	-17	-67	
0.7		-49	-12	0	-12	-49	
0.8	-85	-38	-9	0	-9	-38	-85
0.9	-67	-30	-7	0	-7	-30	-67

Table 2.3: Relative amplitude of the electric field of neighbouring channels (in dB) compared to the amplitude of the centre of the central channel C. Empty cells in the table represents values < -100 dB suppression. Pulses are assumed ideal with no additional pedestals.

From the results presented in table 2.3, it would be expected that only the neighbours on each side of the central channel has sufficiently high amplitude of the electric field to interact with the centre channel, and consequently have an impact on the crosstalk. Based on this observation, the power penalty due to crosstalk, should not depend on the number of OTDM channels as only the two immediate neighbouring channels have sufficient power to affect the central channel C. Thus the simulation should show the same power penalty for 4 x 40 Gbit/s, 8 x 40 Gbit/s, 16 x 40 Gbit/s and 32 x 40 Gbit/s, provided the pulses fulfil the same relation between the FWHM pulse width and the OTDM timeslot, are ideal and do not include additional pedestals.

In Figure 2.18 the power penalty versus the relation between FWHM and the OTDM timeslot is shown for 160 Gbit/s, 320 Gbit/s, 640 Gbit/s and 1280 Gbit/s. The penalties are calculated using the program described above.

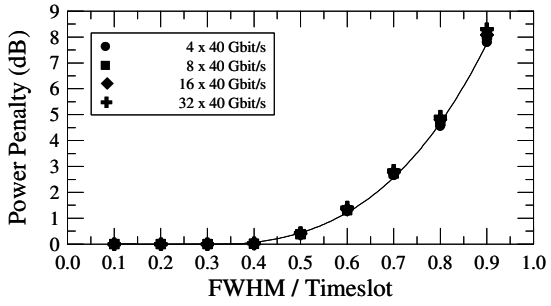

Figure 2.18: Power penalty for multiplexing and demultiplexing ideal Gaussian transform-limited pulses with no pedestal.

As predicted the power penalty is the same for the same ratio between FWHM pulse width and the width of the OTDM timeslot, irrespective of the aggregated bitrate and the total number of OTDM channels. From the figure the best obtainable system for a given FWHM can be determined. For a ratio, T_{FWHM}/T_S of < 0.4 the power penalty is negligible, and if a power penalty for multiplexing and demultiplexing of 1 dB can be tolerated, the ratio between FWHM and the width of the OTDM timeslot should not exceed approximately 0.5. This is summarised in the table 2.4 below.

Bitrate (Gbit/s)	Width of OTDM timeslot (ps)	Maximum FWHM (ps)
4 x 40	6.25000	3.12500
8 x 40	3.12500	1.56625
16 x 40	1.56250	0.78125
32 x 40	0.78125	0.39063

Table 2.4: Maximum temporal FWHM widths corresponding to $0.5T_S$ of the ideal Gaussian pulses with no pedestal in order to keep power penalty below 1 dB

2.6.7 Pulse source requirements for pulses with additional pedestal

As explained previously, the pulse train emitted from the laser will consist of pulses plus an additional pedestal. The pedestal, i.e. PTER, is defined according to Figure 2.13.

The objective for this section is to extract the requirements for the PTER for different FWHM pulse widths [2.56]. As it was concluded in the previous section, a power penalty of 1 dB is expected for ideal Gaussian pulses with pulse widths equal to half of the OTDM timeslot. Consequently, the impact of PTER is not calculated for pulses broader than this.

To illustrate the impact of the PTER in a system affected by incoherent crosstalk, the eye-diagrams for an OTDM signal of 8 x 40 Gbit/s corresponding to an aggregated bitrate of 320 Gbit/s is shown in Figure 2.19 for PTER equal to 25, 33 and 50 dB.

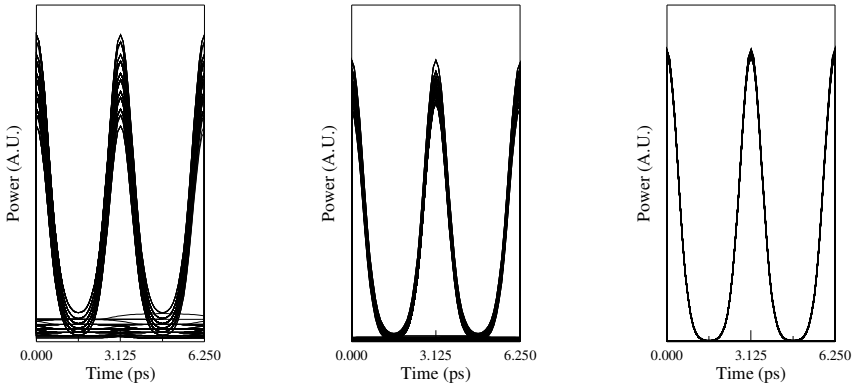

(A) (B) (C)

Figure 2.19: Eye-diagrams for 320 Gbit/s signal with pulses with FWHM pulse widths of 0.9373 ps (0.3 times the timeslot) and with PTER of A) 25 dB, B) 33 dB and C) 50 dB.

From Figure 2.19 it is noticeable how the combination of decreased PTER, which leads to increased incoherent crosstalk, deteriorates the signal. The eye-opening is decreased for decreased PTER resulting in a power penalty.

Based on the developed simulation tool, the impact of PTER was evaluated for different FWHM pulse widths for different aggregated bit rates. In the simulations, the aggregated bit rates were 160 Gbit/s, 320 Gbit/s, 640 Gbit/s and 1280 Gbit/s. It should be noted that the highest bit rate demonstrated hitherto[11] is 640 Gbit/s. Higher aggregated bit rates have been demonstrated, e.g. 1280 Gbit/s [2.2], however this experiment utilised polarisation multiplexing, which imposes more relaxed requirements to the pulse sources due to the perpendicular polarisation states of the neighbouring channels. Because 1280 Gbit/s is the next challenge for single polarisation OTDM systems, the requirements for 1280 Gbit/s is presented. In Figure 2.20, 2.21 and 2.22 the power penalty versus PTER is shown, for FWHM pulse width equal to 0.3, 0.4 and 0.5 times the width of the OTDM timeslot, respectively.

[11] In spring 2006

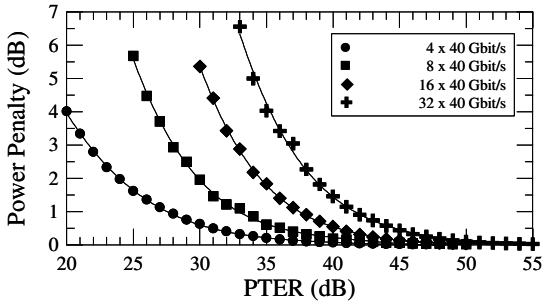

Figure 2.20: Power penalty versus PTER for pulse width FWHM equal to 0.3 times the width of the OTDM timeslot. The 1 dB penalty is obtained for PTER equal to 27, 33, 37 and 41 dB, for 160, 320, 640 and 1280 Gbit/s respectively.

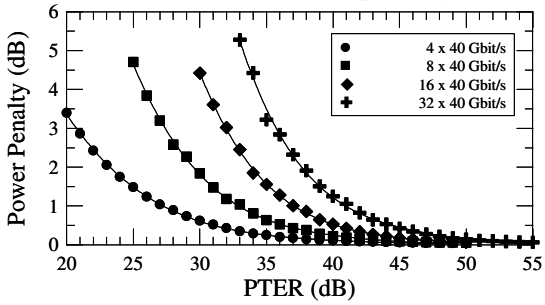

Figure 2.21: Power penalty versus PTER for pulse width FWHM equal to 0.4 times the width of the OTDM timeslot. The 1 dB penalty is obtained for PTER equal to 27, 33, 37 and 41 dB, for 160, 320, 640 and 1280 Gbit/s respectively.

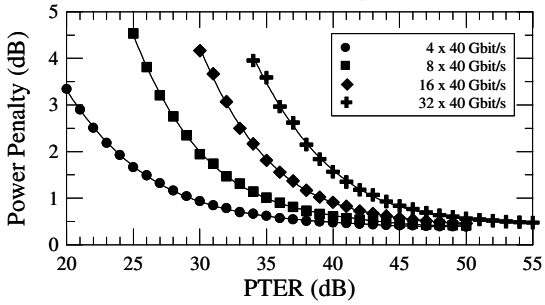

Figure 2.22: Power penalty versus PTER for pulse width FWHM equal to 0.5 times the width of the OTDM timeslot. The 1 dB penalty is obtained for PTER equal to 29, 35, 37 and 43 dB, for 160, 320, 640 and 1280 Gbit/s respectively.

When comparing the results in Figure 2.20 to 2.21 it is concluded, that there is no significant difference between pulse widths with a T_{FWHM}/T_S ratio of 0.3 and 0.4. This is in agreement with Figure 2.18, as the crosstalk due to neighbouring channels when employing ideal Gaussian pulses is negligible for T_{FWHM}/T_S ratios

< 0.4. Consequently the power penalties for the non-ideal pulses are determined by the pedestals, and not the pulse tails from the ideal pulses. When increasing the pulse width, i.e. increasing the ratio T_{FWHM}/T_S, to 0.5, the impact of neighbouring ideal pulse tails combined with the pedestals determines the power penalty, and an increase in the required PTER is necessary, in order to keep the introduced power penalty at 1 dB. It is also noted that for a PTER approaching infinity, the power penalty approaches the results from Figure 2.18.

Direct experimental comparisons for confirming the simulation results have not been performed. However, some of the obtained results can be compared with previous reported work in e.g. [2.57]. The results are similar, i.e. small deviations in power penalties are observed, which are ascribed to parameters in the receiver, e.g. impact of filtering and noise.

An interesting observation is the fact that the requirement for the PTER is increased with approximately 6 dB, when increasing the number of channels from 4 to 8. When increasing the number of channels from 8 to 16, the PTER requirement is only increased with additional 4 dB, and similarly when increasing the number of channels from 16 to 32. As explained previously, the incoherent crosstalk is regarded as noise in the receiver, i.e. the pdf of the incoherent crosstalk determines the BER. For equally distributed random phases, the pdf will change gradually from a distinct non-Gaussian shape for only one crosstalk term, to a Gaussian shaped pdf when increasing the number of crosstalk terms, see e.g. [2.54]. A consequence of this is that the expected sensitivity for a changed number of OTDM channels is not immediately scalable.

From the results presented in this section, the requirements for the transmitter in an OTDM system can be extracted. It should be stressed that the following requirements are conservative, as a design criterion has been the maximum introduction of a 1 dB power penalty for modulating, multiplexing and demultiplexing the pulses.

For Gaussian pulses, the FWHM pulse width should be less than 0.5 times the timeslot. For FWHM pulse widths of approximately 0.4 times the timeslot, the impact of PTER determines the system performance of the pulses, and consequently the effort for decreasing the pulse width further is not awarded with better performance. From Figure 2.22 the PTER for different aggregated bit rates can be extracted to 27, 33, 37 and 41 dB at 160, 320, 640 and 1280 Gbit/s, respectively, when the base rate is 40 Gbit/s

2.6.8 Residual pedestal energy

In the previous sections, the pulses were evaluated in a system context, i.e. the power penalty for multiplexing a number of OTDM channels together and subsequently demultiplexing each channel was evaluated. Requirements in terms of FWHM pulse width and PTER were derived. An interesting comparison to existing literature [2.1] can be made if required, by calculating the residual pedestal energy for specific PTER-levels, and relate it to the simulated power penalties.

By defining the electric field for an ideal Gaussian pulse, 'i' for ideal, and a Gaussian pulse with a pedestal, 'ni' for non-ideal, as

$$E_i(t) = \left[(c + A) \exp\left(\frac{-t^2}{2T_0^2} \right) \right] \exp[i\omega t]$$
$$E_{ni}(t) = \left[c + A \exp\left(\frac{-t^2}{2T_0^2} \right) \right] \exp[i\omega t] \qquad (2.19)$$

the peak power of the pulses is normalised to each other, and the residual energy in the pedestals can be calculated as [2.1]

$$\begin{aligned} \text{Pedestal}(\%) &= \frac{\left| \text{Energy}_{ni} - \text{Energy}_i \right|}{\text{Energy}_{ni}} 100\,\% \\ &= \frac{\left| \int E_{ni}(t)\, E_{ni}^*(t)\, dt - \int E_i(t)\, E_i^*(t)\, dt \right|}{\int E_{ni}(t)\, E_{ni}^*(t)\, dt} 100 \end{aligned} \qquad (2.20)$$

Where the energy is calculated for the timeslot corresponding to the base rate, e.g. 25 ps for a base rate of 40 Gbit/s.

In order to relate the extracted pulse source requirement to the residual pedestal energy, the pedestal energy has been calculated for pulse FWHM widths of 0.4 of the OTDM timeslot as function of the PTER.

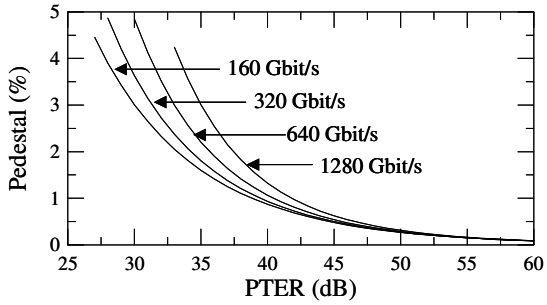

Figure 2.23: Pedestal energy as function of PTER.

The residual pedestal energy corresponding to the required PTER values extracted in the previous section is summarised in table 2.5.

Bitrate (Gbit/s)	PTER (dB)	Pedestal (%)
160	27	4.5
320	33	2.3
640	37	1.6
1280	41	1.1

Table 2.5: Maximum residual pedestal energy.

It should be noted that the calculations for evaluating the residual pedestal energy, are based on pulses with a constant pedestal, see Figure 2.13. If the pulses are non-ideal, but are described by an ideal pulse shape and an additional pedestal, which is not constant in time, then the results in Table 2.5 can only give an indication of required pedestal energy.

2.7 Characterisation of pulses

An important aspect of designing pulse sources is obviously the characterisation of the generated pulses. It is essential to have techniques to obtain reliable measurements of the pulses, in order to e.g. determine if the temporal FWHM and the PTER of the pulses fulfil the target requirements outlined in the previous section.

Ultra short pulse characterisation is a topic, which has evolved into a number of different techniques. Some of the schemes, which can be utilised are

- Auto-correlation [2.58]
- Frequency Resolved Optical Gating (FROG) [2.59]

- Optical Sampling [2.60] [2.61]
- Streak Camera [2.62]

It is indispensable that the pulse source characterisation schemes offer a sensitivity sufficient to resolve the power difference between the peak of the pulse and the pedestal. As outlined in the previous sections, the PTER for a 640 Gbit/s OTDM signal should be higher than 41 dB, which requires an even higher resolution of the pulse source characterisation set-up. It appears that this topic has not been addressed in details.

Which technique should be preferred is beyond the scope of this thesis, as it requires a thorough analysis of each technique in order to make an adequate comparison. In the experiments conducted using the laboratory facilities at COM•DTU, primarily the Auto Correlation technique has been used due to the simplicity of the scheme. Additionally, some work on optical sampling has also been started, but the set-up is still very bulky, complex and noisy and presently cannot be used as a supplement to other high-speed experiments. Consequently, the simulated and extracted requirements in previous sections still need to be verified experimentally.

2.8 Conclusion

In this chapter some of the important parameters an OTDM pulse source should be characterised by are identified. Followed by a survey of some of the promising existing OTDM pulse sources before an experimental implementation of a wavelength tuneable pulse source is suggested and characterised. Because the temporal FWHM width is decreased for increased bit rate, means to compress pulses, inadequate in width, are briefly introduced. A simulation model for evaluating the transmitter is proposed. The model consists of a pulse source characterised by the repetition rate, pulse shape, the FWHM pulse width and the level of possible additional pedestal. The pulses are split into a number of channels defined by the aggregated bit rate and the repetition rate of the pulse train. Each channel is PRBS modulated, delayed and multiplexed together. The OTDM signal is demultiplexed using an ideal square-shaped demultiplexing window with infinite extinction ratio. The demultiplexed channel is limited by the influence of the neighbouring channels in terms of the pulse tails defined by the ideal pulse shape, e.g. Gaussian, and the additional pedestal. The impact of the neighbouring channels is regarded as noise, and the classification is briefly described. The most severe impact of the neighbouring channels is incoherent cross-talk, and a simulation model evaluating the incoherent cross-talk is implemented. Using this model the requirements for the pulse source in terms of FWHM pulse width and maximum allowable pedestal level, i.e. minimum PTER is implemented. The

model is used to extract requirements for 160, 320, 640 and 1280 Gbit/s signals, based on Gaussian pulse trains with repetition rates equal to 40 GHz. The design requirements are based on a maximum introduced power penalty of 1 dB after multiplexing and demultiplexing. Gaussian pulses have been exclusively been used through out the thesis, because equations which includes Gaussian pulses often lead to analytical solutions. As the pulse source requirements are based on simulations, other pulse shapes could have been investigated, but due to time constraints, this was not done. Furthermore, it is expected that the requirements for e.g. hyperbolic secant pulses with a specific FWHM width will be approximately the same as for Gaussian pulses with the same width, as it is the size of the pedestal and not the pulse shape, which has determined the requirements. Finally, it should be noted that the calculations for evaluating PTER requirements are based on pulses with a constant pedestal. If the pulses are non-ideal, but are described by an ideal pulse shape and an additional pedestal, which is not constant in time, e.g. decreasing away from the centre of the pulse, the extracted requirements will be different. Nevertheless, it is believed that the extracted requirements still represent reasonable target values when designing the pulse sources. Finally a short introduction to existing experimental characterisation tools are presented.

2.9 References to chapter 2

[2.1] M. Pelusi, Y. Matsui, A. Suzuki, "Pedestal suppression from compressed femtosecond pulses using a Nonlinear Fiber Loop Mirror", IEEE Journal of Quantum Electronics, Vol. 35, No. 6, pp 867-874 (1999).

[2.2] M. Nakazawa, T. Yamamoto, K. R. Tamura, "1.28 Tbit/s 70 km OTDM transmission using third- and fourth order simultaneous dispersion compensation with a phase modulator", Electronics Letters, Vol. 36, No. 24, pp. 2027-2029 (2000).

[2.3] A. D. Ellis, J. K. Lucek, D. Pitcher, D. G. Moodie, D. Cotter, "Full 10x10 Gbit/s OTDM generation and demultiplexing using electro absorption modulators", Electronics Letters, Vol. 34, No. 18 (1998).

[2.4] P. L. Mason, A. Wonfor, D. D. Marccenac, D. G. Moodie, M. C. Brieriey, R. V. Penty, I. H. White, S. Bouchoule, "The effects of pedestal suppression on gain-switched laser sources for 40 Gbit/s OTDM transmission", Proceedings of 10th Annual Meeting of the IEEE Lasers and Electro-Optics Society (LEOS 1997), San Francisco, California, USA, Vol. 1, pp. 289-90 (1997).

[2.5] B. Mikkelsen, G. Raybon, R.-J. Essiambre, A. J. Stentz, T. N. Nielsen, D. W. Peckham, L. Hsu, L. Grüner-Nielsen, K. Dreyer, J. E. Johnson, "320-Gbit/s Single-Channel Pseudo-linear Transmission over 200 km of Nonzero-Dispersion Fiber", IEEE Photonics Technology Letters, Vol. 12, No. 10, pp. 1400-1402 (2000).

[2.6] M. Schilling, O. Blume, L-H. Nguyen, M. Schmidt, E. Lach, "OTDM Planar Lightwave Components (PLCs) for multiplexing from 40 Gb/s to 80-640 Gb/s", Proceedings of 15th Annual meeting of IEEE Lasers and Electro-Optics Society (LEOS 2002), Glasgow, Scotland, paper ThBB5 (2002).

[2.7] M. Kroh, H. G. Weber, A. T. Clausen, C. Mikkelsen, L. Oxenløwe, A. Siahlo, K. Berg, A. Tersigni, S. Bischoff, J. Mørk, "Report on sources for > 160Gbit/s including first version of the modelocked laser based pulse source without pulse shaper and on design and implementation of Nx40 Gibt/s OTDM multiplexer for Nx40 Gbit/s", TOPRATE deliverable D 3.3 (limited) (2002).

[2.8] M. Pelusi, Y. Matsui, A. Suzuki, "Electrooptic Phase Modulation of Stretched 250-fs pulses for Suppression of Third-Order Fiber Dispersion in Transmission", IEEE Photonics Technology Letters, vol. 11, No. 11, pp. 1461-1463 (1999).

[2.9] A. I. Siahlo, L.K. Oxenløwe, K.S. Berg, A.T. Clausen, K. Yvind, P. Jeppesen, K. P. Hansen, "Using a phase modulator for improvement of the tolerance to second-order dispersion in a 160 Gb/s transmission system", Proceedings of the 29th European Conference on Optical Communication (ECOC'03), Rimini, Italy, paper We4.P.105 (2003).

[2.10] S. Bouchoule, E. Lach, G. Lemestreallan, S. Slempkes, D. Mathoorasing, C. Kazimerski, A. Ougazzaden, "High speed gain-switched laser as very simple 4 x 10 Gbit/s and up to 8 x 10 Gbit/s OTDM source", Proceedings of 24th European Conference on Optical Communication (ECOC'98), Madrid, Spain ,Vol. 1, pp. 215-216 (1998).

[2.11] M. Vaa, "Optical Time Division Multiplexing for high capacity photonic networks", PhD thesis, Technical University of Denmark, Department of Electromagnetic Systems, Lyngby, Denmark (1997).

[2.12] A. Shen, S. Bouchoule, P. Crozat, D. Mathoorasing, J.-M. Lourtioz, C. Kazmierski, "Low timing jitter of gain- and Q-switched laser diodes for high bit rate OTDM applications", Electronics Letters, Vol. 33, No. 22, pp. 1875-1877 (1997).

[2.13] L. Chusseau, C. Kazmirski, "Optimum Linear Pulse Compression of a Gain-Switched 1.5 μm DFB laser", IEEE Photonics Technology Letters, Vol. 6, No. 1, pp. 24-26 (1994).

[2.14] S. Fischer, M. Dülk, M. Bitter, M. Caraccia, E. Gamper, W. Vogt, E. Gini, H. Melchior, W. Hunziker, A. Buxens, H. N. Poulsen, A. T. Clausen, "Ultrafast all-optical demultiplexer based on Mach–Zehnder interferometer with integrated semiconductor optical amplifiers," in Technical Digest of 5th Optoelectronics Communications Conference (OECC'00), Chiba, Japan, paper 14D-1 (best paper award) (2000).

[2.15] K. R. Tamura, M. Nakazawa, "Spectral-smoothing and pedestal reduction of wavelength tunable Quasi-Adiabatically compressed femto-second solitons using a Dispersion-Flattened Dispersion-Imbalanced Loop Mirror", IEEE Photonics Technology Letters, Vol. 11, No. 2, pp. 230-232 (1999).

[2.16] G. P. Agrawal, "Nonlinear Fiber Optics", Second edition, Academic Press, San Diego, California (1995).

[2.17] M. Nakazawa, E. Yoshida, Y. Kimura, "Ultrastable harmonically and regeneratively modelocked polarisation-maintaining erbium fibre ring laser", Electronics Letters, Vol. 30, No. 19, pp. 1603-1605 (1994).

[2.18] A. D. Ellis, R. J. Manning, I. D. Phillips, D. Nesset, "1.6 ps pulse generation at 40 GHz in phaselocked ring laser incorporating highly nonlinear fibre for applications to 160 Gbit/s OTDM networks", Electronics Letters, Vol. 35, No. 8, pp. 645-646 (1999).

[2.19] K. S. Abedin, F. Kubota, "10 GHz, 1 ps regeneratively modelocked fibre laser incorporating highly nonlinear and dispersive photonic crystal fibre for intracavity nonlinear pulse compression", Electronics Letters, Vol. 40, No. 1, pp. 58-59 (2004).

[2.20] E. Yoshida, N. Shimizu, M. Nakazawa, "A 40 GHz 0.9 ps regeneratively mode-locked fiber laser with a tuning range of 1530-1560 nm", IEEE Photonics Technology Letters, Vol. 11, No. 12, pp. 1587-1589 (1999).

[2.21] E. Yoshida, N. Shimuzu, M. Nakazawa, “Measurement of the timing jitter and pulse energy fluctuations of a PLL regeneratively mode-locked Fiber Laser”, IEEE Photonics Technology Letters, Vol. 11, No. 5, pp. 548-550 (1999).

[2.22] K. S. Berg, L. K. Oxenløwe, A. Siahlo, A. Tersigni, A. T. Clausen, C. Peucheret, P. Jeppesen, K. P. Hansen and J. R. Hansen, "80 Gb/s transmission over 80 km and demultiplexing using a highly non-linear photonic crystal fibre", Proceedings of European Conference on Optical Communication, (ECOC'2002), Copenhagen, Denmark, paper 2.1.5 (2002).

[2.23] L. K. Oxenløwe, A. I. Siahlo, K. S. Berg, A. Tersigni, A. T. Clausen, C. Peucheret, P. Jeppesen, K. P. Hansen and J. R. Jensen, "A photonic crystal fibre used as a 160 to 10 Gb/s demultiplexer", Proceedings of Opto-Electronics and Communications Conference (OECC'2002), Yokohama, Japan, post-deadline paper PD1-4 (2002).

[2.24] A. Yariv, “Optical Electronics in Modern Communications – fifth edition”, Oxford University Press, New York, USA (1997).

[2.25] R. Ludwig, S. Diez, E. Erhardt, L. Küller, W. Pieper, H. G. Weber, “A tunable femtosecond modelocked semiconductor laser for applications in OTDM systems”, IEICE Transactions on Electronics. Vol. E81C, No. 2, pp. 140-145 (1998).

[2.26] K. Yvind, “Semiconductor Mode-Locked Lasers for Optical Communication Systems”, PhD thesis, Technical University of Denmark, Department of Communications, Optics & Materials (COM•DTU), Lyngby, Denmark (2004).

[2.27] L. Krainer, R. Paschotta, G. J. Spühler, I. Klimov, C. Y. Teisset, K. J. Weingarten, ”Tunable picosecond pulse-generating laser with repetition rate exceeding 10 GHz”, Electronics Letters, Vol. 38, No. 5, pp. 225-227 (2002).

[2.28] G. J. Spühler, L. Krainer, I. Kilburn, M. Dymott, K. J. Weingarten, R. Paschotta, and U. Keller, "Picosecond pulse-generating laser with repetition rate of 10 GHz and rms timing jitter <100 fs fully tunable over C-band", Technical Digest of conference on Optical Fiber Communication (OFC’03), Atlanta, U.S.A., paper TuL2 (2003).

[2.29] M. Schmidt, E. Lach, K. Schuh, M. Schilling, P. Sillard, G. Veith, "Unrepeatered 320 Gbit/s (8x40 Gbit/s) OTDM transmission over 80 km TeraLight™ fiber link", Proceedings of European Conference on Optical Communication (ECOC'03), Rimini, Italy, paper We4-P.117 (2003).

[2.30] V. Kaman, Y.-J. Chiu, T. Liljeberg, S. Z. Zhang, J. E. Bowers, "Integrated tandem travelling-wave Electroabsorption modulators for > 100 Gbit/s OTDM applications", IEEE Photonics Technology Letters, Vol. 12, No. 11, pp. 1471-1473 (2000).

[2.31] J. H. Lee, T. Kogure, D. J. Richardson, "Wavelength tunable 10-GHz 3-ps pulse source using a dispersion decreasing fiber-based nonlinear optical loop mirror", IEEE Journal of Selected topics in Quantum electronics, Vol. 10, No. 1, pp. 181-185 (2004).

[2.32] M. Schmidt, K. Schuh, E. Lach, M. Schilling, G. Veith, "8x160 Gbit/s (1.28 Tbit/s) DWDM transmission with 0.53 bit/s/Hz spectral efficiency using single EA-modulator based RZ pulse source and demux", Proceedings of European Conference on Optical Communication (ECOC'03), Rimini, Italy, paper Mo3.6.5 (2003).

[2.33] P. Devgan, J. Lasri, R. Tang, P. Kumar, "Ultra-low-jitter multiwavelength synchronised optical pulses for C-, L- and U-bands", Electronics Letters, Vol. 39, No. 18, pp. 1337-1339, (2003).

[2.34] A. T. Clausen, L. Oxenlowe, C. Peucheret, S. N. Knudsen, L. Grüner-Nielsen, A. Bjarklev, S. Barkou, H. N. Poulsen, P. Jeppesen, "Novel single/multiple wavelength RZ pulse source based on four-wave mixing in newly developed highly non-linear fibre", Proceedings of 26th European Conference on Optical Communication (ECOC'00), Münich, Germany, poster P 3.14 (2000).

[2.35] K. Inoue, "Four-Wave Mixing in an Optical Fiber in the Zero-Dispersion Wavelength Region", IEEE Journal of Lightwave Technology, Vol. 10, No. 11, pp. 1553-1561 (1992).

[2.36] P. H. Hedekvist, M. Karlsson and P. A. Andrekson, "Fiber Four-Wave Mixing Demultiplexing with Inherent Parametric Amplification", Journal of Lightwave Technology, Vol. 15, No. 11, pp. 2051-2058 (1997).

[2.37] M. Onishi, T. Okuno, T. Kashiwada, S. Ishikawa, N. Aksaka and M. Nishimura, “Highly Nonlinear Dispersion-Shifted Fibers and Their Application to Broadband Wavelength Converter”, Optical Fiber Technology, Vol. 4, No. 2, pp. 204-214 (1998).

[2.38] O. Aso, M. Tadakuma and S. Namiki, “More than 91 nm Broadband Four-Wave Mixing based fiber parametric wavelength converter”, Proceedings of European Conference on Optical Communication (ECOC´99), Nice, France, Post-Deadline paper PD1-10, pp. 20-21 (1999).

[2.39] L. Grüner-Nielsen, S. N. Knudsen, T. Veng, B. Edvold and C. Larsen ”Design and manufacture of dispersion compensating fibre for simultaneous compensation of dispersion and dispersion slope”, Technical Digest of conference on Optical Fiber Communication Conference (OFC’99), San Diego, California, 1999, paper WM13, pp. 232-234 (1999).

[2.40] A. I. Siahlo, K. S. Berg, A. T. Clausen, L. K. Oxenløwe, A. Tersigni and P. Jeppesen, "160-10 Gb/s demultiplexing by using NOLM", in Proceedings of Quantum Electronics (QE-2002) 4th International Scientific and Technical Conference 2002, p. 122, Minsk, Belarus (2002).

[2.41] A. Siahlo, L. K. Oxenløwe, K. S. Berg, A. T. Clausen, Peter A. Andersen, C. Peucheret, A. Tersigni, P. Jeppesen, K. P. Hansen, J. R. Folkenberg, ” A High-Speed Demultiplexer Based on a Nonlinear Optical Loop Mirror With a Photonic Crystal Fiber, IEEE Photonics Technology Letters, Vol. 15, No. 8, pp. 1147-1149 (2003).

[2.42] T. Sakamoto, F. Futami, K. Kikuchi, S. Takeda, Y. Sugaya, S. Watanabe, “All-optical wavelength conversion of 500-fs pulse trains using Nonlinear-Optical Loop Mirror composed of a Highly Nonlinear DSF”, IEEE Photonics Technology Letters, Vol. 13, No. 5, pp. 502-503 (2001).

[2.43] M. D. Pelusi, H-F. Liu, ”Higher Order Soliton Pulse Compression in Dispersion-Decreasing Optical Fibers”, IEEE Journal of Quantum Electronics, Vol. 33. No. 8, pp. 1430-1439 (1997).

[2.44] M. Nakazawa, E. Yoshida, H. Kubota, Y. Kimura, “Generation of a 170 fs, 10 GHz transform-limited pulse train at 1.55 μm using a dispersion-decreasing, erbium-doped active soliton compressor”, Vol. 30, No. 24, pp. 2038-2040 (1994).

[2.45] A. Mostofi, H. Hatami-Hanza, P. L. Chu, “Optimum Dispersion Profile for Compression of fundamental solitons in Dispersion Decreasing Fibers”, IEEE Journal of Quantum Electronics, “Vol. 33, No. 4, pp. 620-628 (1997).

[2.46] M. Tsuchiya, K. Igarashi, R. Yatsu, K. Taira, K. Y. Koay, M. Kishi, “Sub-100 fs SDPF optical soliton compressor for diode laser pulses”, Optical and Quantum Electronics, Vol. 33, No. 10, pp. 751-766 (2001).

[2.47] S. N. Quist, “Compression of optical pulses”, M. S. project, Technical University of Denmark, Department of Communications, Optics & Materials (COM•DTU), Lyngby, Denmark (1999).

[2.48] Y. Qian, S. Quist, “Optimal design and experimental characterisation of short optical pulse compression using CDPF”, Proceedings of 25th European Conference on Optical Communication (ECOC’99), Nice, France, paper P2.17 (1999).

[2.49] K. C. Chan, H. F. Liu, “Short pulse generation by higher order soliton-effect compression: Effects of optical fiber characteristics”, IEEE Journal of Quantum Electronics, Vol. 31, No. 12, pp. 2226-2235 (1995).

[2.50] K. S. Berg, J. Mulet; M. Kroh, L. K. Oxenløwe, A. T. Clausen, A. N. Siahlo, P. Jeppesen, J. Mørk, S. Ferber, H. G. Weber, ”Report on fibre based short pulse source for ≥ 640 Gbit/s”, Deliverable D 3.5, IST project TOPRATE (IST 2000 28657) (2003).

[2.51] A. Siahlo, A. T. Clausen, J. Seoane, L. K. Oxenløwe, K.S. Berg, P. Jeppesen, O. Brox, S. Bauer, J. Kreissl and B. Sartorius, "Pulse Compression of a 40 GHz DFB based Optical Clock Recovery", Proceedings of the 30th European Conference on Optical Communication (ECOC'04), Stockholm, Sweden, paper We2.5.4 (2004).

[2.52] Peter J. Legg, Moshe Tur, Ivan Andonovic, “Solution Paths to Limit Interferometric Noise Induced Performance Degradations in ASK/Direct Detection Lightwave Networks”, Journal of Lightwave Technology, Vol. 14, No. 9, pp. 1943-1954 (1996).

[2.53] E. L. Goldstein, L. Eskildsen, C. Lin and Y. Silverberg, "Polarization Statistics of Crosstalk-Induced Noise in Transparent Lightwave Networks", Photonics Technology Letters, Vol. 7, No. 11, pp. 1345-1347 (1995).

[2.54] X. Jiang, I. Roudas, K. Jepsen, "Asymmetric probability density function of a signal with interferometric crosstalk in optically amplified systems", Technical Digest of conference on Optical Fiber Communication (OFC'98), San Jose, California, USA, Vol. 3, pp. 151-153 (1998).

[2.55] S. W. Golomb, "Shift Register Sequences", Aegean Park Press, Los Angles, California, USA (1982).

[2.56] A. T. Clausen, H. N. Poulsen, L. K. Oxenløwe, A. I. Siahlo, J. Seoane, P. Jeppesen, "Pulse source requirements for OTDM systems", Proceedings of 16th Annual meeting of IEEE Lasers & Electro-Optics Society (LEOS 2003), Tucson, USA, paper TuY2 (2003).

[2.57] K. S. Jepsen, "High-Speed Optical Signal Processing for High Capacity Optical Networks", PhD thesis, Technical University of Denmark, Department of Electromagnetic Systems, Lyngby, Denmark (1999).

[2.58] J. P. Curtis, J. E. Carroll, "Autocorrelation systems for the measurements of picosecond pulses from injection lasers", International Journal of Electronics, Vol. 60, No. 1, pp. 87-111 (1986).

[2.59] K. W. DeLong, D. N. Fittinghoff, R. Trebino, "Practical Issues in Ultrashort Laser-Pulse Measurements using Frequency-Resolved Optical Gating", IEEE Journal of Quantum Electronics, Vol. 32, No. 7, pp. 1253-1264 (1996).

[2.60] N. Yamada, S. Nogiwa, H. Ohta, "640-Gb/s OTDM Signal Measurement with high-resolution optical sampling System using wavelength-tunable soliton pulses", IEEE Photonics Technology Letters, Vol. 16, No. 4, pp. 1125-1127 (2004).

[2.61] J. Li, M. Westlund, H. Sunnerud, B.-E. Olsson, M. Karlsson, P. A. Andrekson, "0.5-Tb/s Eye-diagram measurement by Optical Sampling using XPM-induced wavelength shifting in Highly Nonlinear Fiber", IEEE Photonics Technology Letters, Vol. 16, No. 2, pp. 566-568 (2004).

[2.62] Product guide HAMAMATSU, http://www.hpk.co.jp

Chapter 3
Clock Extraction

3.1 Introduction

Data transmission systems are depending on Clock Recovery (CR) subsystems, which are able to extract a synchronised clock from an incoming data signal, in order to ensure that the required processing of the data can be carried out. The importance of Clock Recovery is emphasised by making a simple search on Google[12] on "Clock Recovery", showing approximately 330.000 hits[13]. Extracting scientific articles addressing "Clock Recovery" from the electronic database on the library of the Technical University of Denmark results in 3.559 hits[14]. Obviously, a simple search and match on Clock Recovery, reveals a number of different aspects of clock extraction, and certainly not all the hits are related to Optical Time Division Multiplexed (OTDM) systems. Nevertheless, the number of hits emphasises the importance of clock recovery systems.

Figure 3.1 illustrates a simple bit-interleaved OTDM point-to-point transmission system, as already shown and described in chapter 1.

The purpose of the clock in an OTDM system is twofold. It is used to synchronise the switching circuit, used for demultiplexing, by ensuring that the position of the induced Switching Window (SW), see chapter 4, is matched in time with the target OTDM time channel, which should be demultiplexed. Secondly, the clock is applied to the base rate receiver, in order to synchronise the sampling time for the decision circuit. Both the switching circuit and the electrical receiver require a clock at the base rate of the OTDM signal, and consequently the clock extraction circuit should be designed to fulfil this requirement.

[12] www.Google.dk
[13] Hits generated 2006 06 01
[14] Hits generated 2006 06 01

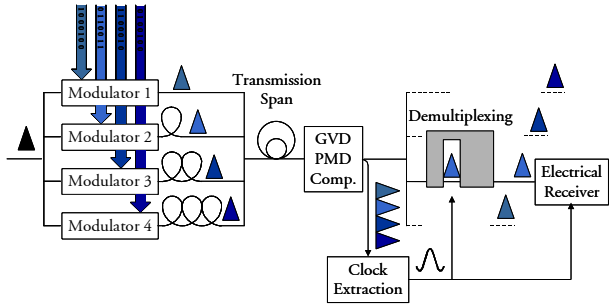

Figure 3.1: Basic bit-interleaved OTDM point-to-point transmission system

Before going into further details, a demarcation of the topic addressed in this chapter is appropriate. The clock extraction circuit blocks considered in this chapter are designed to extract a base rate clock from a continuously incoming high-speed aggregated OTDM signal. In more advanced OTDM systems than the one shown in Figure 3.1, the clock extraction circuits might need to be designed differently and fulfil other requirements.

Instead of an OTDM system based on only two nodes, i.e. a transmitter and receiver node, the system could be expanded to include intermediate nodes as suggested in chapter 5. One potential required functionality in selected nodes would be retiming as part of the regeneration. The CR scheme and requirements used for retiming are not necessarily the same as for the CR unit used in the receiver node. Another communication system, based on high-speed OTDM concepts, is the packet switched OTDM system, which is briefly addressed in chapter 5. When OTDM packets are used for transporting data, the CR circuits in the nodes need to accommodate for the gaps in time between the packets as opposed to the continuous bit steam generated by the bit interleaved OTDM system sketched in Figure 3.1. Clock Recovery schemes and requirements for these specialised OTDM systems are not addressed in this thesis.

A data signal based on external modulation of a Return-to-Zero (RZ) pulse train, can spectrally be described by the combination of a continuously spectrum added discrete frequency components, where the fundamental frequency corresponds to the repetition frequency of the pulse train. The discrete fundamental frequency component is often used to extract a clock signal with the same frequency. The spectrum of an OTDM data signal, which is composed by N time channels, does not contain any frequency components at the base rate of the OTDM signal, but only harmonics corresponding to the aggregated frequency of the OTDM signal [3.1]. As an example, a 160 Gbit/s OTDM signal composed by 16 channels each carrying 10 Gbit/s, would include

discrete frequency components at 160, 320, 480 GHz etc. Hence the extraction of the base rate clock from the OTDM data signal is a non-trivial task and prevents the OTDM system designer from simply injecting the OTDM signal into a standard on-shelf clock extraction circuit, available from existing commercial deployed systems[15]. In [3.2] an elegant modification of existing clock recovery configurations is proposed. The incoming OTDM signal at 100 Gbit/s is detected with a high-speed Photo Detector. The 100 GHz frequency component is injected into a harmonic mixer, along with an electrical local generated clock at 10 GHz. The output signal is used to control a Phase Locked Loop (PLL), and clock extraction at the base rate of the OTDM signal is demonstrated. The principle of the scheme is simple, but the implementation is challenging and the requirements in terms of bandwidth to the electrical components are strict. Even without considering the immense technical challenges by scaling the existing designs to higher bit rates, the present available commercial electronic bandwidth, approximately 100 GHz, prevents the designer from considering this approach for OTDM signals at 160 Gbit/s and above. Consequently other techniques have to be considered.

A simple approach to overcome the potential problem of extracting a base rate clock from the aggregated bit rate could be to transmit two signals – the OTDM signal containing the data on one wavelength and a base rate clock synchronised to the OTDM signal on a different wavelength. This approach has been demonstrated in a number of published experiments including the co-transmission of a 1.28 Tbit/s OTDM signal with a 10 GHz sinusoidal clock, separated 2 nm in wavelength [3.3]. By transmitting the clock on a separate wavelength, the clock can be extracted by optical filtering in the receiver, and applied to e.g. a local laser, which generates the synchronised base rate pulse train required for optical demultiplexing. A modified version of the transmitted clock is to transmit a pulse train, with a repetition frequency of the base rate. If the pulses are sufficiently narrow, the pulses can, after dispersion compensation and filtering, be used directly for demultiplexing in the receiver [3.4]. Obviously, the narrow clock pulses occupy more available bandwidth than the sinusoidal clock signal. A drawback of the transmitted clock scheme is the loss of available bandwidth. As the clock is situated on a separate wavelength, it will occupy bandwidth, which potentially could be used for data transmission.

[15] Small modifications are required if a clock extraction circuit designed for data signal based on Non Return to Zero (NRZ) corresponding to the format used in the deployed systems, was used for a RZ data signals at the same bit rate. NRZ signals do not include any distinct frequency components. However by including a frequency doubler [3.63], a discrete frequency component corresponding to the bit rate is generated, due to the cyclo-stationary properties of the data signal [3.64]. This is opposed to RZ signals, which inherently contain a frequency component corresponding the bit rate, and consequently do not require the pre-processing, i.e. the frequency doubling, before clock extraction. Besides this small modification, the clock recovery should operate for RZ signals.

Finally, timing jitter will influence both the transmitted data and the clock signal in the transmission system. If assuming that the jitter contributions are statistically independent, the maximum allowable transmission length might be limited because the relative jitter between the clock and the data exceeds the maximum tolerable value [3.5]. It should be emphasised that this has not been addressed in literature. In conclusion, transmitted clock is a viable solution, but appears not to represent the optimum solution.

Part of COM•DTU contribution to the European IST project TOPRATE was to implement CR systems operating at bit rates exceeding 100 Gbit/s, e.g. 160 and 320 Gbit/s. In this thesis some of the theoretical considerations on how to design a high-speed OTDM CR systems are presented. The content of the chapter is summarised below.

The outline of this chapter is as follows. First a short summary of reported OTDM Clock Recovery schemes is presented. Partly based on this summary, partly determined by available components, the Opto-electronic Phase Locked Loop (OE-PLL) is chosen as the preferred Clock Recovery scheme.

The OE-PLL used for clock extraction from an incoming high-speed OTDM signal, is based on Optical Phase Detection (OPD) implemented in an electrical PLL configuration. Before going into details with a specific implementation of an OPD, a simple time model explaining the basics of a PLL is introduced. The objective of this model is not to provide a thorough theoretical description of PLL operation, as several excellent PLL books are available, see e.g. [3.6], [3.7], [3.8], [3.9] and [3.10]. However, by introducing the simple model, the principle of operation is explained in a comprehendible way, and serves as the foundation for further discussions. By using the simple model, the modifications of the configuration in order to accommodate clock extraction from an OTDM signal is explained. Based on this model, an example demonstrating the principle of clock extraction from an OTDM signal is simulated. From this example two observations are made:

- When the PLL is extracting the clock, the clock and data signal are in phase quadrature, as opposed to optical demultiplexing where the clock, i.e. the switching window, and the target channel are in-phase.
- Due to the average powers of the data signal and the clock signal, a DC component is introduced in the control signal of the PLL. This DC component does not include any information required to control the PLL. However, this signal can deteriorate the operation of the PLL, and should consequently be compensated.

Four different techniques for compensating this DC component are presented in a literature survey, and one of the techniques is chosen for further investigations within the thesis.

From the theory derived for clock extraction from an OTDM signal, it becomes apparent that the clock pulses, which are injected into the OPD together with the data signal, can be optimised. A simple approach shows the optimum temporal Full Width Half Maximum (FWHM) pulse width for Gaussian pulses for different bit rates.

Before demonstrating the principle of OPD incorporated in a PLL configuration experimentally, a vital design parameter is illustrated by a numerical example where the impact of fibre length, i.e. internal delay within the loop, is examined by evaluating the stability of the feedback loop. The examples show the importance of reducing the length of fibre within the loop. It is important to note, that the delay within the loop is not only due to the fibre patch cords connecting the optical components in the loop. Also some optical components inherently include long delays, e.g. the Erbium doped fibre in the optical amplifiers or the fibre used for compressing the clock pulses from the clock laser.

Finally, an experimental demonstration of 10 GHz clock extraction from a 160 Gbit/s OTDM signal is shown. The PLL incorporates a Semiconductor Optical Amplifier (SOA) as the OPD, and uses the process of Four Wave Mixing (FWM) between the local clock and the incoming OTDM signal to generate the required control signal for the PLL. The results are analysed using the theory derived in the previous sections.

3.2 Reported OTDM clock recovery schemes

A number of groups around the world are addressing clock extraction from high-speed data signals, and in the following sections some of the highlights of previously reported results are presented. The techniques can be divided into two sub-categories - all optical clock extraction and opto-electronic clock extraction. If an optical data signal can be injected into the CR circuit, and the clock is extracted in the optical domain without any conversion to the electrical domain, the principle is labelled all optical CR. If the CR circuit includes O/E and/or E/O conversion the technique is labelled opto-electronic CR. The division in these sub-categories can only be used when describing the principle of operation, as the actual reported implementations do not restrict themselves to this superficial classification.

3.2.1 All optical CR: Mode-locked lasers

In the category of all optical clock extraction, two techniques have been reported based on injection of the optical data signal into a laser, which is either mode-locked lasers or self-pulsating lasers.

By designing a laser that includes a section where the loss (or gain) can be varied in time, the phase of the longitudinal modes supported in the laser can be fixed and mode locking is induced [3.11]. One approach for designing a semiconductor mode-locked laser is to incorporate a saturable absorber within the cavity. Mode locking is now a well-established technique to generate high-quality pulse trains [3.12]. By injecting a data signal into the laser cavity, the data signal will, if the power is sufficiently high, modulate the loss or gain, and hereby mode lock the laser. The mode-locked signal is synchronised to the input data signal, and consequently the generated pulse train corresponds to a clock signal. The cavity length of the laser determines the actual repetition frequency of the clock pulses. In both [3.13] and [3.14] a 160 GHz clock extracted from a 160 Gbit/s data signal is reported, demonstrating the speed potential of the lasers. As stated previously, the extracted clock from the OTDM signal should correspond to the base rate signal. This can in principle be obtained by dimensioning the cavity length of the laser, so the oscillation frequency corresponds to the base rate frequency. Using this appealing simple approach, a 10 GHz clock was extracted by injecting a 160 Gbit/s OTDM signal into the laser [3.15]. One problem, which unfortunately is associated with extraction of sub-harmonic clocks from an aggregated OTDM data signal, is the phase jumps of the extracted clock due to the pattern effects of the data [3.15]. Phase jumps in the clock can severely impair the system performance, and techniques to overcome the problem have been suggested. In [3.16] the data signal was composed by nineteen 10 Gbit/s data channels and a single high power 10 GHz clock pulse train. As the 10 GHz clock pulses contained 1.3 times higher peak power than the other channels, the saturable absorber was modulated with a frequency corresponding to the base rate of the signal. Another technique, which suppresses the pattern induced phase jumps without requiring a special designed data signal, is reported in [3.17] [3.18], where the concatenation of two mode-locked lasers is utilised to extract a 10 GHz clock from a 40 Gbit/s data signal. The first laser is extracting a 40 GHz clock, which subsequently is injected into a 10 GHz laser. By using this approach, the pattern effects are suppressed in the sub-harmonic clock extraction as the injected signal into the second laser is a pulse train and not a data modulated signal. Finally a scheme reported in [3.19] and [3.20] has been used to suppress the phase jumps. A 160 Gbit/s OTDM data signal is injected into the laser and mode locking the laser, which is dimensioned to oscillate at either 40 [3.19] or 80 GHz [3.20]. At the output of the laser, a part of the clock signal is O/E

converted, electrical amplified and filtered by a high Q-filter before being re-applied to the laser section ensuring the fulfilment of mode locking. Using this configuration, a reduction of the phase jumps was reported – without stating the difference in stability of the extracted clock without the feedback loop. Notice, this configuration make the term all-optical clock extraction imprecise, and it could be argued that the scheme should be classified as opto-electronic clock extraction.

3.2.2 All optical CR: Self-pulsating lasers

Another clock extraction scheme is based on the self-pulsating laser. The scheme appears to be similar to the above-mentioned mode locking of a laser by a data signal, because the clock is extracted from the output of the laser after injecting the data signal into the laser. However, the physical mechanism responsible for the generation of a clock is quite different. One particular laser structure, which has been successfully used for clock extraction is the self-pulsating Distributed Feedback (DFB) laser. It consists of 3 different sections, i.e. phase tuning, laser and reflector section [3.21]. The amplitude reflectivity of the laser is very wavelength sensitive, with a sinc-like shape [3.21]. By dimensioning the laser, so the wavelength at which the laser will oscillate at is situated at the steep negative slope of the amplitude reflectivity, a small controlled variation of the oscillation wavelength will induce a large variation in the threshold conditions of the laser. For a given applied current to the gain section of the laser, a low reflectivity corresponds to a high loss in the cavity, which by proper dimensioning of the laser results in a build up of gain without the threshold conditions being fulfilled, i.e. gain equals loss. When the reflectivity of the laser is momentarily increased, the build-up gain immediately fulfils the threshold conditions and Q-switched pulses can be generated and emitted from the laser [3.11]. The designed laser reported in [3.21] can emit pulses without external influence, hence the designation Self-Q-Switching. However, the Q-switching can also be controlled by injecting high power data pulses into the laser. The amplitude modulation of the data signal will, through the alfa-factor, induce a wavelength modulation, and consequently induce the necessary variation in amplitude reflectivity [3.21]. Using this approach, the injected data signal Q-switches the laser, and the emitted pulses are synchronised to the input data signal, i.e. the clock is extracted. Implementing this laser in a 160 Gbit/s OTDM system, it was demonstrated how a 40 GHz optical clock could be extracted from the data signal and subsequently applied to the Electroabsorption Modulator constituting the demultiplexing circuit, resulting in error free operation [3.22]. It appears that the utilisation of a self-pulsating laser for clock extraction requires a pre-processing of the data signal in order to ensure that a amplitude modulation with a repetition frequency corresponding to the base rate of the OTDM signal is present. In [3.22] the

clock recovery device was situated after the switch used for demultiplexing. The set-up demonstrates one of the advantages of the device, even though it requires optical pre-processing the actual pre-processing is identical to the demultiplexing of the signal, and hence does not introduce more components than the actual laser. This is opposed to the Phase Locked Loops discussed later in this chapter, where an optical phase detector equivalent to the required pre-processing when using self-pulsating lasers, is required. For the clock to be extracted using a PLL, the incoming data signal and the local clock needs to be in phase quadrature, and consequently the output signal of the OPD is not the optimum demultiplexed signal and accordingly two different switches are needed, one for the OPD and one for switching and demultiplexing, see Figure 3.10. If the self-pulsating laser is used in a transmission system, a start-up procedure is required whenever the system is switched on or after a break down. How this procedure is envisioned, is not elaborated in literature yet.

The clock signal at the output of the laser is sinusoidal shaped, which is ideal when the demultiplexing circuit is an Electroabsorption modulator. However, if narrow pulses are used to control the demultiplexing circuit as e.g. required in a Non-linear Optical Loop Mirror (NOLM), see chapter 4, some pulse compression is needed. Standard pulse compression techniques can be applied [3.23], enhancing the possible applications of the laser, keeping the demultiplexing and the clock extraction in the optical domain, as opposed to [3.22]. Pulse compression can introduce some significant delay in the set-up due to the length of fibre required, which can deteriorate the stability of the feedback loop. According to [3.24] phase slips are a potential problem, but this problem has not been addressed yet in details for the self-pulsating laser.

3.2.3 Opto-electronic CR: Opto-Electronic Oscillators

In the category of opto-electronic clock extraction, two types have been reported – Opto-Electronic Oscillators (OEO) and OE-PLL.

The Opto-Electronic Oscillator is in principle a simple feedback loop, in which an optical signal is amplitude modulated at a specific frequency corresponding to the clock. The modulated signal is amplified and filtered around the modulation frequency, before it is reapplied to the amplitude modulator. In [3.25] an oscillator was constructed based on a loop consisting of a Mach-Zehnder modulator, a photo detector for converting the optical signal to the electrical domain, electrical amplification, and Q-filtering before the sinusoidal electrical signal is applied as control signal to the modulator. It was investigated how the bias point could determine the behaviour of the feedback loop, i.e. if the loop was bi-stable, oscillating or chaotic. From a clock extraction point-of-view, a stable signal is required, hence the oscillating mode are the design

criteria. OEO's have attracted attention due to the relative simple configuration, and especially Mr. X. S. Yao has treated OEO's in dept both as optical oscillators and as clock recovery circuits see e.g. [3.26], [3.27], [3.28] and [3.29]. Clock extraction was demonstrated, but the results were not directly applicable to OTDM systems. In [3.30] a scheme for base rate clock extraction from an OTDM signal, based on a slightly modified feedback loop, is proposed. In [3.30] a clock extraction circuit for extracting a 2.5 GHz clock from a 10 Gbit/s data signal and extraction of a 10 GHz clock from a 40 Gbit/s data signal are demonstrated, showing the potential of the scheme. The scheme was further refined, and by using a tandem Electroabsorption Modulator (EAM), modulating the first EAM at 10 GHz and the second at 20 GHz, a suitable clock to demultiplex an 80 Gbit/s data signal was generated [3.31]. By modulating the second EAM with a 40 GHz tone, clock extraction from 160 Gbit/s was realised [3.32]. Later, the scheme was implemented using only a single EAM, and clock extraction of a 40 GHz clock from a 320 Gbit/s polarisation multiplexed data signal [3.33] and from a 160 Gbit/s OTDM signal was demonstrated [3.34].

3.2.4 Opto-Electronic CR: Opto-Electronic Phase Locked Loop

The final opto-electronic scheme addressed in this summary is the Opto-Electronic Phase Locked Loop, which like the OEO is based upon a feedback loop. The operational behaviour of the basic Phase Locked Loop can be described as follows. A phase detector compares the phase of the incoming signal with a local generated clock, and generates a signal, which reflects the difference in frequency and phase. The output signal of the phase detector is after some optional filtering applied to a Voltage Controlled Oscillator (VCO), which adjusts the frequency and phase of the local clock, in order to ensure a match between the two signals, i.e. clock extraction [3.6]. In classic PLL theory, the phase detector is designed by means of electronics. However, in order to implement the PLL in an OTDM system where the bit rates are beyond the bandwidth of electronics, optical implementations of the phase detector are required. Using sufficiently fast optical processes compared to the incoming OTDM signal, signals with information of the relative phase difference between the incoming signal and the local clock can be generated. This principle is illustrated in Figure 3.2, where an optical switch suitable for optical demultiplexing is used as the OPD. A local clock generates a pulse train, which is used to induce a Switching Window within the switch. The output power of the OPD is directly related to the relative position, i.e. phase difference, between the control pulses and the data pulses, see Figure 3.2. Converting this signal to the electrical domain by a photo diode and applying it to an electrical PLL, which controls the clock laser, it can be used to extract the clock. Notice,

that the repetition frequency of the control pulses corresponds to the base rate of the OTDM signal.

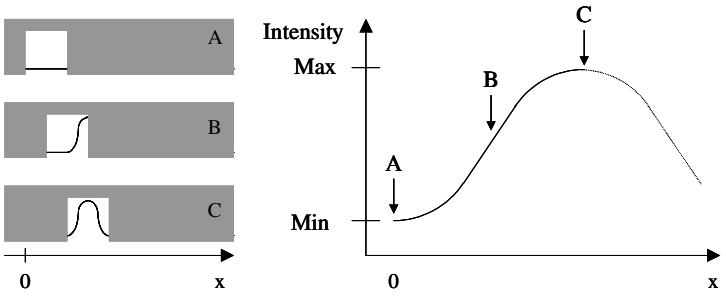

Figure 3.2: Principle of operation for an OPD. The output power of the OPD is a function of the relative position between the Switching Window (in grey) and the data signal.

The technique has successfully been applied to OTDM systems using a number of different optical processes. A 6.3 GHz clock extracted from a 400 Gbit/s data signal using FWM in a SOA for phase comparison, represents clock recovery demonstration from the highest aggregated bit rate presently [3.35]. FWM in SOAs is attractive, as the phase detector, i.e. the SOA, potentially can be monolithically integrated with the local pulse source, simplifying the set-up[16]. In [3.36] the first demonstration of FWM in a SOA using mode-locked lasers for clock extraction was shown, and a 10 GHz clock was extracted from a 160 Gbit/s OTDM data signal, see section 3.7. Other phase detectors implemented in a PLL for clock extraction from OTDM signals are e.g. Cross Gain Modulation (XGM) in SOAs as theoretical predicted in [3.37] and demonstrated in [3.38] where a 6.3 GHz clock was extracted from a 50 Gbit/s data signal. In principle, devices including processes suitable for signal processing at high bit rates can be exploited as the phase detector, hence also Non-Linear Optical Loop Mirrors (NOLM) have been implemented to extract a 10 GHz clock from a 40 Gbit/s data signal [3.39] and 10 GHz Clock Recovery from a 80 Gbit/s data signal [3.40]. Also a SOA in a Sagnac interferometric structure has been used for 10 GHz clock extraction from a 160 Gbit/s data signal [3.41]. Finally, the EAM has attracted significant attention in recent time, partly due to the simplicity of the device and the fact that the device fabrication has reached a high degree of maturity demonstrating sufficiently high bandwidth for signal processing at 160 Gbit/s. In [3.42] two concatenated EAMs were used as the optical phase comparator – the configuration generated

[16] Furthermore, it will reduce the inherent loop delay due to pulse propagation in the configuration, which increases the stability of the loop. This is addressed in more detail in section 3.6.

a 10 GHz frequency component, which was converted to the electrical domain, before injected into a classic electrical 10 GHz clock recovery circuit. In [3.43] only a single EAM was required to obtain the same result.

Instead of generating an optical signal with the frequency corresponding to the clock repetition frequency from which the DC component is extracted, other techniques, which directly generate a DC component (or very low frequent signal) including the required phase information, can be envisaged. This DC component is used to directly control the VCO, reducing a part of the base rate electronics, e.g. 10 GHz electronics. In [3.44] the data signal and the local generated clock are injected bi-directionally into the device. By utilising the fast saturation and the slow recovery effects of the EAM, a control signal including the phase information can be generated and a 10 GHz clock from a 160 Gbit/s data signal was demonstrated. In [3.45] a bi-directional configuration is also implemented. By splitting the incoming data signal into two arms, delaying one signal in the order of 3 ps before injecting the two signals from opposite sides of the device, the optical power of the output signals will depend on the relative position in time of the signals compared to the local clock. By subtracting the two output signals, a control signal for the PLL can be generated. Also this scheme was used to demonstrate 10 GHz clock extraction from a 160 Gbit/s data signal. Finally, an elegant approach using the generated photo current in an EAM is shown in [3.46]. By using a special configuration, it appears that the phase from the clock is decoupled from the data signal, which allows for simultaneously demultiplexing and clock extraction using the same device. By concatenating two EAMs, it is demonstrated that the configuration can be used to extract a 10 GHz clock from a 160 Gbit/s data signal.

3.2.5 Design parameters for CR circuits

The short review presented above reveals that a number of techniques and approaches are available for base rate clock extraction from high bit rate OTDM signals. The techniques are still being developed and refined, and as a direct comparison between the schemes has not been presented yet, it is difficult if not impossible to argue which approach will be the preferred scheme. Furthermore, because OTDM is still a research topic, no standardisations exist. At the moment, developers can only make qualified guesses, on how OTDM systems will be implemented, and which requirements the sub-systems will need to fulfil. In the following, a list of topics is suggested, which could be relevant to compare the different OTDM clock recovery sub-systems.

- Total power consumption of the sub-system
- Physical size of the sub-system including control circuits

- The degree of integration of the sub-system, e.g. monolithically.
- If both the optical and electrical clock are available.
- If the sub-system can be used both to extract the base rate clock and the line rate clock.
- If the CR can be used in packet switched OTDM systems.
- If the optical clock signal is pulsed or sinusoidal.
- What the stability of the sub-system is, i.e. how long can it operate without loosing track of the clock.
- Can the optical clock be extracted without any interface to the electrical domain?
- The jitter of the extracted clock.
- The capture range of the clock recovery system, i.e. the frequency diversity between local clock and data signal, and still obtain clock extraction.

The all-optical schemes, i.e. mode-locked and the self-pulsating lasers, obviously require access to the components. Within the Danish National Technical Research Council programme SCOOP, mode-locked lasers have been designed and fabricated. As the development of these components has been very time consuming, although rewarding in the end, see e.g. [3.12], lasers adequate for clock extraction were not available before the end of this thesis and have consequently not been included in the work. Similarly, access to self-pulsating lasers, has only been available through short periods of time when performing joint experiments with partners within the European IST project TOPRATE. The two Opto-Electronic clock extraction techniques are both very interesting, and the published results indicate promising performance. From literature, comparison between all electrical injected locked oscillators and Phase Locked Loops demonstrate higher locking range (hold-in) and superior phase noise performance of the PLL [3.47]. However, it is unclear if these results can be directly transferred to opto-electronic versions of the schemes introduced in the review. Both designs still need analytical and experimental optimisation and refinement before comparing the performance of the schemes, a comparison, which is beyond the scope of this thesis. Albeit this analysis is still missing, the indicated reported superior phase noise performance combined with previous obtained acquaintance at COM•DTU, see e.g. [3.48], [3.49], [3.50], the OE-PLL based Clock Recovery circuits were chosen as the preferred choice for clock extraction for COM•DTU contribution to the European IST project TOPRATE.

3.3 Time domain PLL Theory

3.3.1 Basic theory for Phase Locked Loops

In Figure 3.3 the basic configuration of a PLL is shown. The PLL consists of a Phase Detector (PD), which compares the phase between the incoming data signal s(t) and the local clock c(t). The output of the PD is lowpass filtered with Loop Filter before the signal e(t) is applied to the VCO.

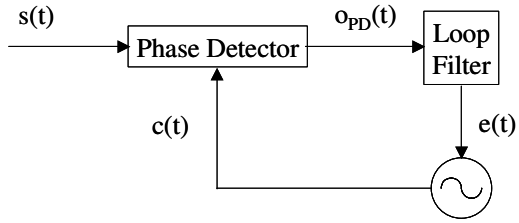

Figure 3.3: Basic Phase Locked Loop (PLL) configuration

Assume that the input signal s(t) can be written as

$$s(t) = S\cos\left(2\pi f_s t + \theta_s\right) \tag{3.1}$$

where f_s is the frequency of the data signal and θ_s is the initial phase of the signal. Assume that the PLL has just been switched on so the clock signal c(t) can be written as

$$c(t) = C\cos\left(2\pi f_c t + \psi_c\right) \tag{3.2}$$

Where f_c is the free-running frequency of the oscillator and ψ_s is the initial phase of the clock.

In the PD, the data signal is multiplied with the control signal. As the multiplication within the PD is characterised by a conversion loss α_{PD}, the output signal from the PD is

$$o_{PD}(t) = \alpha_{PD}\, s(t)\, c(t)$$
$$= \alpha_{PD}\frac{SC}{2}\left[\cos\left(2\pi\left(f_s - f_c\right)t + \left(\theta_s - \psi_c\right)\right) + \cos\left(2\pi\left(f_s + f_c\right)t + \left(\theta_s + \psi_c\right)\right)\right] \tag{3.3}$$

Introducing the conversion efficiency K_{PD} of the PD as ½ α_{PD} SC and filtering away the high frequency components with the loop filter, the control signal to the oscillator, e(t), can be written as

$$e(t) = K_{PD}\cos\left(2\pi\left(f_s - f_c\right)t + \left(\theta_s - \psi_c\right)\right) \tag{3.4}$$

The signal e(t) is applied to the VCO, which controls the output frequency of the local generated clock. After the loop is closed, the tuned clock signal can be written as

$$c(t) = C\cos\left(2\pi f_0 t + \theta_C\right) \tag{3.5}$$

If the frequency difference between s(t) and c(t) is sufficiently small[17], the PLL will adjust the frequency and the phase so the output frequency f_0 is equal to the data signal frequency f_S, leading to a control signal e(t) which is reduced to

$$e(t) = K_{PD}\cos\left(\theta_s - \theta_C\right) \tag{3.6}$$

A relation between the initial phase before and after locking can be derived by comparing the control signal e(t) before and after locking, see eq. (3.2) and (3.5)

$$\psi_c = 2\pi\left(f_s - f_c\right)t + \theta_C \tag{3.7}$$

The control signal e(t) controls the output frequency f_0 of the oscillator by the following relation, which assumes a linear relation between e(t) and f_0 characterised by the oscillator gain factor K_o

$$2\pi f_o = 2\pi f_c + K_o\, e(t) \tag{3.8}$$

Inserting the control signal e(t) for the locked loop, see eq. (3.6), into eq. (3.8), an expression for the output frequency f_0 is found

[17] The term sufficiently small is a design parameter, which can be found by using the techniques described in e.g. [3.7].

$$2\pi f_s = 2\pi f_o = 2\pi f_c + K_o\, e(t) = 2\pi f_c + K_o\, K_{PD} \cos(\theta_s - \theta_C) \quad (3.9)$$

From this expression the following relation can be derived

$$\theta_s - \theta_C = \text{Arccos}\left(\frac{2\pi(f_s - f_c)}{K_o\, K_{PD}}\right) \quad (3.10)$$

With this simplified description of the PLL locking performance, two important observations can be made.

- If the frequency difference between the free-running oscillator and the data signal is small compared to the product of K_oK_{PD} the phase difference between data signal and clock is 90°, i.e. the two signals are in phase quadrature when the PLL is locked.

- If the frequency of the free-running oscillator is not exactly equal to the frequency of the data signal, the locked PLL will include a control signal e(t) which is not exactly 0. However, as the gain factor K_oK_{PD} usually is large, the control signal is quit small.

Because the data signal and the clock are in phase quadrature when the PLL is locked, the data signal and clock signal are often expressed by sine and cosine, respectively, see e.g. [3.6]. Consequently, the control signal e(t) is usually written as

$$e(t) = K_{PD} \sin(\theta_s - \theta_C) \quad (3.11)$$

This convention is used in the rest of this thesis, unless otherwise stated. In section 3.6 the stability of the PLL is addressed by means of the Laplace transformation. The analysis is based on the linear approximation, which in the time domain can be written as

$$e(t) \approx K_{PD} (\theta_s - \theta_C) \quad (3.12)$$

which is true for $\theta_S - \theta_C \ll 1$, see section 3.6.

3.3.2 OTDM CR based on PLL configuration

The simplified configuration in Figure 3.3 was used to extract the clock from a signal s(t), which in an implemented system would represent the data signal. Obviously, the signal s(t) used in the previous section did not contain any

information as the signal was represented by a pure cosine tone. The objective of this section is to modify the configuration in Figure 3.3 to extract the clock at the base rate f_B from the incoming OTDM signal with the aggregated frequency f_s.

Assuming that an OTDM signal is generated by ideal multiplexing of N time channels – it can be shown that the OTDM signal with an aggregated bit rate of $f_s = Nf_B$ has a power spectrum, which consists of both a continuous spectrum and of discrete frequency components, situated at 0, $\pm f_s$, $\pm 2f_s$ etc [3.1]. Neglecting the continuous spectrum the data signal s(t) can be written in a Fourier series as

$$s(t) = S_0 + 2\sum_{j=1}^{\infty} \left|S_j\right| \sin\left(2\pi j f_s t + \theta_{js}\right) \qquad (3.13)$$

Where S_0 is the average (power) of the signal, $\left|S_j\right|$ is the amplitude of the j^{th} Fourier coefficient and θ_{js} is the associated phase. Notice that the sinus and not cosine has been used in the Fourier series, as it was shown in the previous section that the data and clock signal should be in phase quadrature in order to lock, and consequently the notation is arranged in anticipation of this fact.

Using the same configuration as in Figure 3.3 the control signal c(t) would be represented as

$$c(t) = C\cos\left(2\pi f_o t + \theta_C\right) \qquad (3.14)$$

where f_o should lock to the base rate f_B of the OTDM signal. However, the multiplication between s(t) and c(t) would not generate a low frequent control signal e(t). When the OTDM signal consists of N channels, the lowest frequency component would be (N-1) f_s. This obstacle can be overcome by introducing a non-linear transfer function[18] between the oscillator and the Phase Detector as shown in Figure 3.4.

[18] The non-linear transfer function is an abstraction in order to maintain the generality. However, physically the non-linear function could be implemented by applying the electrical sinusoidal signal from the oscillator to a laser, which would generate a pulse train of narrow pulses.

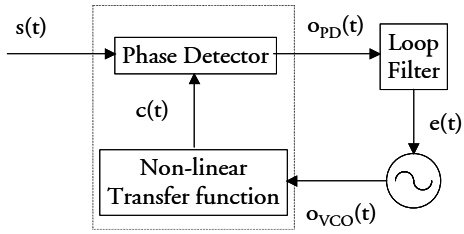

Figure 3.4: PLL configuration for accommodating base rate clock extraction from an OTDM signal

The impact of the non-linear transfer function is shown in Figure 3.5 where the sinusoidal clock from the oscillator with the repetition frequency, which approximately corresponds to the base rate of the OTDM signal, is transformed to narrow pulses. The repetition frequency, i.e. the fundamental frequency, of the pulses is f_o, but also higher order harmonic frequencies are introduced, as shown in Figure 3.5.

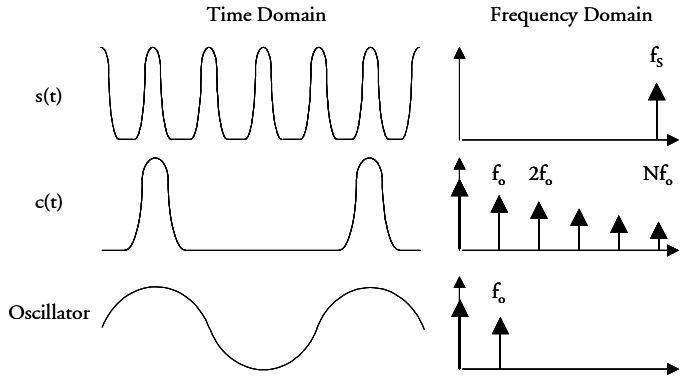

Figure 3.5: The impact of the non-linear transfer function used to introduce frequency components in the clock signal at the data frequency f_s, which corresponds to the aggregated bit rate of the OTDM signal composed by N time channels with base rate frequency of f_B.

From Figure 3.5 it can intuitively be seen that a multiplication between the control signal and the data signal s(t) will produce a DC signal e(t) for the N^{th} harmonic of the clock signal, if $f_o = f_B$, or a low frequent signal e(t) if f_o is close to f_B. Using the same formalism for c(t) as for s(t), i.e. decompose the clock signal into the Fourier series as[19]

[19] It is assumed that a function relating θ_C and θ_{mc} exists. If the phase difference between (θ_C - θ_{mc}) ≠ 0, the static phase difference will be tracked by the PLL [3.7], and thus not prevent clock extraction. The relation between θ_C and θ_{mc} will be assumed in the rest of the chapter.

$$c(t) = C_0 + 2\sum_{m=1}^{\infty} |C_m| \cos\left(2\pi m f_o t + \theta_{mc}\right) \tag{3.15}$$

The output of the PD is calculated as a multiplication between data signal and clock signal are expressed as

$$\begin{aligned} o_{PD}(t) &= \alpha_{PD}\, s(t)\, c(t) \\ &= \alpha_{PD} \left\{ S_0 + 2\sum_{j=1}^{\infty} |S_j| \sin\left(2\pi j f_s t + \theta_{js}\right) \right\} \\ &\quad \left\{ C_0 + 2\sum_{m=1}^{\infty} |C_m| \cos\left(2\pi m f_o t + \theta_{mc}\right) \right\} \end{aligned} \tag{3.16}$$

The low frequency control signal e(t) after the loop filter, which has a bandwidth << f_0, can be derived to (j=1 and m=N)

$$e(t) = \alpha_{PD} S_0\, C_0 + 2\alpha_{PD} S_1\, C_N \sin\left(2\pi\left(f_s - N f_o\right)t + \left(\theta_{1s} - \theta_{Nc}\right)\right) \tag{3.17}$$

when neglecting the low frequent components originating from higher harmonics of s(t) and c(t), e.g. (S_2 , C_{2N}) and (S_3 , C_{3N}) as the power in these frequency components are typically very low compared to (S_0 , C_0) and (S_1 , C_N).

If the frequency difference is sufficiently small, the PLL will adjust the frequency and the phase of the VCO so the PLL is locked to the base rate of the OTDM signal and the control signal e(t) can be written as

$$\begin{aligned} e(t) &= \alpha_{PD} S_0 C_0 + 2\alpha_{PD} S_1 C_N \sin\left(\theta_{1s} - \theta_{Nc}\right) \\ &\triangleq K_{DC} + K_{PD} \sin\left(\theta_{1s} - \theta_{Nc}\right) \end{aligned} \tag{3.18}$$

Where the DC conversion efficiency K_{DC} has been defined as $\alpha_{PD} S_0 C_0$ and the phase detector conversion efficiency, K_{PD} has been defined as $2\alpha_{PD} S_1 C_n$. When the phase difference is zero, i.e. phase quadrature between s(t) and c(t), the control signal e(t) should be zero (neglecting the error signal required to adjust the output frequency from the free running frequency of the oscillator as described in the previous section). As can be seen from eq. (3.18), a constant DC level originating from S_0 and C_0 introduce an offset in e(t). In order to enable extraction of the clock corresponding to the base rate of the data signal

s(t), this offset has to be compensated. This is addressed in section 3.4, where four different schemes for compensating this DC component are analysed.

This section demonstrated how a non-linear transfer function applied to the sinusoidal clock from the oscillator introduces higher harmonics of the oscillator frequency, enabling a Phase Detector to generate a low frequent control signal, which can be used in a PLL to track a clock corresponding to the base rate of the OTDM signal.

3.3.3 Example on control signal for PLL

Before proceeding in the design of a PLL based Clock Recovery, an example based on an OTDM configuration is provided. In Figure 3.6 a simplified OTDM transmitter is shown. The pulse source generates a 10 GHz pulse train of Gaussian pulses with temporal FWHM width of 2.5 ps corresponding to 0.40 times the timeslot for a 160 Gbit/s system, see [3.51] and chapter 2. The pulse train is split into 16 branches, each branch including an external modulator modulating each pulse train with a Pseudo Random Bit Sequence (PRBS) of 2^7-1. Each modulated bit stream is delayed with an appropriate time delay before multiplexed together. If the time delays are designed correctly, the aggregated OTDM signal maintains the PRBS properties of each data channel, see [3.52]. The generated OTDM signal is injected into an optical switch, which is modulated by a 2.34 ps FWHM Gaussian 10 GHz pulse train[20]. The bandwidth of the switch is assumed infinite, and the introduced SW is an exact replica of the control pulse. The output signal of the switch consequently corresponds to a multiplication of the data signal and the control pulses. By varying the position in time of the SW relative to the OTDM signal, and monitor the DC power corresponding to each position of the SW, the control signal for the oscillator can be determined.

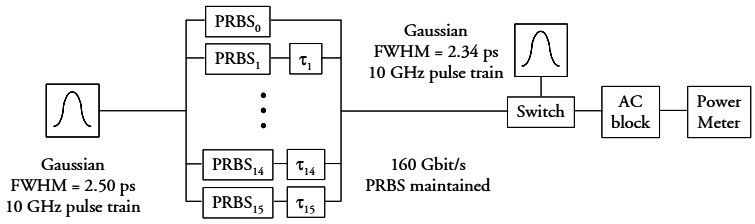

Figure 3.6: OTDM transmitter generating 160 Gbit/s mixed with a 10 GHz pulse train in the mixer. The output signal from the mixer is low-pass filtered by an AC block, i.e. only DC is transmitted through the filter. The output of the filter corresponds to the control signal of the PLL.

[20] The reason for this choice is found in section 3.5

In Figure 3.7 a part of the bit pattern of the 160 Gbit/s OTDM signal is shown together with the corresponding spectrum. Notice the discrete frequency components at DC, 160 and 320 GHz as predicted. In Figure 3.8 a part of the 10 GHz Gaussian clock pulse train is shown with the corresponding spectrum. Notice that the spectrum includes discrete frequency components at 16th harmonic, which is used to generate the control signal.

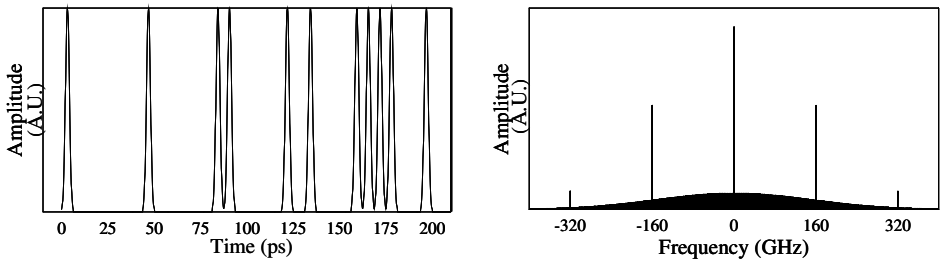

A B

Figure 3.7: (A) pattern of 160 Gbit/s signal with PRBS 2^7-1 (B) corresponding spectrum

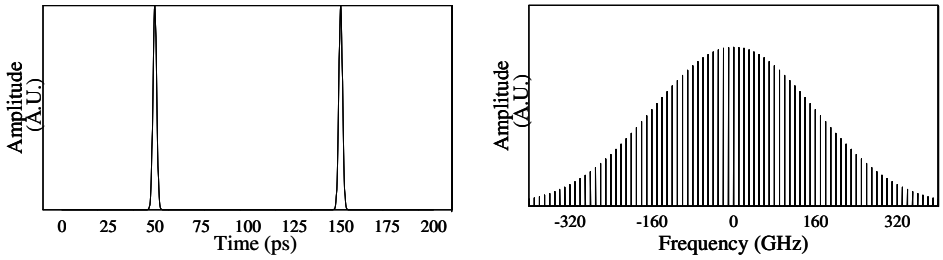

A B

Figure 3.8: (A) pattern of 10 GHz Gaussian pulse train (B) corresponding spectrum

In Figure 3.9 the control signal after the filter is shown as function of the relative time difference between a Gaussian clock pulse and the time-slot of the OTDM signal. It demonstrates the sinusoidal variation of the control signal as function of the time position, i.e. the phase, of the clock signal.

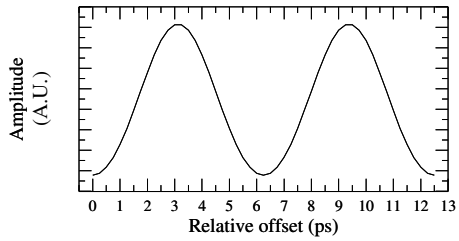

Figure 3.9: Control signal for PLL as function of relative offset between OTDM signal and clock pulse train

Instead of calculating the DC level of the demultiplexed signal, the control signal can, according to the theory derived in the previous sections, be calculated from the Fourier coefficients. This was confirmed by extracting the Fourier coefficients S_0, S_1, C_0 and C_{16} from the spectra in Figure 3.7 and 3.8 and inserting the values into eq. (3.18) and calculating the control signal e(t) showing a perfect match with the depicted results in Figure 3.9.

Figure 3.9 also illustrates how a non-zero control signal e(t) is present, even when the phase quadrature requirement is fulfilled. In order to obtain reliable clock extraction, the DC component has to be compensated, which is addressed in the compensation technique survey in next section. Assuming that the DC component in Figure 3.9 was compensated, the control signal e(t) would show a sinusoidal variation around zero as function of the relative time delay. Due to this variation, e(t) is equal to zero for two different delays, indicating two different operation points for the PLL, where the clock is locked to the data signal. However, in [3.8] the two potential operation points are analysed, concluding that one of the points represents an unstable solution. On Figure 3.9 the zero operation point on the positive slope represents the stable solution, i.e. locking, and the zero operation point on the negative slope represents the unstable solution, i.e. false locking.

It is important to notice, that the output signal from the optical switch when the PLL is locked, does not represent an optimum demultiplexed time channel of the OTDM signal. This is illustrated in Figure 3.10, where the 160 Gbit/s signal from the example above, is demultiplexed with a SW situated in-phase, phase quadrature and out-off-phase.

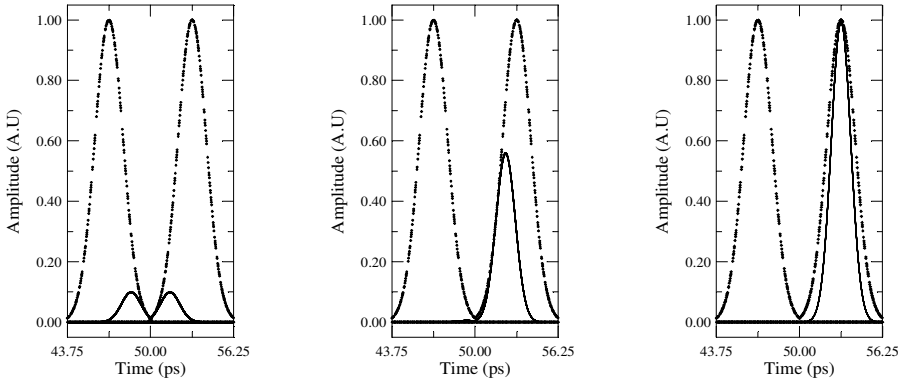

Figure 3.10: 160 Gbit/s data signal (dotted lines) multiplied a clock pulse. The output of the optical switch (full line) is calculated for 3 different situations A) Out-of-phase B) Phase quadrature and C) In-phase

As the eye-diagram in Figure 3.10 B is open and clear, despite of the amplitude and pulse width decrease, the signal could in principle be detected in a receiver. However, compared to the eye-diagram in Figure 3.10 C, an extra introduced power penalty would be expected. If it is required to use the same switch for both optical demultiplexing and clock extraction using OPD based PLL, two different approaches can be used, see [3.53] and configuration four in the next section [3.39].

3.4 Compensation of constant DC component

The following section presents four different techniques for compensating the DC component without any information about the phase difference. The schemes are extracted from existing literature, and one of the techniques is chosen for further investigations within this thesis.

3.4.1 Configuration 1

The constant DC level originating from the DC components from the signal s(t) and the clock pulses c(t) need to be compensated, and consequently the proposed configuration in Figure 3.2 needs to modified. The simplest modification is to subtract a fixed DC signal at the output from either the Phase Detector or the loop filter as illustrated in Figure 3.11.

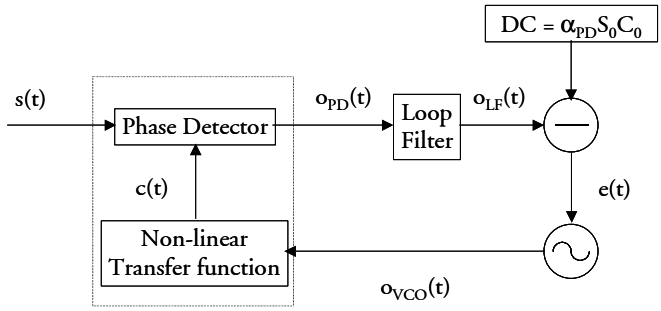

Figure 3.11: Suggested configuration 1 for compensating DC component

Using this configuration the DC component is compensated and the control signal e(t) will only contain information about the phase difference between s(t) and c(t), and consequently the PLL will be able to extract the clock from the data signal. The control signal e(t) can, by modifying the results obtained in eq. (3.18), be written as

$$e(t) = \alpha_{PD}S_0C_0 + 2\alpha_{PD}S_1C_N\sin\left(\theta_{1s}-\theta_{Nc}\right) - DC \tag{3.19}$$

The disadvantage of the scheme can be illustrated by introducing a perturbation Δ in the DC component of the data signal. The new DC component $S_{0\Delta}$ can be written as

$$S_{0\Delta} = S_0\left(1+\Delta\right) \tag{3.20}$$

According to eq. (3.18) the control signal e(t) is then written as

$$\begin{aligned} e(t) &= \alpha_{PD}S_{0\Delta}C_0 + 2\alpha_{PD}S_1C_N\sin\left(\theta_{1S}-\theta'_{NC}\right) - \alpha_{PD}S_0C_0 \\ &= \Delta\alpha_{PD}S_0C_0 + 2\alpha_{PD}S_1C_N\sin\left(\theta_{1S}-\theta'_{NC}\right) \end{aligned} \tag{3.21}$$

Where θ'_{NC} is the phase of the clock when tracking the perturbation Δ. If Δ, and hereby the control signal e(t) is different from zero, the PLL will adjust the phase of the oscillator in order to minimise e(t). Obviously, this is not correct as the phase position within the data signal has not changed, and consequently the extracted clock due to the perturbation will introduce an offset in the timing of the demultiplexing and the decision circuit.

Assuming that the new phase θ'_{NC} can be written as the correct phase θ_{NC} and an offset phase $\Delta\theta_{NC}$

$$\theta'_{NC} = \theta_{NC} + \Delta\theta_{NC} \tag{3.22}$$

The introduced phase due to the perturbation can from eq. (3.21) be derived to

$$\Delta\theta_{NC} = \mathrm{Arcsin}\left(\Delta \frac{S_0 C_0}{2 S_1 C_N} \right) \tag{3.23}$$

Using the Fourier coefficients S_0, S_1, C_0 and C_{16} from the pervious example, the introduced phase offset due to the perturbation can be calculated. In Figure 3.12 the introduced phase offset has been converted to the timing offset within the timeslot of a 160 Gbit/s signal, and is shown as function of the logarithmic perturbation, i.e. $10*\log(S_{0\Delta}/ S_0)$.

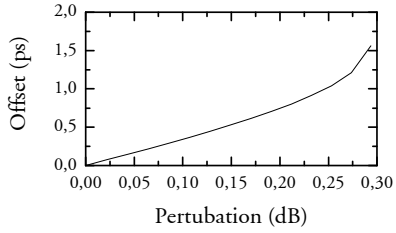

Figure 3.12: Offset in ps as function of the perturbation for set-up shown in Figure 3.11.

In the example the pulse width of the data signal, T_{FWHM}, was 2.5 ps. Comparing with Figure 3.12 and introducing a very relaxed maximum tolerable offset of the clock within the decision circuit[21] of quarter the pulse width, the amplitude fluctuations should still be less than 0.17 dB. Indicating that a very strict control with the amplitude fluctuations at the input to the phase detector is required. Furthermore, an increase of the DC component in the data signal of ~ 0.30 dB will for this set-up prevent the PLL from for tracking the clock at all as the DC level is higher than the 1.

3.4.2 Configuration 2

A more robust configuration in terms of DC fluctuations has been proposed in literature [3.54][3.41], and is shown in Figure 3.13.

[21] This example should only be used as an illustration of the strict requirements to the amplitude tolerances and not as a design requirement of the receiver.

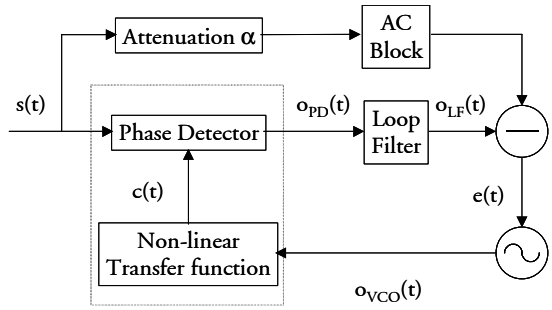

Figure 3.13: Suggested configuration 2 for compensating DC component

The data signal s(t) is split into two branches – one branch includes the Phase Detector and the other branch includes an attenuation α of the data signal and a lowpass filter, which in the ideal case can be regarded as an AC block, thus only S_0 in eq. (3.13) is passing the AC block. By adjusting α to fulfil the following relation

$$\alpha S_0 = \alpha_{PD} S_0 C_0 \tag{3.24}$$

The control signal e(t) can be expressed as

$$\begin{aligned} e(t) &= \alpha_{PD} S_0 C_0 + 2\alpha_{PD} S_1 C_N \sin(\theta_{1S} - \theta_{NC}) - \alpha S_0 \\ &= 2\alpha_{PD} S_1 C_N \sin(\theta_{1S} - \theta_{NC}) \end{aligned} \tag{3.25}$$

as required for the PLL. If a perturbation is introduced in the DC component of the data signal, similar to the treatment of configuration 1, e(t) will be expressed as

$$\begin{aligned} e(t) &= \alpha_{PD} S_{0\Delta} C_0 + 2\alpha_{PD} S_1 C_N \sin(\theta_{1S} - \theta_{NC}) - \alpha S_{0\Delta} \\ &= 2\alpha_{PD} S_1 C_N \sin(\theta_{1S} - \theta_{NC}) \end{aligned} \tag{3.26}$$

where the definition of α is used. The expression for the control signal demonstrates how the impact of possible amplitude fluctuations is reduced by a relatively simple modification of the basic configuration shown in Figure 3.4.

3.4.3 Configuration 3

In Figure 3.14 a more complicated, but very successful configuration is shown [3.35] [3.38]. The configuration is based on the set-up shown in Figure 3.4 with some additional components, i.e. a low-frequent oscillator characterised by a fixed frequency f_Δ and a phase θ_Δ, a Single Side Band (SSB) modulator, a 'N' times frequency doubler[22] and finally an additional mixer. With this modified configuration the two terms in eq. (3.18) will be decoupled.

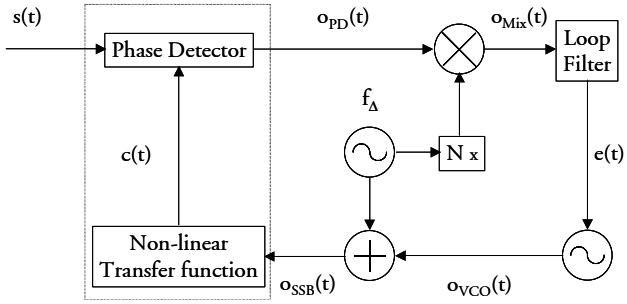

Figure 3.14: Suggested configuration 3 for compensating DC component. Notice the symbol $\oplus$ in this configuration represents Single Sideband Modulation of the oscillator frequency.

The output signal from the oscillator, characterised by f_0 and θ_0, is frequency shifted in the SSB modulator, with a fixed frequency corresponding to the f_Δ. The sinusoidal input signal to the Non-linear Transfer function can expressed as

$$o_{SSB}(t) = K_{SSB} \cos\left(2\pi\left(f_0 + f_\Delta\right)t + \theta_c\left(\theta_0, \theta_\Delta\right)\right) \qquad (3.27)$$

where the conversion efficiency of the SSB modulator, K_{SSB}, has been introduced along with the phase θ_c, which is a function of the phases θ_0 and θ_Δ of the incoming signals. Notice, that the SSB modulator only generates the sum-frequency of the incoming signals (or alternatively the frequency difference).

The clock signal c(t), when assuming a fixed relation between θ_C and θ_{mc}, is then expressed as

[22] N corresponds to the number of OTDM channels.

$$c(t) = C_0 + 2\sum_{m=1}^{\infty} |C_m| \cos\left(2\pi m\left(f_o + f_\Delta\right)t + \theta_{mc}\right) \qquad (3.28)$$

where the conversion efficiency K_{SSB} is included in the Fourier coefficients. After multiplication with the data signal in the Phase Detector, the low-frequent terms at the output of the PD are

$$o_{PD}(t) = \alpha_{PD} S_0\, C_0 + 2\alpha_{PD} S_1\, C_N \sin\left(2\pi\left(f_s - N\left(f_o + f_\Delta\right)\right)t + \left(\theta_{1s} - \theta_{Nc}\right)\right) \qquad (3.29)$$

This signal is the input to the mixer as indicated on Figure 3.14. The other input signal to the mixer is the output signal f_Δ frequency doubled to N times the input frequency as shown in eq. (3.30) below

$$\cos\left(2\pi N f_\Delta t + \theta_{N\Delta}\left(\theta_\Delta\right)\right) \qquad (3.30)$$

where the phase $\theta_{N\Delta}$ is a function of the input phase θ_Δ. When omitting the function description of $\theta_{N\Delta}$ and θ_{Nc} for convenience, the low frequent parts of the signal at the output of the mixer can be described by the following 3 terms

$$o_{MIX}(t) = \begin{cases} 2\alpha_{PD} S_1 C_N \sin\left(2\pi\left(f_s - N f_o\right)t + \left(\theta_{1s} - \theta_{Nc} + \theta_{N\Delta}\right)\right) + \\ \alpha_{PD} S_0 C_0 \sin\left(2\pi N f_\Delta t + \theta_{N\Delta}\right) + \\ 2\alpha_{PD} S_1 C_N \sin\left(2\pi\left(f_s - N\left(f_o + 2f_\Delta\right)\right)t + \left(\theta_{1s} - \theta_{Nc} - \theta_{N\Delta}\right)\right) \end{cases} \qquad (3.31)$$

Using this technique, it can be observed how the two DC components at the output of the Phase Detector are decoupled, and now situated at different frequency components. Assuming that the bandwidth of the loop filter is larger than $(f_s - Nf_o)$ and less than Nf_Δ, the control signal e(t) is then expressed as

$$e(t) = 2\alpha_{PD} S_1 C_N \sin\left(2\pi\left(f_s - N f_o\right)t + \left(\theta_{1s} - \theta_{Nc} + \theta_{N\Delta}\right)\right) \qquad (3.32)$$

If the frequency difference $(f_s - Nf_o)$ is sufficiently small, the control signal applied to the oscillator will tune the output frequency and phase in order to maintain a control signal e(t) = 0. In other words, the configuration shown in Figure 3.14 can be used to extract the clock at the base rate of the OTDM signal.

Introducing a perturbation Δ, so the DC component of the input data signal can be written as $S_{0\Delta} = S_0(1+\Delta)$, it can be concluded due to the decoupling of

the components, that the perturbation will not have an influence on the control signal e(t), and consequently on the clock extraction.

Assuming that the frequency at the output of the oscillator is adjusted to match the base rate frequency of the OTDM signal, a few remarks addressing the phase terms in e(t) can be made. Defining the total phase θ_{tot} as

$$\theta_{tot} = \theta_{1s} - \theta_{Nc}(\theta_o, \theta_\Delta) + \theta_{N\Delta}(\theta_\Delta) \tag{3.33}$$

Introducing an assumed linear dependency characterised by the constants k_1, k_2 and k_3, the total phase is expressed as

$$\theta_{tot} = \theta_{1s} - (k_1\theta_o + k_2\theta_\Delta) + k_3\theta_\Delta \tag{3.34}$$

It is observed that the scheme introduces a constant offset phase defined by the phase θ_Δ, which can be equal to zero depending on the mixer and the SSB. The oscillator will adjust the phase θ_o to include this offset phase, but this will not influence the clock extraction process. Within system context, a constant offset of the clock does not affect the performance of the system, as the offset can be eliminated by fixed time delays to e.g. the switches used for demultiplexing or the decision circuit.

Configuration 3 has been demonstrated successful at high bit rates. However, some disadvantages of the configuration exist. The frequency of the offset frequency should be very carefully chosen, as the bandwidth of the loop filter should be sufficiently high in order to track frequency derivations between signal and oscillator, but sufficiently low to filter out the offset frequency components. A drawback of configuration 3 is the complexity, introducing several components, which potentially can deteriorate the signal, e.g. the SSB and the 'N' times frequency doubler can introduce other frequency components than those described in the previous sections due to imperfections. Finally, the pulse train c(t) is not the clock, but the clock added a low frequent offset frequency. If the implemented OTDM system requires narrow pulses synchronised to the clock, e.g. for demultiplexing, the sinusoidal clock at the output of the oscillator should be tapped and applied to a pulse generator.

Finally, it should be remarked that, as the Switching Window continuously sweep across the data signal, there is no fixed relation between the position of the SW and the data signal. This is opposed to the situation in the basic configuration in Figure 3.3 and configuration 1 and 2 in Figure 3.13 and 3.14.

3.4.4 Configuration 4

In Figure 3.15 a configuration, which with only a few exceptions appears to be similar to the configuration in Figure 3.14, is shown. However, although there are some similarities in the set-up and in the principle, it still constitutes a significantly different operation, see [3.39]. Consequently the technique will be described in the following section.

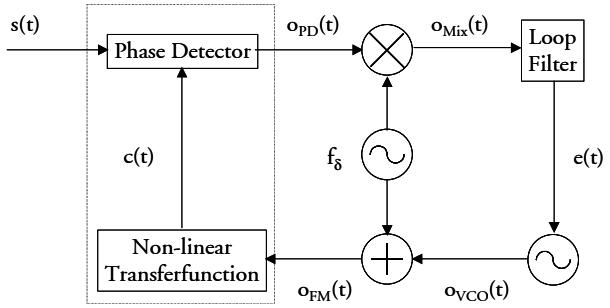

Figure 3.15: Suggested configuration 4 for compensating DC component. Notice the symbol $\oplus$ in this configuration represents Frequency Modulation of the oscillator frequency.

In order to simplify the initial description of the principle of operation, the input data signal s(t) is assumed to be a single sinusoidal tone

$$s(t) = \sin\left(2\pi f_S t + \theta_S\right) \tag{3.35}$$

The output signal from the Voltage Controlled Oscillator is Frequency Modulated (FM) with a modulation index β_m and a frequency f_δ, sometimes referred to as the dither frequency. The FM signal originates from an additional frequency generator, as shown in Figure 3.15. If the non-linear transfer function is bypassed in the initial description, the clock signal c(t) is written as [3.1]

$$c(t) = \cos\left(2\pi f_o t + \theta_C + \beta_m \sin\left(2\pi f_\delta t\right)\right) \tag{3.36}$$

Notice that the phase quadrature relation between s(t) and c(t) is maintained, i.e. s(t) corresponds to sinus and c(t) corresponds to cosine. The output signal of the PD, $o_{PD}(t)$, is calculated as the multiplication between s(t) and c(t). Assuming that the modulation index $\beta_m \ll 1$, the signal $o_{PD}(t)$ can be expressed as

$$o_{PD}(t) \approx \alpha_{PD}\sin\left(2\pi f_S t + \theta_S\right) \left\{\cos\left(2\pi f_o t + \theta_C\right) - \sin\left(2\pi f_o t + \theta_C\right)\beta_m \sin\left(2\pi f_\delta t\right)\right\}$$

$$= \begin{cases} 0.5\,\alpha_{PD}\sin\left(2\pi\left(f_S - f_o\right)t + \theta_S - \theta_C\right) + \\ 0.5\,\alpha_{PD}\sin\left(2\pi\left(f_S + f_o\right)t + \theta_S + \theta_C\right) + \\ 0.5\,\alpha_{PD}\cos\left(2\pi\left(f_S - f_o\right)t + \theta_S - \theta_C\right)\beta_m \sin\left(2\pi f_\delta t\right) - \\ 0.5\,\alpha_{PD}\cos\left(2\pi\left(f_S + f_o\right)t + \theta_S + \theta_C\right)\beta_m \sin\left(2\pi f_\delta t\right) \end{cases} \quad (3.37)$$

From this expression an important observation of the principle can be made. If the frequency of the input signal and the clock is identical, i.e. $f_S = f_o$, two low frequent components are identified, and the output signal of the PD is expressed as

$$o_{PD}(t)\Big|_{f_o = f_S} = \begin{cases} 0.5\,\alpha_{PD}\sin\left(\theta_S - \theta_C\right) + \\ 0.5\,\alpha_{PD}\sin\left(4\pi f_S t + \theta_S + \theta_C\right) + \\ 0.5\,\alpha_{PD}\cos\left(\theta_S - \theta_C\right)\beta_m \sin\left(2\pi f_\delta t\right) - \\ 0.5\,\alpha_{PD}\cos\left(4\pi f_S t + \theta_S + \theta_C\right)\beta_m \sin\left(2\pi f_\delta t\right) \end{cases} \quad (3.38)$$

The amplitude of the frequency component corresponding to the dither frequency is maximised when the phases of s(t) and c(t) are equal to each other, and minimised when the difference between the two phases equal $\pi/2$. In other words, the frequency component is maximum when s(t) and c(t) are in phase quadrature, and equal zero when s(t) and c(t) are phase matched, i.e. in-phase. Consequently, the amplitude of the dither frequency component includes information about the phase difference between data and clock.

In order to access this information, the information is down converted to DC by mixing the signal $o_{PD}(t)$, described in eq. (3.37) with another output branch from the dither frequency generator, as shown in Figure 3.15. The output signal from the mixer, $o_{mix}(t)$, is expressed as

$$o_{mix}(t) = \sin\left(2\pi f_\delta t\right) o_{PD}\left(t\right) \quad (3.39)$$

In order to simplify the expression, only the low frequent components, here defined as frequency components less than f_S, are shown

$$o_{mix}(t) = \begin{cases} 0.25\,\alpha_{PD}\,\beta_m\cos\left(2\pi\left(f_S - f_o\right)t + \theta_S - \theta_C\right) + \\ 0.5\,\alpha_{PD}\sin\left(2\pi\left(f_S - f_o\right)t + \theta_S - \theta_c\right)\sin\left(2\pi f_\delta t\right) \\ 0.25\,\alpha_{PD}\,\beta_m\cos\left(2\pi\left(f_S - f_o\right)t + \theta_S - \theta_C\right)\cos\left(4\pi f_\delta t\right) \end{cases} \quad (3.40)$$

The loop filter is designed with lowpass bandwidth less than the dither frequency. Assuming the frequency difference (f_S-f_o) is less than the bandwidth of the filter, the control signal e(t) is written as

$$e(t) = 0.25\,\alpha_{PD}\,\beta_m\cos\left(2\pi\left(f_S - f_o\right)t + \theta_S - \theta_C\right) \quad (3.41)$$

The control signal applied to the oscillator will change the output frequency and the output phase of the oscillator, so the control signal equals zero. This requirement is fulfilled when

$$f_0 = f_S \qquad ; \qquad \theta_S - \theta_C = \frac{\pi}{2} \quad (3.42)$$

It is observed that when the signals are in-phase, i.e. $\theta_S - \theta_C = \frac{1}{2}\pi$[23], the control signal e(t) equals zero. This is in contrast to the previous configurations, where the error signal was equal zero, when the phases were in phase quadrature, i.e. $\theta_S - \theta_C = 0$.

To adopt clock extraction at the base rate from an OTDM signal, the simplified description above needs to be slightly modified. The OTDM data signal is expressed as

$$s(t) = S_0 + 2\sum_{j=1}^{\infty}\left|S_j\right|\sin\left(2\pi j f_s t + \theta_{js}\right) \quad (3.43)$$

From the previous principle of operation description, the input signal to the non-linear transfer function shown in Figure 3.15 was defined as

$$o_{FM}(t) = \cos\left(2\pi f_o t + \theta_c + \beta_m\sin\left(2\pi f_\delta t\right)\right) \quad (3.44)$$

Assuming that the dither frequency fulfils the requirement - $f_\delta << f_0$ - the FM term $\beta_m \sin(2\pi f_\delta t)$ can be regarded constant for many periods of f_0, and thus be

[23] This relation is due to the definition of s(t) and c(t) including sinus and cosines, respectively.

approximated as a constant phase term. Following the same procedure as in the previous example, the control signal e(t) is written as:

$$e(t) = \alpha_{PD} |S_1||C_N| \beta_m \cos\left(2\pi\left(f_S - Nf_o\right)t + \theta_{1S} - \theta_{NC}\right) \qquad (3.45)$$

Demonstrating that the principle can be used for clock extraction at the base rate of an OTDM signal composed by 'N' channels.

Introducing a perturbation Δ, so the DC component of the input data signal can be written as $S_{0\Delta} = S_0(1+\Delta)$, it can be concluded due to the decoupling of the components, that the perturbation will not have an influence on the control signal e(t), and consequently on the clock extraction.

3.4.5 Advantages and disadvantages of DC compensating schemes

In this section a short resume of the advantages and disadvantages are reiterated. Based on this resume, one scheme is selected as the preferred configuration for clock extraction. It is assumed in the evaluation of the schemes, that the output of the VCO represents the clock in the electrical domain, whereas the term c(t) is an optical signal. It is important to emphasise that c(t) does not automatically represent the optical clock.

Configuration 1:

- Low complexity in implementation
- Bandwidth of Clock Recovery circuit can be modified by adjusting the loop-filter.
- Electrical clock is available.
- Optical clock is available.
- Power fluctuations in incoming DC signal result in misalignment of clock.
- Output signal of OPD is not the demultiplexed signal

Configuration 2:

- Medium complexity in implementation.
- Bandwidth of Clock Recovery circuit can be modified by adjusting the loop-filter.
- Electrical clock is available.
- Optical clock is available.
- Power fluctuations in incoming DC signal are compensated, and do not affect the clock extraction performance.

- Output signal of OPD is not the demultiplexed signal

Configuration 3:

- High complexity in implementation.
- Bandwidth of Clock Recovery circuit can be modified by adjusting the loop filter. However, bandwidth is limited by the off-set frequency as the maximum.
- Electrical clock is available.
- Optical clock is not available, as c(t) represents a pulse train with a repetition frequency equal to the clock added the off-set frequency.
- Additional electrical components can introduce spurious frequency components, which can jeopardise the performance.
- Output signal of OPD is not the demultiplexed signal

Configuration 4:

- High complexity in implementation.
- Bandwidth of Clock Recovery circuit can be modified by adjusting the loop filter. However, bandwidth is limited by the dither frequency as the maximum.
- Electrical clock is available.
- Optical clock is not available, as c(t) represents a pulse train with a repetition frequency equal to the clock added the dither frequency.
- Additional electrical components can introduce spurious frequency components, which can jeopardise the performance.
- Output signal of OPD can be used as the demultiplexed signal including an expected small power penalty due to the dithering of the Switching Window.

Configuration 1 can be excluded immediately, due to the high sensitivity to power fluctuations in the incoming data signal. If this scheme is used, an automatic gain control at the input to the CR circuit is required in order to ensure stable and correct clock extraction. This cancels the advantage of the simplicity of the configuration.

Configuration 3 and 4 are both attractive, and especially configuration 3 has been used to demonstrate clock extraction from the highest aggregated bit rate hitherto. However, two issues counter-argue for utilising the schemes. If optical pulses synchronised to the clock are required for demultiplexing, an additional pulse source controlled by the VCO is required, because the optical clock signal is not accessible. High quality pulse sources adequate for high-speed OTDM systems are often a limited resource in most laboratories. Notice, that albeit configuration 4 offers the possibility for simultaneously clock extraction and

demultiplexing, the configuration can only be used to demultiplex a single channel out of the OTDM signal. If all the channels need to be demultiplexed, as outlined in Figure 3.1, either an optical clock pulse train is required or the clock circuit is required for each individual channel. Secondly, the limitations on bandwidth tuning can impose a problem. As elucidated in section 3.6, the performance of the CR circuit in the presence of jitter can be significantly optimised when varying the bandwidth of the PLL. By using configuration 3 and 4, the CR designer needs to either be limited in bandwidth tuning range or re-design, in terms of frequency, the electronics used at the off-set/dither frequency. This is not considered practical in a laboratory, where the equipment continuously is changed, up-graded or optimised, influencing the specifications of the devices, necessitating continuously optimisation of the implemented CR circuit.

Based on these considerations, configuration number 2 was chosen for further investigations and optimisations in this thesis.

3.5 Optimisation of control signal in PLL

3.5.1 Introduction

From the previous derived theory for OTDM clock extraction, see section 3.3.2, a design parameter for optimising the performance of the Optical Phase Detection is to generate a control signal e(t) with a high contrast, i.e. a large amplitude difference between high and low amplitude. From the definition of K_{PD}, see eq. (3.18) it is observed that an optimised harmonic frequency component of the clock pulse, corresponding to the aggregated bit rate of the OTDM signal, will increase the phase detector conversion efficiency.

In this section a simple approach to optimise the phase detector conversion efficiency is introduced. It is assumed that the sinusoidal clock at the base rate has been transformed using the non-linear transfer function, generating a pulse train with higher harmonic frequency components, and that the pulses of the clock pulse train can be characterised as Gaussian.

3.5.2 Gaussian shaped clock pulses

Assume that the power of the pulses is Gaussian shaped [3.55]

$$c(t) = A \exp\left[-4\ln 2 \frac{t^2}{T_{FWHM}^2} \right] \tag{3.46}$$

where A is the amplitude and T_{FWHM} is the width at FWHM. As the clock pulse train is periodic with a period T_C corresponding to f_0^{-1}, the pulse train can be expressed by its Fourier series. The Fourier coefficients can be derived analytically and the n^{th} Fourier coefficient is expressed as

$$c_n = A\frac{T_{FWHM}}{T_c}\sqrt{\frac{\pi}{4\ln 2}}\exp\left[-\frac{n^2\pi^2}{4\ln 2}\frac{T_{FWHM}^2}{T_c^2}\right] \tag{3.47}$$

The maximum amplitude of the Fourier coefficient can be found by differentiation, revealing the following simple expression for the optimum FWHM width of the Gaussian shaped SW, $T_{FWHMOPT}$.

$$T_{FWHMOPT} = \frac{\sqrt{2\ln(2)}}{\pi n}T_C \tag{3.48}$$

As an example of the existence of an optimum Switching Window for the higher harmonic frequency components, the Fourier coefficient required for extracting a 10 GHz clock from a 160 Gbit/s OTDM signal, i.e. c_{16}, has been calculated as function of T_{FWHM} and shown (normalised) in Figure 3.16.

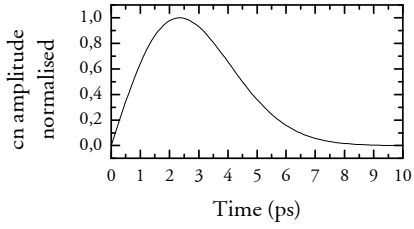

Figure 3.16: Fourier coefficient c_{16} of a Gaussian shaped pulse as function of FWHM

From eq. (3.48), the optimum is found to be 2.34 ps, which is in agreement with the results shown in Figure 3.16. Figure 3.16 also shows how a relative broad range in terms of FWHM will still result in a frequency component, which can be used for clock extraction. In the case of Gaussian shaped switching windows, the width can vary from 0.8 to 4.5 ps without reducing the Fourier coefficient with more than 3 dB for a 160 Gbit/s OTDM system.

In Table 3.1 the optimum T_{FWHM} required for clock extraction from 40, 80, 160, 320, 640 and 1280 Gbit/s is calculated for a base rate of 10 GHz.

Aggregated bit rate	n	T_{FWHM} (ps)
40	4	9.36
80	8	4.68
160	16	2.34
320	32	1.17
640	64	0.58
1280	128	0.29

Table 3.1: Optimised FWHM for Gaussian shaped pulses

From Table 3.1 the narrow switching window widths especially for bit rates above 160 Gbit/s emphasise the challenges foreseen when the bit rate is increased.

The analysis presented above can be repeated for other pulse shapes, thus allowing an optimisation for a specific OTDM system based on a specific switch used for OPD.

3.6 Stability of the PLL

3.6.1 Introduction

An important issue regarding the PLL is the stability. A PLL is a feedback system, which are always, potentially, prone to instabilities, unless the system is carefully dimensioned. If the system is instable, one manifestation can be observed by applying an impulse function at the input to the system, and monitor the output of the system. The transients at the output of the loop will not expire, as opposed to a stable system. Instead, the transients will increase in amplitude, and in principle approach infinity [3.56]. If the feedback loop includes substantial delays, the control circuit of the feedback loop is responding and adjusting to specific characteristics of the input signal, which not necessarily are present when the actual response is feedback in the loop. This can further affect the stability of the loop.

Especially the OPD based PLL can include substantial delays. As outlined in section 3.5, the control pulses inducing the switching window[24] used for mixing

[24] In chapter 4 a survey of different switching schemes used for demultiplexing shows how Switching Windows in most cases are induced by injecting narrow optical control pulses. Assuming that the switching window is an exact replica of the control pulse, switching window and control pulse are interchangeable terms when addressing the OPD.

the incoming clock and data signal have some pulse width range, in which the output signal of the OPD will have an acceptable magnitude. When extracting the clock from extremely high bit rates, the width of the clock pulses will tend to be very narrow. In section 3.5 it was shown, that the optimised width of the clock pulses for CR from a 640 Gbit/s OTDM signal was ~ 600 fs – a requirement lasers with high repetition frequency, i.e. 10 or 40 GHz, will have difficulties in fulfilling, see chapter 2. If the pulse source does not generate sufficiently narrow pulses, pulse compression techniques as outlined in chapter 2, might be used. However, these schemes often require considerable lengths of fibre, thus introducing delay within the loop. Furthermore, a certain optical power of the control pulses before launched into the OPD is also often mandatory in order to utilise the physical process responsible for generating the mixing between local clock and incoming data signal, hence an amplifier is frequently included in the loop. If an Erbium Doped Fibre Amplifier (EDFA) is used, the actual length of the doped fibre, also introduce delays. Consequently, delay in Phase Locked Loops is a very important issue, and should be addressed in more details.

Only a few references can be found in existing literature addressing the impact of loop delays on the performance of the loop. Most of these articles have focussed on communication systems based upon homodyne or heterodyne receivers, demonstrating how the loop delay influences the requirements to the linewidth of the lasers and how the bandwidth of the PLL can be optimised in order to reduce the total phase noise of the extracted clock [3.57][3.58][3.59][3.60][3.61]. The models presented in the articles are very comprehensive and demonstrate important aspects of PLL design including loop delays. However, the references are utilising the minimisation of the phase noise on the error signal for a specific loop delay.

Later in this section, references will be presented showing that the phase noise of the clock depends on the bandwidth of the PLL, and the phase noise can be minimised by proper bandwidth optimisation. However, first the impact of bandwidth on the stability of the PLL is addressed, and it will be demonstrated how the loop delay reduces the variation range of the PLL bandwidth, thus potentially eliminating the possibility of optimising the PLL bandwidth to yield lowest possible phase noise.

3.6.2 PLL stability theory and model

The PLL is a non-linear system, hence the determination of stability constitutes a relative complex problem. However, by using the linear approximation of the PLL an estimate of the stability can be obtained by using e.g. Bode plots [3.6]. A reasonable question is if a stability analysis of a non-linear system based on a

linear analysis is valid? According to [3.8], it is experienced that the fulfilment of the linear stability criterion in general yields a stable system.

Before going into details addressing the stability, the linear approximation is repeated. However, in order to address stability, the time domain analysis of the PLL operation, presented in section 3.3 is transformed to the frequency domain using the Laplace transformation. The derivation below follows any standard textbook addressing PLL operation, see e.g. [3.6]. However, the summary serves the purpose of standardising the terminology to the OTDM clock extraction.

In Figure 3.3 the basic PLL configuration was shown, including a phase detector, a VCO and a non-linear element, ensuring that the clock signal contained the required higher harmonics before injected into the phase detector. The non-linear element is often an abstraction for a laser controlled by the sinusoidal electrical signal from the VCO. As argued in the previous sections, it can be expected that the CR implementation will include a substantial delay situated after the laser. In this presentation the total loop delay is lumped into a single unit right after the laser. The modified PLL is shown in Figure 3.17.

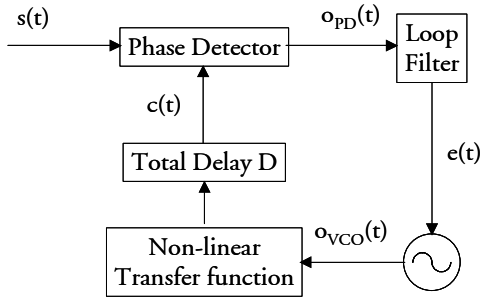

Figure 3.17: Modified PLL configuration including a total loop delay D

From the previous sections, the frequency component of the data signal used for clock extraction was, see eq. (3.18)

$$s(t) = |S_1| \sin\left(2\pi f_S t + \theta_{1S}\right) \tag{3.49}$$

and the frequency component of the local clock signal used for clock extraction from an OTDM signal multiplexed by N channels, see eq. (3.18) was

$$c(t) = |C_N| \cos\left(2\pi N f_0 t + \theta_{NC}\right) \tag{3.50}$$

generating the control signal e(t) used for the feedback loop

$$o_{PD}(t) = \alpha_{PD} |S_1||C_N| \sin\left(2\pi(f_S - Nf_o)t + \theta_{1S} - \theta_{NC}\right) \tag{3.51}$$

defining the two phases as

$$\theta_S(t) = 2\pi f_S t + \theta_{1S}$$
$$\theta_C(t) = 2\pi N f_C t + \theta_{NC} \tag{3.52}$$

the output signal can be expressed as

$$o_{PD}(t) = \alpha_{PD} |S_1||C_N| \sin\left(\theta_S(t) - \theta_C(t)\right) \triangleq K_{PD} \sin\left(\theta_S(t) - \theta_C(t)\right)$$
$$o_{PD}(t) \approx K_{PD}\left[\theta_S(t) - \theta_C(t)\right] \tag{3.53}$$

where the linear approximation is true when the phase difference fulfils $\theta_S(t) - \theta_C(t) \ll 1$. In order to analyse the Bode plot of the linear PLL model, first all the components in the PLL are translated to the Laplace domain (s-domain), using the definition [3.1]

$$L\{f_0(t)\} \triangleq F_0(s) = \int_0^\infty f_0(t) \exp(-st)\, dt \tag{3.54}$$

The phase detector is approximated by subtraction between the phase of the data signal $\theta_S(s)$ and the clock signal $\theta_C(s)$. The PD conversion efficiency K_{PD} is multiplied on the phases. The filter is represented by the transfer function F(s). The oscillator is assumed to be a VCO, which in the time domain can be represented as integration, and consequently as s^{-1} in the Laplace domain [3.6]. The conversion efficiency of the VCO, K_O, is multiplied to the output signal of the VCO and the loop delay D corresponds to e^{-Ds} in the Laplace domain [3.62]. With these definitions, the following relations can be established [3.6]

$$O_{PD}(s) = K_{PD}\left[\Theta_S(s) - \Theta_C(s)\right]$$
$$E(s) = F(s)\, O_{PD}(s) \tag{3.55}$$
$$\Theta_C(s) = \frac{K_0\, E(s) \exp(-Ds)}{s}$$

which are used to derive the open loop gain G(s), the closed loop transfer function H(s) and the corresponding close loop error phase transfer function $\Theta_e(s)$

$$G(s) \triangleq \frac{\Theta_C'}{\Theta_C} = K_{PD}K_O \frac{F(s)}{s}\exp(-Ds) \tag{3.56}$$

$$H(s) \triangleq \frac{\Theta_C(s)}{\Theta_S(s)} = \frac{K_0K_{PD}F(s)\exp(-Ds)}{s + K_0K_{PD}F(s)\exp(-Ds)} = \frac{G(s)}{1+G(s)} \tag{3.57}$$

$$\begin{aligned}\frac{\Theta_e(s)}{\Theta_S(s)} &\triangleq \frac{\Theta_S(s)-\Theta_C(s)}{\Theta_S(s)} = 1 - H(s) \\ &= \frac{s}{s + K_0K_{PD}F(s)\exp(-Ds)}\end{aligned} \tag{3.58}$$

The difference in $\Theta'_C(s)$ and $\Theta_C(s)$ indicate that the loop is open when calculating G(s). In order to exemplify, the Bode plot stability analyses are presented for a specific filter implementation. In Figure 3.18 an active filter is shown, and it consists of an operational amplifier (OA), defined by its gain A, the input resistor R_1 and the feedback coupling of the series connection of resistor R_2 and the capacitor C.

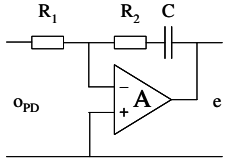

Figure 3.18: Active filter

The transfer function F(s) of the filter in the Laplace domain, when assuming that A is large, can be found as

$$F(s) \triangleq \frac{E(s)}{O_{PD}(s)} \approx \frac{-(R_2Cs+1)}{R_1Cs} \triangleq \frac{-(\tau_2 s+1)}{\tau_1 s} \tag{3.59}$$

The time constants τ_1 and τ_2 are introduced, with definitions evident from eq. (3.59). The approximation is true for large A.

In the following, the minus sign is disregarded, as in most books addressing PLL theory, see e.g. [3.6], [3.7] and [3.8]. The justification for this negligence is

ascribed to the existence of the two operation points, locking and false locking. In order to ensure that the PLL locks to the correct operation point, the loop gain factor $K = -K_O K_{PD}$ should be positive, see [3.8]. Consequently, the minus sign is absorbed into the loop gain factor K.

Inserting eq. (3.59) in the expression of the closed loop transfer function H(s), see eq. (3.57), and introducing K, H(s) can be written as

$$H(s) = \frac{K\frac{\tau_2}{\tau_1}\exp(-Ds)s + \frac{K}{\tau_1}\exp(-Ds)}{s^2 + K\frac{\tau_2}{\tau_1}\exp(-Ds)s + \frac{K}{\tau_1}\exp(-Ds)} \tag{3.60}$$

Introducing the natural frequency ω_N and the damping factor ξ defined as

$$\omega_N = \sqrt{\frac{K}{\tau_1}} \quad ; \quad \xi = \frac{\tau_2}{2}\sqrt{\frac{K}{\tau_1}} = \frac{\tau_2\omega_N}{2} \tag{3.61}$$

H(s) can be written as

$$H(s) = \frac{2\xi\omega_N\exp(-Ds)s + \omega_N^2\exp(-Ds)}{s^2 + 2\xi\omega_N\exp(-Ds)s + \omega_N^2\exp(-Ds)} \tag{3.62}$$

The open loop gain G(s) can be expressed by combining eq. (3.56), (3.59) and (3.61)

$$G(s) = \frac{2\xi\omega_N\exp(-Ds)s + \omega_N^2\exp(-Ds)}{s^2} \tag{3.63}$$

By substituting the parameter s with $i2\pi f$, an expression for the magnitude of G(f) can be found. From the magnitude, an analytical expression for the frequency f_Z at which $G(f_Z)$ is equal to 1, i.e. gain cross over can be found to be

$$|G(f_Z)| = 1 \Rightarrow f_Z = f_N\sqrt{2\xi^2 + \sqrt{4\xi^4 + 1}} \tag{3.64}$$

where $f_N = \omega_N/2\pi$. The argument of G(f) can also be found by algebraic manipulation of eq. (3.63)

$$\mathrm{Arg}(G) = \begin{cases} \mathrm{Arc\,tan}\left(\dfrac{2\xi f}{f_N}\right) - \pi - 2\pi f D \\ \dfrac{180°}{\pi}\left(\mathrm{Arc\,tan}\left(\dfrac{2\xi f}{f_N}\right) - 2\pi f D\right) - 180° \end{cases} \quad (3.65)$$

The term -180° (-π) is due to the two poles at f = 0 Hz.

When analysing the stability of a feedback loop using the Bode plot, the magnitude and the phase of the open loop gain are plotted versus frequency on a logarithmic scale. In principle, the technique is based on plotting the asymptotes of the exact magnitude and phase. However, in [3.6] it is argued that the technique can be used both for the exact and the approximate graphs of the parameters. The Bode criterion for unconditional stability is that the magnitude of the gain G falls below 1 (0 dB), i.e. gain cross over, before the phase shift reaches –180°. The Phase Margin (PM) is consequently defined as the difference between 180° and the phase corresponding to the frequency at gain cross over, i.e. f_Z, see [3.9]. Using this definition, the PM for the active filter can be expressed as

$$PM = 180° + \mathrm{Arg}(G(f_Z)) = \left(\mathrm{Arc\,tan}\left(\frac{2\xi f_Z}{f_N}\right) - 2\pi f_Z D\right)\frac{180°}{\pi} \quad (3.66)$$

In order to design a robust PLL for clock extraction, the PM should be regarded as safety margin in order to allow for inaccuracy in the design model compared to the actual implementation. In [3.10] a rule of thumb is stated – if PM > 45° the system can "usually" be regarded stable. It should be emphasised, that the estimation in eq. (3.66) is based on a number of approximations and assumptions. First of all, the electronic board including the components for the control circuit to the PLL is significantly more complex than outlined in the simple PLL configuration. It includes a number of additional components in the control circuit, which can contribute to the open loop gain characteristic, by reducing the gain cross over frequency, hence reducing the PM. Also spurious effects in the electronic components, e.g. the frequency dependent gain of the OA, can further reduce the possible PM. In principle, these uncertainties should not affect the clock extraction, as they have been taken into account by defining a sufficiently high margin.

In the following example, the acceptable bandwidth of the PLL for a given loop delay within the PLL is calculated. The PLL is based on the loop filter depicted in Figure 3.18, with a damping factor ξ equal to $\sqrt{2}/2$ (=0.707). For a given

length of fibre, the corresponding loop delay D can be calculated. Inserting the value of D, together with the relation between f_Z and f_N in eq. (3.64), the corresponding maximum frequency f_N can be established. In Figure 3.19 the maximum frequency as function of fibre loop length within the loop is depicted for fibre lengths from 1 to 50 meters. For chosen longer fibre lengths, the corresponding bandwidth is stated in table 3.2.

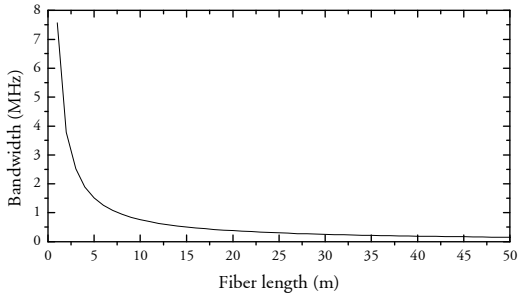

Figure 3.19: Maximum bandwidth of PLL as function of fibre length within PLL, fulfilling a Phase Margin = 45. PLL is designed based upon loop filter in Figure 3.18 with damping factor ξ = 0.707.

Fibre length (m)	Bandwidth (kHz)
100	75.68
200	37.84
300	25.23
400	18.92
500	15.14
600	12.61
700	10.81
800	9.46
900	8.41
1000	7.57

Table 3.2: Maximum bandwidth for varied fibre lengths within the PLL (designed as in Figure 3.17)

From Figure 3.19 it is observed how the allowable bandwidth within the PLL is significantly reduced even for a few meters of fibres. These considerations are important to include in the design of the PLL, as a number of components potentially will include substantial loop delays. As an example, the EDFA, used to boost the signal into the OPD includes non-negligible fibre lengths. If the local pulse source used to generate the optical clock pulse train does not generate sufficiently narrow pulses, see section 3.5 for more detailed specifications, a possible solution is to utilise pulse compression as outlined in chapter 2. However, these pulse compression stages can include hundreds of meters of fibre, thus reducing the maximum acceptable bandwidth to less than 100 kHz. As an example, the pulse compression stages reported in chapter 4 is based on Dispersion Decreasing Fibre (DDF) with a length of 1000 meters.

Other loop filters, which can further reduce or increase the acceptable bandwidth depending on the specific choice can be utilised. This offers the possibility for redesigning the PLL if the stability criterion is not fulfilled. However, notice that the filter type and shape is partly determining the locking behaviour of the PLL, and should not be exchanged without including these considerations into the final implementation design.

From Figure 3.19 it can be concluded that by reducing the total temporal delay within the loop, the acceptable bandwidth of the PLL can be increased without jeopardising stability. A large acceptable variation range of the bandwidth is crucial, because it allows optimisation of another vital clock parameter, the phase noise of the clock. It can be shown how phase- and amplitude-noise on the incoming data signal and from the clock generator are transferred to the clock signal [3.8]. Minimisation of the output phase jitter due to external noise in the data signal requires a loop bandwidth as narrow as possible. However, in order to minimize the output phase jitter due to internal oscillator noise the bandwidth should be as wide as possible [3.7]. Obviously, the two contradicting design requirements necessitate a trade-off in order to optimise the performance. If a substantial temporal delay within the loop is present, it might prevent the optimum trade-off, because the temporal delay dictates a reduced bandwidth of the PLL. A general rule for determining the actual bandwidth of the PLL cannot be stated, as the target bandwidth depends on the noise properties of the incoming data signal and the local clock source, which needs to be characterised for the specific OTDM system.

3.7 CR at 160 Gbit/s using FWM as OPD in a PLL

As part of the contribution from COM•DTU to the European IST project TOPRATE, clock extraction at high bit rates was an important issue and a number of different configurations were successfully investigated at COM•DTU. In this thesis only a single implementation will be described briefly [3.36]. Leif K. Oxenløwe has carried out the experimental work and is acknowledged for kindly providing the results for the thesis. The discussions and the theoretical framework, which has been presented in the previous sections allowing for optimisation and understanding of the Clock Recovery sub-system, were initiated by discussions and analysis of obtained experimental work.

In this section, Clock Recovery from 40, 80 and 160 Gbit/s is presented. The set-up uses a Semiconductor Optical Amplifier as the Optical Phase Detector and the process generating the control signal for the PLL is degenerated FWM between the OTDM signal and the local base rate clock signal.

The CR set-up is shown in Figure 3.20.

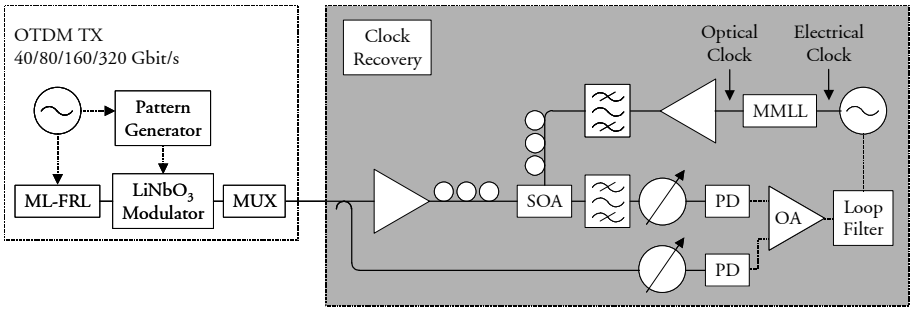

Figure 3.20: Experimental set-up for extracting a 10 GHz clock from 40, 80, 160 Gbit/s. ML-FRL: Mode-locked Fibre Ring Laser. Mux: Multiplexer. SOA: Semiconductor Optical Amplfier. PD: Photo-Detector. OA: Operational Amplifier. MMLL: Monolithic mode-locked Laser.

A Mode-Locked Fibre Ring Laser (ML-FRL) emits 2 ps FWHM pulses with a repetition frequency at 10 GHz at 1554 nm. The pulses are externally modulated using a $LiNbO_3$ modulator, with a PRBS of 2^7-1, multiplexed up to 40, 80, 160 and 320 Gbit/s in a polarisation and PRBS maintaining passive multiplexer. The voltage signal from the VCO is applied to a monolithic mode-locked laser (MMLL), generating a pulse train at 1560 nm with 3 ps FWHM pulses characterised by a timing jitter of approximately 250 fs. The clock signal and the OTDM signal are amplified and merged together and launched into the OPD, here a SOA. When the polarisation states are optimised, the FWM beating between the two signals in the SOA generates the control signal. The power of the FWM product is a direct manifestation of the internal time difference between clock pulses and data pulses. In order to suppress the slow DC fluctuations due to variations in the average power of the incoming OTDM data signal, configuration 2 depicted in Figure 3.13 was used. A branch of the OTDM signal was injected into the OPD whereas the other branch bypassed the OPD. The two branches were terminated by two identical photo detectors (PD), each with a bandwidth of approximately 100 MHz. The relative high bandwidth of the photo detectors ensures that their impact on the total bandwidth of the PLL is negligible. Hence, the bandwidth is primarily defined by the loop-filter, which allows bandwidth optimisations of the phase noise as stated in section 3.6. The signals from the two branches are subtracted using a standard Operation Amplifier configuration before the DC compensated signal is injected into the loop filter, see Figure 3.20, and finally applied to the VCO. The 10 GHz sinusoidal voltage signal from the VCO is applied to the MMLL.

The OPD characteristics were evaluated and the results are shown in Figure 3.21. The results show the expected periodicity in power for all the bit rates. It is noticed how the average power, i.e. the DC level, is increased and the

contrast, i.e. the difference between minimum and maximum power, is decreased for increased bit rates. The reduced contrast for increased bit rates constitutes a severe problem, as the configuration will be more prone to noise. If amplitude noise fluctuations on the data signal are too large, no sufficient feedback signal can be generated to keep tracking the clock. The CR circuit will drop out of lock, and the data signal is outside the tracking range. Consequently, a signal with a high sufficient high contrast is required, to suppress the impact of noise. The term, sufficient high, should be determined for each specific CR circuit after determining the expected noise contributions.

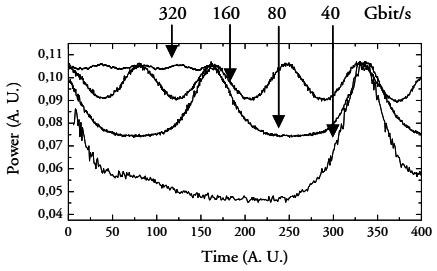

Figure 3.21: Error signal at 40, 80, 160 and 320 Gbit/s as function of time.

From Figure 3.21 it is observed how the contrast in the 320 Gbit/s is almost negligible, although the periodic structure is definitely present. In subsequent experiments, the error signal obtained at 320 Gbit/s was, not surprisingly, not adequate for clock extraction. However, it is important to emphasise that the diminutive contrast obtained in the experimental set-up is not a characteristic inherent for clock extraction from a 320 Gbit/s OTDM signal. As previously stated, the FWHM width of clock pulses and data pulses are 3.9 ps and 2.0 ps, respectively. Comparing these specifications with the requirements derived in chapter 2 and in section 3.5, it would be expected that the performance would be significantly improved by optimising the pulse widths for both pulse sources. Extracting the required information from these sections, it is expected that the combination of Gaussian data pulses with a FWHM width of 1.25 ps ($= 0.40/320 \bullet 10^9$) and Gaussian clock pulses of 1.17 ps, would generate an improved control signal. Using the model explained in 3.5, calculating the control signal using the data from the experimental set-up and with the predicted optimised values, a comparison indeed confirmed a significant improved control signal.

The set-up was used to extract a 10 GHz clock from 40, 80 and 160 Gbit/s. Using a loop filter with a bandwidth of 161 kHz allowed the PLL to extract a clock signal from all three bit rates with timing jitter of approximately 600 fs, which according to [3.5] fulfils the requirements for a 160 Gbit/s OTDM system. Figure 3.22A shows oscilloscope traces of the unlocked clock and 3.22B

the locked clock from an 80 Gbit/s data signal. The traces below the clock signals are the base rate pulse train from the ML-FRL, demonstrating the synchronisation between base rate and extracted clock.

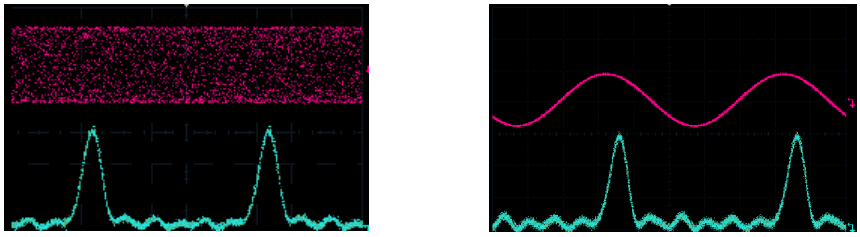

A B

Figure 3.22: A) Upper trace shows unlocked clock. Lower trace the base rate optical pulse train. B) Upper trace shows locked clock extracted from 80 Gbit/s. Lower trace identical to lower trace A).

For the used loop filter, see Figure 3.18, the bandwidth corresponds to $(2\pi\tau_2)^{-1}$ [3.7]. The filter is designed with a damping factor ξ of 0.707, which enables the determination of f_N by using eq. (3.61) and hence the frequency at gain cross over f_Z using eq. (3.64). The total length of fibres and pigtails in the configuration is estimated to approximately 22 meters, corresponding to ~ 110 ns. Thus, the phase margin, which was used to ensure stability, can be calculated to be 51.52°, according to eq. (3.66). Obviously, the phase margin fulfils the rule of thumb, PM > 45°, which suggest that the PLL can be regarded as stable, if the assumptions regarding additional electronics and spurious effects outlined in section 3.5 are fulfilled.

Clock extraction was demonstrated and the results indicate agreement between the theory presented in this thesis and the results obtained.

3.8 Conclusion

In this chapter Clock Recovery for extracting a base rate clock from a high-speed OTDM system was addressed. A short literature survey of different schemes was presented before a simple theory for Optical Phase Detection implemented in a Phase Locked Loop was derived. The signal controlling the OPD based PLL includes a DC term, which needs to be compensated in order to allow Clock Recovery. Four different schemes from literature are examined using the terminology from the derived PLL theory and advantages and disadvantages of the schemes are extracted and a preferred implementation is chosen. An example of how an OPD based PLL can be optimised by choosing the correct width of switching window is presented, showing a relative high

acceptable variation range of temporal FWHM width. Because OPD based PLL implementations can include large temporal delays due to the optical components used in the loop, the impact of the loop stability is addressed by means of Bode plot. The larger time delay of the loop, the narrower acceptable bandwidth of the loop. An example emphasises how significant a reduction in bandwidth even a few meters of fibre can induce. Finally an experimental set-up is presented, demonstrating 10 GHz clock extraction from a 160 Gbit/s OTDM signal. The results are compared to the theory derived in the chapter, indicating agreement between experimental and theoretical work.

3.9 References to chapter 3

[3.1] A. B. Carlson, "Communication systems – An introduction to Signals and Noise in Electrical Communication", McGraw-Hill International Editions, New York, USA (1986).

[3.2] I. D. Phillips et al, "100 Gbit/s optical clock recovery using electrical phaselocked loop consisting of commercially available components", Electronics Letters, Vol. 36, No. 7, pp. 650-651 (2000).

[3.3] M. Nakazawa, T. Yamamoto, K. R. Tamura, "1.28 Tbit/s 70 km OTDM transmission using third- and fourth order simultaneous dispersion compensation with a phase modulator", Electronics Letters, Vol. 36, No. 24, pp. 2027-2029 (2000).

[3.4] J. Seoane, A. I. Siahlo, A. T. Clausen, L. K. Oxenløwe, Z. Xu, P. Jeppesen, "All optical 160 to 10 Gbit/s demultiplexing using co-propagating optical clock", Proceedings of Conference on Lasers & Electro-Optics (CLEO'04), San Francisco, California, USA, paper CThQ4 (2004).

[3.5] M. Jinno, "Effects of Crosstalk and Timing Jitter on All-Optical Time-Division Demultiplexing Using a Nonlinear Fiber Sagnac Interferometer Switch", Journal of Quantum Electronics, Vol. 30, No. 12, pp. 2842-2853 (1994).

[3.6] F. M. Gardner, "Phaselock Techniques", 2nd edition, John Wiley & Sons, New York, USA (1979).

[3.7] R. E. Best, "Phase-Locked Loops – theory, design and applications", McGraw-Hill, Inc., New York, USA (1993).

[3.8] A. Blanchard, "Phase-Locked Loops – application to coherent receiver design", John Wiley & Sons, New York, USA (1976).

[3.9] J. Encinas, "Phase Locked Loops", Chapman & Hall, London, UK (1993).

[3.10] C. L. Phillips and R. D. Harbor, "Feedback control systems", Prentice-Hall, Inc. New Jersey, USA (1988).

[3.11] A. Yariv, "Optical Electronics in Modern Communications 5th edition", Oxford University Press, New York, USA (1997).

[3.12] K. Yvind, "Semiconductor Mode-Locked Lasers for Optical Communication Systems", PhD thesis, Technical University of Denmark, Department of Communications, Optics & Materials (COM•DTU), Lyngby, Denmark (2004).

[3.13] S. Arahira, Y. Ogawa, "All optical 160 Gbps clock extraction using mode-locked laser diodes", Proceedings of the 10th international workshop on femtosecond technology (FST 2003), paper TA-4, p. 52 (2003).

[3.14] T. Ohno, K. Sato, R. Iga, Y. Kondo, T. Ito, T. Furuta, "Recovery of 160 GHz clock from 160 Gbit/s data stream using modelocked laser diode", Electronics Letters, Vol. 40, No. 4, pp. 265-266 (2004).

[3.15] R. Schreieck, M. Kwakernaak, H. Jäckel, "All-optical clock extraction at 160 Gbit/s with monolithic mode-locked laser diodes", IEICE Trans. Electron, Vol. E84-C, No. 6, pp. 841-844 (2001).

[3.16] T. Shimizu, H. Kurita, H. Yokoyama, "All-optical clock extraction performance of a mode-locked diode laser with a novel external-cavity configuration", Technical Digest of conference on Optical Fiber Communication (OFC'98), San Jose, California, USA, paper TuA1 (1998).

[3.17] H. Yokoyama, Y. Hashimoto, H. Kurita, I. Ogura, "Two-stage all-optical subharmonic clock recovery using modelocked semiconductor lasers", Electronics Letters, Vol. 36, No. 18, pp. 1577-1578 (2000).

[3.18] H. Yokoyama, Y. Hashimoto, H. Kurita, I. Ogura, "All-optical subharmonic clock recovery and demultiplexing", Technical Digest of conference on Optical Fiber Communication (OFC'00), Baltimore, Maryland, USA, paper ThP5-1 (2000).

[3.19] T. Ohno, K. Sato, T. Shimizu, T. Furuta, H. Ito, “Recovery of 40 GHz optical clock from 160 Gbit/s data using regeneratively modelocked semiconductor laser”, Electronics Letters, Vol. 39, No. 5, pp. 453-455 (2003).

[3.20] T. Ohno, K. Sato, R. Iga, Y. Kondo, K. Yoshino, T. Furuta, H. Ito, “Recovery of 80 GHz optical clock from 160 Gbit/s data using regeneratively modelocked laser diode”, Electronics Letters, Vol. 39, No. 19, pp. 1398-1400 (2003).

[3.21] B. Sartorius, M. Möhrle, S. Reichenbacher, H. Preir, H-J. Wünsche, U. Bandelow, “Dispersive Self-Q-Switching in Self-Pulsating DFB lasers”, IEEE Journal of Quantum Electronics, Vol. 33, No. 2, pp. 211-218 (1997).

[3.22] O. Brox, S. Bauer, C. Bobbert, G. Bramann, J. Kreissl, B. Sartorius, “160 to 40 Gb/s demultiplexing using a self-pulsating laser based on clock recovery”, Technical Digest of conference on Optical Fiber Communication (OFC’03), Atlanta, Georgia, USA, paper MF85 (2003).

[3.23] A. Siahlo, A. T. Clausen, J. Seoane, L. K. Oxenløwe, K.S. Berg, P. Jeppesen, O. Brox, S. Bauer, J. Kreissl and B. Sartorius, "Pulse Compression of a 40 GHz DFB based Optical Clock Recovery", Proceedings of the 30th European Conference on Optical Communication (ECOC'04), Stockholm, Sweden, paper We2.5.4 (2004).

[3.24] O. Brox, Heinrich-Hertz-Institut, Berlin, Germany, personal communication (2004).

[3.25] A. Neyer, E. Voges, “Dynamics of electrooptic oscillator using an integrated interferometer”, Optics Communication, Vol. 37, No. 3, pp. 169-174 (1981).

[3.26] X. S. Yao, L. Maleki, “High frequency optical subcarrier generator”, Electronics Letters, Vol. 30, No. 18, pp. 1525-1526 (1994).

[3.27] X. S. Yao, L. Maleki, “Converting light into spectrally pure microwave oscillation”, Optics Letters, Vol. 21, No. 7, pp. 483-485 (1996).

[3.28] X. S. Yao, G. Lutes, “A high-speed photonic clock and carrier recovery device”, IEEE Photonics Technology Letters, Vol. 8, No. 5, pp. 688-690 (1996).

[3.29] X. S. Yao, L. Maleki, "Ultralow phase noise dual-loop optoelectronic oscillator", Technical Digest of conference on Optical Fiber Communication (OFC'98), San Jose, California, USA, paper ThT2 (1998).

[3.30] F. Cisternino, R. Girardi, R. Calvani, E. Riccardi, P. Garino, "A regenerative prescaled clock recovery for high-bit-rate OTDM systems", Optical Fiber Technolgy, Vol. 5, No. 3, pp. 260-274 (1999).

[3.31] J. Yu, K. Kojima, N. Chand, A. Ougazzaden, C. W. Lentz, J. M. Geary, J. M. Freund, B. Mason, "Simulataneous demultiplexing and clock recovery of 80 Gb/s OTDM signals using a tandem electro-absorption modulaor", Proceedings of Lasers and Electro-Optics Society (LEOS 2001), San Diego, California, USA paper TuBB4 (2001).

[3.32] J. Yu, K. Kojima, N. Chand, M. Fischer, R. Espindola, T. G. B. Mason, "160 Gb/s single-channel unrepeatered transmission over 200 km of non-zero dispersion shifted fiber", Proceedings of European Conference on Optical Communication (ECOC'01), Amsterdam, Netherlands, Post-Deadline paper PD.M.1.10 (2001).

[3.33] M Schmidt, E. Lach, K. Schuh, M. Schilling, P. Sillard, G. Veith, "Unrepeatered 320 Gbit/s (8x40 Gbit/s) OTDM transmission over 80 km of TeraLight™-reverse TeraLight™ fiber link" Proceedings of European Conference on Optical Communication (ECOC'03), Rimini, Italy, paper We4.P117 (2003).

[3.34] M. Schmidt, K. Schuh, E. Lach, M. Schilling, G. Veith, "8x160 Gbit/s (1.28 Tbit/s) DWDM transmission with 0.53 bit/s/Hz spectral efficiency using single EA-modulator based RZ pulse source and demux", Proceedings of European Conference on Optical Communication (ECOC'03), Rimini, Italy, paper Mo3.6.5 (2003).

[3.35] O. Kamatani, S. Kawanishi, "Prescaled timing extraction from 400 Gb/s optical signal using a Phase Lock Loop based on Four-Wave-Mixing in a Laser Diode Amplifier", IEEE Photonics Technology Letters, Vol. 8, Vo. 8, pp. 1094-1096 (1996).

[3.36] L. K. Oxenløwe, L.J. Christiansen, D. Larsson, K. Yvind, A.T. Clausen, J. Seoane, A. I. Siahlo, B. Sørensen, and P. Jeppesen, "Pre-scaled clock recovery with compact semiconductor devices for ultra high-speed OTDM systems", Proceedings of the 30th European Conference on Optical Communication (ECOC'04), Stockholm, Sweden, paper We3.5.2 (2004).

[3.37] S. Kawanishi, M. Saruwatari, "Ultra-high-speed PLL-type clock recovery circuit based on all-optical Gain modulation in travelling-wave laser diode amplifier", IEEE Journal of Lightwave Technology, vol. 11, No. 12, pp. 2123-2129 (1993).

[3.38] S. Kawanishi, H. Takara, M. Saruwatari, T. Kitoh, "Ultrahigh-speed phaselocked loop-type clock recovery circuit using a travelling-wave laser diode amplifier as a 50 GHz phase detector", Electronics Letters, Vol. 29, No. 19, pp. 1714-1716 (1993).

[3.39] H. Bülow, "Optoelectronic synchronisation scheme for ultrahigh-speed optical demultiplexer", Electronics Letters, Vol. 31, No. 22, pp. 1937-1938 (1995).

[3.40] M. Nakazawa, K. Suzuki, E. Yamada, "NOLM oscillator and its injection locking technique for timing clock extraction and demultiplexing", Electronics Letters, Vol. 32, No. 12, pp. 1122-1123 (1996).

[3.41] L. K. Oxenløwe et al, "Optical clock recovery employing an optical PLL using cross-phase modulation in a Sagnac-Interferometer", Technical Digest of Conference on Lasers and Electro-Optics (CLEO 2001), Baltimore, Maryland, USA, paper CthU2 (2001).

[3.42] D. T. K. Tong, K-L. Deng, B. Mikkelsen, G. Raybon, K. F. Dreyer, J. E. Johnson, "160 Gbit/s clock recovery using electroabsorption modulator-based phase-locked loop", Electronics Letters, Vol. 36, No. 23, pp. 1951-1952 (2000).

[3.43] L. K. Oxenløwe, A. I. Siahlo, K. S. Berg, A. T. Clausen, B. M. Sørensen, K. Yvind, P. Jeppesen, K. P. Hansen, K. Hoppe, J. Hanberg, "A novel 160 Gb/s receiver configuration including a glass crystal pulsed laser, photonic crystal fibre and a simple dynamic clock recovery scheme", Proceedings of the 29th European Conference on Optical Communication (ECOC'03), Rimini, Italy, paper Th2.5.3 (2003).

[3.44] E. S. Awad, P. S. Cho, N. Moulton, J. Goldhar, "Subharmonic optical clock recovery from 160 Gb/s using time-dependent loss saturation inside a single electroabsorption modulator", IEEE Photonics Technology Letters, Vol. 15, No. 12, pp. 1764-1766 (2003).

[3.45] C. Boerner, C. Schubert, C. Schmidt, E. Hilinger, V. Marembert, J. Berger, S. Ferber, E. Dietrich, R. Ludwig, B. Schmauss, H. G. Weber, "160 Gbit/s clock recovery with electro-optical PLL using bidirectional operated electroabsorption modulator as phase comparator", Electronics Letters, Vol. 39, No. 14, pp. 1071-1073 (2003).

[3.46] H-F. Chou, Z. Hu, J. E. Bowers, D. J. Blumenthal, K. Nishimura, M. Usami, "Simultaneous 160 Gb/s demultiplexing and clock recovery by utilising microwave harmonic frequencies in a travelling-wave Electroabsorption modulator", IEEE Photonics Technology Letters, Vol. 16, No. 2, pp. 608-610 (2004).

[3.47] H-C. Chang, A. Borgioli, P. Yeh, R. A. York, "Analysis of oscillators with external feedback loop for improved locking range and noise reduction", IEEE Transactions on Microwave theory and techniques, Vol. 47, No. 8, pp. 1535-1543 (1999).

[3.48] A. T. Clausen, "Optisk klokgendannelse", M.Sc. thesis, Technical University of Denmark, Department of Electromagnetic Systems, Lyngby, Denmark (1997).

[3.49] K. S. Jepsen, "High-Speed Optical Signal Processing for High Capacity Optical Networks", PhD thesis, Technical University of Denmark, Department of Electromagnetic Systems, Lyngby, Denmark (1999).

[3.50] L. K. Oxenløwe, "Optical Signal Processing with semiconductor components", Technical University of Denmark, Department of Communications, Optics & Materials (COM•DTU), Lyngby, Denmark (2002).

[3.51] A. T. Clausen, H. N. Poulsen, L. K. Oxenløwe, A. I. Siahlo, J. Seoane, P. Jeppesen, "Pulse source requirements for OTDM systems", Proceedings of 16th Annual meeting of IEEE Lasers & Electro-Optics Society (LEOS 2003), Tucson, USA, paper TuY2 (2003).

[3.52] M. Kroh, H. G. Weber, A. T. Clausen, C. Mikkelsen, L. Oxenløwe, A. Siahlo, K. Berg, A. Tersigni, S. Bischoff, J. Mørk, "Report on sources for > 160Gbit/s including first version of the modelocked laser based pulse source without pulse shaper and on design and implementation of Nx40 Gibt/s OTDM multiplexer for Nx40 Gbit/s", TOPRATE deliverable D 3.2 (limited) (2002).

[3.53] I. D. Phillips et al, "Simultaneous demultiplexing and clock recovery using a single Electroabsorption modulator in a novel bi-directional configuration", Optics Communication, Vol. 150, No. 1-6, pp. 101-105 (1998).

[3.54] D. T. Tong et al, "High speed clock recovery using an Optoelectronic Phase Locked Loop Implemented with Balanced Photodetection", Proceedings of 11th Annual Meeting of the IEEE Lasers and Electro-Optics Society (LEOS 1999), Orlando, Florida, USA, paper TuZ5 (1999).

[3.55] G. P. Agrawal, "Nonlinear Fiber Optics", Second edition, Academic Press, San Diego, California (1995).

[3.56] O. Jannerup, P. H. Sørensen, "Reguleringsteknik 2. udgave", Polyteknisk forlag, Denmark (1999).

[3.57] M. A. Grant, W. C. Michie, M. J. Fletcher, "The performance of optical phase-locked loops in the presence of non-negligible loop propagation delay", IEEE Journal of Lightwave Technology, Vol. LT-5, No. 4, pp. 592-597 (1987).

[3.58] J. R. Barry, J. M. Kahn, "Carrier synchronisation for homodyne and heterodyne detection of Optical Quadriphase-shift keying", IEEE Journal of Lightwave Technology, Vol. 10, No. 12, pp. 1939-1951 (1992).

[3.59] S. Norimatsu, K. Iwashita, "PLL propagation delay-time influence on linewidth requirements of optical PSK homodyne detection", IEEE Journal of Lightwave Technology, Vol. 9, No. 10, pp. 1367-1375 (1991).

[3.60] S. Norimatsu, K. Iwashita, "Linewidth requirements for optical synchronous detection with nonnegligible loop delay time", IEEE Journal of Lightwave Technology, Vol. 10, No. 3, pp. 341-349 (1992).

[3.61] S. Norimatsu, O. Ishida, "Impact of flicker noise and random-walk noise on a phase-locked loop with finite propagation delay", IEEE Journal of Lightwave Technology, Vol. 12, No. 1, pp. 86-95 (1994).

[3.62] U. Gliese, "Optoelectronics for Space Applications Optical Generation of Microwave Signals", PhD thesis, Technical University of Denmark, Department of Electromagnetic Systems, Lyngby, Denmark (1992).

[3.63] J. K. Holmes, "Tracking performance of the filter and square bit synchronizer", IEEE Transactions on Communications, Vol. COM-28, No. 8, pp. 1154-1158 (1980).

[3.64] L. E. Franks, J. P. Bubrouski, "Statistical properties of timing jitter in a PAM timing recovery scheme", IEEE Transactions on Communications, Vol. COM-22, No. 7, pp. 913-920 (1974).

Chapter 4 Demultiplexing techniques and experiments

4.1 Introduction

After transmission, the ultra fast Optical Time Division Multiplexed (OTDM) data signal should be received and processed. In the transmitter, it was relatively easy to overcome the potential bit rate limitations induced by the low bandwidth of the electronics, see chapter 2. However, in the receiver, the OTDM scheme takes is toll, as detection of the signal is very challenging; both clock recovery and demultiplexing of each tributary channel is required. Clock extraction is thoroughly addressed in chapter 3. Extraction of each individual channel is addressed in the present chapter.

In Figure 4.1 the basic point-to-point bit interleaved OTDM communication system is shown. In the receiver block the extraction of each individual channel is indicated by injecting the data signal into an optical component, i.e. the switch, which applies a Switching Window (SW) on the incoming OTDM signal, thus allowing only the target channel to pass. The possibility of splitting the incoming data signal into an array of switches each extracting a separate data channel is indicated in the figure with dotted lines. However this is not the only receiver structure, which can be implemented in order to extract each tributary channel as discussed in the next section.

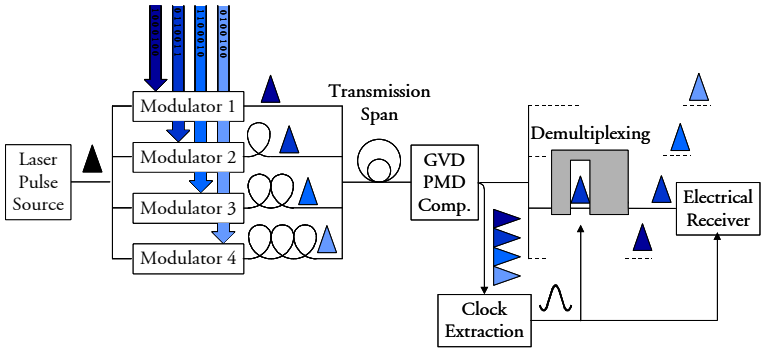

Figure 4.1: Basic OTDM point-to-point communication system.

Ideally, the switch used for demultiplexing should be able to operate as shown in Figure 4.2. Only a single switch is required. As indicated in Figure 4.2, the switch should cyclic toggle between each of the N outlets, corresponding to the number of OTDM channels. Hence, the switch needs to operate at a sufficiently high speed, allowing each separate channel to be routed out at each individual outlet.

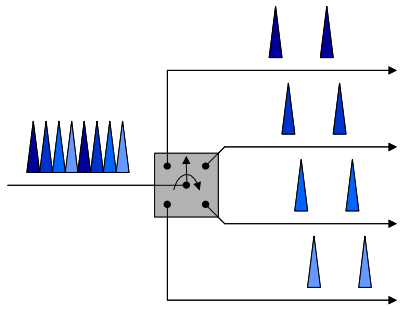

Figure 4.2: Principle of switch in OTDM system

In an OTDM system operating at a bit rate of e.g. 160 Gbit/s, each time slot is 6.25 ps, which corresponds to the absolute maximum switching time. Existing optical commercial switches are relatively slowly, demonstrating switching times in the order of e.g. 100 ns [4.1], more than a factor of ~16.000 too slow compared with the required 160 Gbit/s OTDM switching time. Furthermore, it will probably be challenging to find fast optical switches with a total number of outlets N corresponding to the number of OTDM channels.

Instead the attention has been focussed on optical components, which in general do not offer the functionality sketched in Figure 4.2. Instead the optical switches rely on different processes, which extracts the target channel from the

aggregated OTDM signal, by either passing the target channel and suppressing the remaining channels or by routing the target channel to one outlet of the switch and the remaining channels to another outlet, i.e. complementary demultiplexing. A more detailed description is found in section 4.2, describing the state-of-the-art. The obvious drawback of the utilisation of these switches compared to the simple switch envisioned in Figure 4.2 is the need for a more complex architecture including a number of switches. In [4.2] three different demultiplexing structures are suggested; serial, parallel and tree structure, see Figure 4.3.

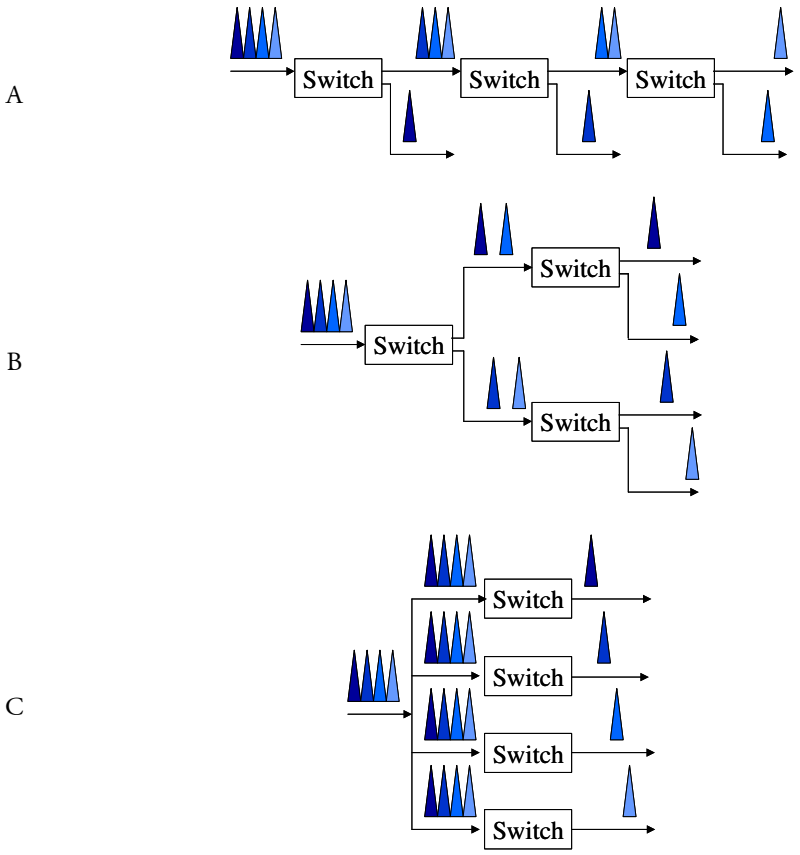

Figure 4.3: Different demultiplexing structure implementations for a point-to-point OTDM system. A) Serial structure B) Tree structure C) Parallel structure.

Inspecting the 3 sketched structures, there are pros and cons for each implementation. Some of the parameters to be considered when choosing the best implementation, includes

- Total number of switches
- Power loss per channel

The number of OTDM channels N is defined as

$$N = 2^n \tag{4.1}$$

where n is an integer. $P_{In,Ch}$ and $P_{Out,Ch}$ are the channel power in and out of the switch and the attenuation x per OTDM channel of each switch is defined as

$$P_{Out,Ch} = x\, P_{In,Ch} \tag{4.2}$$

The total number of required switches to demultiplex all the channels can be derived together with the number of switches each OTDM channel passes. For easing the comparison, the number of switches for each channel is for the serial structure listed for the OTDM channel passing the maximum number of switches, i.e. worst-case. Also the output power of each channel as function of the power per channel at the input to the demultiplexing structure can be found. For the serial structure, the output power is listed for the worst-case channel. In table 4.1 these parameters have been listed for the serial, tree and parallel construction sketched in Figure 4.3.

	Total number of switches	**Number of switches passed for each channel (worst case)**	**Output power each channel (worst case)**
Serial	(N-1)	(N-1)	$x^{(N-1)}P_{In,Ch}$
Tree	(N-1)	n	$x^n P_{In,Ch}$
Parallel	N	1	$\frac{xP_{In,Ch}}{N}$

Table 4.1: Total number of switches, number of switches passed per channel and output power per channel for serial, tree and parallel structure.

It is observed that the total number of switches is basically the same, so from an economical cost-benefit point of view, no preferences can be concluded. The calculation of the (worst-case) power per channel, can perhaps be used to give more convincing arguments for choosing one structure over the others.

A closer look on a 1280 Gbit/s OTDM signal, based on 128 aggregated channels is presented graphically in Figure 4.4. The figure presents the calculated attenuation for the worst-case channel after passing the entire

demultiplexing structure, as function of the switch attenuation x per OTDM channel for the 3 different structures.

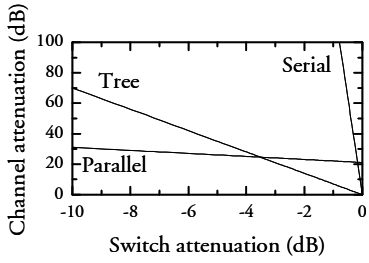

Figure 4.4: Channel attenuation as function of switch attenuation for OTDM signal based on 128 aggregated channels (worst-case).

From the figure, it is clear that the variation of the channel attenuation as function of the power loss in each switch in the parallel structure is quite minimal. The major contribution to the power loss is due to the 1:N splitter in the front of the structure, see Figure 4.3C. The tree and the serial structure in Figure 4.3A and 4.3B do potentially offer the possibility of negligible power loss, assuming minimal switch attenuation. However, the serial structure only offers minimal power loss for extremely small switch losses. As an example, the power loss for the worst-case channel is exceeding 20 dB for only 0.17 dB of power loss per switch, and for 0.5 dB of power loss per switch the worst-case channel loss is more than 60 dB. Contrary to this steep variation in total loss, the tree structure offers approximately 20 db of loss per channel for approximately 3 dB of loss per switch.

Basing a choice of the structure on the power budget will have to depend on the actual implementation of the switch and the actual power loss per switch. A relative high switch loss could suggest either the parallel or the tree structure. However, most switches presented in literature do include amplification, primarily as external amplification, and thus does not necessarily exclude the serial structure. Where to situate the amplifiers ensuring an acceptable Signal to Noise ratio in the receiver block need to optimised.

The component and the process utilised for demultiplexing the signal, can also impose restrictions on the choice of structure. As briefly mentioned previously, some switches route the target channel to one outlet and the other channels to a different outlet, i.e. complementary demultiplexing[25]. This can e.g. be done by utilising constructive and destructive interference in an interferometric

[25] Complementary demultiplexing is also a prerequisite for OTDM networking, see chapter 5.

structure. This feature is not necessary for the parallel structure, but is a prerequisite for tree and the serial structure, as seen in Figure 4.3. Other switches rely on suppression of the remaining channels and are therefore only suitable for the parallel structure, where each channel only passes one specific switch. Consequently, the parallel structure can implement all OTDM demultiplexing switches, whereas tree and serial structure impose additional requirements to the switch.

Finally, Jinno [4.2] points our that the concatenation of switches in the tree and the serial structure, will accumulate imperfections of the switch, such as the impact of a poor switching contrast, i.e. the ratio between the target channel and the remain channels. This problem is obviously not present in the parallel structure.

In conclusion a number of parameters are important, when deciding which structure is the best suited. The choice will largely depend on the specific implementation of the switch, the process it is utilising for demultiplexing, the performance in terms of e.g. power loss per channel and induced cross-talk and finally obviously the total cost of the structure.

In this thesis it has tacitly been assumed that the parallel structure is used, partly due to convention in existing literature, but also due to the convenience when testing and optimising the devices. In the experimental section 4.5 a 320 to 10 Gbit/s demultiplexing experiment is reported. If the tree structure or the serial or tree structure was used, 6 or 31 concatenated switches, respectively, were needed to evaluate the worst-case OTDM channel. However, by assuming that the parallel structure is used, only one single switch is required when evaluating the experimentally implemented 320 Gbit/s OTDM set-up – a tuneable time delay allows evaluation of each individual OTDM channel. Finally, by assuming a parallel structure, important switches such as e.g. Electroabsorption Modulators (EAM), which rely on suppression of the neighbouring channels, can be used and investigated.

4.2 State-of-the-art

4.2.1 Introduction to State-of-the-art

The demultiplexing circuit is used to extract each tributary time channel from the aggregated data signal. The requirements to the switch is quite strict in terms of width of switching window, which can intuitively be understood when inspecting Figure 4.1, and the suppression of the neighbouring channels for ultra high bit rates. This is addressed in more details in successively sections.

Several components and sub-systems have been demonstrated to give very good performance when used as a switching element in OTDM systems. In general the switches can be divided into either Semiconductor Optical Amplifiers (SOA) or fibre based devices, which can be further categorised in interferometric and non-interferometric structures:

- SOA based interferometric switch (SIS)
- SOA based non-interferometric switch (SNIS)
- Fibre based interferometric switch (FIS)
- Fibre based non-interferometric switch (FNIS)

In the following section, the most promising SOA- and fibre-based OTDM switches are briefly summarised. A short description of the principle is presented and a number of key references are given. The intention of the summary is not to give a thorough discussion of each switch, as this is beyond the scope of the thesis, but to emphasise that a number of strong candidates as high-speed switches exist.

4.2.2 SIS: SOA-MZI

A successful switch for OTDM demultiplexing is the Semiconductor Optical Amplifier based Mach-Zehnder interferometer (SOA-MZI), see Figure 4.5.

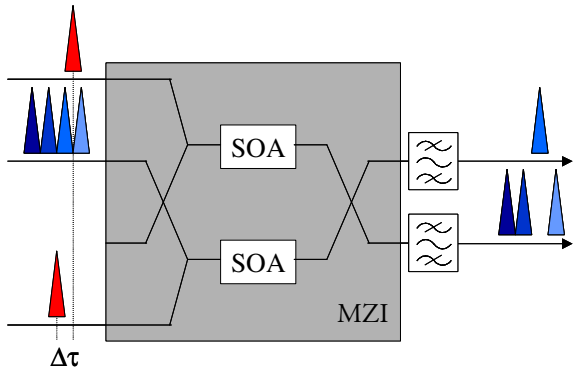

Figure 4.5: Principle of SOA-MZI

A low-power probe signal, i.e. the OTDM signal, injected into the interferometer, will be split and traverse the two arms containing the SOAs and be recombined at the output coupler. Without any external sources, the entire signal will experience destructive interference at e.g. the upper arm and constructive interference at the lower arm. However, by inducing a phase change of π in the target channel, it can be switched from one arm to the other

on a channel-by-channel basis, i.e. demultiplexing. By injecting a high-power narrow control pulse into the SOA, the carriers are almost instantly depleted in the SOA and the refractive index and thus the phase, of the low-power data signal will be altered due to Cross Phase Modulation (XPM). The recovery time for the phase modulation is relatively slow and prevents ultra fast switching [4.3]. By employing a differential scheme as shown in Figure 4.5 and injecting a control pulse into each arm of the interferometer, separated in time by a time delay of $\Delta\tau$, a careful optimisation of the control pulse amplitude and time delay can suppress the impact of recovery time and allow high speed demultiplexing [4.3].

In 2000 a joint experiment between ETH and COM•DTU within the framework of HIGHWAY demonstrated the first 160 to 10 Gbit/s demultiplexing experiment using a monolithically integrated SOA-MZI [4.4]. Error-free operation was not demonstrated due to the quality of the available pulse sources. However, the switching efficiency was determined in a following pump-probe experiment by measuring an extinction ratio of 15 dB 3.125 ps from the centre of the bit [4.5], which was estimated to be sufficient for demultiplexing 160 Gbit/s. Error-free 160 to 10 Gbit/s operation was demonstrated at Siemens in 2001 using the same switches [4.6]. In parallel with the demonstration of the monolithically integrated devices as switches in OTDM demultiplexing experiments [4.4], the use of the hybrid-integrated devices was also shown. Nakamura et al from NEC has been very successful in designing and fabricating SOA array chips, which are mounted on a MZI structured silica-based Planar Lightwave Circuit (PLC). Using this technique 168 Gbit/s [4.7], 252 Gbit/s [4.8] and 336 Gbit/s to 10.5 Gbit/s [4.9] have been demonstrated. A special variant using the hybrid-integrated technique is the gain-transparent interferometer, i.e. the MZI, to demultiplex a 160 Gbit/s OTDM signal at 1550 nm wavelength to 10 Gbit/s using control pulses situated at 1300 nm [4.10]. The advantage of using the switches in the gain-transparent mode is the absence of the unwanted gain-modulation of the data signal and the additional contribution of Amplified Spontaneous Emission (ASE) from the SOA to the data signal [4.10].

The SOA-MZI can, as sketched in Figure 4.5, be used to simultaneously demultiplex an OTDM channel and generate the complementary demultiplexed signal. This is not an inherent feature when implementing a SOA-MZI, but can be introduced by carefully designing two outlets of the device. With two output arms of the component, the switch can be used for all three configurations, i.e. serial, tree and parallel.

4.2.3 SIS: TOAD and SLALOM

The Terahertz Optical Asymmetric Demultiplexer (TOAD) configuration is shown in Figure 4.6.

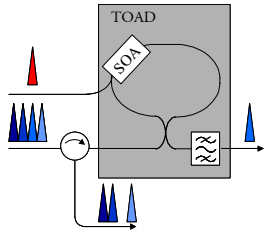

Figure 4.6: The TOAD configuration

The TOAD is a loop mirror, which includes a non-linear element (NLE) situated asymmetrically compared to the midpoint of the loop. When injecting a data-signal into the loop, the data-signal will at the main-coupler of the loop, be split into a clockwise (CLW) and a counter-clockwise (CCLW) signal. The two signals will traverse the loop and recombine at the main-coupler again. Without any external influence the signals will construct destructively at the output and constructively at the input of the coupler, effectively reflecting the data signal. However, by including an internal coupler within the loop and injecting a control signal in the CLW direction of the loop, the interference between the CLW and CCLW data signal can by controlled, and a target channel can be switched from the input of the coupler to the output coupler [4.11]. The mechanism behind the switching is based on the combination of the fast saturation of the NLE by the control pulse and the asymmetric position of the NLE within the loop. If the timing and the power of the control signal is carefully optimised, the control pulse will induce a phase-shift of π for the CCLW target pulse, a phase shift which is not generated when the CLW target pulse is passing the NLE due to the asymmetric position within the loop. The remaining data channels in both the CLW and CCLW signal will either experience no phase shift because the pulses have passed through the NLE before the control pulse has induced the phase shift, or vice versa [4.11]. Even though [4.12] reports switching speed of 250 Gbit/s, this experiment can only be regarded as an experiment evaluating the potential of the switch, as the 250 Gbit/s signal is constructed by only a few pulses. However, in [4.13] a full 160 to 10 Gbit/s OTDM demultiplexing experiment is reported. When comparing the TOAD to e.g. the Symmetrical Mach Zehnder and the Ultrafast Nonlinear Interferometers, there seem to be consensus that the TOAD inherently cannot compete in terms of switching speed [4.14] [4.15][4.16]. By concatenating two TOADS, the speed limit becomes more relaxed on the expense of a more complex structure [4.17].

A quite similar structure with a SOA placed asymmetrically within a loop mirror, is the Semiconductor Laser Amplifier Loop Mirror (SLALOM). The first reported SLALOM differed from the TOAD by avoiding both the control pulse and the internal coupler within the loop [4.18]. The time resolution was determined by the gain recovery of the SOA (SLA) and was consequently significantly slower than the TOAD [4.11]. However, the set-up gradually changed, first by the injection of a control pulse directly into the main coupler [4.19], and finally in a subsequent publication, the SLALOM configuration was identical to the TOAD when used for demultiplexing, as the control pulse was injected into an internal coupler [4.20].

By situating a circulator at the input to the TOAD, the complementary signal can be separated from the input data signal, thus enabling the TOAD for all three configurations.

4.2.4 SIS: UNI and PD-SMZI

In 1996 Patel et al [4.21] suggested the Ultrafast Nonlinear Interferometer (UNI) for OTDM demultiplexing and demonstrated its use by extracting a 10 Gbit/s base rate channel from a 40 Gbit/s OTDM signal. The principle of the UNI is shown in Figure 4.7.

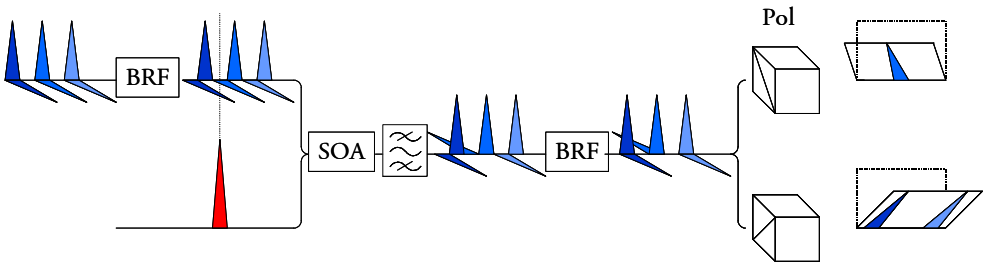

Figure 4.7: Principle of the UNI for demultiplexing.
BRF: Birefringent fibre. POL: Polariser.

An incoming OTDM signal is injected into a birefringent material, e.g. at an angle of 45° into a birefringent fibre, splitting the signal into two orthogonal polarisation states separated in time with a time delay of T. After the polarisation separation, the signal is combined with a control pulse, which is aligned in time with the delayed polarisation component of the target channel. In the SOA, the control pulse induces a relative change in the refractive index, imposing an optical phase change $\Delta\varphi$ of the delayed polarisation state. At the output of the SOA, an optical bandpass filter is used to filter out the control

pulses. The filter is followed by another birefringent material used to counteract the induced time delay T, before the signal is split into two branches each terminated in a polariser. If the phase change $\Delta\varphi$ equals π, the total polarisation angle of the recombined target channel will change 90° compared to the polarisation angel of the input signal [4.22]. Hence, by aligning the angle of the e.g. the upper polariser in Figure 4.7 to match the polarisation angle of the altered target channel, only this channel will pass the polariser while the other channels will be suppressed. Consequently, the target channel is demultiplexed from the OTDM signal. In [4.14] the UNI configuration is successfully demonstrated in a 100 to 12.5 Gbit/s demultiplexing experiment. Obviously, the UNI scheme shown in Figure 4.7 requires a careful adjustment of the input polarisation to the fast and slow axis of the birefringent fibre. This can be overcome by splitting the input data signal into two orthogonal polarisation signals, and injecting the two signals into two parallel slightly modified UNI configurations. By using this configuration a 160 Gbit/s signal was demultiplexed down to 10 Gbit/s [4.23]. The UNI has also been demonstrated in a 160 Gbit/s field trial on installed fibre in the United Kingdom [4.24]. In the terminology of NEC Corporation the principle of the UNI is also named a Polarization-Discriminating Symmetric Mach-Zehnder (PD-SMZ) switch [4.25], and a pump-probe characterisation of the device revealed switching windows in the order of 200 fs [4.26]. By injecting a 3-pulse signal separated 670 fs, pulse demultiplexing was demonstrated with 10 dB of extinction ratio between switched and non-switched pulses, emphasising the high-speed potential of the device.

By including two polarisers at the output of the UNI as shown in Figure 4.7 both the demultiplexed and complementary demultiplexed signal is generated, consequently ensuring that all three configurations are feasible with the UNI as the switch.

4.2.5 SNIS: EAM

The absorption modulation of the EAM has briefly been explained in chapter 2. By applying an electric voltage to the EAM a switching window defined by the applied voltage signal and the transfer-function can be induced. As opposed to the interferometric structures, the absorption modulation does not offer the complementary demultiplexed signal, thus preventing the EAM to be engaged within the serial and the tree structure.

The EAM has been very successful for OTDM switching since one of the first system experiments by Mollenauer et al in 1992, where the EAM was used to demultiplex a 5 Gbit/s to 2.5 Gbit/s [4.27]. The injected aggregated bit rate was the same year increased to 10 Gbit/s [4.28], 40 Gbit/s in 1994 [4.29] and 80

Gbit/s in 1998 [4.30]. As the electrical control signals applied to the EAMs were sinusoidal the corresponding switching window were also approximately sinusoidal, so it was difficult to increase the bit rate further when applying a 10 GHz sinusoidal electrical signal to the EAM as the SW would be to broad. This was overcome in [4.31], were two EAMs were concatenated ensuring a sufficient narrow SW to successfully demultiplex 100 Gbit/s to 10 Gbit/s. By applying a 20 GHz clock to the first EAM and a 10 GHz clock to the second EAM the bit rate could be increased to 160 Gbit/s [4.32]. This principle was further refined, by applying the 10 and 20 GHz sinusoidal clock signals at each end of a single EAM and still obtain 160 to 10 Gbit/s demultiplexing [4.33]. A combination of improved EAM devices and the introduction of commercial available 40 Gbit/s test equipment, resulted in a simplified set-up as only one control signal at 40 GHz and only a single EAM were required to demultiplex 160 Gbit/s to 40 Gbit/s [4.34].

Extracting a 10 or 40 Gbit/s base rate channel from an aggregated OTDM bit rate beyond 160 Gbit/s using an EAM can be cumbersome and is not straight forward even if the EAM in principle is sufficient fast. Two problems exist, when increasing the injected aggregated bit rate into the EAM, as outlined below.

Due to the sinusoidal-shaped transfer-function of the EAM, a pulse-shaped electrical signal with a duty cycle significant lower than 0.5 (corresponding to sinusoidal signal) is required in order to induce a sufficient narrow Switching Window capable of extracting 10 or 40 Gbit/s data signal from an aggregated high-speed OTDM signal. However, generating narrow pulsed electrical signals, with e.g. a base rate of 10 GHz requires electronics with bandwidths significantly larger than 10 GHz, hence jeopardising the fundament of OTDM, i.e. that the electronics should be base rate electronics. Accepting this breach, an example on how to generate pulsed control signals are demonstrated in [4.35] where the superposition of a 10 and 40 GHz clock can be used as the control signal for the two concatenated EAMs used to demultiplex 160 to 10 Gbit/s. The example shows that narrow control signals can be generated, but it also demonstrates how high-speed electronics are required. Generation of electrical signals based on superposition of sinusoidal electrical signals for demultiplexing of signals beyond 160 Gbit/s will most likely be even more challenging and resource demanding. Besides generating the pulsed electrical signal, a second challenge is to ensure a sufficient high bandwidth of the driver amplifiers and electrical interconnection, i.e. the connections used to apply the electrical signal to the EAM [4.36].

An elegant approach suggested by Kodama et al is to monolithically integrate a photo-diode with an EAM (PD-EAM) [4.36]. By injecting a 0.4 ps control pulse into the PD-EAM a switching window sufficiently narrow to demultiplex 160

to 10 Gbit/s was demonstrated [4.36]. The scheme has successfully been used to demultiplex 320 to 10 Gbit/s [4.37] and the high-speed demultiplexing potential was further demonstrated by injecting a data signal comprised of 4 non-modulated pulses corresponding to 500 Gbit/s into the PD-EAM and extracting each of the pulses [4.38]. The required short pulse source in the receiver makes the scheme comparable in complexity with other devices that require optical control signals, e.g. the interferometric techniques reported above.

4.2.6 SNIS: FWM in SOA

Another technique relies on Four-wave Mixing (FWM) in a Semiconductor Optical Amplifier (SOA) between the OTDM data signal and a control pulse train with a repetition rate corresponding to the base rate of the OTDM signal. The two signals will interfere and generate a gain and index grating, which results in both a cross-coupling between the data and control signal and generation of new signals at frequencies determined by the difference in frequency between data and control [4.39]. As the new frequencies require the presence of both a data and control signal, i.e. the equivalent of the logic function AND, FWM can be used to demultiplex the data signal.

In 1996 Morioka et al demonstrated the feasibility of FWM in a SOA by demultiplexing 200 Gbit/s to 6.3 Gbit/s [4.40]. The potential as a realistic candidate for implemented high-speed systems was emphasised by the realisation of a PLC integrated SOA array used to simultaneously demultiplex eight 20 Gbit/s channels from an aggregated OTDM signal of 160 Gbit/s [4.41] and the following 160 Gbit/s transmission experiment [4.42]. FWM is a very fast process and has been reported used as the Optical Phase Detector in a Phase Locked Loop extracting a 6.3 GHz clock from a 400 Gbit/s OTDM signal [4.43], see chapter 4. The quality of the FWM product in the clock extraction experiment could be used to lock a local generated pre-scaled clock to an incoming data signal; however, this is not necessarily sufficient for extracting a time channel error-free from an OTDM signal. Optimisation of the SOA and the FWM process allowing an increase in the bit rate has been investigated to some degree in literature, see e.g. [4.44][4.45][4.46], however without concluding an upper limit for demultiplexing speed.

FWM in semiconductors, and in fibres, see section 4.2.3.2, do not in principle offer both the demultiplexed and complementary demultiplexed signal required for all three configurations in Figure 4.3. However, a complex modification of the set-up can generate both these signals by injecting two control signals into the device (semiconductor or fibre) together with the OTDM signal [4.47], see Figure 4.8.

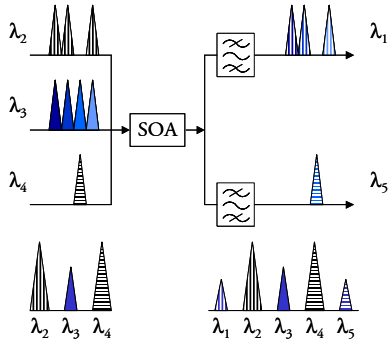

Figure 4.8: Generation of demultiplexed and complementary demultiplexed signal using FWM in SOA [4.47]

One of the control pulse trains at wavelength λ_4 has a repetition frequency corresponding to the base bit rate of the OTDM signal, and is aligned in time with the target channel. The other pulse train at wavelength λ_2 is composed by (N-1) pulses, corresponding to the complementary OTDM signal, with the empty time slot aligned in time to the target channel. By splitting the output signal from the SOA/fibre into two branches filtering each containing an optical bandpass filter centred at the wavelengths of FWM products, the two signals are available and can in principle be used for all three configurations.

When inspecting Figure 4.8 and the principle behind, it is obvious that FWM in both semiconductors and fibre, see section 4.2.3.2, can also, as on of the few techniques, offer the possibility of demultiplexing several base rate channels simultaneously in one single component. The set-up in Figure 4.8 is modified, and M control pulse trains with a repetition frequency corresponding to the base bit rate of the OTDM signal at different angular frequencies, are injected into the SOA. By aligning the control pulse trains to the target channels, M base rate OTDM channels can be switched to different wavelengths. One drawback of this approach is the careful wavelength management; exemplified by injecting a 160 Gbit/s OTDM signal and 16 control pulse trains, the output signal from the semiconductor would include 33 wavelengths (depends on the FWM process). Another drawback is the need for multiple expensive short pulse sources, which most likely counteracts the potential cost reduction and complexity reduction offered by only using a single switch.

4.2.7 FIS: NOLM

The Nonlinear Optical Loop Mirror (NOLM) will be explained in more details in section 4.4, but is briefly described in this section in order to offer a

complete summary of the most important OTDM switches presently considered. The principle is shown in Figure 4.9.

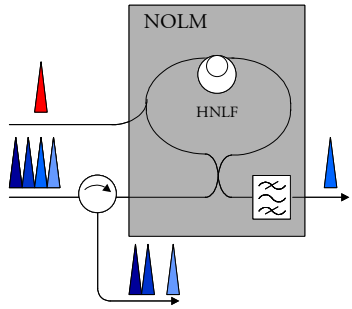

Figure 4.9: Principle of switching using a NOLM

The principle of the NOLM is to some extent similar to the TOAD structure, as it is based on a Sagnac interferometric structure. The NOLM consists of a main-coupler, which is used as inlet and outlet of a fibre loop as seen in Figure 4.9. The fibre loop is composed by a nonlinear fibre as the NLE and an additionally coupler. An OTDM signal is injected into the main-coupler of the NOLM, and is split into a clock-wise (CLW) and a counter clock-wise (CCLW) signal, which traverse the loop. Analogous to the TOAD, the two signals will after the fibre loop be recombined and will without any external source experience destructive interference at the output of the NOLM and constructive interference at the input of the NOLM, thus be reflected (mirrored) back to the same port of the coupler as was used as the inlet to the NOLM. By injecting a high-power control pulse in the CLW direction of the fibre loop, aligned in time to the target channel of the OTDM signal, the control pulse can change the optical phase of the target channel by π due to XPM. After recombination of CLW and CCLW signals, constructive interference is obtained at the output of the NOLM for the target channel, without similar changes for the rest of the OTDM signal, consequently acting as an OTDM demultiplexing switch.

The principle of the NOLM was suggested in 1988 [4.48], although only the data signal was injected into the NOLM utilising Self Phase Modulation (SPM), as opposed to the XPM approach outlined above. However, only two years later the set-up was modified to include a control pulse at another wavelength [4.49], which allowed the NOLM to be used for demultiplexing a non-modulated ~ 1 GHz pulse train to ~ 75 MHz [4.50]. Since then numerous researchers have for almost two decades extensively investigated the NOLM, both theoretical and experimentally, where the four articles by Jinno probably are the most influential [4.2] [4.51][4.52][4.53]. In 1992 64 to 4 Gbit/s demultiplexing was demonstrated using a NOLM based on 14 km of Dispersion Shifted Fibre

(DSF) [4.54]. Increasing the aggregated bit rate to 100 Gbit/s and demultiplexing the signal to 6.3 Gbit/s was shown the year after, when a NOLM was constructed using 6 km of Polarisation Maintaining DSF (PM-DSF) [4.55]. The higher the bit rate, the higher the impact of the group velocity mismatch between the control and the data signal, i.e. walk-off, on the performance [4.2]. In order to demultiplex from even higher bit rates, a NOLM was constructed by concatenating 9 carefully chosen 50 m Dispersion Flattened Fibre (DFF) pieces together, reducing the total walk-off to less than ± 400 fs [4.56]. Using this NOLM, error-free demultiplexing from 640 to 10 Gbit/s was demonstrated [4.57]. Walk-off can be avoided by placing the control and the data signal symmetrically around the zero-dispersion wavelength [4.2]. This was exploited in [4.58], where a 320 Gbit/s OTDM signal was demultiplexed to 10 Gbit/s using 100 m of Highly Nonlinear Dispersion Shifted Fibre implemented in a NOLM. Because the fibre length was very short and the dispersion slope was only 0.032 ps/nm^2/km, the NOLM could also be used to demultiplex 640 to 10 Gbit/s without the symmetrical wavelength management [4.59]. The process of designing and manufacturing commercial available Highly Nonlinear Fibres (HNLF) was further refined by e.g. OFS Fitel Denmark ApS, who provided the fibre for the 320 Gbit/s [4.60] and 640 Gbit/s [4.61] experiments reported in section 4.5. These fibres had a dispersion slope of only 0.013 ps/nm^2/km, so even a length of 500 m did not require special wavelength management at 320 Gbit/s thus easing the actual system design.

4.2.8 FNIS: Kerr-switching

According to [4.62], the principle behind the Kerr switch was already reported back in 1973. A thorough investigation of the Kerr switch was presented in [4.63]. The theory behind Kerr switching is relatively cumbersome relying on XPM between pump and probe with different polarisation [4.62]. Figure 4.10 aids the explanation of the principle behind Kerr switching.

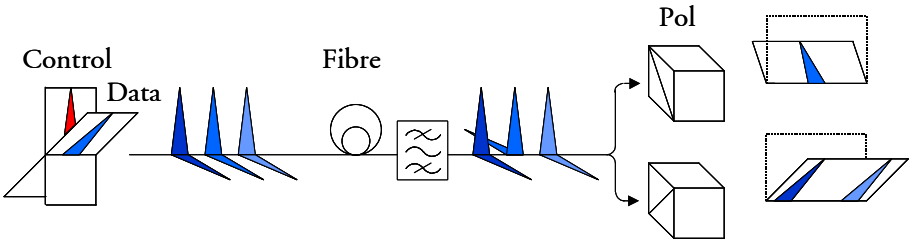

Figure 4.10: Principle behind Kerr switching

The set-up is very simple, as seen at Figure 4.10 [4.62]. A fibre and a pair of polarisers at the output of the fibre are the main components. The orientation

of the polarisers is chosen to be parallel and perpendicular to the linearly polarised probe injected into the fibre; the perpendicular polariser prevents the probe signal to pass. By adding a linearly polarised pump to the probe, with a 45° angle between the polarisation states of the two signals, the polarisation state of the probe can be altered to allow the probe passing the polariser. The probe signal can be composed into a polarisation component perpendicular and parallel with the pump signal. If the power of the pump is sufficiently high, the two probe components will experience a difference in the refractive index due to the pump-induced birefringence. The birefringence will change the phase relation between the two probe components, and the polarisation state of the probe will be changed. By optimising the effect of the induced birefringence the polarisation state of the probe can be altered to match the output polariser consequently ensuring transmission of the probe.

Thus, by injecting a pulse train with a repetition frequency equal to the base rate of the OTDM signal as the pump and aligning the pump signal in time to the target channel of the OTDM signal, which is injected into the fibre as the probe signal, the target channel will be switched to the output of the polariser [4.63]. As the nonlinearity response time is in the order of ~ 2-4 fs [4.62], the high-speed potential of Kerr switching is very promising emphasised in 1995 when the potential of switching a 460 Gbit/s signal was demonstrated [4.64]. Watanabe et al [4.65] utilised both Kerr switching and parametric amplification due to Four-Wave Mixing (FWM) for switching a 10 Gbit/s data channel from a 640 Gbit/s OTDM signal.

As with the UNI, the two polarisers at the output of the Kerr switch as shown in Figure 4.10 allows the generation of both the demultiplexed and complementary demultiplexed signal, and thus can be used in all three configurations.

4.2.9 FNIS: FWM in fibre

Another exploitation of the nonlinear response of the bound electrons of a material to applied optical fields is the FWM [4.62].

Injecting three signals at different wavelengths can, if specific requirements are fulfilled, generate new signal(s) at different wavelength(s), in principle 9 different signals [4.66]. In a WDM transmission system, FWM can limit the performance, and should consequently be suppressed [4.66]. However, FWM can also be used for signal processing e.g. in terms of demultiplexing and switching, which is the objective in this chapter. In order to obtain FWM both frequency and wave vector matching is required [4.62], which due to the impact of chromatic dispersion is not trivially fulfilled without careful

optimisation of the set-up, see e.g. [4.62] and [4.67]. However, by utilising Dispersion Shifted fibres, phase matching in the telecommunication window around 1550 nm can relatively easyly be obtained by situating two of the incoming three wavelengths symmetrically around the zero-dispersion wavelength [4.68]. For OTDM switching purposes, usually partially degenerated FWM is exploited, by injecting only two signals into the fibre, i.e. a high power base rate pulse train and the OTDM signal. Phase matching is obtained by situating the pump on the zero-dispersion wavelength [4.68].

Using this principle of wavelength management, 500 to 10 Gbit/s demultiplexing was demonstrated [4.69], by injecting a 10 GHz pump and a 500 Gbit/s OTDM signal, with centre wavelength separation of 13.7 nm, into 300 meter of PM-DSF. The result is quite remarkable when comparing the estimated walk-off of 1.8 ps between pump and the signal with the 2 ps time slot of a 500 Gbit/s signal. In [4.70] 200 Gbit/s was successfully transmitted over 100 km of fibre, before demultiplexed to the base rate of 6.3 Gbit/s using FWM in 3 km of Dispersion Shifted Fibre.

One of the problems associated with FWM in fibres is the poor conversion efficiency, i.e. relation between FWM product power at the output of the fibre and the probe power at the input of the fibre, which in [4.69] is as low as 2.5 %. Utilising very high pump powers and exploiting parametric amplification, the conversion efficiency can increase to more than 100 % [4.71], and demultiplexing with a gain of 42 dB has been demonstrated for 40 to 10 Gbit/s demultiplexing [4.72]. Another problem with FWM, both in SOAs and in fibres is the polarisation dependence. It can be overcome by modifying the set-up shown in Figure 4.8, on the expense of higher degree of complexity. The highest bit rate demultiplexed using the FWM process in fibre is 100 to 10 Gbit/s demultiplexing with counter propagating pump and signals within a loop mirror [4.73].

It should be noted that the comments regarding the demultiplexed and complementary signals from the SOA switch also applies for the fibre based FWM switch.

4.2.10 Summary on State-of-the-art switches

A short summary of the reported bit rates demultiplexed in different switches, are given in table 4.2. Notice that the references are divided into experiments where the signal is a full OTDM signal with all channels Pseudo Random Bit Sequence (PRBS) modulated as opposed to the demultiplexing of a single pulse train from a signal composed by multiplexing a limited number of pulse trains

without any modulation. The latter can only be regarded as indication of performance.

M	S	Switch	D	CD	Demultiplexing OTDM:Base	Ref
SOA	I	SOA-MZI	X	X	160:10 Gbit/s PRBS	[4.4]
					160:10 Gbit/s PRBS	[4.6]
					336:10 Gbit/s PRBS	[4.9]
		TOAD SLALOM	X	X	160:10 Gbit/s PRBS	[4.13]
					250 Gbit/s : 100 MHz pulses	[4.12]
		UNI PD-SMZI	X	X	160:10 Gbit/s PRBS	[4.23]
					160:10 Gbit/s PRBS	[4.24]
					1492 Gbit/s : 82 MHz pulses	[4.26]
	NI	EAM	X		160:10 Gbit/s PRBS	[4.32]
					160:10 Gbit/s PRBS	[4.33]
					160:40 Gbit/s PRBS	[4.34]
		PD-EAM	X		320:10 Gbit/s PRBS	[4.37]
					500 Gbit/s : 52 MHz pulses	[4.38]
		FWM SOA	X	(X)	200:6.3 Gbit/s PRBS	[4.40]
Fibre	I	NOLM	X	X	640:10 Gbit/s PRBS	[4.57]
					640:10 Gbit/s PRBS	[4.59]
					640:10 Gbit/s PRBS	[4.61]
	NI	Kerr	X	X	460 Gbit/s : 82 MHz pulses	[4.64]
					640:10 Gbit/s PRBS	[4.65]
		FWM fibre	X	(X)	500:10 Gbit/s PRBS	[4.69]

Table 4.2: Summary of most important OTDM switches. M denotes the switch material. S is the structure, i.e. interferometric (I) or non-interferometric (NI). The table lists if the switch offers demultiplexing (D) and/or complementary demultiplexing (CD) by marking an 'X' in the column. An '(X)' indicates possible but modification required. Reported demultiplexing experiments are listed with both references and the aggregated OTDM bit rate and base rate. Experiments have either verified demultiplexing by PRBS or pulse demultiplexing.

For several years switches based on fibre non-linearity easily outperformed switches based on semiconductor devices due to the almost instantaneous response of the non-linear Kerr effect. Albeit semiconductor devices in recent years have started to match fibre devices in demultiplexing speed, fibre based switches still offer the highest demultiplexing rate and is still very attractive and serious candidate as an OTDM switch. At the time of writing this thesis, the highest aggregated OTDM bit rate demultiplexed, is 640 Gbit/s, which have

been demonstrated by utilising either the Kerr switch [4.65] or the NOLM [4.56] [4.59] [4.61].

4.3 Eye Opening Penalty simulation model

In order to estimate the impact of different shapes of the switching window, a simple model is implemented. It consists of an OTDM transmitter, a switch for demultiplexing and extracting the target channel from the aggregated data signal, an ideal photo-detector, a low-pass filter and finally an Eye Opening Penalty (EOP) detector, see Figure 4.11.

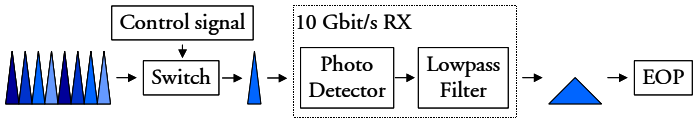

Figure 4.11: OTDM system emulated by simulation tool

The simulation tool is a modified version of the tool used in chapter 2, which was used for evaluating the pulse source requirements. The modified simulation tool does not calculate a Bit Error Rate (BER), but instead the model calculates an EOP. It is important to emphasise that the simulation results based on BER versus EOP cannot be directly compared in terms of e.g. penalty. There are advantages and disadvantages of both evaluation tools, and both can provide insight in the performance of the system. The main reason for using the EOP for evaluating the switch impact is the substantial reduction in simulation time.

A few comments on the simulation tool is outlined below

4.3.1 Transmitter

In the transmitter the data pulse width can be varied as function of the relative width of the OTDM time bit slot. When narrowing the pulse width, the peak power needs to be increased in order to avoid a power penalty originating from the decrease in total pulse energy. The average power P_{AV} of a modulated[26] signal can for a signal based on Gaussian shaped pulses be derived to

$$P_{AV} = \frac{1}{4}\sqrt{\frac{\pi}{\ln 2}}\frac{T_{FWHM}}{T_S}P_C \tag{4.3}$$

[26] Assuming equal number of marks and spaces

Where T_{FWHM}, T_S and P_C are the Full Width Half Maximum width of the pulse, the time bit slot and the peak power of the pulse, respectively. By inspecting eq. (4.3) it is evident, that keeping the product $T_{FWHM}P_C$ constant, the average power of the modulated signal is also kept constant.

In these simulations, the average power of the individual channel is kept constant in order to avoid a power-induced penalty and emphasise the switch-induced penalty. By keeping the average power of each individual channel constant, the total energy of the OTDM signal will vary linearly as function of the number of OTDM channels. In reality, the total acceptable power of the OTDM signal, e.g. in terms of transmission penalty has lower and upper bounds. However, when evaluating an ideal switch with no physical constraints, the total OTDM power is not an issue.

The pulses of the OTDM data signal will experience some short-term variations in the timing position from the ideal position in time, i.e. jitter [4.74]. The timing jitter can originate from the pulse source used to generate the OTDM signal, see e.g. [4.75]. Additionally, transmission of the signal can add random timing jitter to the signal, e.g. due to the interaction between the optical field and acoustic waves [4.76]. Thus, it is imperative to ensure that the system can operate in the presence of timing jitter.

The evaluation of random processes is not straightforward. Techniques have been presented, e.g. in terms of Monte Carlo simulations [4.77], [4.78], Moment Generating Functions [4.79] [4.80] and as analytical expressions based on simplifications and assumptions [4.52][4.81] – techniques, which often are very time consuming. The model presented in this section was before the modification used for Monte Carlo simulations in chapter 2. However, the model put high demands on the total computation time because the simulations needs to be repeated numerous times to ensure that the different combinations of the random process are investigated. To keep the computer processing time to an acceptable level, the Monte Carlo approach was discarded and the EOP simulation tool was adopted due to the relative fast computation time. One of the drawbacks when using the EOP evaluation tool is the fact that the estimated performance of the system will depend solely on the single event, which generates the most deteriorated eye. Monitoring an infinite number of bits, which are all ideal in every respect except for one single deteriorated bit, this single bit will irrespective of the probability of the incidence determine the EOP.

In conclusion, the EOP evaluation tool can be used to reveal how the specific values of the random process impact on the system. However, the interpretation of the results generated by this tool should be cautious and for more detailed investigations the EOP model cannot replace the more accurate

tools such as Monte Carlo simulations and Moment Generating Functions because these tools include the probability for each event.

For the data signal, different temporal offsets of the pulses are investigated as sketched in Figure 4.12. The centre of the pulses carrying the data of the target channel is shifted from the ideal timing position, as shown in Figure 4.12B. Also the impact of neighbouring channels shifted towards the target channel is investigated, see Figure 4.12C. Finally, target and neighbouring channel offsets combined are evaluated.

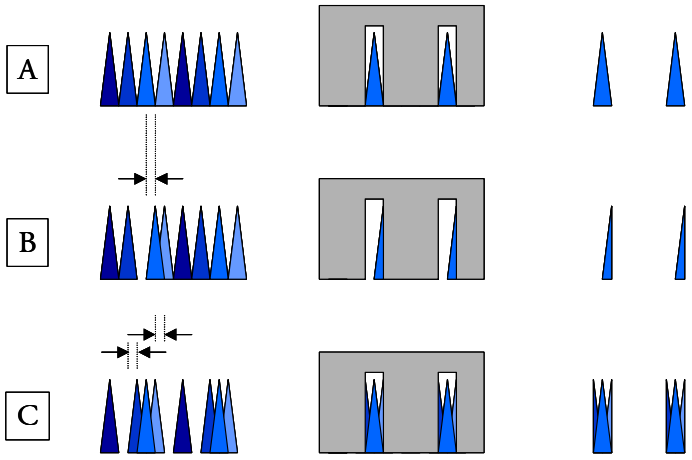

Figure 4.12: Illustration of without (upper) and with (lower) timing jitter.

An important parameter of the data signal is the Pulse Tail Extinction Ratio (PTER), as outlined in chapter 2. For sufficiently high PTER values the impact of PTER on the system performance is negligible. Hence in these simulations, the PTER is assumed fulfilling the requirements extracted in chapter 2, and is consequently ignored.

4.3.2 Switch

The switch in the simulations is completely detached from any physical process, and thus any parameter, e.g. shape, width or extinction ratio of the induced switching window can be changed irrespective if any physical process allows this or not, as indicated in Figure 4.13. Hence, it is possible to establish general rule-of-thumb design values for the switching window.

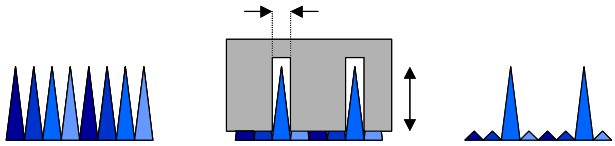

Figure 4.13: Variation of width, extinction ratio and shape of SW and the impact on the demultiplexed signal.

Three shapes of switching windows will be investigated within this thesis. The first SW is Gaussian shaped in order to evaluate the switching performance when the SW is an exact replica of an injected control pulse. The second SW is Super Gaussian shaped, to allow a more square-shaped SW with a flat top, which is included to illustrate how different shapes of SW alters the switching performance. Finally, because the concluding demultiplexing experiment in section 4.5 is using a NOLM as the switch, the SW derived from a simple NOLM model is also included in the comparison. When injecting a Continuous Wave (CW) beam into the switch, the three different types of SW induce a characteristic shape of the output power signal as function of time. The SW shapes in the power domain can analytical be described as

$$P_G(t) = P_{IN} \exp\left(\frac{-t^2}{T_0^2}\right)$$

$$P_{SG}(t) = P_{IN} \exp\left(\frac{-t^{2m}}{T_0^{2m}}\right) \tag{4.4}$$

$$P_{NOLM}(t) = P_{IN}\left(\frac{1-\cos\Delta\phi}{2}\right)$$

Where P_{IN} is the input power of the signal, T_0 is the e^{-1} intensity width, m is the order of the Super Gauss, $\Delta\phi$ is a phase difference controlling the switching. Subscripts G, SG and NOLM denote Gauss, Super Gauss and Non-linear Optical Loop Mirror, respectively. The NOLM expression is derived in a subsequent section. In Figure 4.14 an example is shown of all three SW, normalised to have identical FWHM temporal width.

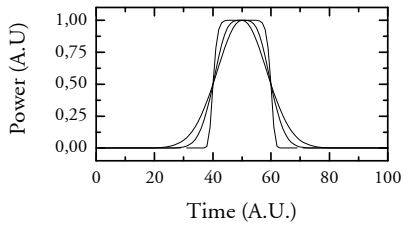

Figure 4.14: Example of three different switching windows evaluated. The steepest slope is the Super Gaussian SW (order m = 5), followed by the simple NOLM model and finally the Gaussian SW.

As previously outlined in chapter 3, the extracted clock will include timing jitter. The clock controls the timing position of the SW, which consequently will vary due to jitter. The impact of timing jitter of the SW is evaluated similar to the timing jitter in the incoming data signal. In Figure 4.15 an offset is added to the ideal timing position of the SW and the outcome is sketched, and when compared to the ideal situation in Figure 4.12A, it indicates erroneous detection. Using the EOP model, the same reservations using the results should be preserved.

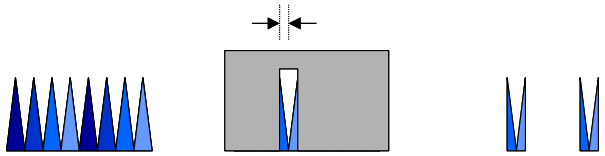

Figure 4.15: Illustration of the effect of timing jitter on the clock controlling the temporal position of the SW.

4.3.3 Receiver

The photo-detector is assumed not to add any noise to the incoming signal. This is in general not true and should be included when optimising a receiver for a specific system, including OTDM receivers. However, relatively thorough investigations of RZ receivers can be found in existing literature, see e.g. [4.82] and are beyond the scope of this thesis. Thus the photo-detector is modelled as a squaring device, squaring the incoming electrical field, with an infinite bandwidth. The photo-current/voltage is subsequently lowpass filtered electrically, emulating both the actual bandwidth of the photo-detector and an additional electrical filter.

The choice of transfer function and bandwidth of the electrical filter, are partly determined by the aforementioned noise contributions from the photo-detector combined with e.g. the accumulated ASE noise from the optical transmission system.

One of the prerequisites of an OTDM system is the exploitation of base rate electronics in the transmitter and the receiver. Thus, the bandwidth of the electrical filter should not exceed base rate, even if the interplay between a specific optical switch for demultiplexing and an electrical filter with higher bandwidth might introduce better performance in terms of e.g. improved sensitivity. A rule-of-thumb states that the typical bandwidth value for RZ transmission is approximately 35 % of the bit rate [4.81]. However, the optimum bandwidth depends on e.g. the pulses used to generate the OTDM signal, whether pre-amplification is included in the receiver configuration and the actual noise distribution. Thus, optimum bandwidths of 50 % and 75 % of the bit rates have been reported [4.82] indicating that no general optimum bandwidth exists for RZ data communication, instead the optimum bandwidth needs to be determined case by case. In the simulations presented below, the filter bandwidth is equal to the 70 % of the bit rate, which is used in Non-Return-to-Zero (NRZ) modulation systems [4.81]. This allows the use of on-shelf base rate receivers, hence reducing the total costs of the OTDM system compared to customised components.

A transfer function often used for the electrical filter in the receiver is the maximal flat time delay filter family labelled the Bessel filters[27] [4.83]. The normalised transfer functions of a 4th order Bessel filters T_{B4} are [4.84]

$$T_{B4}(s) = \frac{105}{s^4 + 10s^3 + 45s^2 + 105s + 105} \tag{4.5}$$

4.3.4 Eye opening detection

After the opto-electrical detection and filtering, the simulation model determines the maximum eye-openings of the 10 Gbit/s back-to-back signal, the 10 Gbit/s signal injected into the switch before received and finally the OTDM signal, i.e. 160, 320, 640 or 1280 Gbit/s demultiplexed in the same switch. The eye opening in this simulation is determined at the single time position within the base rate time slot, resulting in the maximum eye opening when sampling through all the bits. This is in contrast to other published articles, see e.g. [4.85], using the EOP for evaluating optical communication systems, where the impact of timing jitter in the decision circuit is included, by

[27] Or Thomson filter

determining the eye opening in a time interval in each time slot corresponding to the jitter. However, in OTDM the same clock is used, for both triggering the switch used for demultiplexing and the base rate decision circuits, see Figure 4.1, and as the acceptable timing for extracting a channel from an OTDM signal is less than the OTDM time slot, the impact of the same timing jitter on the decision circuit operating within the frame of the base rate time slot, is negligible and is consequently not included in the simulations. Figure 4.16 indicates how the amplitude values required calculating the EOP is determined, and eq. (4.6) defines how the EOP is calculated.

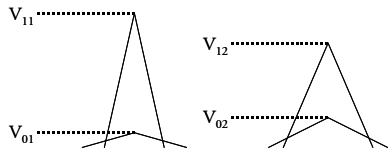

Figure 4.16: Values required to calculate EOP.

$$EOP = 10\log\left(\frac{V_{11} - V_{01}}{V_{12} - V_{02}}\right) \tag{4.6}$$

In the simulations, the Eye Opening Penalty is calculated as the relation between the demultiplexed signal and the 10 Gbit/s back-to-back signal. Two different EOPs are calculated, as seen in Figure 4.17; EOP1 between the demultiplexed 10 Gbit/s data signal and the 10 Gbit/s back-to-back signal and EOP2 between the OTDM signal and the 10 Gbit/s back-to-back signal.

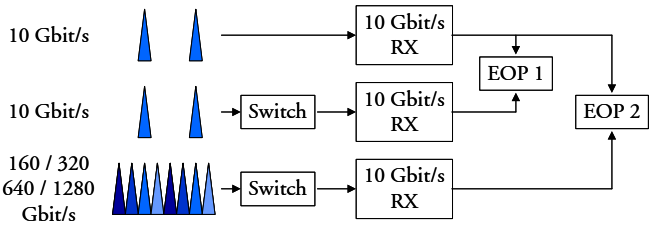

Figure 4.17: Calculation of EOP1 and EOP2 evaluating the impact of the switching window used for demultiplexing.

4.4 Requirements to general switch

4.4.1 General discussion of results

To illustrate the outcome of the aforementioned model, OTDM signals generated by 16, 32, 64 and 128 10 Gbit/s data channels, composed by data pulses with FWHM width corresponding to 0.4 times the time slot of the aggregated bit rate are demultiplexed with both a Gaussian and Super Gaussian shaped SW with varied FWHM. The results are shown in Figure 4.18.

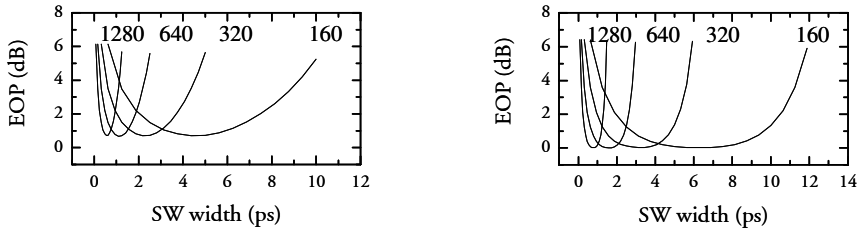

Figure 4.18: Demultiplexing of 160, 320, 640 and 1280 Gbit/s OTDM signals in a switch, with Gaussian (left) and Super Gaussian (right) shaped SW is evaluated by calculating the EOP. Pulses of the data pulses correspond to 0.40 times the OTDM time slot. The width of the SW is varied.

As expected, the optimum performance, i.e. minimum EOP, is obtained for decreasing FWHM SW width for increasing bit rate. This is an obvious consequence of the decreased temporal distance between the data pulses when the bit rate is increased. Thus, in order to extract design parameters for different bit rates, each bit rate should in principle be simulated individually. However, as the only parameters changed when increasing the bit rate are the FWHM width of the SW, T_{FWHMSW}, and the data pulses, T_{FWHM}, the obtained results can be used at arbitrary bit rates, if the widths are specified relatively to the width of the OTDM time slot T_S. Extensive simulations have confirmed this expectation. Consequently, in the following section all results are presented as function of relative width, defined as the ratios T_{FWHM}/ T_S and T_{FWHMSW}/ T_S, and can be scaled to the any required OTDM bit rate.

For discussing the results in more details, a typical result is shown in Figure 4.19, where EOP1 and EOP2 for an OTDM system based on Gaussian pulses with FWHM equal to $0.4T_S$ are depicted as function of the relative switching window width using both a Gaussian and Super Gaussian SW.

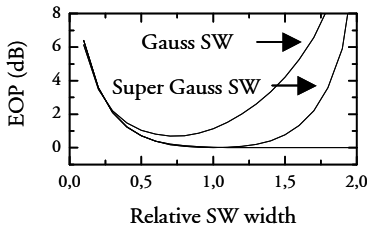

Figure 4.19: EOP1 and EOP2 as function of relative FWHM SW width for an OTDM system based on pulses with FWHM equal to $0.4T_S$ and demultiplexed using a switch with Gaussian and Super Gaussian shaped SW. EOP1 is identical for the two switches.

For the Gaussian and Super Gaussian SW, the two EOP1's are identical. Because the performances for narrow SW are identical, the relative high EOP1, i.e. close to 6 dB, is a consequence of the reduced energy of the target channel after passing the switch and not due to a difference in shaping of the demultiplexed signal because of different SWs. For increased width of the SW, the energy of the demultiplexed 10 Gbit/s data signal is approaching the energy of the 10 Gbit/s back-to-back signal, and thus the EOP is asymptotically decreasing to 0 dB. For narrow SW the EOP for evaluating the switch performance when injecting an OTDM signal into the switch, i.e. EOP2, is identical to EOP1. Hence, increasing the width will reduce EOP2 to a certain point until parts of the neighbouring channels will be present in the output signal of the switch and start introducing significant Inter Symbol Interference (ISI) in the target channel. The increased ISI results in an increased EOP2. Consequently, a switch width exists, which induces a minimum system penalty. It is noted how the Super Gaussian SW introduce a lower minimum EOP penalty and a significantly wider range of SW widths with a low EOP penalty. This is a consequence of the almost vertical edges of the Super Gaussian SW, efficiently suppressing the neighbouring channels to a certain point. From Figure 4.19 the optimum SW width for Gaussian SW is $0.7T_S$ and $1.0T_S$ for the Super Gaussian SW. In the next section a more detailed investigation is presented of the impact of OTDM pulse width on the system performance.

4.4.2 Impact of data pulse widths

In Figure 4.20, EOP2 is depicted as function of the relative SW width for OTDM signals based on pulse trains with relative FWHM equal to 0.2 to 0.9 times the OTDM time slot T_S for both Gaussian and Super Gaussian SW.

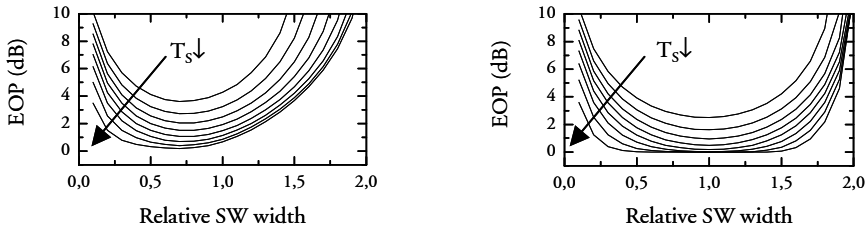

Figure 4.20: EOP2 depicted as function of relative SW width using Gaussian (left) and Super Gaussian (right) SW for demultiplexing OTDM signals based on pulse trains with relative FWHM equal to 0.1 to 0.9 times the OTDM time slot T_S.

In general, the wider the data pulse the higher EOP2, irrespective of the SW width, a trend which is also apparent in chapter 2 where the pulse source requirements are estimated. When the SW widths are narrow, e.g. < $0.5T_S$, the EOP penalty for a specific SW width is increased for increased data pulse width, because an increased part of the target channel energy is suppressed in the switch due to pulse shaping. For relatively broad SW widths exceeding e.g. $0.5T_S$, the EOP is increased due to the impact of ISI. These observations are valid for both the Gaussian and the Super Gaussian SW. As in Figure 4.19 however, there is a distinct difference between the results due to more efficient suppression of neighbouring channels when using the Super Gaussian SW. Interestingly, the optimum widths regardless of data pulse widths are constant ~ $0.7T_S$ and ~ $1.0T_S$ for Gaussian and Super Gaussian SW, respectively. In table 4.3 the minimum EOP's and the corresponding SW widths are summarised for varied data pulse widths. An additional important parameter is the acceptable variation range of SW widths, which maintain adequate performance in terms of EOP. In the tables, the relative variation range of FWHM SW width resulting in 1 dB penalty relative to the minimum EOP is listed.

Relative Pulse Width (T_S)	Gauss			Super Gauss		
	Minimum EOP (dB)	Minimum Width Min EOP (T_S)	1 dB relative variation range (T_S)	Minimum EOP (dB)	Minimum relative width Min EOP (T_S)	1 dB relative variation range (T_S)
0.2	0.19	0.7	0.93	0.0	1.1	1.48
0.3	0.41	0.7	0.85	0.0	1.1	1.33
0.4	0.70	0.7	0.77	0.0	1.0	1.13
0.5	1.07	0.7	0.73	0.2	1.0	1.00
0.6	1.51	0.7	0.72	0.5	1.0	0.90
0.7	2.04	0.7	0.70	1.0	1.0	0.84
0.8	2.72	0.7	0.68	1.6	1.0	0.82
0.9	3.62	0.7	0.65	2.5	1.0	0.82

Table 4.3: Minimum EOP when demultiplexing an OTDM signal based on data pulses with varied FWHM, using a switch inducing a Gaussian or Super Gaussian switching window. Relative variation range of FWHM SW width resulting in 1 dB penalty relative to the minimum EOP is listed.

For increased data pulse widths, the acceptable variation range of the SW width is decreased for both Gaussian and Super Gaussian SW. It is also evident that the acceptable variation range is significant larger for the Super Gaussian SW compared to the Gaussian SW, thus easing the requirements to the switch.

Using table 4.3 an approximately width of the SW can be estimated for any bit rate by scaling the results to target OTDM time slot. However, these results are modified when including impairments of both the data signal and the SW as elaborated upon in the following section.

4.4.3 Impact of extinction ratio (ER) of SW

In the previous simulations, the SW was assumed to be ideal Gaussian and Super Gaussian SW's, which asymptotically approaches zero away from the centre of the SW. However, the actual physical implementation of the switches often induces a narrow SW accompanied with a pedestal, as indicated in Figure 4.13, which limits the suppression of the neighbouring channels and affects the performance of the system. In this section the impact of a pedestal, defined as the extinction ratio between the peak of the SW and the pedestal measured in optical power, is investigated and target design rules are extracted.

A 160 Gbit/s OTDM signal based on data pulses with $0.4T_S$ FWHM width is injected into the switch. The switch is characterised by either a Gaussian or Super Gaussian SW, which are accompanied with a pedestal corresponding to

an ER equal to 5, 10, 15, 20 and 30 dB. The impact of extinction ratio is evaluated by calculating the EOP2 for each ER as function of the SW FWHM width and shown in Figure 4.21.

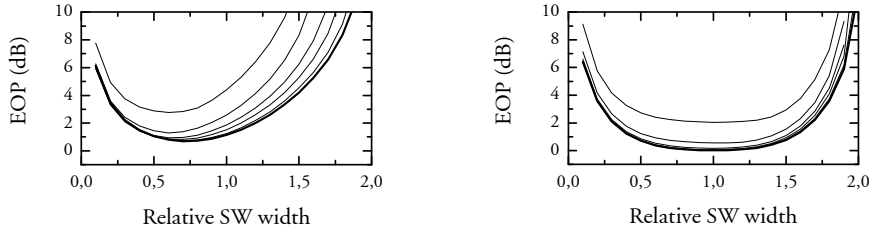

Figure 4.21: EOP as function of FWHM width of SW. ER varied from infinite (bold lines) to 30, 20, 15, 10 and 5 dB. SW is Gaussian (left) and Super Gaussian (right).

Inspecting the EOP dependence on relative SW width, some general observations can be made. When the ER of the SW is decreased from infinity, i.e. ideal SW, to a relative low value of ER, the EOP is increased due to ISI from the neighbouring OTDM channels. For the Gaussian SW, no significant impact is observed for ER ~ 20 dB, especially if the FWHM width of the SW is close to optimum performance. For the Super Gaussian SW, an ER ~ 15 dB reveals negligible difference compared to the ideal Super Gaussian SW, thus more relaxed than the requirements to the Gaussian SW. Another consequence of decreasing the ER is the observed shift of optimum width towards narrower SW for the Gaussian SW, because it reduces the impact of the aforementioned ISI. Albeit, this shift in optimum width is relatively small, as it is shifts from $0.7T_S$ for an ideal Gaussian shaped SW to $0.6T_S$ for a Gaussian SW with ER = 5 dB. For the Super Gaussian SW no shift in optimum width is observed.

4.4.4 Impact of timing jitter

Using the EOP evaluation tool with the restrictions in interpretation of the results, timing jitter can be investigated as a static offset added to the ideal timing position. With this analysis it can be estimated which FWHM SW width is best suited for accommodating demultiplexing jittered OTDM signals.

First the impact of timing jitter on the target channel, as sketched in Figure 4.12B, affects the system performance. In Figure 4.22 the centre of the target channel is displaced from the ideal position with $0.0T_S$ (bold line) to $0.4T_S$, both using a Gaussian SW and a Super Gaussian SW.

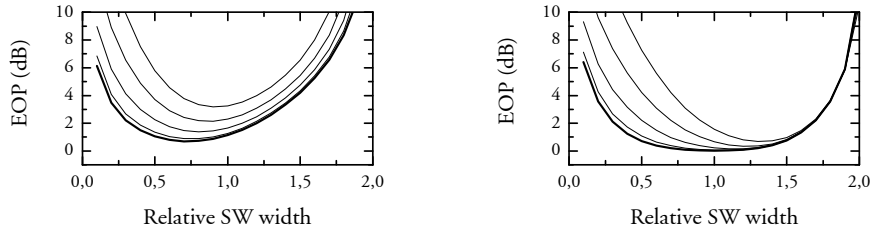

Figure 4.22: EOP as function of FWHM SW width, evaluating the impact of offset of the target channel. Offset is increased from $0.0T_S$ (bold line) to $0.4T_S$. OTDM signal based on pulses with FWHM = $0.4T_S$ is demultiplexed with Gaussian (left) and Super Gaussian (right) switch.

For both shapes of SW, the penalty is increased for increased offset. For the Gaussian SW, the minimum penalty is increased from 0.7 to 3.2 dB. Furthermore, the FWHM SW width corresponding to a minimum penalty is increased, from the optimum width of $0.7T_S$ for no offset to $0.9T_S$ for a static offset of $\pm 0.4T_S$. For the Super Gaussian SW the optimum FWHM SW width for no offset is $1.0T_S$, see table 4.3. However, when the static target channel offset is increased from e.g. $0.0T_S$ to $0.4T_S$, the penalty is increased from 0.0 to 1.6 dB. Additionally, the optimum FWHM SW width is increased from $1.0T_S$ to $1.3T_S$.

Timing jitter on the neighbour data pulses are evaluated as sketched in Figure 4.12C, where the centre of the data pulses in the two immediate neighbour channels statically are moved toward to the centre of the target channel. In Figure 4.22 the neighbouring channels include a static offset varied from $0.0T_S$ to $0.4T_S$ in steps of $0.1T_S$ for both a Gaussian and Super Gaussian SW.

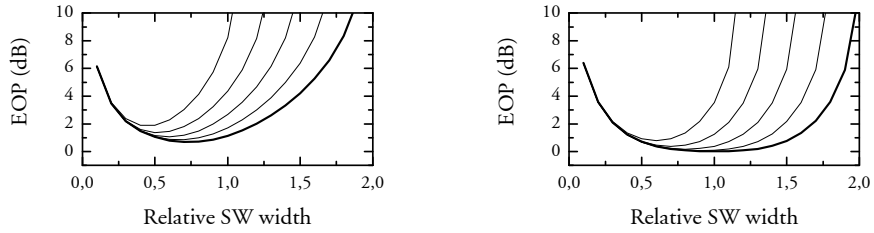

Figure 4.23: EOP as function of FWHM SW width, evaluating the impact of offset of neighbouring channels towards target channel. Offset is increased from $0.0T_S$ (bold line) to $0.4T_S$ in steps of $0.1T_S$ OTDM signal based on pulses with FWHM = $0.4T_S$ is demultiplexed with Gaussian (left) and Super Gaussian (right) switch.

It is noted irrespective of the SW shape, how the acceptable variation range in FWHM SW width is reduced significantly for increased timing jitter, i.e. offset. Thus when implementing a switch in an OTDM system, the requirements to the FWHM SW width becomes increasingly strict, when the associated timing jitter of the data signal is increased.

Furthermore, it is observed, how an OTDM system based on switches optimised to fulfil the previous established optimum FWHM SW width values of $0.7T_S$ for Gaussian SW and $1.0T_S$ for Super Gaussian SW induce a dramatic increase in penalty for increased timing jitter. Instead, the optimum FWHM SW width values are shifted towards more narrow values. For the Gaussian SW, the optimum is shifted from $0.7T_S$ for no offset to $0.4T_S$ for an offset corresponding to $0.4T_S$. The shift in optimum value is even more pronounced for the Super Gaussian SW, with a shift from $1.0T_S$ for no offset to $0.6T_S$ for an offset corresponding to $0.4T_S$.

It is interesting to observe how the two cases of static offset, i.e. offset in the neighbouring channels versus an offset in the target channel, in terms of optimum FWHM SW width seem to counteract each other. Consequently, the influence of an identical offset of both the target channel combined with an offset of the two immediate neighbour channels towards the target channel is investigated and the results are presented in Figure 4.24.

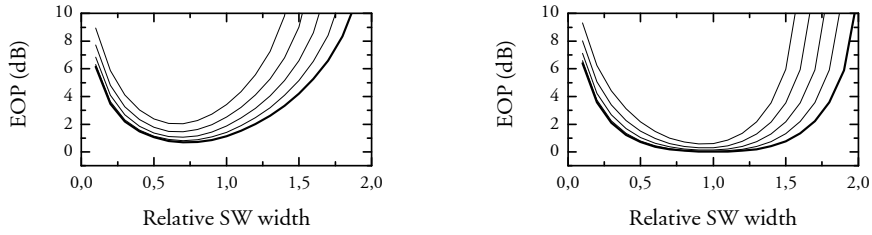

Figure 4.24: EOP as function of FWHM SW width, evaluating the impact of offset moving the neighbouring channels towards target channel and the target channel moved with the same offset away from the ideal timing position. Offset is increased from $0.0T_S$ (bold line) to $0.2T_S$ in steps of 0.05 T_S. OTDM signal based on pulses with FWHM = $0.4T_S$ is demultiplexed with Gaussian (left) and Super Gaussian (right) switch.

The offset is varied from $0.0T_S$ to $0.2T_S$ in steps of $0.05T_S$. The performance when using the Gaussian SW shows an increase in EOP from 0.7 to 2.0 dB with

no shift in optimum SW width. For the Super Gaussian SW, the optimum FWHM SW width is gradually reduced from $1.0T_S$ to $0.9T_S$ with a negligible increase in EOP from 0.0 to 0.6 dB.

In summary, for an offset in the target channel the optimum FWHM SW width is increased, for offsets in the neighbouring channels the optimum FWHM SW width is decreased and for offset in both the target and the neighbouring channels it appears that the optimum FWHM SW widths are approximately identical to the optimum FWHM SW widths determined for signals with ideal timing position. With the reservations due to the static investigation of a random process, FWHM widths of $0.7T_S$ for bell-shaped SW e.g. Gaussian and $1.0T_S$ for more square-shaped SW e.g. like Super Gaussian SW appears to be a good starting point when designing an OTDM system. Furthermore, it appears that the square-shaped form of a Super Gaussian SW is advantageous compared to the bell-shaped SW in terms of induced EOP and in acceptable variation range in SW width.

As outlined in chapter 3, the extracted clock can also include timing jitter, which will be transferred to the temporal position of the SW. As for timing jitter on the data pulses, the results generated with EOP simulation model should be interpreted with caution. In Figure 4.25 the EOP is shown as function of the FWHM SW width for both a Gaussian and a Super Gaussian SW.

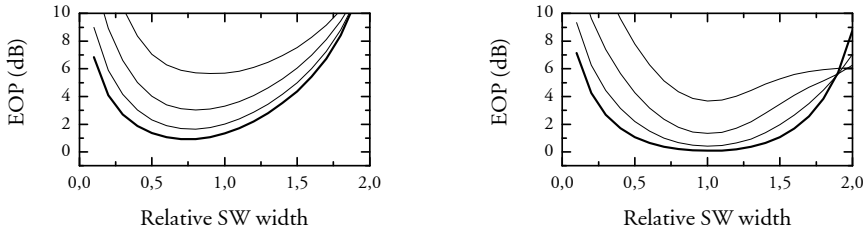

Figure 4.25: EOP as function of FWHM SW width evaluating the impact of SW offset. Offset is increased from $0.0T_S$ (bold line) to $0.4T_S$. OTDM signal based on pulses with FWHM = $0.4T_S$ is demultiplexed with Gaussian (left) and Super Gaussian (right) switch.

The simulation results depicted in Figure 4.25 emphasise how sensitive the system is to timing jitter of the SW, i.e. the controlling clock. Comparing the Gaussian and the Super Gaussian SW, the more squared shaped Super Gauss lowers the relative penalty. It also shows how the optimum FWHM SW width is approximately constant irrespective of the SW offset, unless the jitter is very

high, e.g. < $0.3T_S$. This suggests that the switch cannot be optimised to accommodate for timing jitter on the clock by varying the SW width. The results also emphasise the importance of minimising the timing jitter in the CR circuit.

4.4.5 Summary of requirements general switch

In this section an ideal switch, described by shape and the FWHM width of the SW is implemented irrespective of any physical process. Two different SW shapes have been investigated – a bell-shaped and a square-shaped SW represented by a Gaussian and a Super Gaussian shape, respectively. Based on the simulations it can be concluded that the impact of timing jitter cannot be minimised by varying the width of the SW. However, a Super Gaussian shaped SW is better to reduce the impact of timing jitter than a Gaussian SW, so even though a squared shaped SW is difficult to generate, it will be preferred if possible.

Based on the simulations, the suggested design parameters for the demultiplexing switch are summarised in table 4.4

Shape	Min. ER (dB)	Optimum FWHM SW width (ps)			
		160 Gbit/s	320 Gbit/s	640 Gbit/s	1280 Gbit/s
Gauss	20	4.38	2.19	1.09	0.54
Super Gauss	15	6.25	3.13	1.56	0.78

Table 4.4: Suggested design parameters for switches

4.4 Requirements to NOLM switch

4.4.1 Introduction to NOLM switch

The Non-linear Optical Loop Mirror briefly described in section 4.2.7, is a very attractive candidate for high-speed OTDM switching, due to the fast response of the Kerr effect. This is also emphasised by the fact that switches used to demultiplex the highest aggregated bit rate so far[28] are utilising the Kerr effect either in a NOLM structure or as a Kerr switch, see table 4.2.

In this section, a short introduction to the analytical expressions derived in literature is presented, in order to calculate the switching window induced in the NOLM. The analytical expressions are evaluated using the EOP simulation

[28] In spring 2006

tools described in section 4.3. Rule of thumb design values are extracted from the models.

One problem with the analytical expressions is the underlying assumptions required to derive the equations. Thus, important parameters such as Group Velocity Dispersion and slope, zero-dispersion wavelength are neglected. These parameters can however be included, if numerical evaluation without analytical solutions are acceptable. The coupled non-linear Schrödinger equations (NLSE) are briefly described in this section and used for a general discussion about the design parameters for the NOLM.

4.4.2 Simple NOLM model

Inspecting Figure 4.26, which in principle is identical to the NOLM in Figure 4.9, formalism quite similar to [4.48] describing the functionality of the NOLM can be derived.

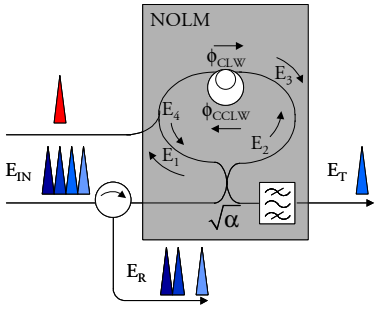

Figure 4.26: NOLM introducing the parameters used to describe the simplified model below

The interferometeric Sagnac structure sketched in Figure 4.26 can for clarification of the principle of operation be represented conceptual as a Mach-Zehnder model, as shown in Figure 4.27, a technique suggested in [4.2].

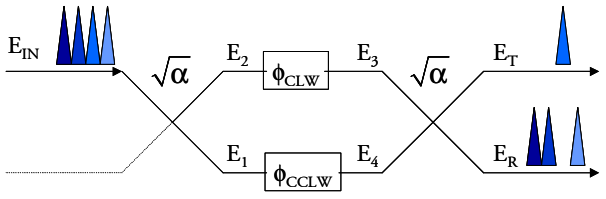

Figure 4.27: Conceptual description of NOLM operation by symbolising the Sagnac interferometer with a Mach-Zehnder representation.

An OTDM signal represented by the optical field E_{IN} is injected into the main coupler of the NOLM. The signal is split into two signals, the clock-wise (CLW) signal E_1 and the counter clock-wise (CCLW) E_2 signal. The main coupler is characterised by a power coupling coefficient α and a negligible insertion loss. The CCLW signal will experience a static phase shift of $\pi/2$ in the main-coupler [4.86], thus the two signals immediately after passing the main coupler of the NOLM can be described as

$$E_1 = \sqrt{\alpha}\, E_{IN}$$
$$E_2 = i\sqrt{1-\alpha}\, E_{IN} \tag{4.7}$$

The two signals traverse the non-linear fibre and by assuming that the power of the data signal is sufficiently low to justify a negligence of Self Phase Modulation, both signals will experience a phase change denoted as ϕ_{CCLW} and ϕ_{CLW} due to XPM induced by the high intensity control pulse. As the control pulse counter propagates through the entire CCLW signal, every channel accumulates the ϕ_{CCLW} phase change. This is opposed to the case for the CLW signal, where only the target channel interacts via XPM with the control pulse and experience the phase change ϕ_{CLW}. Because the interaction length for the CLW signal is substantial larger than the CCLW signal, it can be assumed that $\phi_{CLW} > \phi_{CCLW}$. The two data signals can after transmission through the non-linear fibre be expressed as

$$E_3 = \sqrt{\alpha}\, \exp\left[i\phi_{CLW}\right] E_{IN}$$
$$E_4 = i\sqrt{1-\alpha}\, \exp\left[i\phi_{CCLW}\right] E_{IN} \tag{4.8}$$

When the two signals are combined at the main coupler, depending on the constructive and destructive interference between the two signals, a part of the signal will be reflected E_R and a part of the signal will be transmitted E_T

$$E_R = i\sqrt{1-\alpha}\, E_3 + \sqrt{\alpha}\, E_4$$
$$E_T = \sqrt{\alpha}\, E_3 + i\sqrt{1-\alpha}\, E_4 \tag{4.9}$$

Combining eq. (4.8) and (4.9) the transmitted electrical field can be expressed as

$$E_T = \left\{\alpha \exp\left[i\phi_{CLW}\right] - (1-\alpha)\exp\left[i\phi_{CCLW}\right]\right\} E_{IN} \qquad (4.10)$$

If the power of the incoming OTDM signal P_{IN} and the power of the transmitted power P_T are calculated as[29]

$$P_{IN} = E_{IN}E_{IN}^{*}$$
$$P_T = E_T E_T^{*} \qquad (4.11)$$

and the phase difference between the clock-wise phase and the counter clock-wise phase is defined as $\Delta\phi = (\phi_{CLW} - \phi_{CCLW})$ the transmitted power P_T can be expressed as

$$P_T = \left[1 - 2\alpha(1-\alpha)(1+\cos\Delta\phi)\right] P_{IN} \qquad (4.12)$$

Assuming a power coupling coefficient α = ½, P_T is reduced to the well-known expression [4.51].

$$P_T = \left(\frac{1-\cos\Delta\phi}{2}\right) P_{IN} \qquad (4.13)$$

From eq. (4.13) it can be seen, that maximum power of the target channel is transmitted to the output of the NOLM, when the phase difference $\Delta\phi = \pi$. However, it also important to emphasise, that just keeping a fixed phase difference between counter and clockwise phase equal to π, does not ensure error-free operation when demultiplexing, as illustrated in Figure 4.28. Assume that ϕ_{CLW} varies temporally as an exact replica of an injected Gaussian shaped control pulse defined by the e^{-1} width T_0 (or the FWHM width of the pulse $T_{FWHM} = 2\sqrt{\ln(2)}\,T_0$ [4.62]), $\phi_{CLW}(t)$ can be expressed as

$$\varphi_{CLW}(t) = A_{\phi CLW} \exp\left(\frac{-t^2}{2T_0^2}\right) \qquad (4.14)$$

with the amplitude $A_{\phi CLW}$. If is furthermore assumed that as $\Delta\phi = \phi_{CLW}$ the FWHM width of the SW, T_{FWHMSW} can, by inserting eq. (4.14) into (4.13), be derived to

[29] Ignoring the factor $(2\eta)^{-1}$ [4.96]

$$T_{FWHMSW} = \sqrt{2}\, T_{FWHM} \tag{4.15}$$

The impact of a Gaussian shaped variation in ϕ_{CLW} and the influence of ϕ_{CCLW} is illustrated in Figure 4.28, where a Continuous Wave is injected into an idealised NOLM. The counter clockwise phase ϕ_{CCLW} is varied from 0 to π and the phase difference $\Delta\phi$ is constant π at the centre of the switching window, i.e. $A_{\phi CLW} - \phi_{CCLW} = \pi$.

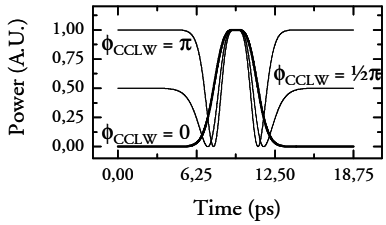

Figure 4.28: CW light with power of 1 switched in NOLM controlled by Gaussian control pulse for ϕ_{CCLW} varied from 0 to π in steps of ½π. Phase difference at peak of SW $\Delta\phi = (\phi_{CLW} - \phi_{CCLW}) = \pi$.

From Figure 4.28 it is observed how maximum power at the centre of the target channel, i.e. time = 9.375 ps, is switched to the output of the NOLM irrespective of the of the ϕ_{CCLW} value. It is also observed how the SW is varied from constructive to destructive interference within the target time slot, i.e. 6.25 to 12.50 ps, for $\phi_{CCLW} > 0$ – a direct consequence when the amplitude ϕ_{CLW} is varied in time from 0 to > π. Finally, it is observed how an increasing ϕ_{CCLW} decreases the Extinction Ratio ER irrespective of the SW induced at the target channel.

Using eq. (4.12) a simple expression for the ER can be derived, assuming that $\Delta\phi = \pi$ at the centre of the target channel and $\Delta\phi = -\phi_{CCLW}$ at the neighbouring channels, when no overlap between control pulse and data pulse occurs.

$$ER = 10\log\left(\frac{1}{\left[1-2\alpha(1-\alpha)\left(1+\cos\left(-\phi_{CCLW}\right)\right)\right]}\right) \tag{4.16}$$

In Figure 4.29, the Extinction Ratio is plotted as function of the power splitting ratio α, for counter clockwise phase ϕ_{CCLW} values varied from 0 to 0.2π in steps of 0.05π. From eq. (4.16) it is clear that ER approaches infinity for $\alpha \rightarrow$ ½ and

$\phi_{CCLW} \rightarrow 0$, however these conditions are difficult to obtain. A random chosen 3-dB coupler[30] revealed power-splitting ratios between 0.4896 and 0.4960, values, which might be optimised by careful selection and splicing of the 3-dB coupler to the NOLM structure. Assuming that α can be fixed between 0.48 and 0.50, the impact of α is quite limited, when ϕ_{CCLW} is different from 0 as seen in Figure 4.29.

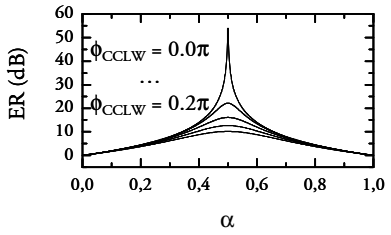

Figure 4.29: Extinction Ratio in dB as function of α for ϕ_{CCLW} values varied from 0 to 0.2π in steps of 0.05π. For increased ϕ_{CCLW} the ER drops.

As pointed out, the counter clockwise phase shift is an inherent artefact of the NOLM structure and thus cannot be eliminated. In Figure 4.30 ER is plotted as function of the ratio ϕ_{CCLW}/π for α varied from 0.50 to 0.45 in steps of 0.01. When ϕ_{CCLW} approaches 0.1π, there is no significant difference in ER for variation of α within practical obtainable values, i.e. 0.45 to 0.50.

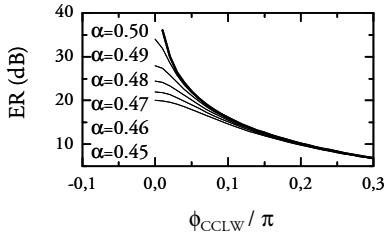

Figure 4.30: ER plotted as function of the ratio ϕ_{CCLW}/π for α varied from 0.50 to 0.45 in steps of 0.01

Using eq. (4.10) and (4.14), the simplified NOLM model can be evaluated in the aforementioned simulation tool. By modelling the phase difference $\Delta\phi$ as a temporal varied pulse shaped profile centred at the target channel, an

[30] JDS Uniphase Model FFC-CKS21B123-003

evaluation of the NOLM can be accessed. Assuming that the phase profile is identical to the control pulse injected into the NOLM, i.e. the phase profile is Gaussian shaped, the 160 to 10 Gbit/s demultiplexing performance in terms of EOP is simulated as function of the FWHM width of the phase profile and shown in Figure 4.31.

Obviously, the phase-difference $\Delta\phi$ has a significant impact on the switching performance. To illustrate this, the simple NOLM model above is implemented in the receiver model described in the simulation tool section 4.3.1. In the simulations, the power splitting ratio α = 0.50, the counter clockwise phase-shift ϕ_{CCLW} = 0 and $A_{\phi CLW}$ are varied from 0.6π to 1.4π in steps of 0.2π.

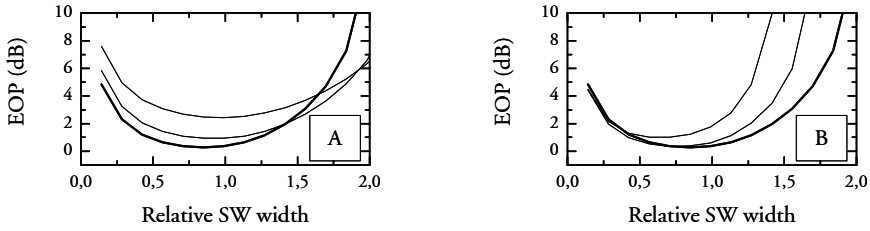

Figure 4.31: Impact of phase-difference $\Delta\phi$ variation. Power splitting ratio α = 0.50, the counter clockwise phase-shift ϕ_{CCLW} = 0. In A, ϕ_{CLW} is varied from 0.6π, 0.8π and 1.0π and in B, ϕ_{CLW} is varied from 1.0π, 1.2π and 1.4π.

For a phase-difference, $\Delta\phi$, less than π it is clear from eq. (4.13) that the power of the switched channel will be less than the input power, thus inducing a power penalty. Because also less power of the neighbouring channels is switched to the base rate receiver, the impact of widened FWHM SW width is more relaxed, hence the crossing EOP curves. For phase-difference $\Delta\phi$ exceeding π, the SW will change the shape of the target channel, a process, which is increasingly dominant for increased $\Delta\phi$. The shaping of the signal, leads to an increased power penalty. The power penalty can be minimised by decreasing the SW width for increased phase-difference $\Delta\phi$, which reduce the impact of shaping. In Figure 4.32 the impact of increased $\Delta\phi$ is illustrated, by plotting a 160 GHz pulse train, a simplified NOLM SW for $\Delta\phi$ = 0.6π. 1.0π and 1.4π with a width corresponding to the optimum for $\Delta\phi$ =1.0π (see Figure 4.31A) and the corresponding demultiplexed signal at the output of the NOLM.

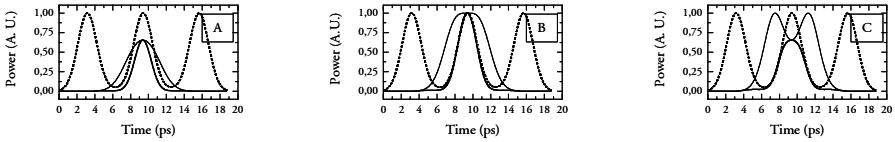

Figure 4.32: Impact of phase-difference $\Delta\phi$ on a 160 GHz switched pulse train. $\Delta\phi$ = 0.6π (A). 1.0π (B) and 1.4π (C) with α = 0.50 and ϕ_{CCLW} = 0. Dashed line is 160 GHz pulse train with FWHM = 0.4T_S. Thin line is SW of NOLM, with FWHM of the Gaussian phase variation of 0.6T_S corresponding to optimum performance for $\Delta\phi$ =1.0π. Bold line is demultiplexed signal.

The difference in EOP for $\Delta\phi$ = 0.6π and 1.4π can be ascribed to the reduction in power for $\Delta\phi$ = 0.6π, as seen in Figure 4.33 where the demultiplexed signals from Figure 4.32A-C are compared.

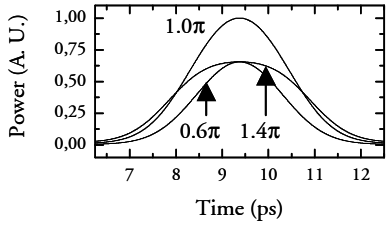

Figure 4.33: Comparison of 160 GHz switched signals for $\Delta\phi$ = 0.6π, 1.0π and 1.4π with α = 0.50, ϕ_{CCLW} = 0 and FWHM of Gaussian phase-change = 0.6T_S.

Based on the simple NOLM model presented in this section, a few guidelines for the design and the operation of the NOLM can be extracted. The SW shape induced from a Gaussian shaped control pulse in a NOLM is in between the shape of Gaussian and Super Gaussian, see Figure 4.14, hence it is expected that the target Extinction Ratio should preferable exceed ~ 20 dB, see table 4.4. From Figure 4.30 the power splitting ratio α should be equal to 0.50 with a tolerance of maximum ±0.03 and the counter clockwise phase change ϕ_{CCLW} < 0.05π. The power of the control pulse should be careful optimised to induce a phase difference $\Delta\phi$ = π and as the optimum FWHM SW width is 0.85T_S, see Figure 4.31, the FWHM width of the Gaussian pulse should be 0.60T_S.

4.4.3 Advanced NOLM model

In the model above, it is assumed that the phase difference has a certain idealised profile. The actual physical process responsible for the phase profile is not included in the model and thus the model does not allow extraction of any design rules, which the NOLM should fulfil. In order to list some of the design parameters an optimised NOLM should fulfil, it is imperative to implement a significantly more complex model for the NOLM including fibre parameters.

The switching performance of the NOLM relies on Cross Phase Modulation between the control signal and the OTDM data signal when propagating through the fibre constituting the NOLM. The NLSE [4.62] introduced in chapter 2 in pulse compression, can be modified to include the interaction between several carriers, by deriving coupled NLSEs [4.62]. The coupled NLSEs covering the NOLM can be written as, when combining [4.62] and [4.2].

$$\frac{\partial A_1}{dz} = -\frac{1}{v_{g1}}\frac{\partial A_1}{dt} - \frac{i}{2}\beta_{21}\frac{\partial A_1^2}{dt^2} + \frac{1}{6}\beta_{31}\frac{\partial A_1^3}{dt^3} - \frac{\alpha_1}{2}A_1 + i\gamma_1\left[|A_1|^2 + 2|A_2|^2 + 2|A_3|^2\right]A_1$$

$$\frac{\partial A_2}{dz} = -\frac{1}{v_{g2}}\frac{\partial A_2}{dt} - \frac{i}{2}\beta_{22}\frac{\partial A_2^2}{dt^2} + \frac{1}{6}\beta_{32}\frac{\partial A_2^3}{dt^3} - \frac{\alpha_2}{2}A_2 + i\gamma_2\left[2|A_1|^2 + |A_2|^2 + 2|A_3|^2\right]A_2$$

$$\frac{\partial A_3}{dz} = -\frac{1}{v_{g3}}\frac{\partial A_3}{dt} - \frac{i}{2}\beta_{23}\frac{\partial A_3^2}{dt^2} + \frac{1}{6}\beta_{33}\frac{\partial A_3^3}{dt^3} - \frac{\alpha_3}{2}A_3 + i\gamma_3\left[2|A_1|^2 + 2|A_2|^2 + |A_3|^2\right]A_3 \qquad (4.17)$$

A is the slowly varying envelope amplitude, v_g is the group velocity, β_2 is the Group Velocity Dispersion (GVD) coefficient, β_3 is the slope of the GVD, α is the attenuation and γ is the non-linear coefficient. Subscripts 1, 2 and 3 denote the control pulse, the clockwise propagating signal and the counter-clockwise propagating signal, respectively. In eq. (4.17) Raman impact and terms requiring phase matching have been excluded.

All parameters have been labelled with different subscripts to allow for wavelength dependency. However, A_2 and A_3 refer to the same wavelength, so $v_{g2} = v_{g3}$, $\beta_{22} = \beta_{23}$, and $\beta_{32} = \beta_{33}$. Furthermore, the wavelength dependence of the attenuation α and the non-linear coefficient can often be ignored, and thus $\alpha_1 = \alpha_2 = \alpha_3 = \alpha$ and $\gamma_1 = \gamma_2 = \gamma_3 = \gamma$.

Coupled NLSEs can relatively easy be numerical solved for co-propagating waves, but for counter-propagating waves the implementation is not straight forward. Consequently, the impact of counter propagating waves is often ignored [4.87] [4.2] and will be in the following.

With these considerations, the coupled NLS equations in eq. (4.17) can then be reduced to

$$\frac{\partial A_1}{dz} = -\frac{1}{v_{g1}}\frac{\partial A_1}{dt} - \frac{i}{2}\beta_{21}\frac{\partial A_1^2}{dt^2} + \frac{1}{6}\beta_{31}\frac{\partial A_1^3}{dt^3} - \frac{\alpha}{2}A_1 + i\gamma\left[|A_1|^2 + 2|A_2|^2\right]A_1$$

$$\frac{\partial A_2}{dz} = -\frac{1}{v_{g2}}\frac{\partial A_2}{dt} - \frac{i}{2}\beta_{22}\frac{\partial A_2^2}{dt^2} + \frac{1}{6}\beta_{32}\frac{\partial A_2^3}{dt^3} - \frac{\alpha}{2}A_2 + i\gamma\left[2|A_1|^2 + |A_2|^2\right]A_2 \quad (4.18)$$

$$\frac{\partial A_3}{dz} = -\frac{1}{v_{g2}}\frac{\partial A_3}{dt} - \frac{i}{2}\beta_{22}\frac{\partial A_3^2}{dt^2} + \frac{1}{6}\beta_{32}\frac{\partial A_3^3}{dt^3} - \frac{\alpha}{2}A_3 + i\gamma|A_3|^2 A_3$$

With eq. (4.18), the impact of the physical parameters on the switching performance can be evaluated. Notice, though that the phase shift induced of the high-power clock pulse on the counter clockwise data signal is not included in this equation due to the approximations outlined above. The phase shift can in principle however be included if using the analytical expression derived in [4.51]. This procedure can be understood by inspecting the Mach-Zehnder structure in Figure 4.27. The two first equations in (4.18) address the amplitude change and the phase change of both the clock and the clockwise propagating signal. The last eq. in (4.18) addresses only the amplitude change of the counter clockwise signal. But adding the analytical phase change impact from [4.51] to the signal after transmission, an expected more precise approximation of the NOLM switching performance can in principle be implemented.

Even without implementing eq. (4.18) a number of comments to the parameter choice can be made. According to [4.62] a simplified expression for the non-linear phase change in the clockwise propagating signal due to cross-phase modulation induced by the co-propagating control pulse, subscript 1, can be derived to

$$\phi_{CLW} = 2A_{eff}\gamma L|E_1|^2 \quad (4.19)$$

where A_{eff} is the effective area and L is the length of the fibre. The most important observation, when inspecting eq. (4.19) is the dependence of γL. The

higher non-linear coefficient γ the shorter length of fibre is required. The length of fibre can have an influence on stability of the fibre-based components, and consequently much work has focused on developing HNLF with very high non-linear coefficients[31]. Up to now it seems that the increase of γ is on the expense of an increase in attenuation α, exemplified in [4.88] where a holey fibre was manufactured with γ = 70 W^{-1} km^{-1} accompanied by an α = 190 dB/km and in [4.89] where the ultra-high γ = 1100 W^{-1} km^{-1} was measured for a Bismuth Oxide fibre with an α = 0.8 dB/m. The presently high values of γ and α do not offer an additional freedom in design, as very short fibre lengths are prerequisite for utilisation. Whether high γ inherently is correlated with high α irrespective of fibre design and materials appears to be an open question.

Other parameters with a potential high impact on the performance of the switching performance of the NOLM are the dispersion parameters, i.e. group velocity, GVD and the slope. As both the OTDM data signal and the control pulses are very narrow in time and the broadening effect of GVD can be quite significant for even small values causing e.g. the data pulses to spread into neighbouring channels and should consequently be minimised, unless the soliton regime is utilised[32]. By using HNL fibres with zero dispersion wavelength λ_0 close to wavelengths of the data and the control signals, the impact of broadening can be reduced. The impact of group velocity can also have a detrimental influence of the switching performance. As seen in eq. (4.18) the control and data signal is travelling through the fibre with two different velocities ν_{g1} and ν_{g2}. If the both the control pulse and the data signal propagate through the fibre with same velocity, the control pulse can be exactly aligned in time to match the position of the target channel, as sketched in Figure 4.34A. However, if e.g. the control pulse travels faster than the data signal, the control pulse is not fixed in time compared to the target channel, indicated in Figure 4.34A with the square box, but can induce a phase shift in parts of the neighbouring channels, leading to switching of both the target channel and the neighbouring channels as seen in Figure 4.34B, which ultimately will induce errors. The velocity mismatch is known as walk-off.

[31] Fibre-based components are prone to instability due to e.g. acoustic waves [4.97], temperature fluctuations [4.63] and polarisation fluctuations of the incoming signal see e.g. [4.98]. Before these problems are solved, the transition of the NOLM from research to commercial components is delayed irrespective of its fast switching properties.

[32] The control pulses will typically have high power and the shape could probably be maintained if utilising the soliton regime. However, the power of the data signals are relatively low and might not fulfil the soliton regime requirements implying that the impact of dispersion should still be minimised.

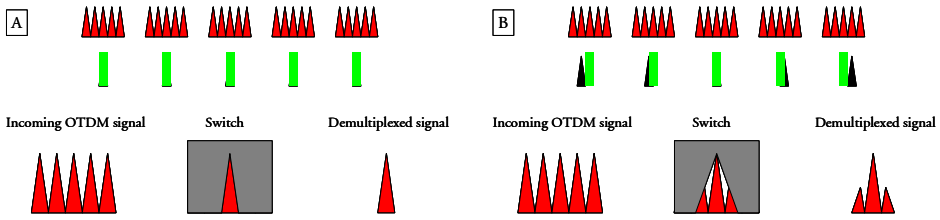

Figure 4.34: Graphic illustration of no walk-off (A) and with walk-off (B) on the switching performance. Square box indicates matched alignment position between control and OTDM data signal.

Different wavelengths for control and data signal are often utilised for inducing switching in the NOLM. In order to ensure a sufficiently high suppression of the control signal at the output of the NOLM using a filter, the control and the data signal wavelength need to be separated with a minimum spacing determined by the spectral pulse width of the signals and the actual filter shape. When the bit rate is increased, the pulse width is decreased, the spectral width is increased and hence the required wavelength separation is increased. With a large separation between the two wavelengths, the walk-off potentially limits the switching performance. How walk-off can be suppressed can be understood by deriving a simple expression as outlined below.

The group velocities can be calculated based on the typical measured fibre values dispersion D and the dispersion slope S. The expression originates from the Taylor series of dispersion D in wavelength λ_0.

$$D(\lambda) = D(\lambda_0) + (\lambda - \lambda_0)\frac{\partial D(\lambda)}{\partial \lambda}\bigg|_{\lambda=\lambda_0} + \frac{1}{2}(\lambda - \lambda_0)^2 \frac{\partial^2 D(\lambda)}{\partial \lambda^2}\bigg|_{\lambda=\lambda_0} + \ldots \qquad (4.20)$$

Assuming that λ_0 is the zero dispersion wavelength, resulting in $D(\lambda_0) = 0$ ps/nm/km, defining the first derivative of D ($\partial D(\lambda)/\partial \lambda$ in $\lambda = \lambda_0$) as the slope S and ignoring higher order terms, dispersion $D(\lambda)$ can be reduced to

$$D(\lambda) = S(\lambda - \lambda_0) \qquad (4.21)$$

which is used in the definition of the group velocity [4.62]

$$D(\lambda) = \frac{\partial \beta_1(\lambda)}{\partial \lambda} = \frac{\partial}{\partial \lambda}\left(\frac{1}{v_g(\lambda)}\right) \qquad (4.22)$$

to finally derive an expression for the group velocity

$$v_g^{-1}(\lambda) = S\frac{(\lambda-\lambda_0)^2}{2} \qquad (4.23)$$

By using eq. (4.23), the walk-off τ, i.e. the mismatch in group velocities between two wavelengths, λ_1 is λ_2, can be expressed as [4.90]

$$\tau = \left|v_g^{-1}(\lambda_1) - v_g^{-1}(\lambda_2)\right| = \frac{1}{2}S(\lambda_1-\lambda_2)(\lambda_1+\lambda_2-2\lambda_0) \qquad (4.24)$$

By situating the control pulse and the OTDM data signal symmetrically around the zero-dispersion wavelength, i.e. $\lambda_1 = \lambda_0-\Delta\lambda$ and $\lambda_2 = \lambda_0+\Delta\lambda$, the impact of walk-off can be suppressed completely. But if this strict requirement is not fulfilled, then the impact of a fixed (non-zero) value of walk-off is increased for an increased bit rate, as the control pulse will start inducing phase shift in the neighbouring channels, hence the acceptable amount of walk-off is partly defined by the bit rate. For switching it can in general be stated, that the non-linear fibre utilised within the NOLM should be characterised by a low value of dispersion slope S, as seen from eq. (4.23). However, walk-off can be utilised to generate a broader SW with flat top, which can be more resilient to the impact of timing jitter [4.53] [4.91].

So without implementing the advanced numerical simulation model, some general engineering design rules can be stated:

- Non-linear coefficient high.
- Attenuation low.
- Dispersion low.
- Dispersion slope low.
- Zero dispersion wavelength situated correct for minimising impact of walk-off.

Using these general guidelines combined both the guiding rules extracted in the two previous sections and with the actual wavelengths and spacing between control and data signal dictated by the available equipment in the laboratory facilities of COM•DTU, several fibres where provided by OFS Fitel Denmark ApS during the project with parameters allowing an improved performance of the switching performance of the NOLM. No new fibres where designed or fabricated specifically for this project, instead a search in the available fibre databases by especially Dr. Lars Grüner-Nielsen at OFS Fitel Denmark ApS[33], resulted in the optimised fibres.

[33] Acknowledgement to the enthusiasm with which OFS Fitel Denmark ApS supported with fibres and a special thank you to Dr. Lars Grüner-Nielsen for his never-ending willingness to find the best suited fibres for the NOLM.

4.5 Demultiplexing at 320 Gbit/s and beyond

4.5.1 Introduction to 320 to 10 Gbit/s demultiplexing experiment

During the last few years, a large number of OTDM experiments including demultiplexing have been performed at COM•DTU. Several of these experiments were carried out within the framework of the European IST project TOPRATE. As outlined in the state-of-the art section, fibre based switches still offer the highest demultiplexing rate, with the two outstanding experiment reporting 10 Gbit/s signal extraction from a 640 Gbit/s OTDM signal using either fibre based XPM in a NOLM [4.57] or Kerr switching [4.65]. Within the TOPRATE project, no research in components for ultra high switching, i.e. above 160 Gbit/s, were carried out, which dictated the decision of using fibre based components for the experiments. During the TOPRATE project the aggregated bit rate was continually increased from e.g. 80 [4.92], 160 [4.93], 320 [4.60] to 640 Gbit/s [4.61] by careful

- Optimisation of the experimental set-ups.
- Selection of fibres matched to high-speed operation.
- Design rules presented in previous sections.
- Better equipment.
- Increased know-how.

In this section, the results from a 320 Gbit/s OTDM experiment are presented.

As previously mentioned one of the drawbacks when utilising a NOLM is the impact of walk-off between the control pulse and the OTDM signal. One approach used to reduce the impact of walk-off is presented in [4.56] and used in [4.57]. A special fibre is constructed by carefully choosing and concatenating nine 50 m fibre segments with alternating walk-off between control and data signal, hence effectively constructing a fibre with less than 100 fs of walk-off. Another approach is to place the wavelengths of the control and data signal symmetrically around the zero dispersion wavelength, thus suppressing the walk-off, as demonstrated in [4.58] where a 320 Gbit/s OTDM signal was demultiplexed to 10 Gbit/s. Here a NOLM based on a commercially available Highly Non-Linear Fibre (HNLF) is used to successfully demultiplex a 320 Gbit/s OTDM signal to 10 Gbit/s without utilising any special wavelength management, thus allowing for a simpler implementation of the switch in ultra-high speed systems.

4.5.2 Experimental set-up

The key to obtain these results was a commercially available 500 m Highly Non-linear Fibre (HNLF) with a non-linear coefficient γ = 10.5 ps/nm/km and a total insertion loss, including connectors, of ~ 5 dB. The fibre was designed to exhibit flat dispersion for a relatively broad wavelength range and was characterised by a zero-dispersion wavelength λ_0 of 1561 nm and a dispersion slope S of 0.013 ps/nm^2/km. This HNLF was implemented in the NOLM and used in the experimental set-up shown in Figure 4.35, which was used to generate a 320 Gbit/s OTDM signal and to demultiplex the signal to 10 Gbit/s.

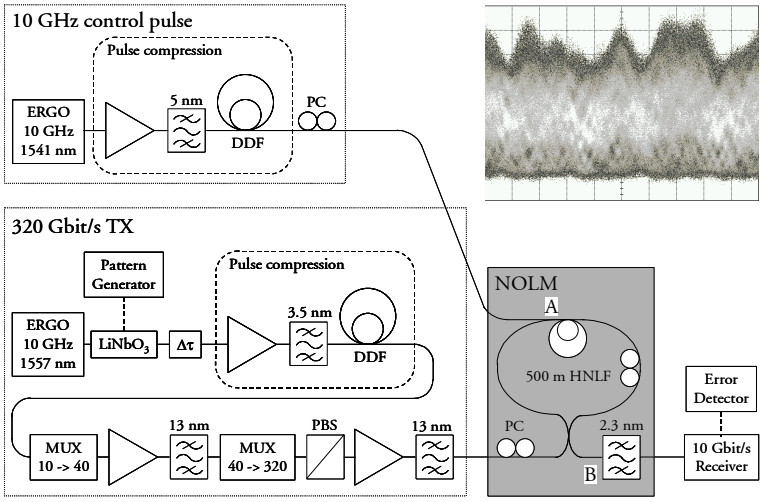

Figure 4.35: Experimental set-up for generating and demultiplexing the 320 Gbit/s OTDM signal. The inset shows the eye-diagram of the 320 Gbit/s signal.

An Erbium Glass Laser Oscillator (ERGO) [4.94] emits a 10 GHz pulse train at 1557 nm. The pulses are externally modulated with a Pseudo Random Bit Sequence (PRBS) at 2^7-1 using a $LiNbO_3$ modulator before they are injected into a pulse compression stage, comprised of a high-power EDFA, a 3.5 nm Optical Bandpass Filter (OBF) and 1 km of Dispersion Decreasing Fibre (DDF), see chapter 2. Pulses are generated with a temporal Full Width Half Maximum (FWHM) of 1 ps corresponding to a T_{FWHM} = $0.32T_S$, which approximately is in accordance with the specifications derived in chapter 2. The 10 Gbit/s signal is multiplexed up to 40 Gbit/s using a passive PRBS and polarisation maintaining fibre delay multiplexer. After additional amplification and filtering, using a 13 nm OBF, the signal is multiplexed up to 320 Gbit/s using a Planar Lightwave Circuit (PLC) [4.95]. A subsequent Polarisation Beam Splitter (PBS) is used to ensure single polarisation state of the 32 time channels.

The amplitude variations seen in the OTDM signal in Figure 4.35 is due to imperfect multiplexing and small polarisation variations of each channel. The 320 Gbit/s OTDM signal is amplified, and its State of Polarisation (SOP) is adjusted using a polarisation controller (PC) before being injected into the NOLM. The control pulses required to demultiplex the 320 Gbit/s signal are generated by an additional ERGO, synchronised to the same synthesiser as the data ERGO. The emitted pulses at 1541 nm are amplified, filtered and injected into a similar pulse compression stage, generating 1 ps FWHM width pulses. A control pulse with a width of 1 ps would according to the simple NOLM model in section 4.4, induce a SW with a FWHM width of 1.41ps, which corresponds to a FWHM SW width of $0.45T_S$ assuming Gaussian pulses, thus slightly more narrow than the optimum width, see Figure 4.31. However, due to the, albeit small, walk-off, the width of the SW will be slightly increased[34]. After aligning the SOP of the control pulses to be parallel with the data signal, the pulse train is injected into the NOLM. Within the NOLM, the OTDM signal is split into two signals propagating clockwise (CLW) and counter-clockwise (CCLW). The target channel of the CLW propagating OTDM signal is co-propagating with the high power control pulse and thus accumulates a non-linear phase shift induced by XPM. After propagation through the entire loop, the two signals are recombined in the coupler, and if the power and the shape of the control pulse are optimised, the target channel experiences constructive interference at the output port of the NOLM, and the channel is demultiplexed [4.51]. The control signal is suppressed by a 2.3 nm OBF centred at the wavelength of the OTDM signal. Finally, the demultiplexed 10 Gbit/s data signal is injected into a pre-amplified 10 Gbit/s receiver including an Error-detector. The purpose of the tuneable time-delay $\Delta\tau$ situated after the modulator in the 320 Gbit/s TX is two-fold: to optimise the position between control pulse and target channel for best demultiplexing and to ensure that each individual time channel can be demultiplexed.

The wavelength separation between control and OTDM signal is 16 nm, which is determined by interplay between wavelength tuneability of the lasers, the gain bandwidth of the optical amplifiers, which for an EDFA typically lies between 1535 and 1570 nm and finally the induced cross-talk from the control pulse when filtering the data signal. The dispersion and the corresponding relative propagation delay, calculated as the length L times the group-velocity, see eq. (4.24), is shown in Figure 4.36.

[34] The FWHM SW width is not measured because the required optical bandpass filter at the output of the NOLM used to suppress the control pulse will determine the width and the shape of the measured SW.

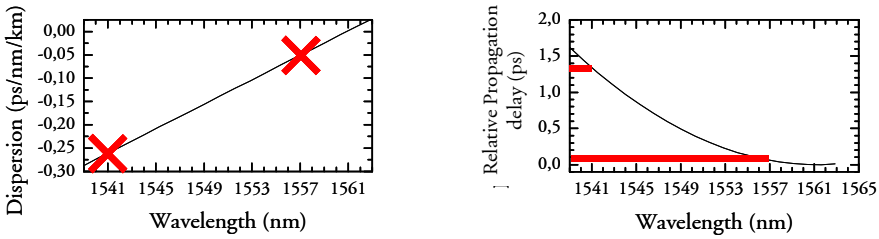

Figure 4.36: Dispersion as function of wavelength for 500 m of HNLF used for 320 to 10 Gbit/s demultiplexing (left). Relative propagation delay as function of wavelength (right). Crosses and lines correspond to values for control and data signals.

From 4.36 and from eq. (4.24) the walk-off can be estimated to ~1.2 ps corresponding to ~ 38 % of the OTDM time slot.

4.5.3 Experimental results

In Figure 4.37 the spectra of control and data signals measured at point A and B, see the experimental set-up Figure 4.35 are shown, illustrating ~20 dB drop in data power as a single time channel is extracted from the OTDM signal.

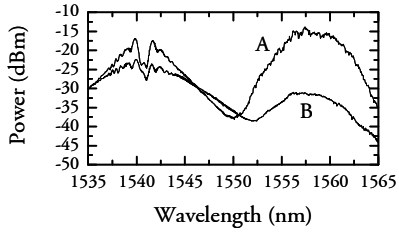

Figure 4.37: Spectra of control and data signal measured at point A and B (see Figure 4.35).

In Figure 4.38 the BER curves for the back-to-back configuration, i.e. the 10 Gbit/s data signal at the output of the compression stage is injected directly into the 10 Gbit/s receiver, and for the 320 to 10 Gbit/s demultiplexed signal for one of the 32 time channels. The introduced power penalty is ~ 2.7 dB.

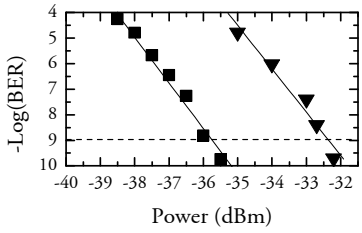

Figure 4.38: BER measurements for 10 Gbit/s back-to-back configuration based on compressed pulses and after 320 to 10 Gbit/s demultiplexing.

In Figure 4.39 the 10 Gbit/s demultiplexed electrical (upper trace) and the optical (lower trace) eye-diagrams corresponding to the sensitivity at the BER = 10^{-9} are shown.

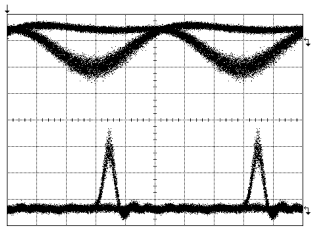

Figure 4.39: 10 Gbit/s demultiplexed electrical (upper trace) and the optical (lower trace) eye-diagrams corresponding to the sensitivity at the BER = 10^{-9}.

The performance of the entire OTDM signal was evaluated as shown in Figure 4.40, where the sensitivity of all the 32 channels is shown. All channels are error-free with an average sensitivity of –30.1 dBm, hence the average power penalty compared to the 10 Gbit/s compressed pulses is ~ 4.9 dB. The fluctuations in sensitivity observed in Figure 4.40 are ascribed to amplitude variations due to small splitting deviations of the couplers implemented in the multiplexer, as can be observed in the 320 Gbit/s eye-diagram shown as inset in Figure 4.35.

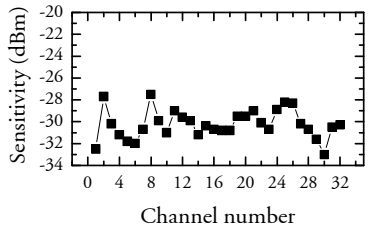

Figure 4.40: Sensitivity measured for all time channels constituting the 320 Gbit/s signal.

In conclusion, a NOLM based on commercially available HNLF has been implemented and used to successfully demultiplex all 32 channels constituting a 320 Gbit/s OTDM signal down to 10 Gbit/s. The used HNLF has been designed with a low dispersion slope of 0.013 ps/nm2, which reduces the introduced walk-off between control and data signal and thus alleviates the need for special wavelength management of the OTDM system.

It should be emphasised that the walk-off of 1.2 ps was acceptable for 320 Gbit/s demultiplexing. However, when using the same fibre with the same wavelength allocation, subsequent 640 Gbit/s experiment failed to generate error-free demultiplexing. This was however overcome by using another fibre with a slightly higher dispersion slope of 0.016 ps/nm^2/km but with a more advantageous zero-dispersion wavelength of 1551 nm, thus reducing the walk-off to less than 250 fs [4.61]. Error-free operation corresponding to BER = 10^{-9} was demonstrated for one channel with a high power penalty of 12.5 dB.

4.4 Summary

In this chapter, the power budgets and the number of required components for different OTDM switch structures have been addressed. It is concluded that the system performance of an OTDM system based on a serial and tree switch structure are very prone to even small switch attenuation values, as opposed to the parallel structure. A thorough state-off-the-art switch survey is presented. A simple simulation model to evaluate the impact of different switch shapes was presented and design rules were extracted for ideal switches. A simple model for a NOLM was subsequently derived and evaluated to extract the design rules for a specific switch. The simple model was modified to include the physical processes responsible for the switching and a general discussion of the fibre parameters was presented. Finally, the results from the model were used to design an experimental set-up for demonstrating 320 to 10 Gbit/s

demultiplexing. By changing the fibre implemented in the NOLM to a fibre with less walk-off, 640 Gbit/s demultiplexing was subsequently demonstrated, albeit with large power penalty.

4.5 References to chapter 4

[4.1] Agiltron, Nano Speed™ 2x2 Solid State Fiber-optic switch, www.agiltron.com

[4.2] M. Jinno, "Effects of Group Velocity Dispersion on Self/Cross Phase Modulation in a Nonlinear Sagnac Interferometer Switch", Journal of Lightwave Technology, Vol. 10, No. 8, pp. 1167-1178 (1992).

[4.3] B. Mikkelsen, "Semiconductor Optical Amplifiers: Amplification and Signal Processing", Ph.D. thesis, Technical University of Denmark, Department of Electromagnectic Systems (1994).

[4.4] S. Fischer, M. Dülk, M. Bitter, M. Caraccia, E. Gamper, W. Vogt, E. Gini, H. Melchior, W. Hunziker, A. Buxens, H. N. Poulsen, and A. T. Clausen, "Ultrafast all-optical demultiplexer based on Mach–Zehnder interferometer with integrated semiconductor optical amplifiers," in Technical Digest of 5th Optoelectronics Communications Conference (OECC'00), Chiba, Japan, paper 14D-1 (best paper award) (2000).

[4.5] M. Dülk, St. Fischer, M. Bitter, M. Caraccia, W. Vogt, E. Gini, H. Melchior, W. Hunziker, A. Buxens, H. N. Poulsen and A. T. Clausen "Ultrafast all-optical demultiplexer based on monolithic Mach-Zehnder interferometer with integrated semiconductor optical amplifiers", Journal of Optical and Quantum Electronics, vol. 33, pp. 899-906 (2001).

[4.6] M. Heid, S. Spälter, G. Mohs, A. Färbert, W. Vogt, H. Melchior, "160-Gbit/s demultiplexing based on monolithically integrated Mach-Zehnder interferometer", Proceedings of 27th European Conference on Optical Communication (ECOC'01), Amsterdam, Holland, Vol. 6, pp. 82-83 (2001).

[4.7] S. Nakamura, Y. Ueno, K. Tajima, J. Sasaki, T. Sugimoto, T. Kato, T. Shimoda, M. Itoh, H. Hatakeyama, T. Tamunuki, T. Sasaki, "Demultiplexing of 168-Gb/s Data Pulses with a hybrid-integrated Symmetric Mach-Zehnder All-optical Switch", Photonics Technology Letters, Vol. 12, No. 4, pp. 425-427 (2000).

[4.8] S. Nakamura, Y. Ueno, J. Sasaki, K. Tajima, “Error-free demultiplexing at 252 Gbit/s and low-power-penalty, jitter-tolerant demultiplexing at 168 Gbit/s with integrated Symmetric Mach-Zehnder all-optical switch”, Proceedings of 27th European Conference on Optical Communication (ECOC’01), Amsterdam, Holland, paper Th.F.2.2 (2001).

[4.9] S. Nakamura, Y. Ueno, K. Tajima, “Error-free all-optical demultiplexing at 336 Gb/s with a hybrid-integrated Symmetric-Mach-Zehnder switch”, Technical Digest of conference on Optical Fiber Communication (OFC’02), Anaheim, California, USA paper FD3-1 (2002).

[4.10] S. Diez, C. Schubert, R. Ludwig, H.-J. Ehrke, U. Feiste, C. Schmidt, H.G. Weber, "160 Gbit/s all-optical demultiplexer using hybrid gain-transparent SOA Mach-Zehnder interferometer", Electronics Letters, Vol. 36, No. 17, pp. 1484-1486 (2000).

[4.11] J. P. Sokoloff, P. R. Prucnal, I. Glesk, M. Kane, “A Terahertz Optical Asymmetric Demultiplexer (TOAD)”, Photonics Technology Letters, Vol. 5, No. 7, pp. 787-790 (1993).

[4.12] I. Glesk, J. P. Sokoloff, P. R. Prucnal, “Demonstration of all-optical demultiplexing of TDM data at 250 Gbit/s”, Electronics Letters, Vol. 30, No. 4, pp. 339-341 (1994).

[4.13] K. Suzuki, K. Iwatsuki, S. Nishi, M. Saruwatari, “Error-free demultiplexing of 160 Gbit/s pulse signal using optical loop mirror including semiconductor laser amplifier”, Electronics Letters, Vol. 30, No. 18, pp. 1501-1503 (1994).

[4.14] K. L. Hall, B. S. Robinson, “Bit error rate charecterization of 100 Gb/s all-optical demultiplexers”, Technical Digest of Conference on Lasers and Electro-Optics (CLEO 1999), Baltimore, Maryland, USA, paper CTuW1 (1999).

[4.15] C. Schubert, J. Berger, S. Diez, H. J. Ehrke, R. Ludwig, U. Feiste, C. Schmidt, H. G. Weber, G. Toptchiyski, S. Randel, K. Petermann, “Comparison of Interferometric All-optical Switches for Demultiplexing Applications in High-Speed OTDM systems”, Journal of Lightwave Technology, Vol. 20, No. 4, pp. 618-624 (2002).

[4.16] P. Toliver, R. J. Runser, I. Glesk, P. R. Prucnal, "Comparison of three nonlinear optical switch geometries", Technical Digest of Conference on Lasers & Electro-Optics (CLEO 2000), San Francisco, California, USA, paper CWD2 (2000).

[4.17] B. C. Wang, V. Baby, W. Tong, L. Xu, M. Friedman, R. J. Runser, I. Glesk, P. R. Prucnal, "A novel fast optical switch based on two cascaded Terahertz Optical Asymmetric Demultiplexers (TOAD), Optics Express, Vol. 10, No. 1, pp. 15-23 (2001).

[4.18] M. Eiselt, "Optical Loop Mirror with semiconductor laser amplifier", Electronics Letters, Vol. 28, No. 16, pp. 1505-1507 (1992).

[4.19] M. Eiselt, W. Pieper, H. G. Weber, "All-optical high speed demultiplexing with a semiconductor laser amplifier in a loop mirror configuration", Electronics Letters, Vol. 29, No. 13, pp. 1167-1168 (1993).

[4.20] M. Eiselt, W. Pieper, H. G. Weber, "SLALOM: Semiconductor Laser Amplifier in a Loop Mirror", Journal of Lightwave Technology, Vol. 13, No. 10, pp. 2099-2112 (1995).

[4.21] N. S. Patel, K. A. Rauschenbach, K. L. Hall, "40-Gb/s Demultiplexing Using an Ultrafast Nonlinear Interferometer (UNI)", Photonics Technology Letters, Vol. 8, no. 12, pp. 1695-1697 (1996).

[4.22] C. Bintjas, K. Vlachos, N. Pleros, H. Avramopoulos, "Ultrafast Nonlinear Interferometer (UNI)-Based Digital Optical Circuits and Their Use in Packet Switching", Journal of Lightwave Technology, Vol. 21, No. 11, pp. 2629-2637 (2003).

[4.23] C. Schubert, J. Berger, U. Feiste, R. Ludwig, C. Schmidt, H. G. Weber, "160-Gb/s Polarization insensitive All-Optical Demultiplexing Using a Gain-transparent Ultrafast Nonlinear Interferometer (GT-UNI)", Photonics Technology Letters, Vol. 13, No. 11, pp. 1200-1202 (2001).

[4.24] E. Tangdiongga, J. P. Turkiewicz, H. Rohde, W. Schairer, G. Lehmann, E. S. R. Sikora, Y. R. Zhou, A. Lord, D. Payne, G. D. Khoe, H. de Waardt, "160 Gbit/s OTDM add-drop networking using 275 km installed fibres", Electronics Letters, Vol. 40, No. 9, pp. 552-553 (2004).

[4.25] K. Tajuma, S. Nakanura, Y. Ueno, "Semiconductor nonlinearities for ultrafast all-optical gating", Journal of Measurement Science and Technology, Vol. 13, No.11, pp. 1692-1697 (2002).

[4.26] S. Nakamura, Y. Ueno, K. Tajima, "Ultrafast (200 fs switching, 1.5-Tb/s demultiplexing) and High-repetition (10 GHz) Operations of a Polarization-Discriminating Symmetric Mach-Zehnder All-optical Switch", Photonics Technology Letters, Vol. 10, No. 11, pp. 1575-1577 (1998).

[4.27] L. F. Mollenauer, E. Lichtman, G. T. Harvey, M. J. Neubelt, B. M. Nyman, "Demonstration of error-free soliton transmission over more than 15.000 km at 5 Gbit/s single-channel, and over more than 11.000 km at 10 Gbit/s in two-channel WDM", Electronics Letters, Vol. 28, No. 8, pp. 792-794 (1992).

[4.28] M. Suzuki, H. Tanaka, Y. Matsushima, "10 Gbit/s optical demultiplexing and switching by sinusoidal driven InGaAsP Electroabsorption modulators", Electronics Letters, Vol. 28 No. 10, pp. 934-935 (1992).

[4.29] A. D. Ellis, T. Widdowson, X. Shan, D. G. Moodie, "Three-node, 40 Gbit/s OTDM network experiment using electro-optic switches", Electronics Letters, Vol. 30, No. 16, pp. 1333-1334 (1994).

[4.30] D. D. Marcenac, A. D. Ellis, D. G. Moodie, "80 Gbit/s OTDM using Electroabsorption modulators", Electronics Letters, Vol. 34, No. 1, pp. 101-103 (1998).

[4.31] G. Raybon, B. Mikkelsen, R. –J. Essiambre, J. E. Johnson, K. Dreyer, L. E. Nelson, "100 Gbit/s single-channel transmission over 200 km TrueWave® and 160 km conventional fiber with EAM source and demultiplexer", Proceedings of 25th European Conference on Optical Communication (ECOC'99), Nice, France, paper WeC2-5 (1999).

[4.32] B. Mikkelsen, G. Raybon, R. –J. Essiambre, K. Dreyer, Y. Su, L. E. Nelson, J. E. Johnson, G. Shtengel, A. Bond, D. G. Moodie, A. D. Ellis, "160 Gbit/s single-channel transmission over 300 km nonzero-dispersion fiber with semiconductor based transmitter and demultiplexer", Proceedings of 25th European Conference on Optical Communication (ECOC'99), Nice, France, paper PD2-2 (1999).

[4.33] H. Chou, Y. Chiu, J. Bower, W. Wang, D. Blumenthal, "160 Gb/s to 10 Gb/s OTDM demultiplexing using a Travelling-wave Electroabsorption Modulator", Technical Digest of conference on Optical Fiber Communication (OFC'03), Atlanta, Georgia, USA, paper ThX2 (2003).

[4.34] E. Lach, M. Schmidt, K. Schuh, B. Junginger, G. Veith, "Advanced 160 Gbit/s OTDM system based on wavelength transparent 4 x 40 Gbit/s ETDM transmitters and receivers", Technical Digest of conference on Optical Fiber Communication (OFC'02), Anaheim, California, USA, paper TuA2 (2002).

[4.35] J-L. Augé, M. Cavallari, M. Jones, P. Kean, D. Watley, A. Hadjifotiou, "Single channel 160 GB/s OTDM propagation over 480 km of standard fiber using a 40 GHz semiconductor mode-locked laser pulse source", Technical Digest of conference on Optical Fiber Communication (OFC'02), Anaheim, California, USA, paper TuA3 (2002).

[4.36] S. Kodama, T. Yoshimatsu, T. Ito, T. Ishibashi, "160-Gbit/s error-free demultiplexing operation by a monolithic PD-EAM optical gate", Technical Digest of conference on Optical Fiber Communication (OFC'02), Anaheim, California, USA, paper TuU2 (2002).

[4.37] S. Kodama, T. Yoshimatsu, H. Ito, "320-Gbit/s Error-free demultiplexing operation of a Monlithic PD-EAM Optical gate", Technical Digest of conference on Optical Fiber Communication (OFC'03), Atlanta, Georgia, USA, paper ThX5 (2003).

[4.38] S. Kodama, T. Yoshimatsu, H. Ito, "500 Gbit/s optical gate monolithically integrating photodiode and Electroabsorption modulator", Electronics Letters, Vol. 40, No. 9, pp. 555-556 (2004).

[4.39] A. Mecozzi, J. Mørk, "Saturation effects in nondegenerate Four-Wave Mixing between short optical pulses in Semiconductor Laser Amplifiers", Journal of Selected Topics in Quantum Electronics, Vol. 3, No. 5, pp. 1190-1207 (1997).

[4.40] T. Morioka, H. Takara, S. Kawanishi, K. Uchiyama, M. Saruwatari, "Polarization-independent all-optical demultiplexing up to 200 Gbit/s using four-wave mixing in a semiconductor laser amplifier", Technical Digest of conference on Optical Fiber Communication (OFC'96), San Jose, California, USA, paper WH1 (1996).

[4.41] I. Shake, H. Takara, K. Uchiyama, I. Ogawa, T. Kitoh, T. Kitagawa, M. Okamoto, K. Magari, Y. Suzuki, T. Morioka, "160 Gbit/s full optical time-division demultiplexing using FWM of SOA-array integrated on PLC", Electronics Letters, Vol. 38, No. 1, pp. 37-38 (2002).

[4.42] T. Ohara, H. Takara, I. Shake, K. Mori, K. Sato, S. Kawanishi, S. Mino, T. Yamada, M. Ishii, I. Ogawa, T. Kitoh, K. Magari, M. Okamoto, R. V. Roussev, J. R. Kurz, K. R. Parameswaran, M. M. Fejer, "160-Gb/s OTDM Transmission Using Integrated All-Optical MUX/DEMUX With All-Channel Modulation and Demultiplexing, Photonics Technology Letters, Vol. 16, No. 2, pp. 650-652 (2004).

[4.43] O. Kamatani, S. Kawanishi, "Prescaled Timing Extraction from 400 Gb/s Optical Signal Using a Phase Lock Loop Based on Four-Wave-Mixing in a Laser Diode Amplifier", Photonics Technology Letters, Vol. 8, No. 8, pp. 1094-1096 (1996).

[4.44] M. A. Summerfield, R. S. Tucker, "Optimization of Pump and Signal Powers for Wavelength Converters Based on FWM in Semiconductor Optical Amplifiers", Photonics Technolgy Letters, Vol. 8, no. 10, pp. 1316-1318 (1996).

[4.45] N. K. Das, Y. Yasuhiro, T. Kawazoe, H. Kawaguchi, "Analysis of Optical DEMUX Characteristics Based on Four-Wave Mixing in Semiconductor Optical Amplifiers", Journal of Lightwave Technology, Vol. 19, No. 2, pp. 237-246 (2001).

[4.46] S. Jansen, G. Khoe, H. de Waardt, M. Heid, S. Spälter, E. Meissner, C. Weiske, A. Schoepflin, "Optimizing the Wavelength Configuration for FWM-Based Demultiplexing in a SOA", Technical Digest of conference on Optical Fiber Communication (OFC'03), Atlanta, Georgia, USA, paper ThO5 (2003).

[4.47] A. Buxens, H. N. Poulsen, A. T. Clausen, P. Jeppesen, "Simultaneous All-optical add-drop multiplexing functionality using bi-directional four wave mixing in a semiconductor optical amplifier", Proceedings of 25th European Conference on Optical Communication (ECOC'99), Nice, France, paper I-248 (1999).

[4.48] N. J. Doran, D. Wood, "Nonlinear-optical loop mirror", Optics Letters, Vol.13, No. 1, pp. 56-58 (1988).

[4.49] K. J. Blow, N. J. Doran, B. K. Nayar, B. P. Nelson, "Two-wavelength operation of the nonlinear fiber loop mirror", Optics Letters, Vol. 15, No. 4, pp. 248-250 (1990).

[4.50] K. J. Blow, N. J. Doran, B. P. Nelson, "Demonstration of the nonlinear fibre loop mirror as an ultrafast all-optical demultiplexer", Electronics Letters, Vol. 26, No. 14, pp. 962-964 (1990).

[4.51] M. Jinno, T. Matsumoto, "Nonlinear Sagnac Interferometer Switch and Its applications", Journal of Quantum Electronics, Vol. 28, No. 4, pp. 875-882 (1992).

[4.52] M. Jinno, "Effects of Crosstalk and Timing Jitter on All-Optical Time-Division Demultiplexing Using a Nonlinear Fiber Sagnac Interferometer Switch", Journal of Quantum Electronics, Vol. 30, No. 12, pp. 2842-2853 (1994).

[4.53] M. Jinno, "All Optical Signal Regularizing/Regeneration Using a Nonlinear Fiber Sagnac Interferometer Switch with Signal-Clock Walk-Off", Journal of Lightwave Technology, Vol. 12, No. 9, pp. 1648-1659 (1994).

[4.54] P. A. Andrekson, N. A. Olsson, J. R. Simpson, D. J. Digiovanni, P. A. Morton, T. Tanbun-Ek, R. A. Logan, K. W. Wecht, "64 Gb/s All-optical demultiplexing with the Nonlinear Optical-Loop Mirror", Photonics Technology Letters, Vol. 4, No. 6, pp. 644-647 (1992).

[4.55] K. Uchiyama, H. Takara, S. Kawanishi, T. Morioka, M. Saruwatari, T. Kitoh, "100 Gbit/s all-optical demultiplexing using nonlinear optical loop mirror with gating width control", Electronics Letters, Vol. 29, No. 21, pp. 1870-1871 (1993).

[4.56] T. Yamamoto, E. Yoshida, M. Nakazawa, "Ultrafast nonlinear optical loop mirror for demultiplexing 640 Gbit/s TDM signals", Electronics Letters, Vol. 34, No. 10, pp. 1013-1014 (1998).

[4.57] M. Nakazawa, E. Yoshida, T. Yamamoto, E. Yamada, A. Sahara, "TDM single channel 640 Gbit/s transmission experiment over 60 km using 400 fs pulse train and walk-off free, dispersion flattened nonlinear optical loop mirror", Electronics Letters, Vol. 34, No. 9, pp. 907-908 (1998).

[4.58] H. Sotobayashi, C. Sawaguchi, Y. Koyamada, W. Chujo, “Ultrafast walk-off-free nonlinear optical loop mirror by a simplified configuration for 320 Gbit/s time-division multiplexing signal demultiplexing”, Optics Letters, Vol. 27, No. 17, pp. 1555-1557 (2002).

[4.59] H. Sotobayashi, W. Chujo,T. Ozeki, “Inter-wavelength-band conversions and demultiplexing of 640 Gbit/s OTDM signals”, Technical Digest of conference on Optical Fiber Communication (OFC’02), Anaheim, California, USA, paper WM2 (2002)

[4.60] A. T. Clausen, A. Siahlo, J. Seoane, L. K. Oxenløwe, P. Jeppesen, "320 to 10 Gbit/s demultiplexing using a NOLM based on commercially available components”, Electronics Letters, Vol. 41, No. 5, pp. 265-266 (2005).

[4.61] A. I. Siahlo, A. T. Clausen, L. K. Oxenløwe, J. Seoane, P. Jeppesen, "640 Gb/s OTDM Transmission and Demultiplexing using a NOLM with Commercially Available Highly Non-linear Fiber", Technical Digest of Conference on Lasers & Electro-Optics (CLEO 2005), Baltimore, Maryland, USA, paper CTuO1 (2005) (Invited).

[4.62] G. P. Agrawal, “Nonlinear Fiber Optics, Second edition”, Academic Press, San Diego, California, USA (1995).

[4.63] T. Morioka, M. Saruwatari, “Ultrafast All-optical switching utilizing the Optical Kerr Effect in Polarization-Maintaining Single-Mode Fibers”, Journal on Selected Areas in Communications, Vol. 6, No. 7, pp. 1186-1198 (1988).

[4.64] O. Dühr, F. Seifert, V. Petrov, “Ultrafast Kerr demultiplexing up to 460 Gbit/s in short optical fibers”, Applied Optics, Vol. 34, No. 24, pp. 5297-5300 (1995).

[4.65] S. Watanabe, R. Okabe, F. Futami, R. Hainberger, C. Schmidt-Langhorst, C. Schubert, H. G. Weber, “Novel Fiber Kerr-switch with parametric Gain: Demonstration of Optical Demultiplexing and sampling up to 640 Gb/s”, Proceedings of the 30th European Conference on Optical Communication (ECOC'04), Stockholm, Sweden, Paper Th4.1.6 (2004).

[4.66] N. Shibata, R. P. Braun, R. G. Waarts, "Phase-Mismatch dependence of Efficiency of Wave Generation Through Four-Wave Mixing in a Single-Mode Optical Fibre", Journal of Quantum Electronics, Vol. QE-23, No. 7, pp. 1205-1210 (1987).

[4.67] C. Lin, W. A. Reed, A. D Pearson, H. –T. Shang, "Phase Matching in the minimum-chromatic-dispersion region of single-mode fibers for stimulated four-photon mixing" Optics Letters, Vol. 6, No. 10, pp. 493-495 (1981).

[4.68] K. Inoue, "Four-Wave Mixing in an Optical Fiber in the Zero-Dispersion Wavelength Region", Journal of Lightwave Technology, Vol. 10, No. 11, pp. 1553-1561 (1992).

[4.69] T. Morioka, H. Takara, S. Kawanishi, T. Kitoh, M. Saruwatari, "Error-free 500 Gbit/s all-optical demultiplexing using low-noise, low-jitter supercontinuum short pulses", Electronics Letters, Vol. 32, No. 9, pp. 833-834 (1996).

[4.70] S. Kawanishi, H. Takara, T. Morioka, O. Kamatani, M. Saruwatari, "200 Gbit/s, 100 km time-division-multiplexed optical transmission using supercontinuum pulses with prescaled PLL timing extraction and all-optical demultiplexing", Electronics Letters, Vol. 31, No. 10, pp. 816-817 (1995).

[4.71] P. O. Hedekvist, M. Karlsson, P. A. Andrekson, "Fiber Four-Wave Mixing Demultiplexing with Inherent Parametric Amplification", Journal of Lightwave Technology, Vol. 15, No. 11, pp. 2051-2058 (1997).

[4.72] J. Hansryd, P. A. Andrekson, "O-TDM Demultiplexer with 42 dB Gain Based on a Fiber Optical Parametric Amplifier", Proceedings of 26th European Conference on Optical Communication (ECOC'00), Munich, Germany, paper 1.1.3 (2000).

[4.73] T. Morioka, S. Kawanishi, K. Uchiyama, H. Takara, M. Saruwatari, "Polarisation-independent 100 Gbit/s all-optical demultiplexer using four-wave mixing in a polarisation-maintaining fibre loop", Electronics Letters, Vol. 30, No. 7, pp. 591-592 (1994).

[4.74] International Telecommunication Union - Telecommunication standardisation sector of ITU (ITU-T), "G.810: Definitions and terminology for synchronisation networks", (1996).

[4.75] K. Yvind, "Semiconductor Mode-locked lasers for optical communication systems", PhD thesis, Research Center COM, Technical University of Denmark (2003).

[4.76] E. M. Dianov, A. V. Luchnikov, A. N. Pilipetskii, A. M. Prokhorov, "Long-range interaction of picosecond solitons through excitation of acoustic waves in optical fibers", Applied Physics B (Photophysics and Laser Chemistry), Vol. B54, No. 2, pp. 175-180 (1992).

[4.77] T. Georges, "Study of non-Gaussian timing jitter statistics induced by soliton interaction and filtering", Optics Communications, No. 123, pp. 617-623 (1996).

[4.78] V. S. Grigoryan, C. R. Menyuk, R.-M. Mu, "Calculation of Timing and Amplitude jitter in dispersion-managed optical fiber communications using lineraization", Journal of Lightwave Technology, Vol. 17, No. 8, pp. 1347-1356 (1999).

[4.79] J. J. Reilly, B. Tech, J. R. F. da Rocha, K. Schumacher, "Influence of timing errors on the performance of direct-detection optical-fibre communication systems", IEE Proceedings J (Optoelectronics), Vol. 132, No. 6, pp. 309-313 (1985).

[4.80] J. Zhang, M Yao, X. Chen, L. Xu, M. Chen, Y. Gao, "Bit error rate analysis of OTDM system based on moment generating function", Journal of Lightwave Technology, Vol. 18, No. 11, pp. 1513-1518 (2000).

[4.81] G. P. Agrawal, "Fiber-optic communication systems – second edition", John Wiley & Sons, Inc, New York, USA (1997).

[4.82] P. J. Winzer, M. Pfennigbauer, M. M. Strasser, W. R. Leeb, "Optimum filter bandwidths for optically preamplified RZ and NRZ receivers", Journal of Lightwave Technology, Vol. 19, No. 9, pp. 1263-1273 (2001).

[4.83] D. Marcuse, C. R. Menyuk, "Simulation of single-channel optical systems at 100 Gb/s", Journal of Lightwave Technology, Vol. 17, No. 4, pp. 564-569 (1999).

[4.84] R. Schaumann, M. E. V. Valkenburg, "Design of analog filters", Oxford University Press (2001)

[4.85] P. I. Reyes, M. Sumetsky, N. M. Litchinitser, P. S. Westbrook, “Reduction of group delay ripple of multi-channel chirped fiber grating using adiabatic UV correction”, Optics Express, Vol. 12, No. 12, pp. 2676-2687 (2004).

[4.86] G. P. Agrawal, “Applications of nonlinear fiber optics”, Academic Press, San Diego, California, USA (2001).

[4.87] J. Yu, X. Zheng, C. Peucheret, A. T. Clausen, H. N. Poulsen, P. Jeppesen. “All Optical Wavelength Conversion of Short Pulses and NRZ Signals Based on a Nonlinear Optical Loop Mirror", Journal of Lightwave Technology, Vol. 18, No. 7, pp. 1007 (2000).

[4.88] W. Belardi, J. H. Lee, K. Furusawa, Z. Yusoff, P. Petropoulos, M. Ibsen, T. M. Monro, D. J. Richardson, "A 10 Gbit/s tuneable wavelength converter based on Four-Wave Mixing in highly nonlinear holey fibre", Proceedings of 28th European Conference on Optical Communication (ECOC'02), Copenhagen, Denmark (2002).

[4.89] J. H. Lee, T. Nagashima, T. Hasegawa, S. Ohara, N. Sugimoto, T. Tanemura, K. Kikuchi, “Wavelength conversion of 40-Gbit/s NRZ Signal using Four-Wave Mixing in 40-cm-long Bismuth Oxide Based Highly-Nonlinear Optical Fiber”, Technical Digest of conference on Optical Fiber Communication (OFC’05), Anaheim, California, USA, paper PDP23 (2005).

[4.90] S. Bigo, E. Desurvire, B. Desruelle, “All-optical RZ-to-NRZ format conversion at 10 Gbit/s with nonlinear optical loop mirror”, Electronics Letters, Vol. 30, No. 22, pp. 1868-1869 (1994).

[4.91] J. Lee, M. Ibsen, D. Richardson, L. Oxenløwe, K. Berg, A. Clausen, P. Jeppesen, "Timing jitter tolerant all-optical TDM data demultiplexing at 80 Gbit/s using fiber Bragg grating based rectangular pulse switching technology", in Technical Digest Optical Fiber Communication Conference (OFC’03), paper TuH7, Atlanta, Georgia, U.S.A. (2003).

[4.92] K. S. Berg, L. K. Oxenløwe, A. Siahlo, A. Tersigni, A. T. Clausen, C. Peucheret, P. Jeppesen, K. P. Hansen and J. R. Hansen, "80 Gb/s transmission over 80 km and demultiplexing using a highly non-linear photonic crystal fibre", Proceedings of European Conference on Optical Communication, (ECOC'2002), Copenhagen, Denmark, paper 2.1.5 (2002).

[4.93] A. I. Siahlo, K. S. Berg, A. T. Clausen, L. K. Oxenløwe, A. Tersigni, P. Jeppesen, "160-10 Gb/s demultiplexing by using NOLM", in Proceedings of Quantum Electronics (QE-2002) 4th International Scientific and Technical Conference 2002, p. 122, Minsk, Belarus (2002).

[4.94] G. J. Spühler, L. Krainer, I. Kilburn, M. Dymott, K. J. Weingarten, R. Paschotta, and U. Keller, "Picosecond pulse-generating laser with repetition rate of 10 GHz and rms timing jitter <100 fs fully tunable over C-band", Technical Digest of conference on Optical Fiber Communication Conference 2003 (OFC'03), Atlanta, U.S.A., paper TuL2 (2003).

[4.95] M. Schilling, O. Blume, L-H. Nguyen, M. Schmidt, E. Lach, "OTDM Planar Lightwave Components (PLCs) for multiplexing from 40 Gb/s to 80-640 Gb/s", Proceedings of 15th Annual meeting of IEEE Lasers and Electro-Optics Society (LEOS 2002), Glasgow, Scotland, paper ThBB5 (2002).

[4.96] A. Yariv, "Optical Electronics in Modern Communications – fifth edition", Oxford University Press, New York, USA (1997).

[4.97] B.-E. Olsson, N. Lagerqvist, A. Boyle, P. A. Andrekson, "Elimination of Acoustic Sensitivity in Nonlinear Optical Loop Mirrors", Journal of Lightwave Technology, Vol. 17, No. 2, pp. 343-346 (1999).

[4.98] T. Sakamoto, H. C. Lim, K. Kikuchi, "All-optical polarisation-insensitive time-division demultiplexer using a Nonlinear Optical Loop Mirror with a pair of short polarization-maintaining fibers", Photonics Technology Letters, Vol. 14, No. 12, pp. 1737-1739 (2002).

Chapter 5
OTDM networking

5.1 Introduction

In the previous chapters, different aspects of basic bit-interleaved Optical Time Division Multiplexed (OTDM) systems have been addressed in terms of components and functionalities. The OTDM technique offers the possibility of supporting huge traffic amounts by increasing the total aggregated bit rate. However through out the entire thesis up to now, it has been tacitly assumed that the OTDM system was a point-to-point system, as shown in Figure 5.1, i.e. the data traffic is generated in the transmitter node A and transmitted to the receiver node B. For a more detailed description of the subsystems constituting node A and B, please refer to previous chapters.

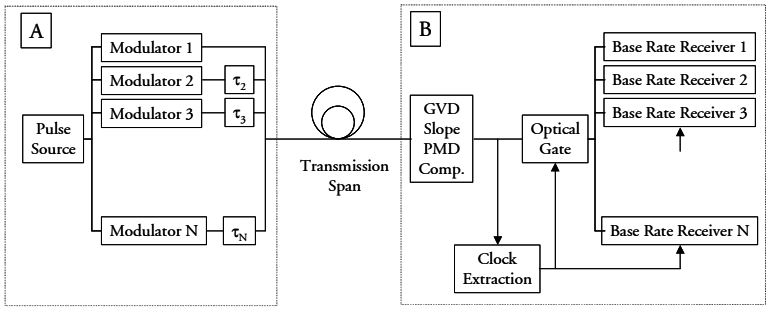

Figure 5.1: OTDM system used for point-to-point transmission.

The OTDM system shown in Figure 5.1 is basically a data pipeline, offering the possibility of transmitting large amounts of data from one point to another, i.e. node A to B.

An important question when examining Figure 5.1 is whether the OTDM technique is limited to this architecture or if the technique can be applied to more complex network architectures? It is obvious that if the OTDM technology can be applied into a versatile number of applications and architectures, the more attractive the technology will be.

Without introducing any assumptions or new subsystems, two different architectures can be suggested. Defining the subsystems within node A in Figure 5.1 as an OTDM transmitter and the subsystems within node B as an OTDM receiver, the OTDM technology shown in Figure 5.1, can be used to ensure data traffic from A to B and B to A by implementing two parallel OTDM systems as illustrated in Figure 5.2.

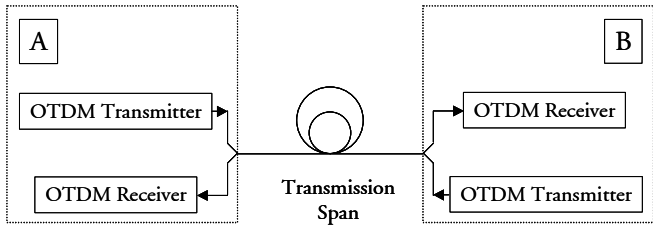

Figure 5.2: Two parallel OTDM systems used to allow for bi-directional transmission.

By introducing a single OTDM transmitter and a number of OTDM receivers in a star structure, as in Figure 5.3, high capacity broadcasting can be implemented. If each OTDM receiver only extracted a single channel of the aggregated OTDM data signal by optical demultiplexing, the architecture could be used to transmit unique data streams to each individual node[35]. Considering this architecture, it is evident that none of the subsystems defining the OTDM transmitter or the receiver include the possibility of identifying the OTDM channel addressed to the specific node. If the proposed structure should be implemented, some additional functionalities have to be defined and developed.

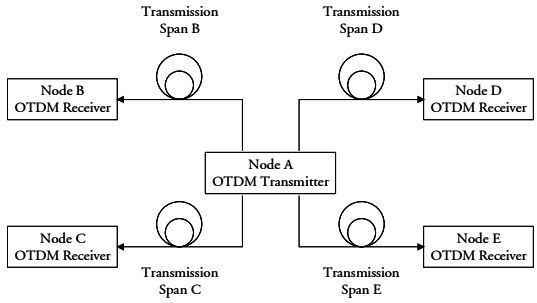

Figure 5.3: Star architecture based on OTDM technology used for broadcasting

[35] This architecture is similar in performance to a WDM architecture and is only included for illustrative purpose.

The objective of this chapter is to give a review of some of the functionalities, which are required in order to implement OTDM network architectures. A scheme to implement a specific functionality, i.e. channel identification, will be addressed in details as only a few references can be found in existing literature.

The scheme in Figure 5.1 is based on bit-interleaving a number of channels in the time domain, and the next section will address the required functionalities for this architecture. Bit interleaved OTDM systems have a number of advantages and drawbacks. By exploiting some of the potential advantages of OTDM, an architecture based on Optical Packet Multiplexing OTDM, can be implemented, offering the possibility of dynamically routing the packets through the network. A short survey of reported packet switched OTDM networks is presented in section 5.5 with a following discussion.

5.2 OADM node functionalities

5.2.1 OTDM OADM nodes

The first steps to introduce OTDM in networks include the introduction of additional nodes between the transmitter, i.e. node A, and the final receiver, node B, see Figure 5.1. Within the intermediate nodes of the system, it is required that a number of the OTDM channels from the aggregated data signal can be dropped, and a number of new bit streams can be inserted into the vacant time slots. The component within the node is labelled an Optical Add Drop Multiplexer (OADM). In Figure 5.4 a system including two additional nodes are shown. A single OTDM channel is dropped in each of the nodes, and a new channel is added as sketched in the figure, but in principle several channels can be dropped and added as discussed in subsequent sections.

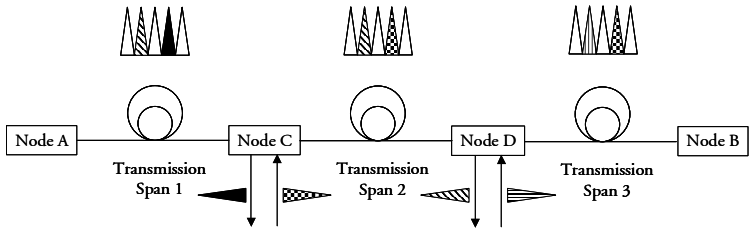

Figure 5.4: OTDM network including additional intermediate nodes based on Optical Add-Drop Multiplexing.

Figure 5.4 illustrates how an OTDM signal generated in node A, after transmission is injected into the first OADM node, i.e. node C. Within the OADM the target channel is dropped and an incoming single time channel

fulfilling the requirements in terms of FWHM and base rate of the OTDM signal is inserted instead of the dropped channel. This is repeated in node D, before the OTDM signal is received in node B.

The principle shown in Figure 5.4 is simple, and does not reveal any of the challenges, which are associated with the actual implementation of the add-drop node. In Figure 5.5 some suggested required functionalities within the add-drop node is included.

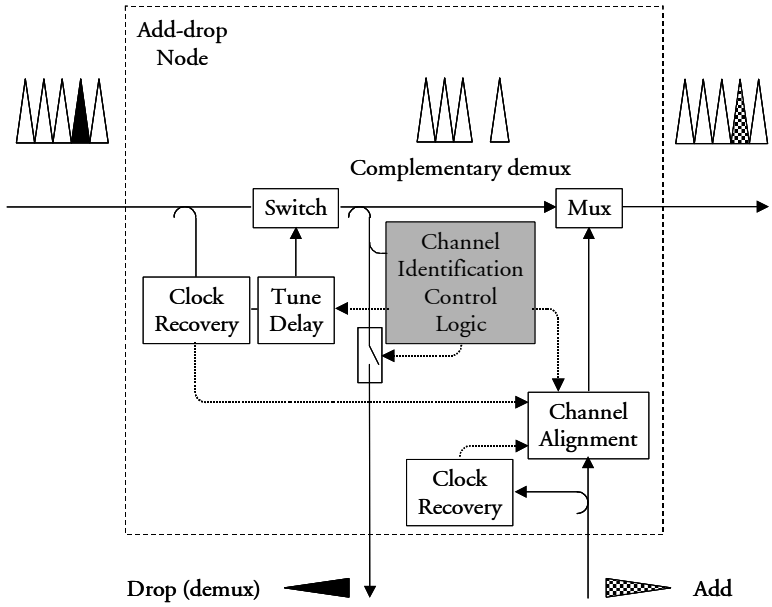

Figure 5.5: Optical Add Drop Multiplexer (OADM) node, showing some of the required functionalities required in order to drop target channel and add a new time channel in the empty time slot.

From Figure 5.5 several subsystems can be identified

- Clock Recovery circuits.
- Switch for demultiplexing and complementary demultiplexing.
- Tuneable optical or electrical time delays.
- Channel identification and corresponding control logic.
- Channel Alignment circuit.
- Multiplexing circuit (Mux).

The principal operation of the OADM will be explained in the following, describing the functionality of the subsystems.

As outlined in chapter 4 a control signal with a repetition frequency corresponding to the base rate of the OTDM signal is required for extracting a base rate channel from the aggregated OTDM signal. The control signal can be generated, by extracting the base rate clock of the aggregated OTDM signal. In Figure 5.5 a branch of the incoming OTDM signal is injected into the Clock Recovery (CR) Circuit. In chapter 3, the Clock Recovery theory based on Optical Phase Detection (OPD) implemented in a Phase Locked Loop (PLL) configuration is described, and it is shown that a clock extracted at the base rate of an aggregated OTDM signal is locked to one of the OTDM channels but not a predetermined channel, i.e. the locking process will scan through the OTDM channels until the locking conditions are fulfilled and thus the locking channel is randomly picked. Consequently, a fixed time delay between the Clock Recovery and the Demultiplexing Circuit can be determined, ensuring perfect alignment between the induced Switching Window (SW) in the switch and an OTDM channel. However, this fixed time delay enables demultiplexing of an OTDM channel, but without any certainty that the extracted channel is the target channel to be dropped in the OADM node, e.g. the black channel in Figure 5.5. It is important to emphasise that this delay line do not jeopardize the synchronisation of the Clock Recovery between the OTDM signal and the clock

By injecting a branch of the demultiplexed signal into a Channel Identification Circuit, this circuit will examine if the demultiplexed channel indeed is the correct channel. How this information can be extracted and used in the circuit is the objective of next section. If the demultiplexed channel does not correspond to the target channel, the Channel Identification Circuit Control Logic will increment the value of the time delay in steps corresponding to the OTDM time slot. In this manner the Channel Identification Circuit can scan through all the OTDM channels, monitoring when the target channel is dropped in the node. When the target channel is identified and dropped, the Channel Identification Circuit Control Logic will open a switch, passing the bit stream out of the OADM without further processing[36]. In section 5.3.6 the scanning process is discussed in some detail.

The Demultiplexing Circuit, also labelled optical gate or switch, should generate two signals – the demultiplexed channel and the complementary demultiplexed signal, i.e. the dropped channel and the OTDM signal without the dropped channel, respectively.

The complementary demultiplexed signal includes a vacant time slot in the OTDM signal, where a new channel, referred to as the add channel, can be

[36] Additional processing in order to interface the base rate data signal to e.g. a LAN network is not considered further within this section.

inserted. In Figure 5.5 a new channel is injected into the OADM. It is assumed that the repetition frequency of the add channel is identical to the base rate of the OTDM channel, otherwise the configuration in Figure 5.5 has to be extended with a circuit enabling the repetition frequency of the add channel to be modified. It is however not assumed that the add channel is aligned in time to the empty slot. A branch of the add channel is injected into a Clock Recovery Circuit extracting the clock of the add signal. As opposed to the clock extracted from the aggregated OTDM signal, the alignment between the add data channel signal and the add clock is well established, because the add signal is a base rate signal (see chapter 3 for more details). The two clock signals are used as input to the Channel Alignment Circuit. This circuit can compare the phase of the two clocks and control a tuneable time delay, ensuring that the add channel is matched in time to an OTDM timeslot. As the Channel Identification Circuit has extracted the information of the position between the base rate clock extracted from the OTDM signal and the position of the target channel, it can be used as an additional control signal into the Channel Alignment Circuit, hereby shifting the tuneable time delay with the required additional time delay in order to align the add channel to the vacant time slot in the complementary demultiplexed signal.

After alignment of the add channel, it is injected together with the complementary demultiplexed signal into the Multiplexing Circuit where the two signals are merged together. The Multiplexing Circuit can e.g. be a passive coupler. It is however important to equalise the peak power of the add channel to the same level as the peak power of the remaining channels in the complementary demultiplexed signal. This could be realised by using Variable Optical Attenuators (VOA).

How the Channel Identification Circuit is implemented is strongly related to how the channel information is applied to the target channel. This is addressed in section 5.3. The Channel Alignment Circuit is primarily some simple electronic logic comparing the three input signals, generating the required control signal for the tuneable time delay.

Clock Recovery Circuits have been presented in chapter 3 and will consequently not be addressed further in this chapter. The switch used for demultiplexing in Figure 5.5 has a lot in common with the switches presented in chapter 4 and summarised in table 4.2. However, in the depicted configuration in Figure 5.5, both the demultiplexed channel and the complementary demultiplexed channel should be presented. A number of circuits offer both signals at the output of the component as described in chapter 4. The optical switch should fulfil some strict requirements in terms of suppression of the empty time slot in the complementary demultiplexed signal - this has been addressed in details in [5.1].

The tuneable time delays need to offer a tuning range of a full OTDM base rate time slot, in order to ensure that e.g. the add channel can be aligned to the vacant time slot of the complementary OTDM signal. A few schemes for tuneable optical time delays have been demonstrated in the literature. In Figure 5.6 a technique based on wavelength converters is shown [5.2].

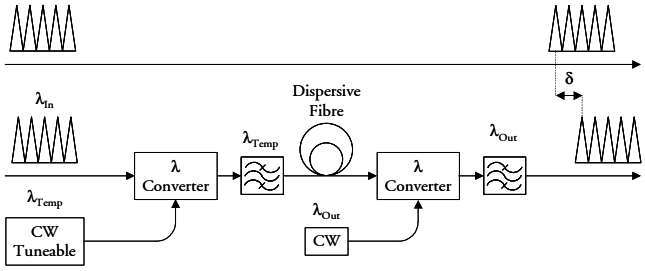

Figure 5.6: Tuneable time delay based on wavelength converters.

An optical data stream or pulse train, which needs to be delayed, is injected into the delay structure. First, the data stream is wavelength converted to an internal temporary wavelength λ_{Temp}. The wavelength-converted signal is subsequently injected into a dispersive element, which introduces a specific time delay of the signal due to wavelength dependent group velocity. Consequently, by adjusting the wavelength of the internal signal, the relative delay can be controlled. At the output of the dispersive element, an additional wavelength converter is used to convert the signal back to the original wavelength of the data signal[37], and a relative delay δ between the original signal and the output signal is introduced. The granularity of the delay is limited by the tuneable Continuous Wave (CW) source, which in practice should not be an issue. An optical time delay of 100 ps corresponding to a full OTDM base rate timeslot was reported. A more severe limitation of the technique is the complexity of the set-up, with two wavelength converters. However, in [5.2] the configuration was evaluated, using Semiconductor Optical Amplifier (SOA) based interferometric devices. These devices offer in principle the possibility of integration on a chip, which could to some degree limit the physical size and increase the stability of the scheme.

Another time delay structure is reported in [5.3], where a number of delay stages placed between an input and an output modulator is used to select a specific OTDM channel within the signal. The scheme is relatively simple as opposed to the technique in [5.2]. As the granularity is equal to the time slot,

[37] Notice, the structure can also be used as an interface between different networks, and consequently the wavelength is not necessarily equal to the input wavelength.

i.e. it can be used to select the target OTDM channel, it should be sufficient for the set-up in Figure 5.5 when dropping a channel. For the synchronisation of the incoming channel, which should be added, the granularity of the time delay might have to be higher. The structure in it self inherently introduce significant losses depending on the number of delay stages, thus as with the previous suggested tuneable time delay requires optical amplification.

As it is obvious from the above description, an indispensable part of an OTDM system, which includes OADM nodes, is the Channel Identification. In literature only a few groups have proposed schemes for channel identification, which will be briefly explained in the next section, before a novel architecture will be proposed.

5.3. Channel identification

With the configuration shown in Figure 5.5 it is possible to implement an add-drop node in an OTDM network architecture. However, in the previous section it has been assumed, that information in the target data channel is available, allowing the Channel Identification Circuit to determine if the demultiplexed channel is the target channel or not. If the demultiplexed channel is not the correct channel, the Channel Identification Circuit Control Logic, will shift the tuneable delay in order to scan through all the OTDM channels, in order to extract the target channel.

Examining the OTDM transmitter in Figure 5.1 reveals that none of the subsystems within the transmitter apply this information to any of the bit streams. From an optical point of view, all the OTDM channels are identical. The information could be embedded in some of the bits constituting the individual bit streams, by following a specified protocol. This can be done, but will increase the complexity of the node, and will be avoided in the present configuration as processing capabilities will be required[38]. Consequently, the required information has to be procured by other means.

Identification of a specific OTDM channel within the aggregated data signal has not been addressed in much detail within the existing literature, and consequently this topic represents a vital challenge, if the OTDM technique has to penetrate the barrier from point-to-point systems to network systems with several add-drop nodes.

[38] In section 5.5 where an introduction to Optical Packet Multiplexed OTDM networks is presented, the address information is available in the header of the packets.

5.3.1 Previous reported techniques for channel identification

In [5.4] the principle OTDM transmitter constituting node A in Figure 5.1 has been modified, by including polarisation controls in the N branches, as shown in Figure 5.7.

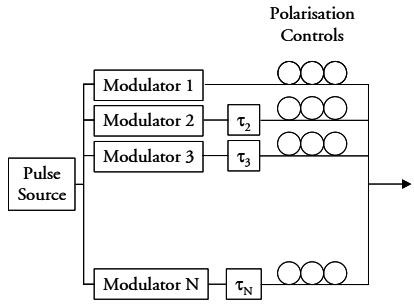

Figure 5.7: OTDM transmitter including polarisation controls in each branch.

By careful adjusting the State Of Polarisation (SOP) in each branch, an OTDM signal can be generated where the SOP of channel 1 is perpendicular to the (N-1) other channels, as illustrated in Figure 5.8. By placing a polariser in the receiver, aligned to channel 1, a base rate data signal, e.g. 10 Gbit/s, can be extracted, as shown in Figure 5.8. This signal can subsequently be injected into a base rate Clock Recovery Circuit, e.g. operating at 10 GHz. With this approach, the CR is locked uniquely to a specific time channel, thereby allowing channel identification. The proposed scheme is an elegant approach to allow channel identification. As the technique resembles the Alternate Polarisation OTDM transmission, where the SOP of every bit is perpendicular to its neighbours, and as this technique has been very successful, see e.g. [5.5] [5.6], this suggested implementation can be a good choice for channel identification. A drawback is the potential impact on the signal of components with Polarisation Dependent Loss (PDL) and Polarisation Mode Dispersion (PMD), which could jeopardise the scheme – simulations, including non-linear effects and PMD, have to be carried out, in order to evaluate the transmission performance and thereby the feasibility. An additional issue, which has not been addressed in [5.4], is how the polariser in the receiver dynamically will adapt to the random changes in polarisation due to the transmission. As the scheme is based on discrimination of channel 1, it is indispensable to solve this problem.

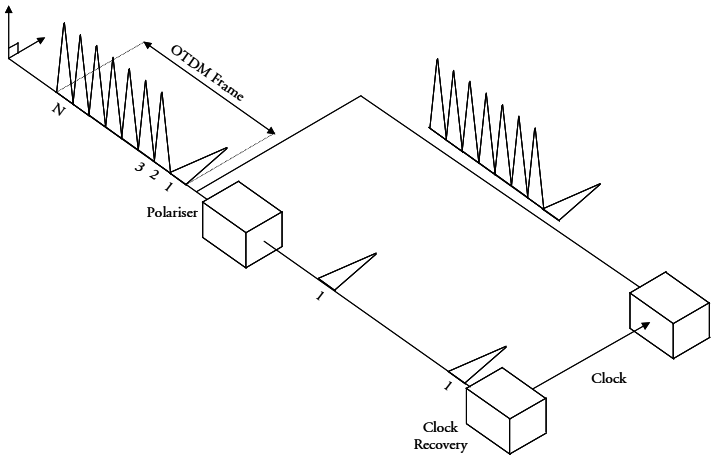

Figure 5.8: OTDM signal composed by N channels. The SOP of channel 1 is perpendicular to the other (N-1) channels.

In [5.7] and [5.8] another technique is reported based on amplitude difference between channel 1 and the other (N-1) OTDM channels. The OTDM transmitter in Figure 5.1 is modified, by including optical attenuators in each branch[39]. By decreasing the power level of the (N-1) channels compared to channel 1, see Figure 5.9, the spectral properties of the OTDM signal is changed. From chapter 3 it is known that the aggregated OTDM signal does not include any discrete frequency components at the base rate clock. However, with the proposed modifications a base rate frequency component has been introduced, which can be used to extract the clock [5.7], see Figure 5.9A. In [5.7] a loop mirror is used as a threshold device in order to extract the header bits by increasing the power level ratio between peak power of channel 1 and the other channels in the receiver, hereby reducing the introduced power level difference in the receiver. In [5.8] the threshold device is a modified Terahertz Asymmetric Optical Demultiplexing (TOAD) circuit. At the output of the threshold device, both the header bits are available and the complementary demultiplexed data signal. The header bits are used as control signal for the Demultiplexing Circuit, demultiplexing the data from the OTDM data stream, see Figure 5.9B. As in [5.4], the unique locking of the CR to a specific channel in both schemes, allows for channel identification.

One of the advantages of the proposed scheme is the generated base rate frequency component, allowing for simpler clock extraction as opposed to the PLL based approach, explained in chapter 3. A drawback of the architecture is

[39] In Figure 5.1 it is assumed that the peak power levels of each channel inherently were equalised. In reality optical attenuators would be included in the transmitter, whereby the proposed modification does not constitute an increase in complexity.

the additional optical subsystems, i.e. the threshold device, which increase the complexity. Furthermore, the system is prone to saturations effects, which could equalise the peak powers of all the channels, hereby removing the channel information. An advantage of the set-up in Figure 5.8B is the self-clocking properties of the scheme, allowing for asynchronous data transmission e.g. in optical packet multiplexed networks, see section 5.5. A drawback is that one bit out of the frame is required to be a fixed pattern, corresponding to only marks.

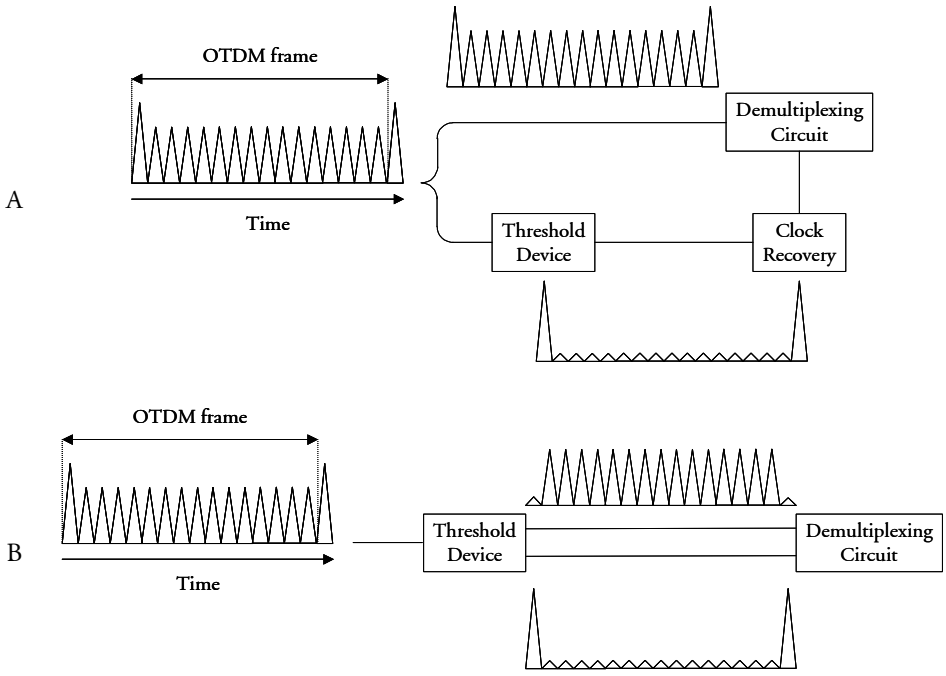

Figure 5.9: Modified OTDM signal, by increasing the peak power of channel 1 compared to the other (N-1) channels. A) Corresponds to the suggested set-up in [5.7] and B) to the set-up in [5.8].

Finally, a scheme proposed in [5.9] exists. The header bit of the frame is introduced by modulating a fixed pattern in the header bit with Binary Phase Shift Keying (BPSK) and the other bits with Amplitude Shift Keying (ASK). By implementing a homodyne receiver a clock signal corresponding to the base rate of the OTDM signal can be extracted. Both the transmitter and receiver are quite complex compared to the previous mentioned configurations. Furthermore, the header bit does not contain any data information as the pattern is fixed.

In the following section a novel scheme based on pilot tone modulation is proposed.

5.3.2 Channel identification based on pilot tone modulation

A novel approach for channel identification is presented in this section based on sinusoidal amplitude modulation of one of the OTDM channels. In Figure 5.10 the proposed transmitter is shown. A pulse source is generating a pulse train with a repetition frequency corresponding to the base rate of the OTDM signal. The pulse train is split into N branches, each branch including an external data modulator. In one of the branches an additional external modulator is included, labelled pilot in the Figure, applying a low frequent (frequency f_p) Amplitude Modulation (AM) on the pulse train. Each of the branches includes an appropriate time delay in order to multiplex the N pulse trains in the time domain.

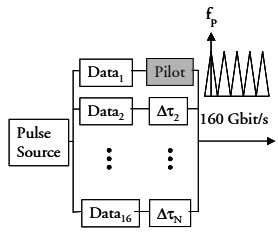

Figure 5.10: OTDM Transmitter including one branch with additional modulator for applying amplitude modulation serving as the pilot tone. The frequency of the pilot tone is f_p

Part of an OTDM network, including a transmitter, a dispersion compensated transmission span and an Add-drop node, relying on the pilot tone scheme is shown in Figure 5.11 [5.10], adapting the set-up shown in Figure 5.5 to the pilot tone scheme.

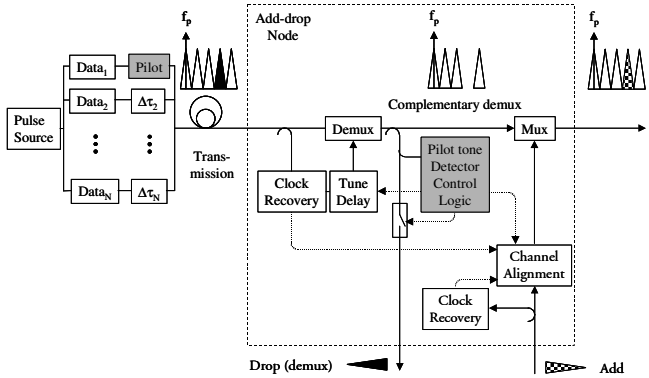

Figure 5.11: Pilot tone scheme implemented in an OTDM network.

The transmitter is generating an OTDM signal as explained and shown in Figure 5.10. The OTDM signal is injected into the dispersion compensated transmission span and received in the add-drop node. One of the OTDM channels, marked as black in Figure 5.10, should be dropped in the Add-drop node and another channel, chequered in the Figure, should be added in the generated vacant timeslot. In this scheme it is predefined that the pilot tone modulated channel constitutes channel number 1, and the black marked channel is number 4, i.e. the network in its current implementation is static with no means to dynamically reallocate a specific channel to a specific node.

As most of the sub-systems in Figure 5.11 are similar to the sub-systems constituting Figure 5.5, the functionalities will not be addressed further in this section – only sub-systems specifically addressing the Channel Identification Circuit will be explained.

A part of the demultiplexed signal is injected into the Pilot Tone Detector, which detects the power at the pilot tone frequency. If the demultiplexed channel does not correspond to the pilot tone modulated channel, the power of the pilot tone does not exceed the internal threshold set in the control logic of the pilot tone circuit. In this case, the control logic generates an electrical signal, controlling the tuneable time delay between the CR and the demultiplexing circuit, to increment the time delay with a step in time corresponding to one OTDM time slot. The next OTDM channel is consequently demultiplexed and checked. This process is repeated until the pilot tone modulated OTDM channel corresponds to the demultiplexed channel. After the pilot tone channel is recognised, the control logic can apply a new electrical signal to the tuneable time delay, controlling the time delay to increment/decrement the position of the SW the number of OTDM time slots in order to ensure that demultiplexing

of the correct channel. This routing is based on fixed traffic, determining that e.g. channel 4 is destined for this specific node.

Correspondingly, as the pilot tone control logic has recognised the position of the pilot tone modulated channel, is has simultaneously recognised the position of the vacant time slot. Consequently, it controls an additional time delay encapsulated in the Channel Alignment Circuit between the new chequered Add channel and the multiplexing circuit, labelled mux, see Figure 5.11.

A key component in the scheme is the pilot tone detector and the control logic. Within this thesis, the actual hardware has not been designed and fabricated. However, it is envisioned to consist of a photo detector with a bandwidth sufficiently high in order to detect the pilot tone frequency, a bandpas filter centred at the pilot tone frequency and a subsequent electrical circuit monitoring the electrical power. As the frequency of the pilot tone is low, the required electronics for the pilot tone detector is correspondingly low speed, and should consequently keep the expenses of the circuit acceptable.

5.3.3 Numerical example illustrating the pilot tone scheme

In order to ensure the unique identification of the pilot tone modulated channel based on the electrical power, it is imperative that the power at the pilot tone varies significantly as function of the position of the SW. In this section this is illustrated by a numerical investigation.

The schematic shown in Figure 5.12 is used to evaluate the scheme. It consists of a pulse source generating a pulse train of Gaussian pulses with FWHM width of 0.4 times the timeslot of a 160 Gbit/s data signal as described in chapter 2. The pulses are split into 16 arms. In the simplified set-up the branches do not include any data modulation, only the appropriate time delays. One of the branches furthermore includes an ideal Amplitude Modulator, applying the pilot tone modulation to one of the channels. The modulation index of the AM can be varied. The 16 arms are bit interleaved and injected into an ideal demultiplexing circuit, which is characterised by a Gaussian shaped SW. At the output of the demultiplexing circuit, the demultiplexed signal can be visualised in time, i.e. oscilloscope, and in frequency, i.e. spectrum analyser. The spectrum is used to determine the power at the pilot tone frequency.

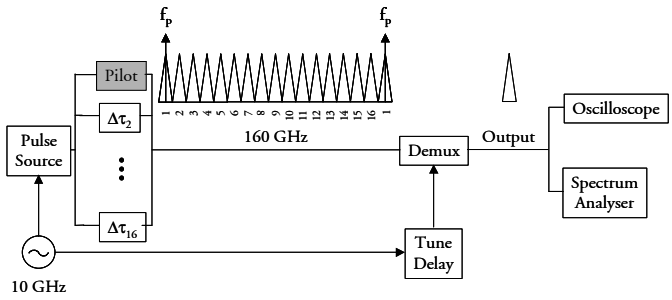

Figure 5.12: Numerical set-up used to evaluate the pilot tone scheme.

In order to ensure a sufficient resolution between the discrete spectral components, f_p is chosen to 200 MHz. This choice is related to the used FFT routine and is not a design criterion for the scheme. In a subsequent section a suggested lower frequency is determined based on the cut off frequency of components constituting the network. The modulation index in the shown example is 0.3, which introduce significant amplitude of the discrete pilot tone frequency component without resulting in a high receiver penalty (see subsequent section).

The pulse train emulating the pilot tone modulated OTDM channel, can be written as follows:

$$P_p(t) = \frac{1}{1+m}\left(1+m\cos\left(2\pi f_p t\right)\right)\sum_{k=-\infty}^{\infty} A\exp\left(\frac{-\left(t-kT_B\right)^2}{2T_o^2}\right) \qquad (5.1)$$

Where k is an integer, A is the amplitude in power, T_0 is the e^{-1} intensity point of the Gaussian pulse, T_B is the period of the pulse train, i.e. the base rate time slot of the OTDM signal, f_p is the pilot tone frequency and m is the modulation index. The factor $(1+m)^{-1}$ is included to ensure that maximum amplitude of the signal does not exceed the amplitude of the input signal[40].

As an example the Gaussian pulse train is pilot tone modulated with a modulation index m = 0.3 as shown in Figure 5.13A. In Figure 5.13B a zoom on the spectral components between 9 to 11 GHz of the channel with and without pilot tone modulation is shown.

[40] The maximum, the average and the minimum amplitude A_{Max}, AV, A_{Min} can be calculated to be 1, 1/(1+m) and (1-m)/(1+m) respectively. Defining the variation in amplitude $\Delta A = A_{Max}-AV = AV-A_{Min}$ the modulation index can be calculated as $\Delta A/AV = m$ [5.11].

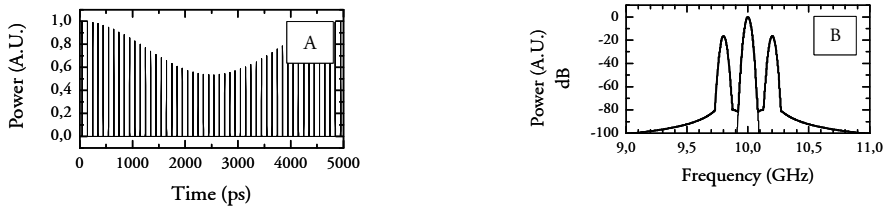

Figure 5.13: (A) 10 GHz pulse train pilot tone modulated with modulation index m = 0.3. (B) Spectrum of pulse train without pilot tone modulation (thin line) and with pilot tone modulation (bold line).

Inspecting the spectrum in Figure 5.13B it can be observed how the power is centred in the discrete 10 GHz discrete frequency component when no pilot tone is applied to the pulse train, i.e. the thin line in Figure 5.13B. When applying the pilot tone, the expected two sidebands around the 10 GHz component appear. Notice, the power of the 10 GHz component is normalised for easy comparison. Additionally, a pilot tone modulated sideband would be observed around the DC component, which is the component envisaged to be used in an implemented system. However, in the experimental set-up described in a forthcoming section the 10 GHz component was inspected because it allowed a simple monitoring of the presence of a 10 Gbit/s data signal simultaneously.

The modulation index m can in principle be determined in the time domain, albeit not practically in the laboratory due to the resolution of the oscilloscopes. Instead the modulation index can be calculated from the spectrum, by extracting the power of the 10 GHz component P_{10} and the modulation induced side band component P_p and using the following relation [5.11]

$$m = \sqrt{\frac{4\,P_p}{P_{10}}} \tag{5.2}$$

As explained previously, the power in the frequency components induced by the pilot tone modulation is used to determine the channel number. Consequently it is important to obtain a significant difference in received pilot tone power, as function of the relative position of the SW to the pilot tone modulated OTDM channel.

Performing the simulation based on the set-up shown in Figure 5.12, and tuning the time delay and consequently the relative position of the SW

compared to the OTDM signal, the pilot tone power for each position can be extracted from the spectrum. In Figure 5.14 the pilot tone power is shown as function of the relative position between the pilot tone modulated OTDM channel and the SW for m = 0.3 and a 4.37 ps FWHM width of the SW, see chapter 4.

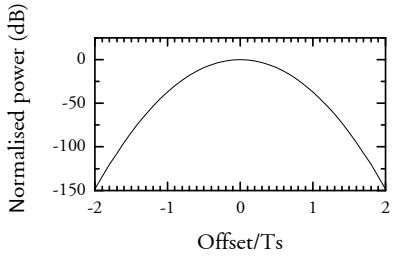

Figure 5.14: Power of discrete pilot tone as function of detuning between the centre of the pilot tone modulated channel and the Switching Window.

It is observed that a significant difference in power is obtained when demultiplexing the pilot tone modulated channel and the neighbouring channels. When detecting the pilot tone power in the immediate neighbouring channels, the power has dropped 37 dB compared to the power in the actual pilot tone modulated signal. Increasing the offset further, the power drops even lower until the power reaches the power level of a pure Gaussian pulse train, which in these simulations are approximately –200 dB. The variation in pilot tone power is determined solely by the width and shape of the switching window and is identical irrespective of the modulation index m. Hence an even higher suppression of the pilot tone power can be designed by e.g. decreasing the temporal width of the SW. However, this might introduce an overall penalty to the OTDM system, as the switch does not fulfil the requirements for fully optimised performance (see chapter 4).

The relative variation in pilot tone power as function of the temporal position of the SW is important, because the pilot tone circuit is envisaged to monitor the pilot tone power for each demultiplexed channel. The circuit can determine whether the channel is pilot tone modulated or not by introducing a threshold within the control logic used for making a simple binary decision. A threshold level covered by the variation range between the pilot tone powers measured in the target channel and the immediate neighbour channel appears to be a reasonable choice.

Albeit, the variation of the normalised pilot tone power as function of the offset between pilot tone modulated channel and the SW is not correlated to the value of m, the absolute value of the pilot tone power is correlated to m as

expressed by eq. (5.3). The simulations presented in this section are based on ideal conditions and hence the Signal to Noise Ratio (SNR) between a noise floor and the peak of the pilot tone power is very high, and are in the simulations only present due to computational and software related uncertainties. However, in a real system, the SNR is expected to decrease because noise will be introduced in the system. If the absolute power of the pilot tone component is low, the actual SNR useable for the pilot tone logic can be significant lower than the variation predicted in the simulations thus potentially jeopardising the detection.

In conclusion, from a design point of view a high absolute pilot tone power, and consequently a high modulation index, is attractive, as the decision circuit will be more robust to noise. However, an increased pilot tone modulation applied to the pilot tone channel will due to the amplitude variation introduce a power penalty when received. The impact of the pilot tone amplitude modulation of an OTDM channel is addressed in the following section.

5.3.4 Power penalty due to pilot tone modulation

A simple way to illustrate the impact of pilot tone modulation on a Gaussian pulse train carrying data is to calculate the Eye Opening Penalty (EOP) as function of the modulation index m, using the simulation tool described in chapter 4.

EOP simulations calculate the penalty from the worst-case eye. Consequently, instead of simulating a pilot tone sinusoidal modulated Gaussian pulse train as outlined in eq. (5.1), the data modulated signal is multiplied with the factor causing the most degraded signal. In this case (1-m)/(1+m) leads to a minimum amplitude of the data modulated signal. The EOP is calculated as the ratio between eye opening with and without pilot tone modulation using eq. (4.6). The simulations can be summarised as shown in Figure 5.15.

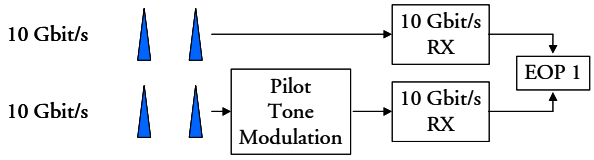

Figure 5.15: Principle of EOP simulations addressing impact of modulation index m of the pilot tone modulation

The EOP as function of modulation index is shown in Figure 5.16.

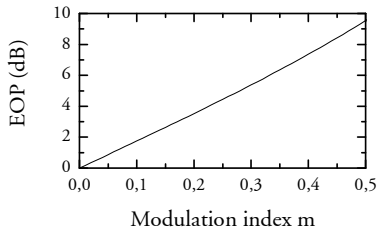

Figure 5.16: EOP as function of modulation index m of pilot tone modulation

From Figure 5.16 it can be seen that a modulation index of ~ 0.06 corresponding to a reduction of the amplitude from 1 to 0.89, induces an EOP of 1 dB. This indicates a high penalty dependence to even relative moderate modulation indices. However, as emphasised in chapter 4, the results generated by the EOP simulations should be interpreted cautiously because the results are based on the worst-case sample irrespective of the probability of this incidence and can consequently not be used to evaluate the Bit Error Rate (BER). Because a significant number of the total data bits will not experience the maximum amplitude reduction, the impact of the modulation index m on the BER is expected to be more relaxed.

An analytical expression including the modified probability density functions (pdf) due to pilot tone modulation is presented in [5.12]. In [5.13] the theory for detection of signals using a receiver, described by the presence of Gaussian distributed noise is derived. The well-known expression for the error probability, usually described by the BER, is

$$BER = \frac{1}{4}\left[\operatorname{erfc}\left(\frac{I_1 - I_d}{\sigma_1\sqrt{2}} \right) + \operatorname{erfc}\left(\frac{I_d - I_0}{\sigma_0\sqrt{2}} \right) \right] \tag{5.3}$$

Where I_0 and I_1 are the average currents, corresponding to a received space ('0') or mark ('1'), respectively. The noise associated with the received bits is represented by the variances in the received spaces and marks, σ_0 and σ_1. I_d is the threshold within the receiver, used to decide whether the received bit was a mark or a space. Defining the Q parameter as

$$Q = \frac{I_1 - I_0}{\sigma_1 + \sigma_0} \tag{5.4}$$

It can be shown that an optimised threshold exists, leading to a reduced expression for the minimum BER [5.13]

$$\mathrm{BER} = \frac{1}{2}\,\mathrm{erfc}\left(\frac{Q}{\sqrt{2}}\right) \tag{5.5}$$

Applying the sinusoidal Amplitude Modulation to the data modulated pulse train changes the probability density function of the received signal. This is illustrated in Figure 5.17, where the initial Gaussian distribution of the mark signal transformed, as the modulation index *m* is increased from 0.1 to 0.5.

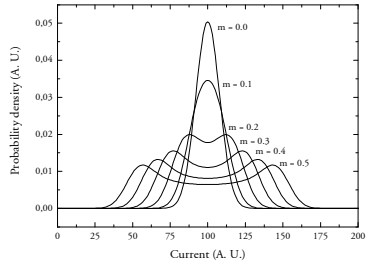

Figure 5.17: Probability density for a received mark, with pilot tone modulation m varied from 0.0 to 0.5 in steps of 0.1.

To calculate the BER for the pilot tone modulated signal, a modification of the BER expression in eq. (5.3) and (5.5) are required. Mathematically, the received probability density function can be described as a convolution of the initial Gaussian distribution with the pdf of the sinusoidal signal [5.12]. Utilising the mathematical tools developed in [5.14], an expression of the BER can be derived [5.12]. However, in order to obtain an expression, which can be analytically accessed, an approximation is introduced in [5.12]. It is assumed that the power penalty primarily stems from the instant, when the mark signal is a minimum due to the AM, see e.g. Figure 5.17 for an intuitive justification of this assumption. Introducing the parameter μ as

$$\mu = \frac{1-(\sigma_0/\sigma_1)}{1-(I_0/I_1)} \tag{5.6}$$

The modified BER for a pilot tone modulated signal can be expressed as [5.12]

$$\mathrm{BER} = \frac{1}{4}\left[\mathrm{erfc}\left(\frac{Q}{\sqrt{2}}\right) + \mathrm{erfc}\left(\frac{Q}{\sqrt{2}}(1-m\mu)\right)\right] \tag{5.7}$$

Notice, just like the EOP simulations presented above, eq. (5.7) is based on the assumption that the bits with lowest amplitude primarily introduce the penalty. Hence, eq. (5.7) will also lead to a pessimistic penalty as function of the modulation index m. The primary goal of this section was to indicate how the pilot tone modulation for increased modulation index m starts degrading the signal. A simple simulation model and a referenced analytical expression have been presented. A modulation index of 0.3 would introduce an EOP of ~ 5 dB.

5.3.5 Experimental investigation of pilot tone impact

Choice of pilot tone frequency

Using the pilot tone scheme in an Optical Network, it is imperative that the tone is available in the entire network, and is consequently not cut off in some of the components constituting the network.

One of the key components in an optical network is the EDFA. The relative slow gain dynamics in the EDFA's result in a high pass characteristic of the device [5.12] dictates that the choice of pilot tone frequency should be chosen higher than the cut-off frequency of the EDFA.

In Figure 5.18 an example showing the relative pilot tone power measured on an electrical spectrum analyser after a specific EDFA[41] as function of the pilot tone frequency, demonstrating a 3-dB cut-off frequency of approximately 55 kHz.

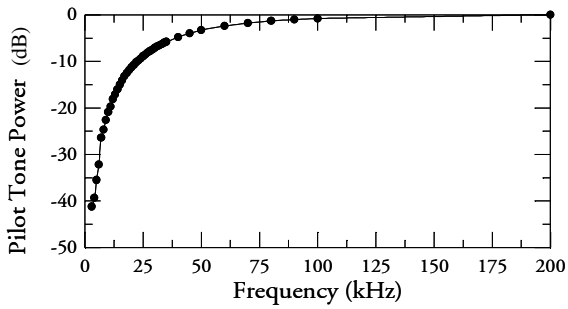

Figure 5.18: Pilot tone power after an EDFA as function of the pilot tone frequency f_p. The 3 dB cut-off frequency is approximately 55 kHz.

When determining an appropriate pilot tone frequency, the decision is partly based on the cut-off frequency of each individual EDFA implemented in the

[41] Highwave Optical Technologies

optical network. However, also the impact of the total cut-off frequency when concatenating a number of EDFA's needs to be included when determining the pilot tone frequency as the total cut-off frequency of the system will be larger than each individual EDFA cut-off frequency.

Finally, an additional parameter affecting the choice of the pilot tone frequency is the separation between the pilot tone frequency and the bandwidth of the high frequency data. According to [5.15] the frequency of the pilot tone should be sufficiently low not to enter the bandwidth of the high frequency data.

When implementing the pilot tone scheme, all these inputs should be included when choosing the actual pilot tone frequency.

Impact of Pilot Tone Modulation on System performance

As elucidated in section 5.3.4, the Pilot Tone Modulation will introduce a power penalty in the receiver, due to the convolution between the sinusoidal modulation and the noise characterising the data and the receiver. In the following section, an experimental investigation is presented [5.10].

If the ratio, Δ_S, measured in dB on the spectrum analyser, between the power of the OTDM base rate frequency and the pilot tone frequency is defined as

$$\Delta_S = 10 \log\left(\frac{P_{10}}{P_p}\right) \tag{5.8}$$

The modulation index m can be calculated as

$$m = \sqrt{\frac{4}{10^{\Delta_S/10}}} \tag{5.9}$$

Which is more convenient than eq. (5.2), as the power of the frequency components experimentally typically will be monitored on a logarithmic scale on the spectrum analyser. In Figure 5.19, Δ_S is shown as function of m.

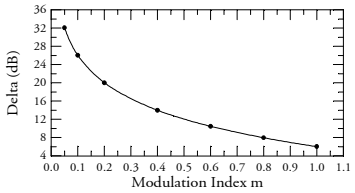

Figure 5.19: Δ_S is shown as function of m

In Figure 5.20 a zoom on the measured experimentally obtained electric spectra of four signals are shown, corresponding to a modulation index m of 0.00, 0.39, 0.53 and 0.59[42], see Figure 5.19. In Figure 5.21 the measured BER is depicted for a 10 Gbit/s data modulated signal. This signal would be the pilot tone modulated channel depicted in Figure 5.12. Examining the figure, it can be seen that both slope and sensitivity, i.e. power corresponding to BER = 10^{-9}, are significantly affected by the pilot tone modulation.

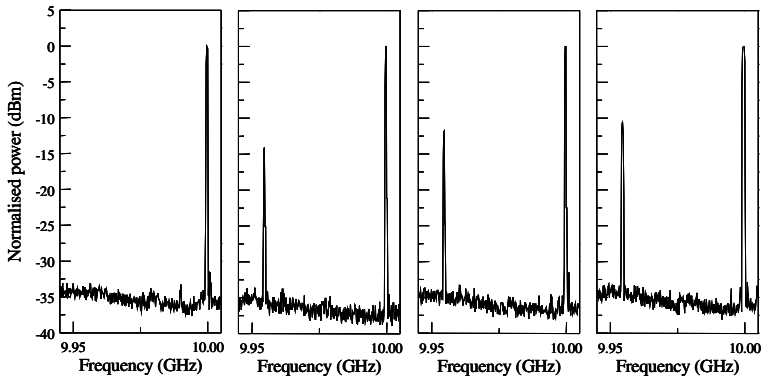

Figure 5.20: Zoom on the experimentally measured electrical spectra of data signals applied pilot tone modulation with modulation index *m* ranging from 0.00, 0.39, 0.53 and 0.59, starting from left to right.

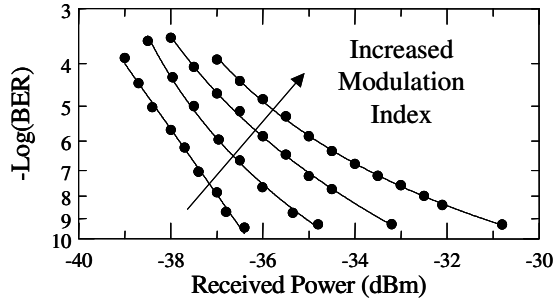

Figure 5.21: Experimentally measured BER curves for data signal applied pilot tone modulation with a modulation index *m* of 0.00, 0.39, 0.53 and 0.59.

If a power penalty of 1 dB is acceptable, then m can approximately be 0.3 for this specific system. This value is significantly higher than the predicted value

[42] Notice, that in [5.10] the modulation indices were incorrectly stated as *m* of 0.00, 0.27, 0.35 and 0.41.

based on EOP simulations, thus emphasising that EOP simulations only address the worst-case scenario. Examining Figure 5.20, a distinct pilot tone frequency component is available, with an estimated SNR of ~ 20 dB. This indicates that the electrical circuit encapsulated in the Pilot Tone Detector Circuit should be able to detect the power. This indication is further supported, when measuring the contrast using the set-up shown in Figure 5.22.

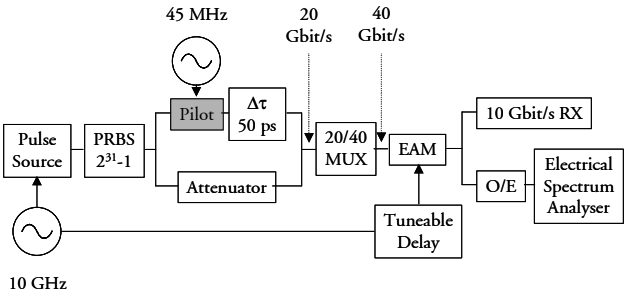

Figure 5.22: Experimental set-up for evaluating contrast.

In Figure 5.22 the pulse source is controlled by an electrical signal, generating a 10 GHz pulse train. The signal is PRBS modulated with a sequence length of 2^{31}-1 before the data signal is split into two branches. In one of the branches, an additional modulator is included, used to apply the 45 MHz pilot tone to the data signal. An optical time delay is used to ensure that the relative time difference between the upper branch and the lower branch is equal to i*50 ps, where i is an integer, hereby generating a 20 Gbit/s data signal, when bit interleaving the upper and the lower branch. In the lower branch, an optical attenuator is adjusted in order to obtain same peak power when no pilot tone is applied and the pilot tone modulator is a passive component. The 20 Gbit/s is injected into a passive fibre delay multiplexer, multiplexing the signal from 20 to 40 Gbit/s[43]. The 40 Gbit/s data signal is demultiplexed using an Electroabsorption Modulator (EAM) driven by the same synthesiser as the pulse source. By inserting a tuneable time delay between the synthesiser and the EAM, the relative position of the Switching Window to the data signal can be varied. The pilot tone power can be monitored as function of the position of the SW, by injecting the O/E converted demultiplexed signal into an electrical spectrum analyser. In Figure 5.23 the pilot tone power is depicted as function of the relative position of the SW from the centre of one channel to the next, demonstrating a contrast of 18 dB. Comparing with Figure 5.20 this would correspond to a reduction of the SNR from ~ 20 to ~ 2 dB. The contrast is an artefact of the extinction ratio of the switch, i.e. the EAM. The example

[43] With this structure, two out of four channels in the OTDM signal are pilot tone modulated. Due to available equipment, this was the only way to generate a 40 Gbit/s OTDM signal.

illuminates what kind of magnitude the variation of pilot tone power the network should be capable of detecting. As the pilot tone does not carry any information or data, it is believed that the obtained contrast is sufficient for reliable decision, i.e. whether the demultiplexed channel is the pilot tone modulated data signal or not.

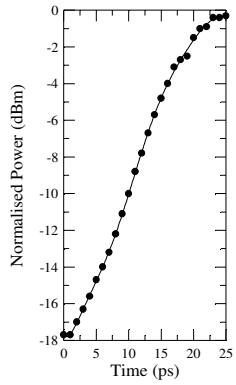

Figure 5.23: Normalised pilot tone power as function relative position of SW to data signal.

In this section, the impact of pilot tone modulation on a data signal has been experimentally evaluated. It has been demonstrated, that a pilot tone modulation introducing sufficient power for detection in a pilot tone detection circuit without introducing unacceptable power penalties, can be obtained.

5.3.6 Discussion of pilot tone scheme

In section 5.3.2 a scheme for channel identification based on pilot tone modulation was proposed, and in section 5.3.5 the impact of pilot tone modulation on system performance was evaluated experimentally and design parameters in terms of frequency and modulation index were proposed.

One of the major advantages of the scheme is the use of relatively low speed electronics, which would limit the costs of the technique, but also limit the technological problems, which can occur when designing high-speed electronic circuits. An additional advantage of the scheme is the limited required SNR of the pilot tone frequency component, as no data is transmitted on the pilot tone frequency.

One apparent drawback, is the cumbersome scanning through the channels, until the pilot tone modulated channel is recognised, followed by the tuning of the time delay until the target channel is demultiplexed. However, the OTDM

network, which the pilot tone scheme is based upon, is a static bit interleaved OTDM system where it is pre-defined which OTDM channel is destined to which node. Consequently, when the target channel has been identified, the pilot tone tracking procedure is not further required, unless the Clock Recovery at the input to the node, looses track of the data signal. Hence, the tracking process is not continuously required.

The principle was demonstrated at 40 Gbit/s but can without any modifications be used in OTDM systems with higher aggregated bit rates.

In order to demonstrate the versatility of the pilot tone scheme, the scheme is proposed implemented in semi static OTDM networks as outlined in section 5.4.

5.4 Uni-directional OTDM ring network

In the previous sections some of proposed functionalities in a bit interleaved OTDM system are proposed, with special focus on the channel identification. A reasonable question now, is whether an OTDM network can be designed based on the techniques in the previous chapters and the architectures for the OADM in preceding sections?

5.4.1 Pilot tone modulation for channel identification

In order to elaborate more on the design of the OADM, an architecture as shown in Figure 5.24 is proposed [5.16]. It is based on a uni-directional ring with 4 nodes. It is assumed that full connectivity is possible, i.e. every node can transmit and receive from all the other nodes as indicated in the figure. The nomenclature A→B is defined as transmission of a channel from node A to node B

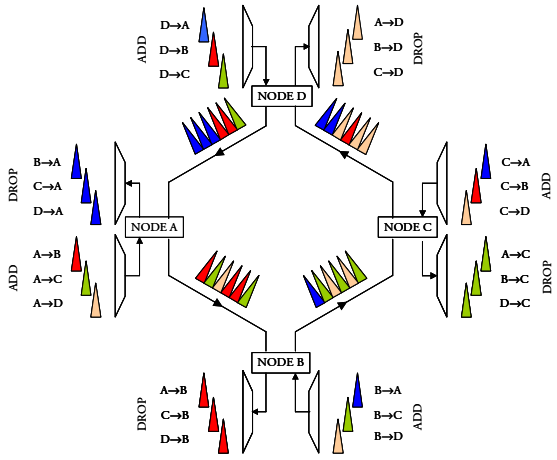

Figure 5.24: OTDM network with full connectivity based on an uni-directional ring with 4 nodes.

From Figure 5.24 an important distinction from Figure 5.5 can be observed. If full connectivity between all nodes is required simultaneously, each OADM need the possibility to add and drop a number of channels consecutively – the minimum number of channels is the total number of nodes in the network subtracted 1. This will either necessitate that the switch can demultiplex the required channels simultaneously or require a number of switches working together. If the latter implementation is required, the switches need to be concatenated, i.e. serial processing in order to ensure that the complementary demultiplexed signal with vacant time slots corresponding to all the channels are available. One approach could be to concatenate the required number of switches, generating the complementary demultiplexed signal by dropping one channel at a time, before adding all the new channels. Another approach would be to drop one channel, add a channel, drop the next channel, followed by the adding of the second channel until all the required processing was completed. Notice, that the proposed Pilot Tone Detector scheme is still valid. The first demultiplexing circuit is used to identify the channel numbers. When this relation is established, the switches are closed, and the Control logic will control the Time delays to the demultiplexing circuits and the Channel Alignment circuits.

An important observation based on these considerations, is how the complexity of the nodes are directly scalable with an increase in the number of nodes. This will in the proposed architecture, in practice invoke a limit on the network size.

Another parameter, which can limit the network size, is the required number of OTDM channels in order to connect all the nodes within the system. With

origin in Figure 5.24, the required number of OTDM channels can be listed as in table 5.1, where the input and output data streams, i.e. the OTDM signal, to each node is listed.

Channel Number	Node A		Node B		Node C		Node D	
	In	Out	In	Out	In	Out	In	Out
1	B→A	A→B	A→B	B→A	B→A	B→A	B→A	B→A
2	C→A	A→C	A→C	A→C	A→C	C→A	C→A	C→A
3	D→A	A→D	A→D	A→D	A→D	A→D	A→D	D→A
4	C→B	C→B	C→B	B→C	B→C	C→B	C→B	C→B
5	D→B	D→B	D→B	B→D	B→D	B→D	B→D	D→B
6	D→C	D→C	D→C	D→C	D→C	C→D	C→D	D→C

Table 5.1: Transmission matrix

In each node, the time slot corresponding to a dropped signal from a specific node, is immediately reused to add a data channel to the same node, ensuring full use of all channels in the bit interleaved signal. In the example only 6 channels are required.

If the number of nodes in the ring is *n*, a general expression for the minimum required OTDM channels N can be derived to

$$N = \sum_{i=1}^{n-1} i = \frac{n(n-1)}{2} \tag{5.10}$$

Based on eq. (5.11) the number of channels as function of the number of nodes in the system can be calculated, see Table 5.2.

Nodes	Channels	Nodes	Channels
		16	120
		17	136
3	3	18	153
4	6	19	171
5	10	20	190
6	15	21	210
7	21	22	231
8	28	23	253
9	36	24	276
10	45	25	300
11	55	26	325
12	66	27	351
13	78	28	378
14	91	29	406
15	105	30	435

Table 5.2: Number of OTDM channels as function of number of nodes

From the table it can be seen how the number of OTDM channels increases dramatically when the number of nodes is increased. For 16 nodes, the minimum number of channels should be 120[44].

The total number of OTDM channels is limited by the total available aggregated OTDM bit rate, which consequently can limit the number of nodes. In Figure 5.25 the aggregated bit rate in the network is shown as function of the number of nodes for a base rate of 2.5, 10 and 40 Gbit/s.

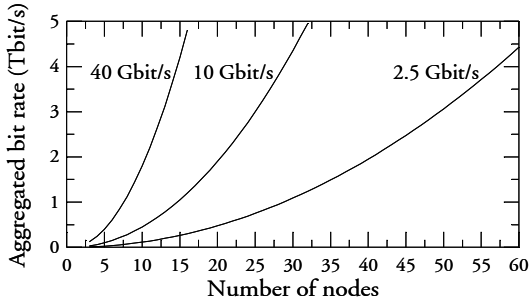

Figure 5.25: Aggregated bit rate in the OTDM network as function of the number of nodes for base rate varied from 2.5, 10 and 40 Gbit/s

[44] Note that this is the minimum of channels, which only allows data corresponding to the base rate of the OTDM signal to be transmitted from one node to another, i.e. the users are homogenous. If the users are heterogeneous and higher capacity is required between two nodes, the number of OTDM channels will need to be increased correspondingly.

From Figure 5.25 the maximum number of nodes in the system can be extracted for various maximum aggregated bit rates. At present, the highest demonstrated aggregated bit rate is 1.28 Tbit/s [5.5], but the future might show even more impressing results, breaking through 2 Tbit/s and beyond. In table 5.3 the maximum nodes for different aggregated bit rates are specified.

Aggregated bit rate (Tbit/s)	Base rate (Gbit/s)		
	2.5	**10**	**40**
1	29	15	8
2	41	21	11
3	50	25	13
4	58	29	15
5	64	33	17

Table: 5.3: Maximum nodes for specified aggregated bit rates

It is observed that a relatively large network including 29 nodes can be designed. However, the data capacity between each node will be limited to 2.5 Gbit/s, which is comparable or even less than existing WDM based networks, and consequently this is not considered advantageous. For 10 and 40 Gbit/s base rate OTDM networks, the number of nodes is limited to 15 and 8, respectively, for an aggregated bit rate of 1 Tbit/s. For a 2 Tbit/s OTDM system, the number of nodes has only increased to 21 and 11 for the 10 and 40 Gbit/s base rate system.

The total aggregated OTDM bit rate is determined by the transmission impairments due to the narrow pulses combined with the performance of each sub-system constituting the OTDM networks, e.g. Clock Recovery circuits, see chapter 3, and switches used for demultiplexing and complementary demultiplexing, see chapter 4. In chapter 2 the requirements to the pulse source in terms of Pulse Tail Extinction Ratio (PTER) were estimated. The results showed how the requirement to the pulse pedestals were increased as the number of OTDM channels was increased. For an aggregated signal composed of 32 channels each carrying 40 Gbit/s the PTER should be higher than 41 dB, which is regarded as strict requirement. Increasing the number of channels further will, under the assumptions established in chapter 2, result in even stricter requirements. The results in [5.5] are based on 128 channels each carrying 10 Gbit/s, and in this experiment polarisation multiplexing have been facilitated in order to reduce the pulse interaction. The upper limit of OTDM channels have not been established, but table 5.2 emphasise the challenges the network designer will face when dimensioning a network in terms of transmitter requirements.

In conclusion the maximum number of nodes in a uni-directional OTDM ring based on full connectivity is relatively small, due to

- Complexity of OADM architecture is increased as the number of nodes is increased.
- An increase in the number of nodes increases the number of OTDM channels, and consequently increases the requirements to the sub-systems constituting the OTDM network, e.g. pulse sources in terms of PTER.
- The maximum available aggregated bit rate within the ring.

If, however, the network designer can accept a limited number of nodes, OTDM networks can offer a huge capacity. As an example, consider a uni-directional ring structure with 8 nodes, which are homogenous, i.e. identical in terms of transmitted and received capacity. The number of required OTDM channels is 28 according to Table 5.2. If the system is based on a 40 Gbit/s base rate, each node should be capable of dropping and adding seven 40 Gbit/s OTDM channels from the 1120 Gbit/s OTDM ring, as shown in Figure 5.26.

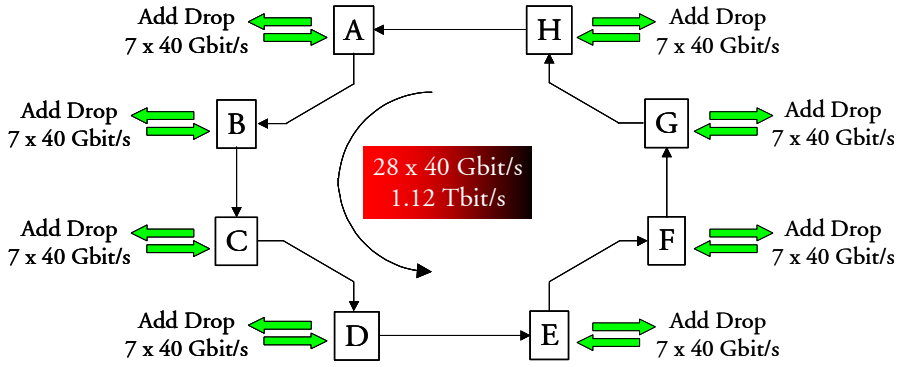

Figure 5.26: OTDM uni-directional ring network of homogenous users

By reducing the number of nodes to 6, the required number of channels is reduced to only 15 thus requiring an aggregated bit rate of 600 Gbit/s. However, by keeping the aggregated bit rate to 1120 Gbit/s, as in the 8 nodes scenario, some of the nodes are allowed to both transmit and receive more traffic than the initial 40 Gbit/s to chosen nodes. As an example, four of the nodes are users with small need for capacity while the remaining two users have a high demand for capacity between each other. By allocating the extra 13 channels, i.e. 28-15, the two nodes have 14 channels in total for data transmission between each other. If the system is based on a 40 Gbit/s base rate,

the network allocates 560 Gbit/s between the two high-end users, as seen in Figure 5.27.

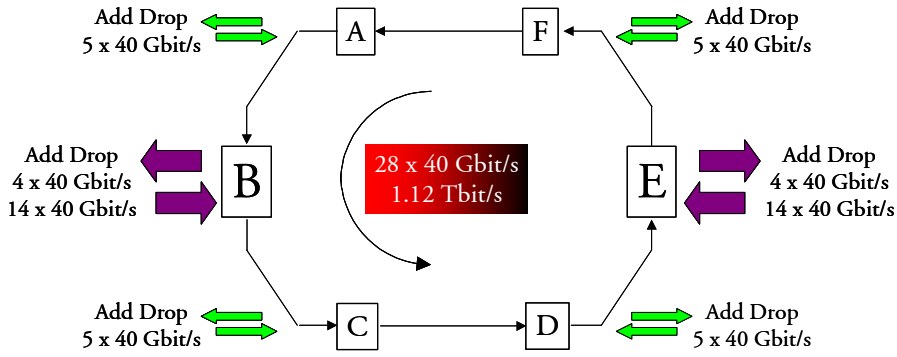

Figure 5.27: OTDM uni-directional ring network of heterogeneous users

The proposed architecture appears to be well suited for high capacity transmission between a limited number of nodes. One application could be the use of the OTDM network to connect a number of e.g. Local Area Networks (LAN) or Metropolitan Area Networks (MAN), using the nodes as the interface between these networks. The actual implementation will not be further commented within this thesis.

It should be emphasised that no general conclusions should be extracted from the example above, as a number of other architectures should be investigated thoroughly. However, the example based on the architecture shown in Figure 5.24 serves as an example to illustrate how advantages and potential problems for OTDM networks should be considered. The example shows how OTDM can be a good candidate for some applications, but it also illustrates that OTDM is not an obvious candidate for a number of other applications, e.g. networks of large number of nodes. Albeit, WDM ring networks with full connectivity also start to be quite complex when the number of nodes is increased beyond 5, see e.g. [5.17].

5.4.2 Routing based on pilot tone scheme

In the previous section, an OTDM network based on a uni-directional ring with full connectivity was suggested. It was argued that the structure appears to be a good choice, if the network consists of a limited number of nodes, and high capacity is required. It was also argued that the network could be dimensioned to allow the users represented by the nodes, to be heterogeneous, i.e. the users were a mixture between high and low bandwidth users.

One important assumption, which has not been addressed previously, but has been implied in the discussions, was the existence of a static data pattern. When dimensioning the network, it has been pre-defined how many channels each node can receive and transmit. A possible consequence of this design is the potential low utilisation of the available bandwidth. If e.g. node B in Figure 5.24 does not have any data to transmit to node D, the specific time channel allocated for transmission between the two nodes will not be used. Even if e.g. node C needs to transmit more data to node D, the system cannot recognise the vacant time channel and exploit it. If the traffic pattern indeed is static, and the data traffic between the different nodes in reality is present at all time, then this will not impose a problem. On the contrary, as the system complexity will be kept to a minimum.

However, can the bit interleaved OTDM network be used if the traffic pattern is dynamically changing? The bit interleaved OTDM approach described in the previous chapters and sections, does not immediately offer this functionality. By modifying the proposed pilot tone scheme, an OTDM system making dynamical routing feasible, can be sketched.

In Figure 5.24 the transmission between specific nodes where allocated to assigned bit slots in the OTDM system. Using the pilot tone scheme, each node is instead assigned a specific pilot tone. This is illustrated in Figure 5.28, where the example with four nodes shown in Figure 5.24 is modified, adopting the pilot tone modulation.

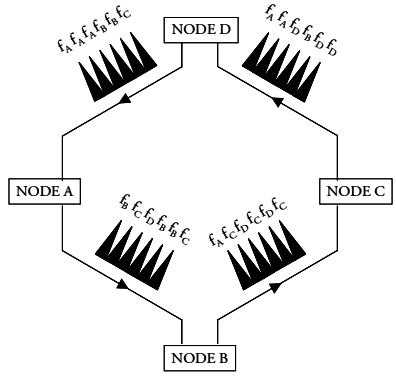

Figure 5.28: OTDM ring network based on uni-directional ring, with pilot tone identification.

In the example node A e.g. is assigned a low frequent pilot tone f_A, node B is assigned f_B etc. If an OTDM channel is modulated with this frequency, the

Channel Identification Circuit within node A, will recognise this channel and ensure that the channel is dropped. With this approach, it is possible to utilise the available bandwidth more efficiently, as any node can transmit data if the time slot are empty. The OADM node structure will certainly increase in complexity as more functionalities are required. In Figure 5.29 a proposed modified OADM structure is outlined.

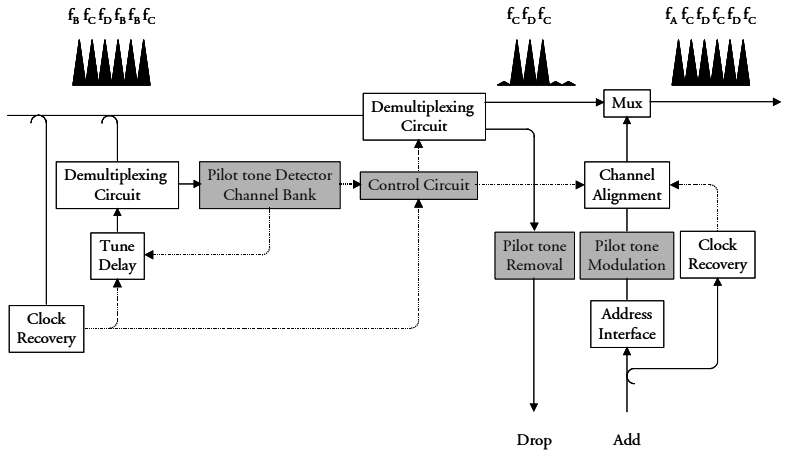

Figure 5.29: Proposed structure of an OADM allowing for dynamical allocation of the channels, based on the pilot tone scheme.

One of the main modifications compared to Figure 5.24 is the separate demultiplexing circuit used for the Pilot Tone Detector. As the destination of the OTDM channels potentially are changing dynamically, it is required to monitor the OTDM channels continuously. The tuneable delay, controlled by the Clock Recovery and the Pilot Tone Detector Circuit, is varied, enabling the demultiplexing circuit to scan through all the channels. A Channel Bank stores the information regarding the addresses of the OTDM channels and if any of the channels are vacant (e.g. no pilot tone present). The information is used to control the switch where the actual demultiplexed channels are dropped. Notice, that the actual implementation of the switch can consist of several components as discussed previously. The dropped channels are pilot tone modulated, so before routing the signal further to another network, the modulation should be removed. Pilot tone removal has been demonstrated previously [5.18] using electrically modulation of a Semiconductor Optical Amplifier. Before the new channels can be added to the OTDM signal, it is essential to extract the destination node. This information is assumed to be embedded in each data signal, which constitute the add channels. An Address Interface extracts the target node address, and ensures that each add channel is

modulated with the appropriate pilot tone frequency before they are added to the complementary demultiplexed signal, as explained previously. Please note that pilot tone modulation will consist of parallel modulators, allowing for adding several channels to the OTDM signal.

The proposed scheme in Figure 5.29 emphasises how the complexity is significantly increased for each new required functionality. However, it also demonstrates that a network topology can be designed using the developed optical technologies explained in this and former chapters. The control circuits will be electronic boards, which maximally should be operated at frequencies corresponding to the base rate of the OTDM signal. The actual allocation of vacant time slots in each node, allowing for dynamically changing the traffic pattern, has not been addressed in the above. This is partly related to the maximum number of channels, which can be added and dropped in a node - the more channels, the more flexibility. However, the more channels, the more complex the demultiplexing circuit including the switches will be, combined with an increase in the price per node, as the number of sub-systems and components will scale with channel number. A trade off between price and functionality will be required. Furthermore, when designing a network where the traffic is not static determined as in Figure 5.4 there are a number of requirements to the topology [5.19]:

- The network should provide a guaranteed bandwidth (GBW) to all the users.
- It should offer bandwidth on demand (BOD) if some users require more bandwidth
- It should use the network resources in an efficient matter and ensure a fair distribution of the bandwidth between all the users.

The proposed architecture is a sketch of how to implement dynamic routing based on bit interleaved OTDM. The scheme can optically be implemented with existing sub-systems presented in this and former chapters. However, it is indispensable to develop an appropriate protocol for the network, before such systems can be implemented.

In this section it has been demonstrated how the bit interleaved OTDM system can be expanded to include a number of nodes by introducing add drop multiplexing. Some of the required functionalities have been explained, with special focus on channel identification. An example of an OTDM network based on a uni-directional ring has been used to expose some of the potential challenges a network designer could encounter when dimensioning an OTDM network. In the proposed structure, it is shown how the number of nodes in the system will be limited. A scheme for channel identification has been proposed

and evaluated experimentally. The introduced power penalty due to the increase complexity and the deterioration of the data signals can be reduced to less than 1 dB of power penalty. The pilot tone scheme can be used to allow for dynamical changes in the traffic pattern. Some of the needed functionalities within the node have been suggested. Advantages and disadvantages have been clarified and future work with special focus on the development of the protocol has been outlined.

The restriction in number of nodes and the limited ways of changing the destination of the OTDM channels using bit interleaved OTDM, have encouraged a few groups in the world to address other network implementations based on OTDM technology. Instead of bit interleaving a number of bit streams, the groups have been investigating the OTDM technology implemented in packet switched networks. The thesis will give a short survey of the present state of the reported work.

5.5 Packet switched OTDM networks

5.5.1 Introduction

Looking at the configuration in Figure 5.1, showing the basic OTDM bit interleaved system, and the suggested modified systems in Figure 5.4 where the system includes a number of Add-drop nodes and finally in Figure 5.24 and 5.28 where the network has been further modified allowing for the unique identification of the channel number, one important observation can be done. The bit interleaved OTDM system is primarily used as data pipelines, i.e. systems where huge amounts of data can be transferred from one node to a few nodes, with a limited possibility of accommodate for dynamical changes in the different traffic patterns.

It can be argued that bit interleaving OTDM systems, including the outlined possibility for routing, can be characterised as a circuit switched network, as the connection, i.e. light paths, between the nodes are maintained until all data has been transmitted. As opposed to circuit switching, there exist another technique, which is more efficient in terms of utilisation of the bandwidth, i.e. packet switched network [5.20], which enables dynamic routing of the data. In packet switched network each transmitter generates packets, which consist of header with the address information of the receiver, and a payload containing the data for the receiver.

In Figure 5.30 the uni-directional ring with four nodes has been modified to accommodate for the packet topology. The figure shows how a packet can be composed by a payload with a bit rate corresponding to the high-speed OTDM

bit rate, and a header, which can have a reduced bit rate and another modulation format if required. In the figure, each packet are separated by a guard-band in order to ensure that the target node has time to process the packet, i.e. drop the packet, before it needs to check the next packet.

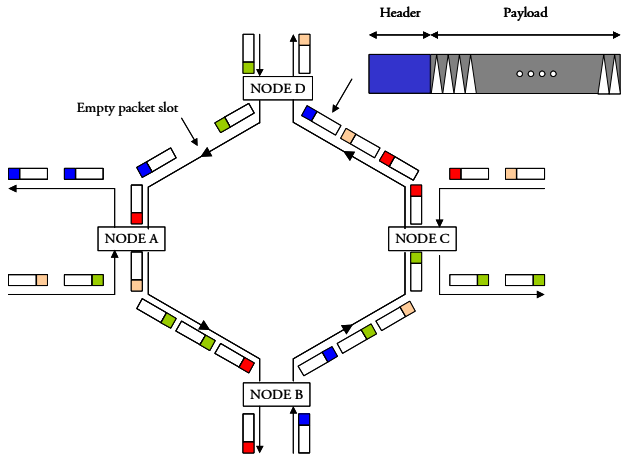

Figure 5.30: Uni-directional ring based on packet switching.

If the OTDM technology has to be used in a packet switched network environment, it needs to be modified, as previously stated, in order to accommodate for the requirements that dynamic traffic patterns introduce [5.19] in terms of GBW, BOD and efficiency, see section 5.4.2.

How to design a packet switched network based on the OTDM technique is beyond the scope of this thesis, as a full network design addressing all the topics covering from the physical layer including designing subsystems with specific functionalities, to protocols and management of the network, is challenging. A good introduction to design of optical networks is given in [5.20], including a small survey of some of the work presented by a few groups in the world.

An important question when reading this thesis and considering the packet switched network, is whether the techniques in the previous chapters developed for bit interleaved OTDM are sufficiently versatile to be applied to packet switched network, e.g. by modifying the existing designs?

5.5.2 Required functionalities

In order to answer this question, an example extracted from [5.21], which is not included in the survey of [5.20], is shortly presented, focusing on the required optical functionalities in the network. A group at the Institute of

Communication Networks at Vienna University of Technology, has investigated, how a packet based OTDM system can be designed and implemented. The principle is based on a high speed OTDM backbone structure, connecting a number of nodes constituting the network. The data transmitted on the OTDM link is based on packets, each packet divided into a header and a high-speed payload. Each node includes a packet compression stage, which ensures that incoming packets from low speed networks are sufficiently compressed allowing the packets to occupy a reduced bandwidth at the OTDM backbone. A decompression stage serves as a reverse interface, as it decreases the bit rate sufficiently for the low speed network. This scheme is labelled Optical Packet Compression Time Division Multiplexing (OPC-TDM), and can be found in e.g. [5.22], [5.23] or [5.21]. In Figure 5.31, a simplified access node is shown based on [5.21].

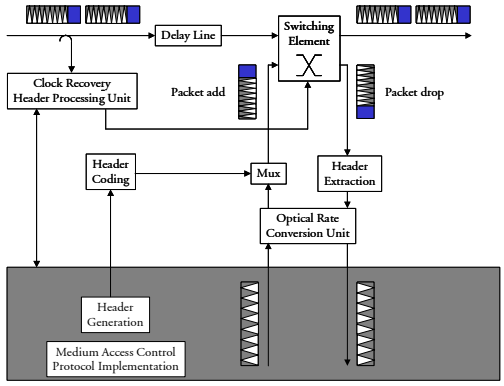

Figure 5.31: Access node in Optical Packet Compression Time Division Multiplexed system, based on [5.21].

In Figure 5.31 the incoming data to each node consist of a header and a payload. The bit rate of the header is not necessarily equal to the high-speed bit rate of the payload, but can be at lower bit rates, in order to simplify the address extraction. In each access node within the network, a coupler is used to tap the packets into a clock recovery circuit and a header-processing unit. As the header-processing unit is not extracting the destination address of the packet instantaneously, i.e. header processing latency, the packet at the other coupler output is delayed before it enters the optical switch. If the packet is destined for this specific node, the clock recovery and the header-processing unit will apply a control signal to the switch, which enables the switch to drop the packet. As the information in the header is obsolete after the packet has been dropped in the node, the payload and the header are separated in the header extraction circuit. The high-speed payload is expanded to lower bit rates, using a packet decompression circuit, in order to allow e.g. electronic

processing. To add a low speed packet to the high-speed OTDM backbone, first the packet is compressed using the optical rate conversion unit, which essentially compresses the packet in time. The Media Access Control (MAC) unit generates the header address, applies the address to the header-coding unit, where the optical header is modulated before the header is multiplexed together with the compressed packet. The full packet, i.e. header and payload, is injected into the switch, which ensures that the packet is situated on the OTDM backbone.

From this simplified description of the access node, a number of optical functionalities have been introduced.

- Clock Recovery
- Optical switch
- Time delay
- Header extraction
- Optical bit rate conversion units
- Header coding

Some of the functionalities have been addressed previously in this thesis, and will consequently briefly be examined within the context of packet switched networks. Other functionalities, such as the optical switch and the header coding will not be further addressed. Finally, some of the key functionalities, which are dispensable in bit interleaved OTDM, but not for the proposed packet switched OTDM network are shortly reviewed, as they represent some exiting new features, adding to the versatility of OTDM.

Clock Recovery

In chapter 3, clock recovery circuits have been investigated, with focus on clock extraction using Optical Phase Detection implemented in a Phase Locked Loop design. The theory and the results are based on bit interleaved OTDM data signals, and the question is if the presented implementations can be used for packet switched networks? First of all, the clock circuits developed in chapter 3 extracted a pre-scaled clock corresponding to the base rate of the OTDM signal. In Figure 5.31, the clock is used to read information in the header, which is not necessarily equal to the bit rate of the high-speed payload or the base rate of the OTDM signal. Furthermore, the clock is used to control the switching element, which most probably only needs a limited number of control signals in order to ensure a packet to be dropped. These two observations suggest that modifications are required, if the OPD based PLL clock recovery circuit should be used for the packet switched network. However, the actual modifications cannot be proposed in this thesis, as a number of parameters related to the

network are not defined in the proposed topology. Some of the unspecified issues, which influences the possible modifications are listed below

- Is the OTDM backbone based on synchronous or asynchronous packet arrival
- How many bits do the payload and the header contain and is the payload variable length?
- How fast is it expected that the Clock Recovery circuit should lock to the incoming packet, i.e. magnitude of the lock-in time of the Clock Recovery?
- A related question is how many skipped bits are acceptable before the Clock Recovery have locked to the packet?
- What is the maximum time between packet arrivals?
- What is the maximum number of consecutive zeros within a packet?
- What is the minimum time between each packet, i.e. guard band?
- What is the bit rate of the header and the payload?

These questions need to be answered before a possible OPD based PLL can be designed, and before the question addressing feasibility can be answered.

A few groups have proposed schemes, developed in order to accommodate packet switched networks, by generating distinct control signals in the node when a packet arrives to the node. One example of this is the configuration reported in [5.8]. The first bit of the packet, defined as the marker bit, has an increased peak power compared to the other bits in the packet. By injecting the packet into a threshold device, the marker bit can be extracted and this bit or pulse is the signal, which announces the arrival of a packet to the node. Another scheme is reported in [5.24], where the gain response of a SOA is used to distinct the first bit of the packet from the consecutive bits. These two examples can be used to synchronise the optical switch, and drop the packets. However, the schemes apparently do not offer the possibility of extracting the required clock, and the schemes should consequently be implemented in parallel with clock extraction circuits.

Time delays

Time delays are important in bit interleaved and in the proposed packet switched networks. In the bit interleaved OTDM systems, see section 5.2, the time delays are primarily used to tune the clock, which introduces the Switching Window in the switch, in order to ensure that the correct OTDM channel is dropped in the node. In packet switched networks the necessity of time delays is introduced due to the header processing latency. However, depending on the actual implementation of the topology of the network, possible conflicts between packets on the OTDM backbone and packets, which

should be added, can be foreseen. In this situation buffers are required [5.20]. The time delays or buffers in the packet switched network should be capable of storing full packets, which can consist of a large number of bits – in [5.25] packets sizes between 10 to 100 kbits are envisaged, which in a 640 Gbit/s OTDM backbone system would correspond to time delays in the order of 15 to 150 ns. This is opposed to the tuneable time delays in bit interleaved OTDM systems, in which the maximum tuning range in time is equal to the frame time of the OTDM signal, i.e. the base rate time slot, which equals 25 or 100 ps if the base rate is 40 or 10 Gbit/s. The time delays referred to in section 5.2.1 cannot be expected to offer delays in the magnitude of several ns. Instead, buffers based on optical fibres incorporated in loops, can be used as the delay, by exploiting the transmission delay in fibres. In [5.26] a 9 kbit packet, with an aggregated bit rate of 80 Gbit/s was stored for 30 seconds, demonstrating the potential of this technique. As the delays are related to the roundtrips within the loop, this particular buffer inherently only offers fixed delays, which can be a drawback due to the limited tuneability.

Optical bit rate conversion units

One of the key functionalities in the proposed topology is the optical bit rate conversion units, which compress the packets to the high-speed OTDM bit rate of the backbone or decompress packets dropped in the node, to bit rates which can be handled by e.g. electronics. A short introduction to two of the techniques reported in literature is presented below.

In [5.27] and [5.28] a compression scheme based on a fibre loop is presented. An input packet with bits separated T_{in} in time, is via a 2x2 switch injected into a fibre loop. The length of the fibre is carefully adjusted so the propagation time within the loop, ensures that when the first bit has propagated through the entire loop, and the second bit is injected into the loop, the two bits will be separated T_{out} in time. Using this technique, the entire packet can be compressed. As a number of only partly compressed packets will continuously be available at the output of the 2x2 switch, an additional switch is used to guarantee that only the fully compressed packet is switched into the succeeding system.

The scheme presented in [5.27] and [5.28] is simple and elegant. However, a few remarks should be addressed to the technique. The switch at the output of the loop, needs to introduce a Switching Window, which is very well defined, with steep leading and falling edges defined by the minimum separation in time between the partly compressed packets and furthermore a good extinction ratio of the switching, in order to ensure an acceptable quality of the compressed packet. If this is not obtained, the compressed packet can introduce impairments in the other packets, when it is added to the OTDM backbone.

The need of a high quality switch reveals that although no switch is included in the packet switched OTDM network in Figure 5.31, the technique is still included on a subsystem level. The techniques presented in chapter 4, should in this case be modified in order to accommodate for the requirements of this specific implementation.

One required functionality, which is not addressed in [5.27] and [5.28], is the synchronisation between in the incoming packets and the switch at the output of the loop in order to make certain that the compressed packet is switched correctly into the subsequent system.

A drawback of the technique is the asymmetric accumulation of losses in the loop. By injecting a packet of N bits into the loop, the first bit will propagate N times in the loop and the last bit will propagate 1 time in the loop, introducing a variation in peak amplitude of the bits due to the losses in the fibres. If the fibre loop is used both as compression and decompression stage, this skew in amplitude is levelled out [5.29]. However, the impact on transmission properties on the OTDM backbone of packets composed of bits with different amplitude should be addressed, before it can be concluded if the scheme indeed can be implemented.

Another scheme is presented in [5.30], where the compression of the packets are introduced by injecting the packet into a structure similar to the laboratory multiplexer. The packet is injected into the device and split into two branches. The packet will propagate through the two arms, before the two signals are merged together. If the time separation between the bits in the uncompressed packet is T_{in} and the target separation between the bits after full compression is T_{out}, the relative time delay between the two arms should be $(T_{in}- T_{out})$. By adding additional stages, implemented similarly to the first stage, with an increment in the relative time delay between the two arms corresponding to $2(T_{in}- T_{out})$, $4(T_{in}- T_{out})$ etc, a compressed packet can be obtained at the output of the concatenated stages. The structure is referred to as a delay line lattice, and by injecting a N bit packet into $q = \log_2(N)$ concatenated stages, a compressed packet is generated at the output of the lattice. Like the optical rate conversion unit based on optical fibre loop, several incomplete compressed packets are available at the output of the lattice, and a switch is used to ensure that the correct compressed packet is passed into the subsequent system. The lattice can be used bi-directionally, and in this case the lattice would also act as a decompression stage. Also for the time delay lattice, the synchronisation of the switch is an issue. As opposed to the previous technique, all the bits will propagate through the same number of couplers and will consequently experience an identical reduction in peak power.

A concern initiated by the suggested techniques, is the number of bits in the packet, which can be compressed. If the packet has a length of e.g. 65.536 bits, the number of stages required would be q = 16, corresponding to a 48 dB decrease in peak power of all the bits. If this is not acceptable, a structure based on a number of parallel lattices has been suggested [5.31]. It should be noticed that the structure in [5.31] presents a significant increase in complexity as it introduces a number of additional gates, which would require very accurate synchronisation.

Header extraction unit

A header extraction unit separates the header and the payload. If a switch can be designed for the optical rate conversion unit, the same device can perform the required demultiplexing of the payload. The edges of the Switching Window should be sufficiently steep, in order to suppress the impact of the header.

Additional sub-systems and required functionalities.

It should noticed, that the pulse source requirements extracted in chapter 2 should be fulfilled for the pulses constituting the payload. The actual requirements depend on the bit rate of the payload.

5.5.3 Summary of packet switched OTDM networks

In this section a short survey of the reported work in packet switched network based on the OTDM scheme. It has been shown how a number of the existing OTDM functionalities described in the previous chapters can be modified to accommodate for packet transmission. A number of groups have reported different approaches for implementing the systems and taking starting point in one specific suggested implementation, the functionality is explained. The suggested topologies demonstrate that the OTDM scheme can in principle be implemented based on the existing developed sub-systems. However, a number of issues, as observed in this section still need to be addressed, before a full demonstration can be tested.

5.6 Conclusion

In this chapter the bit interleaved OTDM point-to-point system is proposed expanded to include several nodes in a network. In the nodes, specific OTDM channels need to be dropped and new data channels need to be added into the vacant time slots. Some of the sub-systems required to enable this performance are listed with special focus on channel identification. Channel identification is

an indispensable functionality within a node, and a short summary of previous reported channel identification schemes is presented. A novel channel identification technique is suggested based on pilot tone modulating one of the OTDM channels. The pilot tone modulation scheme is explained in detail and a numerical example shows its potential. Finally the scheme is characterised in an experimental demonstration at 40 Gbit/s but is believed to be applicable to higher bit rates without any further modifications. The scheme is based on relatively low-speed electronics, which should keep the costs to an acceptable level. A uni-directional OTDM ring network is suggested incorporating the pilot tone scheme for channel identification. The dimensioning of the system in terms of capacity and number of nodes is presented. As the ring network is based on a static traffic pattern with no means to accommodate for dynamic changes, a modification is briefly outlined. This is based on pilot tone modulation of each individual OTDM channel, where the pilot tone frequency refers to the address of a specific node. The example emphasise how the complexity is increased for more advanced network structures. Finally, a short introduction to the work of the few other groups in the world, which have addressed OTDM in packet switched networks, is given.

5.7 References to chapter 5

[5.1] K. S. Jepsen, Ph.D. Thesis, "High-speed Optical Signal Processing for High Capacity Optical Networks", Technical University of Denmark, Department of Electromagnetic Systems, Kongens Lyngby, DK-2800, Denmark (1999).

[5.2] A. T. Clausen, K. S. Jepsen, A. Buxens, B. Mikkelsen, K. E. Stubkjaer: "Interface for 10 Gbit/s bit-synchronisation and format and wavelength conversion with 3R capabilities", Electronics Letters, Vol. 34, No. 16, pp. 1554-1555 (1998).

[5.3] K-L. Deng, K. I. Kang, I. Glesk, P. Prucnal, "A 1024-channel fast tunable delay line for ultrafast all-optical TDM networks", IEEE Photonics Technology Letters, Vol. 9, No. 11, pp. 1496-1498 (1997).

[5.4] X. Lei, Y. Minyu, C. Minghua, Z. Jianfeng, C. Zingzhong, G. Yizhi and C. Chen, "All Optical Frame Clock Extraction with polarization Flag in OTDM system", Technical Digest of 5th Asia Pacific Conference on communications/4th Optoelectronics and Communications Conference (APCC/OECC'99), Beijing, China, Vol. 1, pp. 363-363 (1999).

[5.5] M. Nakazawa, T. Yamamoto, K.R. Tamura, "1.28Tb/s - 70 km OTDM transmission using third- and fourth-order simultaneous dispersion compensation with a phase modulator", Electronics Letters, Vol. 36, No. 24, pp. 2027-2029 (2000).

[5.6] A. I. Siahlo, A. T. Clausen, L. K. Oxenløwe, J. Seoane, P. Jeppesen, "640 Gb/s OTDM Transmission and Demultiplexing using a NOLM with Commercially Available Highly Non-linear Fiber", Technical Digest of Conference on Lasers & Electro-Optics (CLEO 2005), Baltimore, Maryland, USA, paper CTuO1 (2005) (Invited).

[5.7] Z. Xiang, P. Ye, K. J. Guan and J. L. Lin, "Theoretical analysis of an OTDM frame synchronisation scheme", Optics Communications, Vol. 154, No. 1-3, pp. 19-22 (1998).

[5.8] K. L. Deng, I. Glesk, K. I. Kang and P. R. Prucnal, "Unbalanced TOAD for Optical Data and Clock Separation in Self-Clocked Transparent OTDM Networks", IEEE Photonics Technology Letters, Vol. 9, No. 6, pp. 830-832 (1997).

[5.9] B. Li and P. Ye, "OTDM frame synchronization and channel recognition method based on alignment signal with BPSK modulation", Proceedings of Optical Fibre Conference (OFC'98), paper WM35 (1998).

[5.10] A. T. Clausen, J. Bennike, L.K. Oxenløwe, J. Seoane, A.I. Siahlo and P. Jeppesen, "Pilot tone modulation used for channel identification in OTDM networks", Proceedings of Conference on Lasers & Electro-Optics (CLEO'04), San Francisco, California, USA, paper CThQ7 (2004).

[5.11] A. B. Carlson, "Communication systems – An introduction to Signals and Noise in Electrical Communication", McGraw-Hill International Editions, New York, USA (1986).

[5.12] M Murakami, T. Imai and M. Aoyama, "A remote supervisory System based on subcarrier overmodulation for submarine optical amplifier systems", Journal of Lightwave Technology, Vol. 14, No. 5, pp. 671-677 (1996).

[5.13] G. P. Agrawal, "Fiber-Optic Communication Systems", John Wiley & Sons, Inc., Second edition, United States of America (1997).

[5.14] S. O. Rice, “Statistical properties of a Sine Wave Plus Random Noise”, Bell System Technology Journal, Vol. 27, No. 1, pp. 109-157 (1948).

[5.15] F. Heismann, M. T. Fatehi, S. K. Korotky and J. J. Veselka, “Signal Tracking and performance monitoring in multi-wavelength optical networks”, Proceedings of European Conference on Optical Communication (ECOC’96), paper WeB.2.2 (1996).

[5.16] A. T. Clausen, L. K. Oxenløwe, A. Siahlo, J. Seoane and P. Jeppesen, "Expansion of Point-to-Point OTDM Systems to a Ring Network", Proceedings of the 30th European Conference on Optical Communication (ECOC'04), Stockholm, Sweden, paper Th2.6.3 (2004).

[5.17] A. Buxéns Azcoaga, Ph.D. thesis “40 Gb/s Optical Transmission Systems”, Technical University of Denmark, Department of Department of Communications, Optics and Materials (COM), Kongens Lyngby, DK-2800, Denmark (2003).

[5.18] A. Klock, S. L. Danielsen, B. Mikkelsen, K. E. Stubkjaer, M. Schilling, K. Wünstel, W. Idler, “Pilot Tones in Networks with nonlinear elements”, IEEE Photonics Technology Letters, Vol. 10, No. 3, pp. 448-450 (1998).

[5.19] R. Barry, V. Chan, K. L. Hall, E. Kintzer, J.D. Moore, K. A. Rauschenbach, H. Hauss, E. Ippen, W. Wong and M. Haner, “All-optical network consortium – Ultrafast TDM Networks”, IEEE Journal of Selected Areas in Communications, Vol. 14, No. 5, pp. 999-1013 (1996).

[5.20] R. Ramaswami, K. N. Sivarajan, “Optical Networks – a practical perspective”, Academic press, Second edition, United Kingdom (2002).

[5.21] S. Aleksic, “Packet-switched OTDM networks employing the packet compression/expansion technique”, Photonic Network Communications, Vol. 3, No. 1/2, pp. 273-288 (2003).

[5.22] S. Aleksic, K. Bengi, V. Kjajinovic, ”OPC-TDM network performance improvement by the use of full-scalable optical packet compression/decompression units”, Proceedings of the 5th Working Conference on Optical Network Design and Modelling (ONDM 2001), pp. 263-273 (2001).

[5.23] S. Aleksic, "An ultra-fast photonic ring network employing Optical Packet Compression – Time Division Multiplexing (OPC-TDM) scheme, Electrical Engineering, Vol. 83, No. 4, pp. 223-229 (2001).

[5.24] Z. Yongpeng, Y. Peida, "Simple self synchronization scheme for OTDM packet networks", Proceedings of 15th Annual Meeting of the IEEE Lasers and Electro-Optics Society (LEOS 2002), Glasgow, Scotland, paper WA3 (2002).

[5.25] J. D. Moores, J. Korn, K. L. Hall, S. G. Finn and K. A. Rauschenbach, "Ultrafast Optical TDM Networking: Extension to the Wide Area", IEICE Trans. Electron, Vol. E82-C, No. 2, pp. 157-169 (1999).

[5.26] J. Moores, "80 Gbit/s 9kbit optical pulse storage loop", Technical Digest of Optical Fibre Conference 1997 (OFC'97), paper TuQ3 (1997).

[5.27] H. Toda, F. Nakada, M. Suzuki, A. Hasegawa, "An optical packet compressor based on a fiber delay loop", IEEE Photonics Technology Letters, Vol. 12, No. 6, pp. 708-710 (2000).

[5.28] H. Toda, F. Nakada, M. Suzuki, A. Hasegawa, "An optical packet compressor using a fibre loop for a feasible all optical TDM network", Proceedings of 25th European Conference on Optical Communication (ECOC'99), paper C3.6 (1999).

[5.29] A. S. Acampora, S. I. A. Shah, "A packet compression/decompression approach for very high speed optical networks", Proceedings of Telecommunications Symposium, paper 2.5.1 (1990).

[5.30] P. Toliver, K-L. Deng, I. Glesk, P. R. Prucnal, "Simultaneous optical compression and decompression of 100 Gb/s OTDM packets using a single bidirectional optical delay line lattice", IEEE Photonics Technology Letters, Vol. 11, No. 9, pp. 1183-1185 (1999).

[5.31] S. Aleksic, V. Krajinovic, K. Bengi, "A novel scalable optical packet compression/decompression scheme", Proceedings of European Conference of Optical Communication (ECOC'01), Amsterdam, paper WeP51 (2001).

Chapter 6
Summary and discussion

Internet traffic is growing and is expected to continuously grow in the future partly due to new broadband services and partly due to new users. Analysis indicates that the existing capacity will soon be exploited 100 % when upgrading the networks with existing communication systems, even when assuming a reasonable increase of the capacity with additional 20 % per year. Thus, lack of capacity can impose limitations on the traffic. It is important to focus on techniques, which can increase the capacity on the existing installed optical infrastructure, and OTDM is one out of several options. This thesis has focussed on bit interleaved OTDM systems, both point-to-point systems and partially OTDM networks.

A bit interleaved point-to-point OTDM system can be split into several sub-systems, each performing required specific functionalities enabling the system to operate error-free. In this thesis three subsystems have been addressed, i.e. the pulse source, the clock recovery and the switch used for demultiplexing.

In chapter 2 the requirements to the pulse source were discussed by extracting a number of characterisation parameters, which are important when implementing the sources in an OTDM system. Due to the shape of the Return-to-Zero pulses emitted from the pulse source, part of the pulse tails will overlap the neighbouring channels. Presented theory showed that both the power of the tails and the interferometric beating between the data signal in the OTDM timeslot and the pulse tails can corrupt data detection. A detailed simulation model was implemented in order to extract requirements for both the temporal FWHM width and the PTER. The results showed that a FWHM width of approximately 0.4 times the OTDM timeslot is optimum irrespective of the aggregated OTDM bit rate. The requirements to the PTER are very strict, with PTER increasing from 27, 33, 37 to 41 dB for bit rates of 160, 320,

640 and 1280 Gbit/s, respectively. Finally, a short introduction to pulse source characterisation tools was given.

Chapter 3 was devoted to the Clock Recovery sub-system. Standard Phase Locked Loop theory was modified to allow clock extraction from a high-speed OTDM signal, which does not include a distinct component at the base rate frequency. Four different OTDM clock recovery schemes were examined and compared theoretically before one specific design was chosen. The chosen design was based on a dynamic compensation of the inherent DC component of the PLL control signal, which does not include any phase information. Based on the modified PLL theory, means to optimise the performance of the Clock Recovery was outlined, by deriving the optimum temporal FWHM width of the switch used for optical phase detection. Because optical Clock Recovery systems often include substantial length of fibres due to the utilised components, the impact of time delays in the PLL on the stability was addressed using a simple model based on Bode plots. An example was presented to demonstrate how the acceptable bandwidth of the PLL is reduced significantly for even a few meters of fibre. Finally, the theoretical results were used to analyse the results from a Clock Recovery experiment extracting a 10 GHz clock from a 160 Gbit/s OTDM signal, confirming agreement between theory and experiments.

Demultiplexing of the tributary channels was addressed in chapter 4. Because no switches presently can demultiplex all channels simultaneously, an array of switches is required. A short discussion of different switch array topologies, i.e. serial, tree and parallel structures was presented before the advantages and disadvantages were summarised. The preferred structure largely depends on the specific switch used in the system. In this thesis the parallel structure was preferred because it allows evaluation of the OTDM system using only one single switch as opposed to tree and serial structure. A summary of switches used successfully in ultra-high speed systems was presented. A simple simulation model was implemented in order to evaluate the impact of the temporal FWHM width of the SW, ER of the SW, the SW shape and timing jitter. All these parameters are completely detached from any physical process, and can consequently be changed to any value irrespective of any physical process allows this or not. For Gaussian shaped SW the ER should be above 20 dB and the width should optimally be 0.70 times the OTDM timeslot. For Super Gaussian (order m = 5) the ER is more relaxed leading to acceptable results when ER exceeds 15 dB. The temporal FWHM width should be approximately equal to the timeslot. Theory for a simple Non-linear Optical Loop Mirror (NOLM) was presented and implemented in the simple simulation tool, enabling design rules for the power splitting ratio of the input coupler, the induced phase changes due to the counter propagating data and to the temporal FWHM width of the SW of the control pulse. Finally, a 320 to 10

Gbit/s demultiplexing experiment using a NOLM constructed by 500 m Highly Non Linear Fibre (HNLF) was presented. Because the fibre exhibits low dispersion slope, no special wavelength management was used to avoid walk-off between control and data pulses. All 32 channels were demultiplexed error-free.

Finally in chapter 5 the point-to-point system was expanded to include more nodes thus enabling network structures. Some of the nodes need to support dropping and adding of OTDM channels. This is achieved by first demultiplexing the target channel destined for the node and route it towards its destination. Secondly, by generating the complementary demultiplexed signal, which is the original OTDM signal with a vacant time slot in the timeslot corresponding to the target channel. Finally, by adding the new channel into the vacant timeslot the full add-drop process is completed. In the thesis a suggested add-drop node structure was sketched emphasising the additional functionalities, which are new compared to point-to-point systems. One indispensable function is Channel Identification, which ensures certainty that the dropped channel indeed is the target channel for the specific node. Only a few groups in the world have addressed Channel Identification, and the schemes were summarised before a novel technique based on pilot tone modulation of one of the OTDM channels was suggested. The scheme is attractive because it is based on low-speed electronics and thus should keep the costs and complexity to an acceptable level. A numerical example demonstrates the impact of pilot tone modulation on the system performance and design parameters were extracted. An experimental 40 Gbit/s demonstration is presented confirming that an easy traceable pilot tone can be imposed on an OTDM channel without deteriorating the signal unacceptably. Assuming the existence of Channel Identification functionalities, an OTDM ring network was suggested and designed in order to clarify how OTDM can perform in network structures. The total number of nodes is determined by the total number of OTDM channels, which are correlated to the base rate and the total aggregated OTDM bit rate. The maximum OTDM bit rate is limited by constraints imposed by the transmission span and the sub-systems constituting the OTDM system such as e.g. the pulse source. Finally a short introduction to packet switched OTDM networks reported by other groups was given, emphasising some of the difficulties still remaining unsolved.

Some of the work presented in this thesis has been focusing on deriving and presenting some of the required design rules enabling optimum performance of OTDM bit interleaved systems. By utilising the results presented in the previous chapters it should be possible to both improve the performance of OTDM systems at bit rates already demonstrated at e.g. 320 and 640 Gbit/s but the results from this thesis should also serve as tools for enabling single polarisation OTDM point-to-point systems breaking the record at 640 Gbit/s.

One important question, which has not been addressed in this thesis, is however, what are the future challenges for OTDM?

As 640 Gbit/s single polarisation OTDM systems have been demonstrated by several groups in the world and additionally 1280 Gbit/s using alternate polarisation has successfully been evaluated, it seems likely that 1280 Gbit/s on a single polarisation indeed is feasible and should be one of the goals in the near future for OTDM researchers around the world. Thus, part of future OTDM research should aim on continuously increasing the total aggregated bit rate both by optimising already existing subsystems and by utilising new schemes e.g. using newly discovered physical processes allowing high-speed signal processing.

One topic faced in future OTDM research, which has not been addressed in the existing literature, is to determine what is the ultimate aggregated bit rate both theoretically and practically. For the bit rates demonstrated hitherto experiments in the laboratories have indicated that error-free operation is achievable by simply optimising the existing components constituting the OTDM system. It would nevertheless be expected that at some point, a fundamental physical restriction would limit the maximum achievable bit rate. Which physical mechanisms that can restrict the ultimate bit rate and to which limit is an essential question for future research.

Another subject of profound interest is how OTDM can penetrate into the commercial systems. Despite the fact that the concept of OTDM was suggested 40 years ago, no commercial systems have been deployed yet. The reasons for this are manifold as discussed in the following.

Stability of OTDM components

In order for OTDM systems to even be considered as serious candidates for systems carrying real data, as opposed to the Pseudo Random Bit Sequences (PRBS) utilised in most laboratory demonstrations, it is inevitable to develop the OTDM components and the subsystems so they fulfil stability requirements matching existing deployed systems. As discussed in chapter 4, fibre based components for e.g. switching are often used due to the fast Kerr effect, and these components serve as good examples of the challenges faced by potential OTDM network designers. Any researcher who experimentally have been working with e.g. a Non-linear Optical Loop Mirror (NOLM), see chapter 4, will testify how sensitive the NOLM is to external environmental influence such as e.g. temperature, and operation of the NOLM requires a continuous optimisation of e.g. the state-of-polarisation and temporal position of the input signal in order to ensure error-free operation. Before a NOLM can be used in real systems, the stability needs to be ensured by reducing the influence of

external sources and/or by implementing automatic feedback systems, which continuously optimise the performance by e.g. varying a polarisation controller at the input to the NOLM. Hence, stabilisation of the OTDM components and subsystems are indispensable but yet uncultivated work and needs attention before OTDM is feasible in real data carrying systems.

OTDM in network environment

The work reported in literature on OTDM systems has primarily focused on point-to-point systems, thus investigating how an ultra-high capacity can be generated in the transmitter by bit interleaving a number of low bit rate signals together and transmit the aggregated high-speed signal over a transmission span before processed and detected in the receiver. It is however often vaguely suggested in the same papers that OTDM can be used in more advanced networks, albeit without going into details about the actual envisioned implementation and structure. As described in chapter 5, only a few groups in the world including COM•DTU have pursued in more details how OTDM can be utilised in networks. Reading these suggested structures it appears that no consensus has been obtained on how OTDM can be used and the proposed structures often ignore a potential interplay with existing networks and the data transfer protocols used. Hence, substantial work still lay ahead of the OTDM community to clarify whether OTDM can be used as an additional technology available for network designers to increase the total capacity of the networks by exploiting the interplay between OTDM and currently utilised technologies or if it is beneficial to replace some of these technologies with OTDM. This decision will require interactive work between the OTDM researchers and network planners in order to determine network topology, node structure and required functionalities, e.g. channel identification and add-drop multiplexing as discussed in chapter 5, and how the OTDM implementation might need to be modified to allow adoption of specific data protocols hence ensuring the operability of OTDM in network topologies including more than a transmitter and receiver node.

Specific applications for OTDM

In parallel with the work on investigating how OTDM in general can be utilised in network environments, it is also of interest to identify, if some specific applications will benefit from utilising the OTDM scheme for data transfer instead of present employed techniques. As one of the strong points of OTDM is the ability to handle large amount of data, a criteria for choosing well-suited applications for OTDM could be to identify environments where data generation and distribution require huge capacity. Finding and exploiting these potential niches are important OTDM research topics, as these niches

could be the starting point for deploying high-speed OTDM systems in real data carrying systems.

Cost efficiency of OTDM systems

Wavelength Division Multiplexed (WDM) systems deployed in existing networks can be designed and implemented using standardised components thus benefiting from relatively low prices due to the reduced costs associated with large scale production. OTDM components and subsystems are still in the research phase both in terms of optimisation of performance and stability, and have consequently not matured yet. Thus the costs of OTDM components are expected to be relatively high because they are customised research components. One objective for OTDM development must be to ensure that the total cost of the system is competitive with existing technologies when making the relevant cost-benefit analysis. The cost-benefit analysis will however not only include initial expenditures but also the operational costs. One operational parameter, which is of great concern when designing a system, is the power consumption. The higher the power consumption, the higher the costs so the power consumption should obviously be reduced to keep the expenditures of the OTDM system to an acceptable level. An additional incitement for keeping the power consumption of the entire system low is the risk of global warming. The energy used in telecommunication is typically produced in big power plants utilising fossil fuel, which unfortunately as an unwanted by-product emit carbon dioxide (CO_2) suspected to contribute to global warming. The Kyoto protocol puts constraints on the total acceptable CO_2 emission for each country and consequently ultimately on the total energy consumed by e.g. telecommunication systems.

So in conclusion, OTDM constitutes an attractive scheme to increase the total capacity of data carrying systems, and this thesis has presented some of the required design rules enabling optimum performance of OTDM systems. However, before OTDM can be utilised it still faces a number of challenges in terms of e.g. stability, cost efficiency and compatibility with existing network protocols and topologies.

Appendix A
PhD publications

Papers

[p1] K. S. Jepsen, A. T. Clausen, B. Mikkelsen, H. N. Poulsen, K. E. Stubkjaer, "All-optical network interface for bit synchronisation and regeneration", Proceedings of 23th European Conference on Optical Communication (ECOC'97), Edinburgh, UK, post-deadline paper Th3C.8 (1997).

[p2] K. S. Jepsen, B. Mikkelsen, A. T. Clausen, H. N. Poulsen, K. E. Stubkjaer, M. Vaa, "High-speed OTDM switching", Technical Digest of Conference on Lasers & Electro-Optics (CLEO 1998), San Francisco, California, USA, invited paper CMA1 (1998).

[p3] K. S. Jepsen, B. Mikkelsen, M. Vaa, H. N. Poulsen, A. T. Clausen, K. E. Stubkjaer, R. Hess, M. Duelk, W. Vogt, E. Gamper, E. Gini, P. A. Besse, H. Melchior, "Simultaneous all-optical add and drop multiplexing of 40 Gbit/s OTDM signals using monolithically integrated Mach-Zehnder interferometer", Technical Digest of conference on Optical Fiber Communication (OFC'98), San Jose, California, USA, paper ThN2 (1998).

[p4] A. T. Clausen, K. S. Jepsen, A. Buxens, B. Mikkelsen, K. E. Stubkjaer: "Interface for 10 Gbit/s bit-synchronisation and format and wavelength conversion with 3R capabilities", Electronics Letters, Vol. 34, No. 16, pp. 1554-1555 (1998).

[p5] K. S. Jepsen, A. Buxens, A. T. Clausen, H. N. Poulsen, B. Mikkelsen, K. E. Stubkjaer: "20 Gbit/s optical 3R regeneration using polarisation-independent monolithically integrated Michelson interferometer", Electronics Letters, Vol. 34, No. 5, p. 472-474 (1998).

[p6] R. Hess, M. Duelk, W. Vogt, E. Gamper, E. Gini, P. A. Besse, H. Melchior, K. S. Jepsen, B. Mikkelsen, M. Vaa, H. N. Poulsen, A. T. Clausen, K. E. Stubkjaer, S. Bouchoule, F. Devaux: "Simultaneous all-optical add and drop multiplexing of 40 Gbit/s OTDM signals using monolithically integrated Mach-Zehnder interferometer", Electronics Letters, Vol. 34, No. 6, p. 579-580 (1998).

[p7] A. T. Clausen, A. Buxens, K. S. Jepsen, H. N. Poulsen, K. E. Stubkjaer: "Polarization-independent 3R regenerator at 20 Gbit/s using a monolithically integrated semiconductor optical amplifier based Michelson Interferometer", Technical Digest of 3rd Optoelectronics and Communications Conference (OECC'98), Chiba, Japan, paper 13A1-3 (1998).

[p8] K. E. Stubkjaer, S. L. Danielsen, A. Kloch, P. B. Hansen, K. S. Jepsen, H. N. Poulsen, D. Wolfson, A. T. Clausen, E. Limal, A. Buxens: "All-optical wavelength converters", Technical Digest of 3rd Optoelectronics and Communications Conference (OECC'98), Chiba, Japan, paper 16B3-1 (1998).

[p9] K. E. Stubkjaer, K. S. Jepsen, A. T. Clauen, H. N. Poulsen, A. Buxens, S. L. Danielsen, P. B. Hansen, A. Kloch, D. Wolfson: "High-speed photonic processing", The Rank Prize Funds - Mini-symposium on Ultrafast Photonic Processing and Networks, Grasmere, Cumbria, UK (1998).

[p10] A. T. Clausen, A. Buxens, K. S. Jepsen, H. N. Poulsen, K. E. Stubkjaer: "3R regeneration at 20 Gbit/s using a monolithically integrated Semiconductor Optical Amplifier based Michelson Interferometer", The Rank Prize Funds - Mini-symposium on Ultrafast Photonic Processing and Networks, Grasmere, Cumbria, UK (1998).

[p11] A. Buxens, A. T. Clausen, H. N. Poulsen, K. S. Jepsen, K. E. Stubkjaer, C. Bornholdt, O. Brox, M. Möhrle, B. Sartorius, "40 to 10 Gbit/s demultiplexing using a self-pulsating DFB laser for clock recovery", Proceedings of 24th European Conference on Optical Communication (ECOC'98), Madrid, Spain, Vol. 1, pp. 507-508 (1998)

[p12] K. S. Jepsen, H. N. Poulsen, A. T. Clausen, A. Buxens, K. E. Stubkjaer, "Investigation of cascadability of add-drop multiplexers in OTDM systems", in Proceedings of 24th European Conference on Optical Communication (ECOC'98), Madrid, Spain, Vol. 1, pp. 619-620 (1998).

[p13] A. Buxens, H. N. Poulsen, A.T. Clausen, K. S. Jepsen, K. E. Stubkjaer: "New Bi-directional Mid Span Spectral Inversion using Bi-directional Four Wave Mixing in Semiconductor Optical Amplifiers", Proceedings of 24th European Conference on Optical Communication (ECOC'98), Madrid, Spain, post-deadline paper, Vol. 3, pp. 97-98 (1998).

[p14] H. N. Poulsen, K. S. Jepsen, A. T. Clausen, A. Buxens, K. E. Stubkjaer, R. Hess, M. Duelk, H. Melchior, "Fast Optical Signal Processing in High Bit Rate OTDM Systems", Proceedings of 11th Annual Meeting of the IEEE Lasers and Electro-Optics Society (LEOS 1998), Orlando, Florida, USA, invited paper TuI1 (1998).

[p15] K. E. Stubkjaer, Kloch A., P. B. Hansen, H. N. Poulsen, D. Wolfson, K. S. Jepsen, A. T. Clausen, E. Limal, A. Buxens: "Wavelength converter technology", IEICE Transactions on Electronics, Vol. E82-C, Issue 2, p. 338-348 (1999).

[p16] K. E. Stubkjaer, Kloch A., P. B. Hansen, H. N. Poulsen, D. Wolfson, K. S. Jepsen, A. T. Clausen, E. Limal, A. Buxens: "Wavelength converter technology", IEICE Transactions on Electronics, Vol. E82-B, Issue 2, p. 390-400 (1999).

[p17] S. Bischoff, A. Buxens, H. N. Poulsen, A. T. Clausen, J. Mørk: "Bi-directional four wave mixing in semiconductor amplifiers for mid span spectral inversion: Theory and experiments", Technical Digest of Conference on Lasers and Electro-Optics (CLEO 1999), Baltimore, Maryland, USA, paper CTuW3 (1999).

[p18] S. Bischoff, A. Buxens, H. N. Poulsen, A. T. Clausen, J. Mørk, "Bi-directional four wave mixing in semiconductor amplifiers for mid span spectral inversion: Theory and experiments", Vol. 17, No. 9, pp. 1617-1625 (1999).

[p19] A. Buxens, A. T. Clausen, H. N. Poulsen, P. Jeppesen, "10 Gb/s bi-directional gating in semiconductor optical amplifiers for optical cross-connects exploiting network connection-symmetry", Proceeedings Photonics in Switching 99, Santa Barbara, California, USA, Vol. 32, pp 127-131 (1999).

[p20] X. Xheng, F. Liu, A. T. Clausen, A. Buxens, "High performance wavelength converter based on semiconductor optical and Mach-Zehnder interferometer add/drop multiplexer", Technical Digest of Optical Amplifiers and their Applications (OAA'99), Nara, Japan, pp. 132-134 (1999).

[p21] A. T. Clausen, A. Buxens, H. N. Poulsen, L. Oxenløve, P. Jeppesen, "Polarisation-independent Bi-directional Four Wave Mixing for Mid Span Spectral Inversion", Proceedings of 25th European Conference on Optical Communication (ECOC'99), Nice, France, paper I-146 (1999).

[p22] A. Buxens, H. N. Poulsen, A. T. Clausen, P. Jeppesen, "Simultaneous All-optical add-drop multiplexing functionality using bi-directional four wave mixing in a semiconductor optical amplifier", Proceedings of 25th European Conference on Optical Communication (ECOC'99), Nice, France, paper I-248 (1999).

[p23] H. N. Poulsen, P. Varming, A. Buxens, A. T. Clausen, I. Muñoz, P. Jeppesen, C. V. Poulsen, J. E. Pedersen, L. Eskildsen: "1607 nm DFB Fibre Laser for Optical Communication in the L-band", Proceedings of 25th European Conference on Optical Communication (ECOC'99), Nice, France, paper I-70 (1999).

[p24] S. Bouchoule, R. Lefevre, E. Legros, F. Devaux, H. Melchior, M. Duelk, R. Hess, E. Lach, H. Bülow, G. Veith, J. R. Burie, J. F. Cadiou, F. Brillouet, J. Hourany, D. Hoffman, B. Sartorius, K. S. Jepsen, A. T. Clausen, A. Buxens, H. N. Poulsen, K. E. Stubkjaer, H. Burkhard, H.-J. Schöll, D. Nesset, A. E. Kelly, D. Marcenac, R. V. Penty and I. H. White, "Photonic technologies for ultra-high-speed information highways, I. 40 Gbit/s TDM components and subsystems", Optical Fiber Technology, Vol. 5, No. 3, pp. 275-300 (invited paper) (1999).

[p25] H. N. Poulsen, A. Buxens, A. T. Clausen, P. Jeppesen, M. Dulk, S. Fischer, E. Gamper, W. Vogt, W. Hunziker, E. Gini, H. Melchior, "Wavelength conversion from C- to L-band at 10 Gbit/s including transmission over 80 km of SSMF", Technical Digest of Conference on Lasers & Electro-Optics (CLEO 2000), San Francisco, California, USA, paper CWI2 (2000).

[p26] A. Buxens, A. T. Clausen, H. N. Poulsen, P. Jeppesen, S. Fischer, M. Dulk, E. Gamper, W. Vogt, W. Hunziker, E. Gini, H. Melchior, "All-optical regenerative OTDM add/drop multiplexing at 40 Gbit/s using monolithic InP Mach-Zehnder interferometer", Technical Digest of Conference on Lasers & Electro-Optics (CLEO 2000), San Francisco, California, USA, paper CWD3 (2000).

[p27] A. Buxens, H. N. Poulsen, A. T. Clausen, P. Jeppesen, "All-optical OTDM to WDM signal format translation and OTDM add-drop funcionality using bi-directional four wave mixing in a semiconductor optical amplifier". Electronics Letters, Vol. 36, No. 2, pp. 156-158 (2000).

[p28] A. Buxens, H. N. Poulsen, A. T. Clausen, P. Jeppesen, "Gain flattened L-band EDFA based on up-grading a C-band EDFA using forward ASE pumping in an EDF section". Electronics Letters, Vol. 36, No. 9, pp. 821-823 (2000).

[p29] M. Dülk, S. Fischer, E. Gamper, W. Vogt, W. Hunziker, E. Gini, H. Melchior, H. N. Poulsen, A. T. Clausen, A. Buxens, P. Jeppesen, "Efficient regenerative wavelength conversion at 10 Gbit/s over C- and L-band (80 nm span) using a Mach-Zehnder interferometer with monolithically integrated semiconductor optical amplifiers". Electronics Letters, Vol. 36, No. 3, pp. 241-243 (2000).

[p30] S. Fischer, M. Dülk, E. Gamper, W. Vogt, W. Hunziker, E. Gini, H. Melchior, A. Buxens, H. N. Poulsen, A. T. Clausen, "All-Optical Regenerative OTDM Add/Drop Multiplexing at 40 Gbit/s using Monolithic InP Mach-Zehnder Interferometer", Photonics Technology Letters, Vol. 12, No. 3, pp. 335-337 (2000).

[p31] J. Yu, A. Buxens, A. Clausen, P. Jeppesen, "16x10 Gb/s WDM Bi-Directional Gating in a Semiconductor Optical Amplifier for Optical Cross Connects Exploiting Network Connection-Symmetry", Photonics Technology Letters, Vol. 12, No. 6, pp. 702-704 (2000).

[p32] J. Yu, A. Clausen, H. N. Poulsen, P. Jeppesen, X. Zheng, C. Peucheret. "40 Gb/s wavelength conversion in a cascade of an SOA and a NOLM and demonstration of extinction ratio improvement". Electronics Letters, Vol. 36, No. 11, pp. 963-964 (2000).

[p33] J. Yu, X. Zheng, F. Liu, C. Peucheret, A. T. Clausen, H. N. Poulsen, P. Jeppesen. "8 x 40 Gbit/s, 55km WDM Transmission Over Conventional Fiber Using A New RZ Optical Source", Photonics Technology Letters, Vol. 12, No. 7, pp. 912-914 (2000).

[p34] J. Yu, X. Zheng, C. Peucheret, A. T. Clausen, H. N. Poulsen, P. Jeppesen. "40 Gb/s All-Optical Wavelength Conversion Based on a Nonlinear Optical Loop Mirror", Journal of Lightwave Technology, Vol. 18, No. 7, pp. 1001-1006 (2000).

[p35] J. Yu, X. Zheng, C. Peucheret, A. T. Clausen, H. N. Poulsen, P. Jeppesen. "All Optical Wavelength Conversion of Short Pulses and NRZ Signals Based on a Nonlinear Optical Loop Mirror", Journal of Lightwave Technology, Vol. 18, No. 7, pp. 1007 (2000).

[p36] H. N. Poulsen, A. T. Clausen, A. Buxens, L. Oxenloewe, C. Peucheret, C. Rasmussen, F. Liu, J. Yu, A. Kloch, T. Fjelde, D. Wolfson, P. Jeppesen, "Ultra fast all-optical signal processing in semiconductor and fiber based devices", Proceedings of 26th European Conference on Optical Communication (ECOC'00), Munich, Germany, invited paper 7.4.1 (2000).

[p37] M. Dulk, S. Fischer, E. Gamper, W. Vogt, W. Hunziker, E. Gini, E. H. Melchior, H. N. Poulsen, A. T. Clausen, A. Buxens, P. Jeppesen, "Efficient and robust regenerative all-optical wavelength converter for C- and L-band (80 nm span) and for data rates up to 40 Gbit/s", Proceedings of Conference on Lasers and Electro-Optics, CLEO 2000, Vol. 39, pp. 276-277 (2000)

[p38] A. T. Clausen, L. Oxenlowe, C. Peucheret, S. N. Knudsen, L. Grüner-Nielsen, A. Bjarklev, S. Barkou, H. N. Poulsen, P. Jeppesen, "Novel single/multiple wavelength RZ pulse source based on four-wave mixing in newly developed highly non-linear fibre", Proceedings of 26th European Conference on Optical Communication (ECOC'00), Munich, Germany, poster P 3.14 (2000).

[p39] J. Yu, Y. Qian, A. T. Clausen, H. N. Poulsen, R. Jeppesen, S. N. Knudsen, "40 Gbit/s pulsewidth-maintained wavelength conversion based on a high-nonlinearity DSF-NOLM", Electronics Letters, Vol. 36, No. 19, pp. 1633-1634 (2000)

[p40] S. Fischer, M. Dülk, M. Bitter, M. Caraccia, E. Gamper, W. Vogt, E. Gini, H. Melchior, W. Hunziker, A. Buxens, H. N. Poulsen, A. T. Clausen, "Ultrafast all-optical demultiplexer based on Mach–Zehnder interferometer with integrated semiconductor optical amplifiers," in Technical Digest of 5th Optoelectronics Communications Conference (OECC'00), Chiba, Japan, paper 14D-1 (best paper award) (2000).

[p41] L. K. Oxenloewe, A. T. Clausen, H. N. Poulsen, "Wavelength conversion in an electroabsorption modulator," Proceedings of 26th European Conference on Optical Communication (ECOC'00), Munich, Germany, paper 9.4.4 (2000).

[p42] S. Bischoff, A. Buxens, S. Fischer, M. Duelk, A. T. Clausen, H. N. Poulsen, and J. Mørk, "Comparison of all-optical co- and counter-propagating high-speed signal processing in SOA-based Mach-Zehnder interferometers", Optical and Quantum Electronics, Vol. 33, pp. 907-926 (2001).

[p43] A. T. Clausen, C. Peucheret, L. Oxenlowe, H. N. Poulsen, P. Jeppesen, "OTDM and WDM systems", Danish Optical Society DOPS-NYT, Vol. 16, No. 2, pp. 9-12 (2001).

[p44] A. T. Clausen, L. Oxenløwe, C. Peucheret, H. N. Poulsen, P. Jeppesen, S. N. Knudsen, L. Grüner Nielsen, "10-GHz return-to-zero pulse source tunable in wavelength with a single- or multi wavelength output based on four-wave mixing in a newly developed highly nonlinear fiber", Photonics Technology Letters, Vol. 13, no. 1, pp. 70-72 (2001).

[p45] M. Dülk, S. Fischer, M. Bitter, M. Caraccia, W. Vogt, E. Gini, H. Melchior, W. Hunziker, A. Buxens, H. N. Poulsen, A. T. Clausen "Ultrafast all-optical demultiplexer based on monolithic Mach-Zehnder interferometer with integrated semiconductor optical amplifiers", Optical and Quantum Electronics, vol. 33, pp. 899-906 (2001).

[p46] M. L. Nielsen, A. T. Clausen, T. Fjelde, L. Oxenløwe, A. Klock, H. Poulsen, D. Wolfson, "All-optical signal processing employing interferometric structures" in Proceedings of OSP/COST International Workshop, Copenhagen, Denmark, paper VII-1 (2001).

[p47] K. E. Stubkjaer, T. Fjelde, D. Wolfson, A. Kloch, H. N. Poulsen, A. T. Clausen, "Functional elements for high-speed optical processing", International symposium on contemporary photonics technology (CPT'01), Tokyo, Japan, pp. 55-58 (2001).

[p48] A. I. Siahlo, K. S. Berg, A. T. Clausen, L. K. Oxenløwe, A. Tersigni, P. Jeppesen, "160-10 Gb/s demultiplexing by using NOLM", in Proceedings of Quantum Electronics (QE-2002) 4th International Scientific and Technical Conference 2002, p. 122, Minsk, Belarus (2002).

[p49] K. S. Berg, L. K. Oxenløwe, A. Siahlo, A. Tersigni, A. T. Clausen, C. Peucheret, P. Jeppesen, K. P. Hansen and J. R. Hansen, "80 Gb/s transmission over 80 km and demultiplexing using a highly non-linear photonic crystal fibre", Proceedings of European Conference on Optical Communication, (ECOC'2002), Copenhagen, Denmark, paper 2.1.5 (2002).

[p50] L. K. Oxenløwe, A. I. Siahlo, K. S. Berg, A. Tersigni, A. T. Clausen, C. Peucheret, P. Jeppesen, K. P. Hansen, J. R. Jensen, "A photonic crystal fibre used as a 160 to 10 Gb/s demultiplexer", Proceedings of Opto-Electronics and Communications Conference (OECC'2002), Yokohama, Japan, post-deadline paper PD1-4 (2002).

[p51] J. Lee, M. Ibsen, D. Richardson, L. Oxenløwe, K. Berg, A. Clausen, P. Jeppesen, "Timing jitter tolerant all-optical TDM data demultiplexing at 80 Gbit/s using fiber Bragg grating based rectangular pulse switching technology", in Technical Digest Optical Fiber Communication Conference (OFC'03), paper TuH7, Atlanta, Georgia, U.S.A. (2003).

[p52] A. Tersigni, V. Calle, A. T. Clausen, L. Oxenløwe, J. Mork, P. Jeppesen, "Polarisation independent optical sampling using four-wave mixing", Technical Digest of Conference on Lasers & Electro-Optics (CLEO 2003), Baltimore, Maryland, USA, paper CMR2 (2003).

[p53] A. Tersigni, V. Calle, A. T. Clausen, P. Jeppesen, K. P. Hansen and J. R. Jensen "Optical Sampling at 80 Gbit/s Using Photonic Crystal Fiber", Technical Digest of 8th OptoElectronics and Communcations Conference (OECC'03), Shanghai, China, paper 16D2-3 (2003)

[p54] L. K. Oxenløwe, A. Siahlo, P. Andersen, K. S. Berg, A. T. Clausen, P. Jeppesen, K. P. Hansen, J. R. Folkenberg, "Complete transmission system with highly non-linear dispersion shifted photonic crystal fibre as the demultiplexer", Proceedings of Conference on Lasers & Electro-Optics (CLEO'03), Baltimore, U.S.A., paper CFJ1 (2003).

[p55] A. Siahlo, L. K. Oxenløwe, K. S. Berg, A. T. Clausen, Peter A. Andersen, C. Peucheret, A. Tersigni, P. Jeppesen, K. P. Hansen, J. R. Folkenberg, " A High-Speed Demultiplexer Based on a Nonlinear Optical Loop Mirror With a Photonic Crystal Fiber, IEEE Photonics Technology Letters, Vol. 15, No. 8, pp. 1147-1149 (2003).

[p56] J. H. Lee, L. K. Oxenløwe, M. Ibsen, K. S. Berg, A. T. Clausen, D. J. Richardson, P. Jeppesen, "All-Optical TDM Data Demultiplexing at 80 Gb/s with Significant Timing Jitter Tolerance Using a Fiber Bragg Grating Based Rectangular Pulse Switching Technology", Journal of Lightwave Technology, Vol. 21, No. 11, pp. 2518-2523 (2003).

[p57] L. K. Oxenløwe, A. I. Siahlo, K. S. Berg, A. T. Clausen, B. M. Sørensen, K. Yvind, P. Jeppesen, K. P. Hansen, K. Hoppe, J. Hanberg, "A novel 160 Gb/s receiver configuration including a glass crystal pulsed laser, photonic crystal fibre and a simple dynamic clock recovery scheme", Proceedings of the 29th European Conference on Optical Communication (ECOC'03), Rimini, Italy, paper Th2.5.3 (2003).

[p58] Z. Xu, L. K. Oxenløwe, A. I. Siahlo, K. S. Berg, A. T. Clausen, Q. N. T. Le, C. Peucheret, K. Rottwitt, P. Jeppesen "Experimental characterisation of distributed Raman amplification in a standard single mode fibre based 160 Gbit/s transmission system", Proceedings of the 29th European Conference on Optical Communication (ECOC'03), Rimini, Italy, paper Tu4.7.2 (2003).

[p59] A. I. Siahlo, L.K. Oxenløwe, K.S. Berg, A.T. Clausen, K. Yvind, P. Jeppesen, K. P. Hansen, "Using a phase modulator for improvement of the tolerance to second-order dispersion in a 160 Gb/s transmission system", Proceedings of the 29th European Conference on Optical Communication (ECOC'03), Rimini, Italy, paper We4.P.105 (2003).

[p60] A. Tersigni, V. Calle, A. T. Clausen, P. Jeppesen, K. P. Hansen. J. R. Jensen "Optical Sampling at 80 Gbit/s Using Photonic Crystal Fiber", Proceedings of the 29th European Conference on Optical Communication (ECOC'03), Rimini, Italy, paper We4.P.129 (2003).

[p61] A. T. Clausen, H. N. Poulsen, L. K. Oxenløwe, A. I. Siahlo, J. Seoane, P. Jeppesen, "Pulse source requirements for OTDM systems", Proceedings of 16th Annual meeting of IEEE Lasers & Electro-Optics Society (LEOS 2003), Tucson, USA, paper TuY2 (2003).

[p62] D. Zibar, L. K. Oxenløve, A. T. Clausen, J. Mørk, " Theoretical and experimental Investigation of a Balanced Phase-Locked Loop Based Clock Recovery at a Bit Rate of 160 Gb/s", Proceedings of 16th Annual meeting of IEEE Lasers & Electro-Optics Society (LEOS 2003), Tucson, USA, paper TuY5 (2003).

[p63] A. Siahlo, L. K. Oxenløwe, K. S. Berg, A. T. Clausen, Peter A. Andersen, C. Peucheret, A. Tersigni, P. Jeppesen, K. P. Hansen, J. R. Folkenberg, " A High-Speed Demultiplexer Based on a Nonlinear Optical Loop Mirror With a Photonic Crystal Fiber, IEEE Photonics Technology Letters, Vol. 15, No. 8, pp. 1147-1149 (2003).

[p64] A. T. Clausen, J. Bennike, L.K. Oxenløwe, J. Seoane, A.I. Siahlo and P. Jeppesen, "Pilot tone modulation used for channel identification in OTDM networks", Proceedings of Conference on Lasers & Electro-Optics (CLEO'04), San Francisco, California, USA, paper CThQ7 (2004).

[p65] J. Seoane, A. I. Siahlo, A. T. Clausen, L. K. Oxenløwe, Z. Xu, P. Jeppesen, “All optical 160 to 10 Gbit/s demultiplexing using co-propagating optical clock”, Proceedings of Conference on Lasers & Electro-Optics (CLEO’04), San Francisco, California, USA, paper CThQ4 (2004).

[p66] L. K. Oxenløwe, K. S. Berg, A. T. Clausen, J. Seoane, A. I. Siahlo and P. Jeppesen, “Specialty fibers for 160, 320 and 640 Gb/s signal processing” Proceedings of Conference on Lasers & Electro-Optics (CLEO’04), San Francisco, California, USA, paper CThQ1 (2004)

[p67] A. I. Siahlo, A. T. Clausen, L. K. Oxenløwe, J. Seoane, Z. Xu, P. Jeppesen, “Tunable dispersion compensation using phase modulation in receiver part”, Technical Digest of conference on Optical Fiber Communication (OFC’04), Los Angeles, California, USA, paper ThU4 (2004)

[p68] Z. Xu, J. Seoane, A. Siahlo, L. Oxenløwe, A. T. Clausen, C. Peucheret, K. Rottwitt, P. Jeppesen, “Experimental characterization of dispersion maps with Raman gain in 160 Gb/s systems”, Proceedings of Conference on Lasers & Electro-Optics (CLEO’04), San Francisco, California, USA, paper CWA20 (2004).

[p69] A. T. Clausen, L. K. Oxenløwe, A. Siahlo, J. Seoane and P. Jeppesen, "Expansion of Point-to-Point OTDM Systems to a Ring Network", Proceedings of the 30th European Conference on Optical Communication (ECOC'04), Stockholm, Sweden, paper Th2.6.3 (2004).

[p70] L. K. Oxenløwe, L.J. Christiansen, D. Larsson, K. Yvind, A.T. Clausen, J. Seoane, A.I. Siahlo, B. Sørensen, and P. Jeppesen, "Pre-scaled clock recovery with compact semiconductor devices for ultra high-speed OTDM systems", Proceedings of the 30th European Conference on Optical Communication (ECOC'04), Stockholm, Sweden, paper We3.5.2 (2004).

[p71] J. Seoane, A. I. Siahlo, A. T. Clausen, L. K. Oxenløwe, P. Jeppesen, M. Schmidt, M. Schilling and E. Lach, "Ultra high-speed demultiplexing using a NOLM based on commercially available highly non-linear fibre", Proceedings of the 30th European Conference on Optical Communication (ECOC'04), Stockholm, Sweden, paper We1.5.4 (2004).

[p72] A. Siahlo, A. T. Clausen, J. Seoane, L. K. Oxenløwe, K.S. Berg, P. Jeppesen, O. Brox, S. Bauer, J. Kreissl and B. Sartorius, "Pulse Compression of a 40 GHz DFB based Optical Clock Recovery", Proceedings of the 30th European Conference on Optical Communication (ECOC'04), Stockholm, Sweden, paper We2.5.4 (2004).

[p73] E. Lach, M. Schmidt, M. Witte, K. Schuh, H. Buelow, F. Buchali, A. T. Clausen, L. K. Oxenløwe, B. Sartorius, C. Kazmierski, S. Vorbeck, R. Leppla, E. Le-Rouzic, B. Cuenot, A. Richter, R. Ramos, R. Llorente, G. Charlet, P. Pecci, D. Rouvillain, "DWDM transmission at ultra-high channel bitrates: European TOPRATE project view", Proceedings of the 30th European Conference on Optical Communication (ECOC'04), Stockholm, Sweden, paper Tu1.1.2 (2004)

[p74] M. Galili, L.K. Oxenløwe, D. Zibar, A.T. Clausen, P. Jeppesen, "160 Gb/s Raman-Assisted SPM Wavelength Converter" Proceedings of 30th European Conference on Optical Communication (ECOC'04), Stockholm, Sweden, post-deadline paper Th4.3.1 (2004).

[p75] A. T. Clausen, L. K. Oxenløwe, A. Siahlo, J. Seoane, P. Jeppesen "Experimental and Theoretical Investigation of Systems with Potential for Terabit Capacity", SPIE International Symposium on Information Technology and Communication (ITCOM 2004), Philadelphia, Pennsylvania, USA, paper 5596-09 (2004).

[p76] L. K. Oxenløwe, L. J. Christiansen, D. Larsson, K. Yvind, A. T. Clausen, J. Seoane, A. I. Siahlo, B. Sørensen, P. Jeppesen, "Low-jitter pre-scaled clock recovery with compact semiconductor components for ultra high-speed OTDM systems", Proceedings of 9th OptoElectronics and Communications Conference/3rd International conference on Optical Internet (OECC'04/COIN), Yokohama, Japan, paper 16E3-5 (2004)

[p77] D. Zibar, L. K. Oxenløwe, A. T. Clausen, J. Mørk, P. Jeppesen, "Analysis of the Effects of Time Delay in Clock Recovery Circuits Based on Phase-Locked Loops", Proceedings of 17th Annual meeting meeting of IEEE Lasers & Electro-Optics Society (LEOS 2004), Rio Mar, Puerto Rico, paper TuR 4 (2004).

[p78] A. I. Siahlo, J. Seoane, A. T. Clausen, L. K. Oxenløwe, P. Jeppesen, "320 Gb/s Single-Polarization OTDM Transmission over 80 km Standard Transmission Fiber", Technical Digest of conference on Optical Fiber Communication (OFC'05), Anaheim, California, USA, paper OFF3 (2005).

[p79] A. I. Siahlo, A. T. Clausen, L. K. Oxenløwe, J. Seoane, K. S. Berg, Z. Xu, J. Zeng, P. Jeppesen, "Phase Modulation for Post-Compensation of Dispersion in 160 Gb/s Systems", IEEE Photonics Technology Letters, Vol. 17, No. 2, pp. 498-500 (2005).

[p80] A. I. Siahlo, A. T. Clausen, L. K. Oxenløwe, J. Seoane, P. Jeppesen, "640 Gb/s OTDM Transmission and Demultiplexing using a NOLM with Commercially Available Highly Non-linear Fiber", Technical Digest of Conference on Lasers & Electro-Optics (CLEO 2005), Baltimore, Maryland, USA, paper CTuO1 (2005) (Invited).

[p81] A. T. Clausen, A. Siahlo, J. Seoane, L. K. Oxenløwe, P. Jeppesen, "320 to 10 Gbit/s demultiplexing using a NOLM based on commercially available components", Electronics Letters, Vol. 41, No. 5, pp. 265-266 (2005).

[p82] M. Galili, L. K. Oxenløwe, D. Zibar, A. T. Clausen, P. Jeppesen, H.-J. Deyerl, N. Plougmann, M. Kristensen, "Characterisation of Systems for Raman-Assisted High-Speed Wavelength Conversion", Technical Digest of Conference on Lasers & Electro-Optics (CLEO 2005), Baltimore, Maryland, USA, paper CMQ2 (2005).

[p83] D. Zibar, J. Mørk, L. K. Oxenløwe, M. Galili, A. T. Clausen, " Timing Jitter Analysis for Clock Recovery Circuits Based on an Optoelectronic Phase-Locked Loop (OPLL)", Technical Digest of Conference on Lasers & Electro-Optics (CLEO 2005), Baltimore, Maryland, USA, paper CMZ4 (2005).

[p84] J. Seoane, A. T. Clausen, L. K. Oxenløwe, A. I. Siahlo, P. Jeppesen, "Spectral Efficiency Limits for Binary Modulation in Ultra High Bit Rate Optical Networks", Technical Digest of 10th Optoelectronics and Communcations Conference (OECC'05), Seoul, Korea, paper 7P-003 (2005).

[p85] M. Galili, L. K. Oxenløwe, D. Zibar, A. T. Clausen, H.-J. Deyerl, N. Plougmann, M. Kristensen, P. Jeppesen, "160 Gb/s Notch-Filtered Raman-Assisted XPM Wavelength Converter", Proceedings of the 31st European Conference on Optical Communication (ECOC'05), Glasgow, United Kingdom, paper Mo4.5.5 (2005).

[p86] L. K. Oxenløwe, D. Zibar, M. Galili, A. T. Clausen, L.J. Christiansen, P. Jeppesen, "Filtering-Assisted Cross-Phase Modulation in a Semiconductor Optical Amplifier Enabling 320 Gb/s Clock Recovery", Proceedings of the 31st European Conference on Optical Communication (ECOC'05), Glasgow, United Kingdom, paper We3.5.5 (2005).

[p87] D. Zibar, L. K. Oxenløwe, J. Mørk, M. P. Sørensen, M. Galili, A. T. Clausen, B. M. Sørensen, P. Jeppesen, "Detailed modelling and experimental characterisation of an ultra-fast optoelectronic clock recovery circuit", Proceedings of the 31st European Conference on Optical Communication (ECOC'05), Glasgow, United Kingdom, paper We4.P.111 (2005).

[p88] T. Tokle, L. K. Oxenløwe, J. Seoane, A. T. Clausen, P. Jeppesen, "160 Gbit/s Single Channel Data Generation using Multilevel Optical RZ-DPSK-ASK Modulation and Optical Time Division Multiplexing", Proceedings of the 31st European Conference on Optical Communication (ECOC'05), Glasgow, United Kingdom, paper We3.2.5 (2005).

[p89] L. K. Oxenløwe, D. Zibar, M. Galili, A. T. Clausen, L. J. Christiansen, P. Jeppesen, "Clock recovery for 320 Gb/s OTDM data using filtering-assisted XPM in an SOA", Technical Digest of Conference on Lasers & Electro-Optics Europe (CLEO Europe 2005), Munich, Germany, paper CI3-4-MON (2005).

[p90] M. Galili, L. K. Oxenløwe, H. C. Hansen Mulvad, D. Zibar, A. T. Clausen, P. Jeppesen, “160 Gb/s Raman-Assisted Notch-Filtered XPM Wavelength Conversion and Transmission”, Technical Digest of conference on Optical Fiber Communication (OFC’06), Anaheim, California, USA, paper OWW2 (2006)

[p91] D. Zibar, L. K. Oxenløwe, H. C. Hansen Mulvad, J. Mørk, M. Galili, A. T. Clausen, Palle Jeppesen, ”The Impact of Gating Timing Jitter on a 160 Gb/s Demultiplexer”, Technical Digest of conference on Optical Fiber Communication (OFC’06), Anaheim, California, USA, paper OTuB2 (2006)

[p92] D. Zibar, J. Mørk, L. K. Oxenløwe, A. T. Clausen, P. Jeppesen, “Reduction of Timing jitter by Clock Recovery based on an Optical Phase-Locked Loop”, Technical Digest of Conference on Laser-Electro Optics (CLEO 2006), Long Beach, California, USA, paper CMJ4 (2006).

[p93] L. K. Oxenløwe, M. Galili, A. T. Clausen, P. Jeppesen, "Generating a Square Switching Window for Timing Jitter Tolerant 160 Gb/s Demultiplexing by the Optical Fourier Transform Technique", accepted at 32nd European Conference on Optical Communication (ECOC'06)

[p94] M. Galili, L.K. Oxenløwe, H. C. Hansen Mulvad, A.T. Clausen, P. Jeppesen, "Raman-Assisted XPM Wavelength Conversion at 320 Gb/s" accepted at 32nd European Conference on Optical Communication (ECOC'06)

[p95] H. C. Hansen Mulvad, M. Galili, L. K. Oxenløwe, L.Grüner-Nielsen, A. Clausen, Palle Jeppesen, "Simultaneous Add-Drop Multiplexing at 80 Gbit/s in a Nonlinear Optical Loop Mirror" accepted at 32nd European Conference on Optical Communication (ECOC'06)

[p96] M. Galili, L.K. Oxenløwe, H.C.H. Mulvad, A.T. Clausen and P. Jeppesen, “Cross Phase Modulation Wavelength Conversion of 320 Gb/s Data” accepted at European Optics Society Annual Meeting 2006, Topical Meeting on Extreme Optics (EOS 2006 TOM2)

[p97] L. K. Oxenløwe, M. Galili, H. C. H. Mulvad, A. T. Clausen, D. Zibar, P. Jeppesen, "Solutions for ultra-high speed optical wavelength conversion and clock recovery" submitted to 8th International Conference on Transparent Optical Networks (ICTON 2006).

[p98] L. K. Oxenløwe, M. Galili, H.C. Mulvad Hansen, A.T. Clausen, P. Jeppesen "Reduced timing sensitivity in all-optical switching using flat-top control pulses obtained by the optical Fourier transform technique" accepted at International Conference on Photonics in Switching 2006, paper O9.3

[p99] M. Galili, H. C. Hansen Mulvad, L. K. Oxenløwe, A. T. Clausen, P. Jeppesen "Low-penalty Raman-Assisted XPM Wavelength Conversion at 320 Gb/s" submitted to 19th Annual meeting of IEEE Lasers & Electro-Optics Society (LEOS 2006)

[p100] H. C. Hansen Mulvad, L. K. Oxenløwe, M. Galili, A. T. Clausen, P. Jeppesen, L. Grüner-Nielsen, "Simultaneous 160 Gb/s Add-Drop Multiplexing in a Non-Linear Optical Loop Mirror" submitted to 19th Annual meeting of IEEE Lasers & Electro-Optics Society (LEOS 2006)

Deliverables

[D01] A. T. Clausen, H. N. Poulsen, "Clock recovery based on phase detection in semiconductor optical amplifiers", HIGHWAY deliverable D 25 (restricted) (1998).

[D02] E. Lach, H. Bülow, G. Veith, B. Sartorius, D. Hoffmann, A. T. Clausen, H. N. Poulsen, "Final reports on clock recovery", HIGWAY deliverable D 31 (restricted) (1998).

[D03] A. T. Clausen, H. N. Poulsen, C. Peucheret, J. Bennike, "Report on 8 x 40 Gb/s WDM RZ experiment", METEOR deliverable D 09 (public) (2000).

[D04] G. Eisenstein, A. T. Clausen, D. Dahan, J. Lasri, J. Seoane, "Report on 8 X 40 Gbit/s WDM NRZ Experiments", METEOR deliverable D 15 (restricted) (2001).

[D05] S. Boge, J. Seoane, A. T. Clausen, "Report on 8 x 40 Gbit/s WDM NRZ experiment – Addendum", METEOR deliverable D 15 Addendum (public) (2002).

[D06] A. T. Clausen, L. Oxenløwe, A. Siahlo, K. S. Berg, P. Jeppesen, "Pulsesource requirements for 160 Gbit/s, 640 Gbit/s and 1 Tbit/s transmission systems", TOPRATE deliverable D 3.1 (limited) (2002).

[D07] H. Bülow, H. Akzünger, F. Buchali, G. Thielecke, A. Clausen, A. Siahlo, L. Oxenløwe, C. M. Weinert, J. Marti, F. Ramos, R. Llorente, R. Clavero, E. Corbel, "Report on 160 Gbit/s transmission impairment analysis, dispersion (GVD, PMD) mitigation and novel Orthogonal-OTDM technique principles", TOPRATE deliverable D 2.1 (restricted), 2002 08 31 (2002).

[D08] M. Kroh, H. G. Weber, A. T. Clausen, C. Mikkelsen, L. Oxenløwe, A. Siahlo, K. Berg, A. Tersigni, S. Bischoff, J. Mørk, "Report on sources for > 160Gbit/s including first version of the modelocked laser based pulse source without pulse shaper and on design and implementation of Nx40 Gibt/s OTDM multiplexer for Nx40 Gbit/s", TOPRATE deliverable D 3.2 (limited) (2002).

[D09] E. Lach, K. Schuh, M. Schmidt, A. T. Clausen, L. Oxenløwe, A. Siahlo, K. Berg, A. Tersigni, "Report on concepts and laboratory testbeds for Nx160 Gbit/s DWDM transmission", TOPRATE deliverable D 5.1 (limited) (2002).

[D10] A. T. Clausen, J. Mørk, L. K. Oxenløwe, M. Schmidt, E. Lach, "Report on design and implementation of EAM based demux for 160 Gbit/s and SOA based interferometric devices from > 160 Gbit/s and on techniques for optical phase detection", TOPRATE deliverable D 4.2 (restricted) (2003).

[D11] J. Gehler, H. Bülow, F. Buchali, A. Clausen, A. Siahlo, L. Oxenløwe, J. Marti, F. Ramos, R. Llorente, R. Clavero, "Report on concepts for static/dynamic dispersion compensation and novel OTDM/DWDM principle transmission impairments", TOPRATE deliverable D 2.2 (restricted) (2003)

[D12] K. S. Berg, J. Mulet, M. Kroh, L. K. Oxenløwe, A. T. Clausen, A. N. Siahlo, P. Jeppesen, J. Mørk, S. Ferber, H. G. Weber, "Report on fibre based short pulse source for ≥ 640 Gbit/s and improved ECMLL", TOPRATE deliverable D 3.5 (limited) (2003).

[D13] A. T. Clausen, A. Siahlo, L. Oxenløwe, J. Seoane, E. Lach, K. Schuh, M. Schmidt, H. Aksuenger, B. Junginger, P. Pecci, "Report on Nx160 Gbit/s OTDM DWDM and 640 Gbit/s transmission system experiments", TOPRATE deliverable D 5.2 (restricted) (2003).

[D14] A. I. Siahlo, A. T. Clausen, L. Oxenløwe, J. Seoane, C. M. Weinert, "Report on system optimisation and dispersion management for OTDM/WDM transmission at 160 Gbit/s and beyond", TOPRATE deliverable D 2.3 (restricted) (2004).

[D15] M. Schmidt, M. Witte, F. Buchali, E. Corbel, A. I. Siahlo, A. T. Clausen, L. K. Oxenløwe, J. Seoane, R. Llorente, R.Clavero, J.Perez, "Report on dynamic dispersion compensation (GVD, PMD) and channel monitoring", TOPRATE deliverable D 2.4 (restricted) (2004).

[D16] C. Kazmierski, J. Decobert, F. Blache, E. Lach, M. Schmidt, K. Schuh, B. Junginger, J. Mulet, J. Mørk, A. Clausen, M. Kroh, H.G. Weber, "Final report on design and implementation of OTDM sources for Nx160 Gbit/s DWDM and ≥ 640 Gbit to >1 Tbit/s based on EAM, mode-locked laser, soliton effect and supercontinuum", TOPRATE deliverable D 3.6 (restricted) (2004).

[D17] L.K. Oxenløwe, A.T. Clausen, A. Siahlo, J. Seoane, M. Schmidt, K. Schuh, B. Junginger, E. Lach, O. Brox, C. Bobbert, T. Tekin, B. Sartorius, "Final report on ultra-high speed OTDM receiver for 160 Gbit/s DWDM and ≥ 640 Gbit/s (including reports on demultiplexer for >160 Gbit/s based on fiber non-linearities, on clock-recovery subsystems based on optical phase detection and phase locked loop and on the potential of self-pulsating DFB lasers for demultiplexing in OTDM systems)", TOPRATE deliverable D 4.4 (restricted) (2004).

[D18] D. Rouvillain, E. Corbel, P. Pecci, E. Lach, M. Schmidt, M. Witte, A. T. Clausen, J. Seoane, A. I. Siahlo, L. K. Oxenløwe, "Final report on Nx160Gbit/s OTDM-DWDM and single channel 640 Gbit/s and up to 1 Tbit/s system experiments and subsystem tests", TOPRATE deliverable D 5.3 (restricted) (2004).

[D19] M. Schmidt, M. Witte, F. Buchali, E. Corbel, A. I. Siahlo, A. T. Clausen, L. K. Oxenløwe, J. Seoane, R. Llorente, R. Clavero, J. Perez, "Public report on Terabit/s Transmission aspects within TOPRATE", TOPRATE deliverable D 2.5 (public) (2004).

[D20] C. Kazmierski, J. Decobert, F. Blache, E. Lach, M. Schmidt, K. Schuh, B. Junginger, J. Mulet, J. Mørk, A. Clausen, M. Kroh, C. M. Weinert, H. G. Weber, E. Le Rouzic, "Final public report on design and implementation of OTDM sources for Nx160 Gbit/s DWDM and ≥ 640 Gbit to >1 Tbit/s based on EAM, modelocked laser, soliton effect and supercontinuum", TOPRATE deliverable D 3.7 (public) (2004).

[D21] L. K. Oxenløwe, A. T. Clausen, A. Siahlo, J. Seoane, M. Schmidt, K. Schuh, B. Junginger, E. Lach, O. Brox, C. Bobbert, T. Tekin, B. Sartorius, "Public report on High speed demultiplexers and receivers within TOPRATE", TOPRATE deliverable D 4.5 (public) (2004).

[D22] E. Lach, M. Schmidt, M. Witte, K. Schuh, D. Rouvillain, E. Corbel, P. Pecci, A. T. Clausen, J. Seoane, A.I. Siahlo, L.K. Oxenløwe, "Public report on Terabit/s system demonstrators and lab experiments within TOPRATE", deliverable D 5.4 (public) (2004).